Dissimilar laser welding of NiTi shape memory alloys

by

Amirali Shamsolhodaei

A thesis
presented to the University of Waterloo
in fulfillment of the
thesis requirement for the degree of
Doctor of Philosophy
in
Mechanical and Mechatronics Engineering

Waterloo, Ontario, Canada, 2021

Examining Committee Membership

The following served on the Examining Committee for this thesis. The decision of the Examining Committee is by majority vote.

External Examiner	Professor Mohammad Jahazi Department of Mechanical Engineering, Ecole de technologie superieure (ETS), Canada
Supervisor(s)	Professor Norman Y. Zhou and, Professor Peng Peng Department of Mechanical and Mechatronics Engineering, University of Waterloo, Canada
Internal Member	Professor Adrian P. Gerlich, Department of Mechanical and Mechatronics Engineering, University of Waterloo, Canada
Internal Member	Professor Ehsan Toyserkani, Department of Mechanical and Mechatronics Engineering, University of Waterloo, Canada
Internal-external Member	Professor Scott Walbridge, Department of Civil and Environmental Engineering, University of Waterloo, Canada

AUTHOR'S DECLARATION

This thesis consists of material all of which I authored or co-authored: see Statement of Contributions included in the thesis. This is a true copy of the thesis, including any required final revisions, as accepted by my examiners.

I understand that my thesis may be made electronically available to the public.

Statement of Contribution

This thesis includes seven chapters: an introduction and literature review (Chapters 1 and 2) which represents a review paper (manuscript is ready to submit), and a series of four data chapters starting from Chapter 3 to 6 including published or under-review manuscripts the candidate authored.

The manuscripts have been modified to the style of the thesis. The candidate is the primary author in all manuscripts. It should be noted that most of the work in the lab (except where noted) including sample preparations, welding of the samples, mechanical testing, characterizations, and writing were done by the candidate. The following co-authors have contributed to the current work as outlined below:

Professor Norman Zhou supervised the research progress, advised the research direction, reviewed and edited the manuscripts. Professor Peng Peng oversaw research progress, had participated in technical discussions, reviewed and edited the thesis.

Chapter 1 and 2

Professor Norman Zhou supervised the research progress, advised the research direction, reviewed and edited the manuscripts. Professor Peng Peng oversaw research progress, participated in technical discussions, and reviewed and edited the thesis.

A Shamsolhodaei, J Li, B. Panton, JP Oliveira, A Michael, A Vivek, G Daehn, P Peng, YN Zhou, "A review on the dissimilar welding of NiTi shape memory alloys using fusion and solid state processes", Ready to submit

The candidate is the primary author of this review paper and the sections used in this thesis. Jianxiong Li from Ohio State University (OSU) authored the solid state process section of the manuscript, which is entirely excluded from Chapter 2. Boyd Panton (OSU), Joao Pedro Oliveira (Universidade Nova de Lisboa), Andrew Michael (UW), Anupam Vivek (OSU), Glenn Daehn (OSU) assisted with editing and provided feedback on the manuscript. Prof. Zhou and Prof. Peng's roles were as described earlier.

Chapter 3

A. Shamsolhodaei, Y.N. Zhou, & A. Michael (2019). Enhancement of mechanical and functional properties of welded NiTi by controlling nickel vaporisation. Science and Technology of Welding and Joining, 24(8), 706-712.

Dr. Andrew Michael was a Ph.D. student at the University of Waterloo who supported with editing the manuscript, technical comments, and editorial support. The role of Prof. Zhou was as described earlier.

A Shamsolhodaei, M.H. Razmpoosh, C. Maletta, P. Magaro, Y.N. Zhou. (2021). A comprehensive insight into the superelasticity measurement of laser welded NiTi shape memory alloys. Materials Letters 287, 129310.

Dr. Razmpoosh from University of Toronto supported the Electron Probe Micro Analyzer (EMPA) to measure the Ni loss inside the fusion zone of the welded samples used in Fig 3-4 and helped with the editing of the manuscript. Dr. Maletta and Pietro Magaro from University of Calabria (Italy) supported the nanoindentation tests at room and elevated temperature to measure the local superelasticity of the welded samples. The role of Prof. Zhou was as described earlier.

Chapter 4

A. Shamsolhodaei, J.P. Oliveira, N. Schell, E. Maawad, B. Panton, Y.N. Zhou, (2020). Controlling intermetallic compounds formation during laser welding of NiTi to 316L stainless steel. Intermetallics, 116, 106656.

Norbert Schell and Emad Maawed from Institute of Materials Physics, Helmholtz-Zentrum Hereon (Germany) supported with Synchrotron XRD results (Figure 4-7). The roles of J.P. Oliveira, B. Panton and Prof. Zhou were as described earlier.

A. Shamsolhodaei, Q. Sun, X Wang, B. Panton, H. Di, Y.N. Zhou. (2020). Effect of Laser Positioning on the Microstructure and Properties of NiTi-Copper Dissimilar Laser Welds. Journal of Materials Engineering and Performance, 29(2), 849-857.

Dr. Qian Sun and Dr. Xiaonan Wang were visitor scholars at the Center of Advanced Materials Joining and helped with designing and performing some of the experiments and co-authoring the manuscript. Prof. Di supported in editing and reviewed the manuscript. The role of Prof. Panton and Prof. Zhou were as described earlier.

Chapter 5

A Shamsolhodaei, JP Oliveira, B Panton, B Ballesteros, N Schell, YN Zhou. (2021), Superelasticity preservation in dissimilar joint of NiTi shape memory alloy to biomedical PtIr, Materialia 16, 101090.

B Ballesteros helped with providing Transmission Electron Microscope images (Figure 5-3) and N. Schell helped with providing Synchrotron XRD (Figure 5-4). The role of J.P. Oliveira, B. Panton and Prof. Zhou were as described earlier.

Chapter 6

A. Shamsolhodaei, B. Panton, A. Michael, P. Changizian, Y.N. Zhou. (2021), Laser alloying as an effective way to fabricate NiTiPt shape memory alloy, Metallurgical and Materials Transaction A (2021):1-11.

Dr. Pouyan Changizian (Queens University) supported with providing Transmission Electron Microscopy images (Figure 6-11 and 6-12 and Table 6-2). The role of other authors was described earlier.

A Shamsolhodaei, P Peng, H Torbati-Sarraf, N Chawla, YN Zhou. Laser microwelding as a novel alloying process to fabricate NiTiPt high temperature shape memory alloys (Ready to submit).

Dr. Torbati-Sarraf and Prof. Chawla from University of Purdue supported with providing 3D X-ray tomography images (Figure 6-14 and 6-15) and reviewing the manuscript. The role of other authors were described earlier.

Abstract

Welding of NiTi shape memory alloys has a great importance since it has a wide application in the medical industry due to the NiTi unique biocompatibility, superelasticity and shape memory effect. Laser microwelding is one of the leading candidates in manufacturing methods for medical devices due to its low heat input, minimum heat affected zone and good reproducibility. Despite all these benefits, some challenges such as formation of hard and brittle intermetallic compounds and selective vaporization, inherent in this technique still exist. Therefore, it is important to study and develop methods and parameters to minimize detrimental effects, such as the mentioned issues.

To have a basic understanding of the effect of laser parameters, similar laser welding of NiTi has been applied and the results show that applying high power resulted in Ni evaporation and changing the transformation temperature, and hence, the formation of the martensite phase within the fusion zone. These outcomes in addition to unfavorable texture inside the fusion zone (FZ) are the primary reasons for deterioration of superelasticity for the high power sample.

Laser offsetting strategy in the dissimilar weld of NiTi to stainless steel and pure Cu was studied to control the intermetallic compound formation and flow characteristics inside the fusion zone. Adopting laser offsetting welding on NiTi/SS joint could increase the mechanical response of the welded samples by suppressing the brittle intermetallics and modifying the microstructure. However, in the case of NiTi/Cu although the positioning of the laser varied the degree of the microstructure homogeneity, the mixing pattern and the presence of $Ni_xTi_yCu_z$ intermetallic compounds, it did not have any significant effect on the mechanical properties of the welds.

In the case of the NiTi/PtIr dissimilar joint, it was shown that by selecting proper parameters the NiTiPt phase formed in the fusion zone, which has a strong bonding with both base materials, causing superelasticity preservation in NiTi/PtIr joint. The mentioned NiTiPt, contains the P-phase and $Ti_2(Ni, Pt)_3$ nano-precipitates, which are the main characteristics of this high temperature shape memory alloy. This resulted in fabrication of NiTiPt high temperature shape memory alloy wire with a significant superelasticity at 250°C. This work could open a door to obtaining a better understanding of laser microwelding of NiTi shape memory alloys and improving its weld quality and functional properties and additionally making use of the laser microwelding potential to fabricate high temperature shape memory alloys by alloying a third element into the NiTi.

Keywords: NiTi Shape memory alloys; Welding and Joining; Dissimilar microwelding; Laser microalloying; Advanced characterization; Biomaterials.

Acknowledgements

I would like to express my gratitude and appreciation to my supervisors Prof. Norman Y. Zhou and Prof. Peng Peng for all their valuable comments, advice and encouragements throughout my PhD studies as well as giving the opportunity to pursue my research and academic goals. Their great knowledge of material science and welding processes helped me a lot to stay on track during my PhD journey.

I would also like to thank Dr. Joao Oliveira from Lisboa, Dr. Boyd Panton from Ohio State University, Dr. Andrew Michael from Cloud DX, Dr. Mohammadhadi Razmpoosh, Dr. Pablo Enrique, Dr. Xiaonan Wang and Dr. Qian Sun and all my friends in CAMJ group. My gratitude also goes to the Natural Sciences and Engineering Research Council of Canada (NSERC) for supporting this study. I would like to thank the researchers at the Canadian Centre for Electron Microscopy (CCEM) all of their support with transmission electron microscopy and electron backscattered diffraction equipment.

I would also like to acknowledge Baylis Medical Company for their relentless support, resources and practical industrial experience. I would like to thank Dr. Foss Jiao from Baylis Medical Company for all his support and great help.

Finally, I would like to thank my family for their continued love and support throughout my PhD program: my wife Pendar, my parents Maryam and Mehdi, my brothers Amirhossein and Amirreza. My successes in life would not be possible without them. They all inspired me and provided constant encouragement always and during this journey with their relentless love and support.

Dedication

To my family:

My beautiful & supportive wife, my beloved parents, and my dear brothers

Table of Contents

List of Figures

List of Tables

Chapter 1 Introduction

1.1 Background

The global growing demand of medical device manufacturing has an expected growth rate of approximately 5 percent annually[1]. Today Canada is the eighth largest medical device market. The United States, Canada's largest trading partner in the medical industry, accounts for roughly 45% of global sales [1]. This level of importance to the Canadian market points undoubtedly to the importance of continued improvement in this sector.

The production and fabrication of medical devices is a vast field in which the physical connection of these devices is required to meet certain standards. This entails that they should have a pertinent level of mechanical strength and functional properties, depending on their applications. One of the leading candidates in manufacturing methods for medical devices is laser microwelding, which is chosen in place of other welding and joining processes due to its low heat input, high energy density, minimum heat affected zone and good reproducibility. It should be mentioned that rather than joining and welding, laser processing could also be beneficial to fabrication of medical devices. Despite all of the aforementioned benefits, there are some challenges inherent in this technique such as the formation of brittle intermetallic compounds, segregations, vaporization of different elements and porosity.

An additional challenge stems from the fact that various biomaterials are being integrated into complex multi-component systems to take advantages of their individual properties, which results in dissimilar materials needing to be welded together. For instance, NiTi's shape memory effect and superelasticity can be integrated with the biocompatibility and superior mechanical properties of stainless steel or the high electric conductivity of PtIr, depending on the specific use[2]. Consequently, it is important to develop effective methods that can minimize detrimental effects, such as the aforementioned issues. These methods could consist of controlling process variables and parameters, adopting different joint configurations, using interlayers and applying solid state processes.

1.2 Objective

The focus of this thesis is on dissimilar microwelding of NiTi alloys to other biomaterials (Stainless Steel 316L, Cu and Pt-Ir) and improving its mechanical and functional properties through welding parameter control. In this regard, the potential of dissimilar laser welding of NiTi to other material to fabrication high temperature ternary NiTi shape memory alloys will be discussed. Therefore, the main objectives of this thesis are:

a. Understanding the challenges during laser welding of NiTi related to microstructural features, non-ideal phases and changes in transformation temperatures.

b. Correlating the relationships between microstructure (grain structure and texture) of NiTi joints and their functional behavior by adopting different laser process parameters and configuration.

c. Applying the optimized welding parameters to preserve the mechanical properties and functional aspects of NiTi such as superelasticity in dissimilar laser welding.

d. Adopting laser microwelding processing of NiTi shape memory alloy enabling laser alloying to fabricate ternary high temperature shape memory alloys.

1.3 Thesis outline

The thesis consists of seven chapters. Chapter 1 is an introduction presenting the motivation and the objectives of the current research. Chapter 2 details a thorough literature review over the physical metallurgy, laser processing and laser welding and some fabrication method related to NiTi shape memory alloys. At the end of this chapter the effect of third element in the NiTi medical alloys are discussed.

Chapter 3 discusses the Ni vaporization of NiTi alloys during welding and the effect of laser parameters on the microstructure and texture and therefore mechanical properties of welded NiTi alloys. Chapter 4 discusses the formation of hard and brittle intermetallic compound and non-ideal microstructural features stemming from the complex flow behavior of the fusion zone of dissimilar NiTi joints. In this regard, offsetting laser welding method has been proposed in dissimilar laser welding of NiTi to stainless steel and NiTi to pure Cu welded joints.

As the focus of this thesis, Chapter 5 & 6 investigate two main issues in dissimilar welding of NiTi alloys for medical device applications. The first one is how to preserve the superelastic response of NiTi material after welding with other biomaterial, while the second issue is to increase the x-ray visibility of NiTi medical devices using laser microwelding technique. Therefore, Chapter 5 studies the dissimilar welding of NiTi to PtIr wire and discusses how it is possible to preserve the superelasticity of the welded joints. The microwelding enabled alloying of Pt and NiTi material to fabricate a high temperature shape memory alloy (NiTiPt) which has also a great influence on the increasing of x-ray visibility of NiTi medical devices is presented in Chapter 6. Finally, Chapter 7 will conclude the thesis and recommendation for future works.

Chapter 2 Literature Review

2.1 Introduction of NiTi

NiTi shape memory alloys are the best-known smart materials due to the superior performance of their functional properties, namely shape memory effect and superelasticity. In comparison to other shape memory alloys, such as Fe-Mn-Si, Cu-Zn-Ak and Cu-Al-Ni, the NiTi alloys have less instability, less impracticability and better thermomechanical performance [3,4]. Therefore, they have a wide variety of applications mainly in biomedical, aerospace and automotive industry [5]. NiTi is an intermetallic compound (IMC) that consisting of equiatomic or near equiatomic Ti and Ni elements, as seen in the Ni-Ti phase diagram in Figure 2-1. It should be mentioned that with only a slight deviation from the equiatomic composition, other IMCs namely Ni_3Ti, Ni_3Ti_2, Ni_3Ti_4 (all in Ni rich NiTi) and Ti_2Ni (in Ti rich NiTi), could be formed [6].

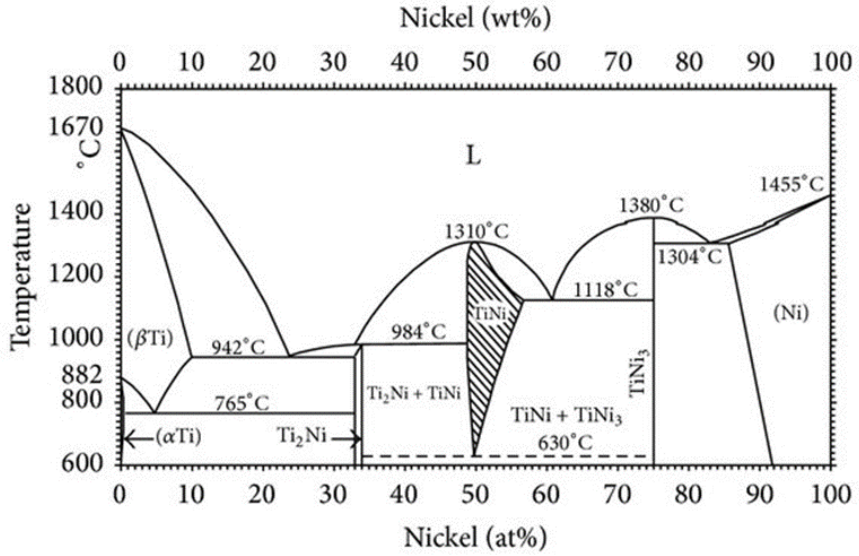

Figure 2-1 Phase diagram of Ni-Ti [6].

NiTi shape memory alloys were first proposed for use as implants in dentistry in 1962 [7], followed by using the NiTi as superelastic braces in 1972, and then approved for orthopedic surgery by US Food and Drug Administration (FDA) in 1989 [8]. Since then, many new biomedical applications have been introduced to the market. NiTi has exhibited superior high corrosion resistance, biocompatibility and can be produced to respond at the temperature of the human body. The most important aspect of NiTi is actually that its superelastic behavior mimics the stress-strain behavior of human bones and tendons. As a result, the NiTi stents are compliant to bend in vessels while the stainless steel stents tend to force blood vessel straight [5].

Therefore, for many complex medical treatments and surgical procedures, there is a vital need for precise and reliable miniature instruments to achieve accurate positioning and functioning. These devices can be used in many fields such as orthopedics, neurology, cardiology and radiology and some examples are endodontics, stents (Figure 2-2-a), bone staples, guidewires and catheters. Aside from medical devices which is the main focus of this thesis, NiTi is used in other industrial field such as aerospace (Figure 2-2-b), auto (Figure 2-2-d), robotics (Figure 2-2-c and e) and actuators (Figure 2-2-g). In all those applications the knowledge over joining and welding of NiTi SMA is inevitable.

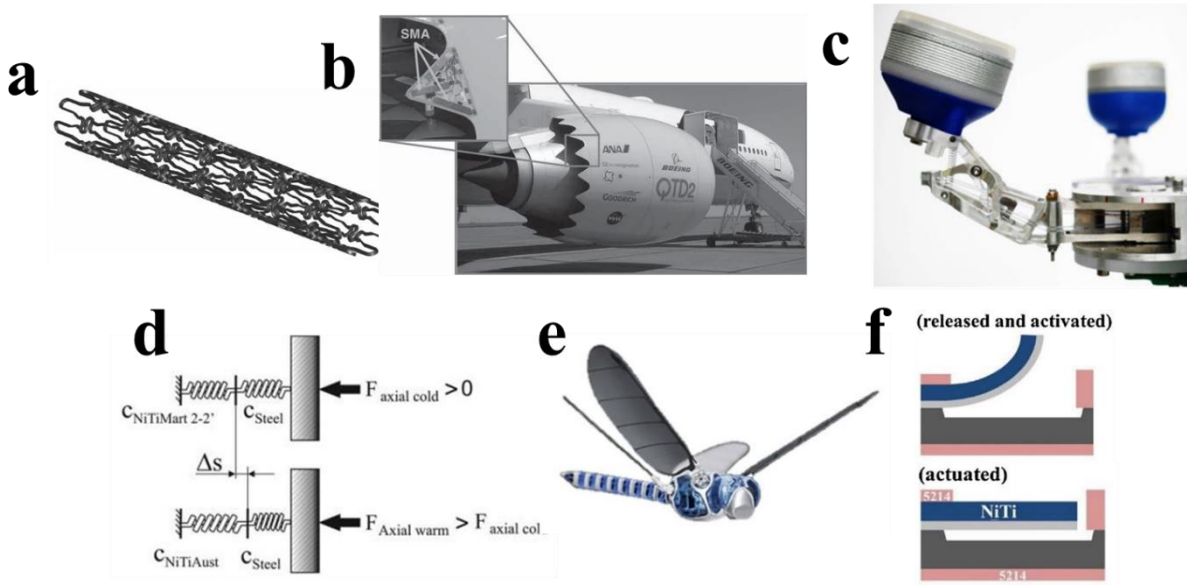

Figure 2-2 Some of NiTi applications: a) Stents[9], b) Boeing variable geometry chevron[10], c) Shape memory vacuum grippers[11], d) Auto clutch[12], e) Flying robots [5] and f) MEMS thermal actuators [13].

NiTi has two main phases, martensite and austenite, that can transform between each other either by temperature or by deformation. The austenite phase has a B2 (CsCl-type) ordered cubic structure with a lattice constant of a≈0.3015 nm at room temperature and the martensite phase (B19') is twin-based with 24 different variants[14] and a monoclinic type crystal structure. However, under appropriate thermomechanical processing a third phase, named "R-phase", can be present also via martensitic transformation with trigonal crystal structure. The condition for R-phase to be stable typically require the presence of Ni_4Ti_3, dislocations or stress fields in the austenite matrix [6].

In the shape memory alloys, the martensite/austenite interface is mobile and this leads to a thermoelastic phase transformation with low internal friction, which can be detected by thermal analysis [15]. Usually, the martensite phase transforms into the austenite phase by heating over austenite start and austenite finish temperatures (A_s and A_f) in an exothermic reaction. Reverse transformation occurs

in the same way by cooling the austenite phase, crossing the martensite start temperature (M_s), martensite finish temperature (M_f) and showing an endothermic reaction [16].

Microstructures of undeformed NiTi austenite and martensite are in two different scales as shown in Figure 2-3: martensite crystallites formed within each parent grain are in a submicron scale as is marked by blue lines in Figure 2-3-a and the parent grains are visible at with an average grain size of ~10μm in Figure 2-3-b. It should be mentioned that the blue lines in Figure 2-3-a are different orientations of martensite crystallites belonging to aforementioned the 24 different B19' variants formed inside each grain as the NiTi cooled through martensitic transformation in free-load condition. In this context, the word crystallite is normally used to emphasize a material volume that consists of a single martensite lattice orientation [17]. However, when the material is fully austenitic, the grains are visible and defined by a single austenite lattice orientation.

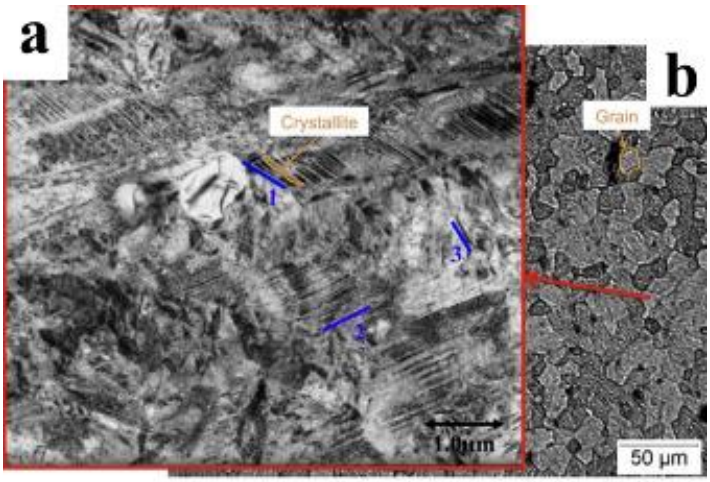

Figure 2-3 Microstructure of NiTi shows a) lath-like martensite crystallites formed inside each parent grain and b) grain structure of austenite phase. Blue lines show some of the different orientation of martensite crystallites [17].

As mentioned before, martensite and austenite phase can transform between each other by applying and removal of stress/strain. In this regard, tensile behavior of NiTi alloy obtained below the M_f (martensite finish temperature, corresponding to the blue curve in Figure 2-4) and above the A_f (austenite finish temperature corresponding to the red curve in Figure 2-4) are used to demonstrate isothermal uniaxial stress-strain response. Each curve entails different regimes: regime i) is related to the elastic deformation of the material in both phases, regime ii) is inelastic deformation which contains a reversible transformation, regime iii) is elastic and reversible deformation of either detwinned martensite (blue curve) or stress induced martensite (red curve) and regime iv) is related to plastic deformation of the final phase that is irrecoverable. Yield 1 is the transition from regime i to ii. In regime ii a stress plateau occurs due to stress induced martensite phenomena in austenite phase (red

curve) or martensite detwinning (martensite reorientation) when the material is deformed in the martensite phase (blue curve). It is interesting to mention that in both cases these strains are both inelastic and recoverable strains of the NiTi since they are expected to be fully recovered through phase transformation via unloading or applying heat (above A_f). Further straining causes a rehardening event after yielding the induced martensite (in red curve)/reoriented martensite (in blue curve) at the end of regime ii and entering regime iii of the stress-strain curve of the material. This region is recoverable and is the elastic deformation of stress induced (red curve) or detwinned (blue line) martensite. Finally upon reaching Yield 2 the transition to irrecoverable and plastic deformation of martensite starts [17].

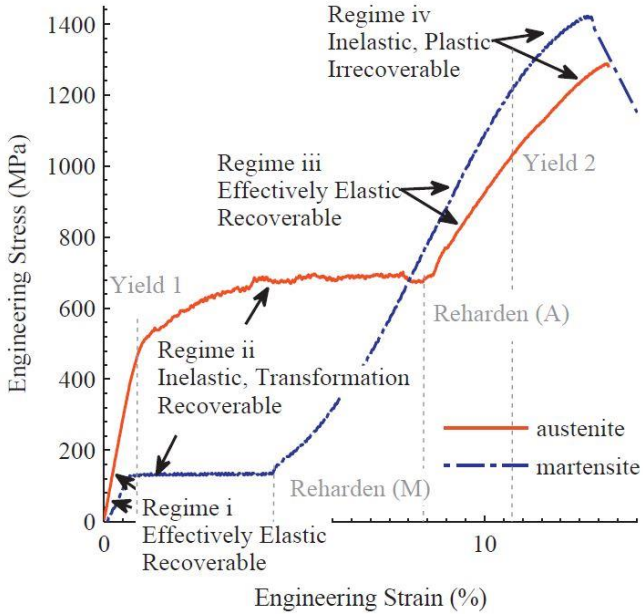

Figure 2-4 Tensile response of NiTi wire at martensite (blue line) and austenite (red line) [17].

The mentioned reversible and thermoelastic transformation between twinned-martensite and austenite is the main reason for the functional properties of NiTi, which are superelastic effect (SE) and shape memory effect (SME). Figure 2-5 shows these properties in macroscopic and atomic scale. Basically, in martensite phase stability (Figure 2-5-a) the condition for shape memory effect arises when an applied deformation is recovered completely by heating. In this case, twinned martensite first transforms to detwinned martensite via loading. After unloading and heating, the detwinned martensite transforms to the austenite phase and recovers its original shape. For the superelastic effect (Figure 2-5-b), the austenite phase is the dominant phase, and it absorbs a considerable amount of deformation through a stress-induced martensite transformation. After unloading, the shape recovers (8-12%) without large residual strains by reverse transformation from martensite to austenite [6,16]. Here, M_d is the temperature below which the martensite transformation can be induced by stress, and above it

NiTi in the austenite phase behaves like any other material and has a typical elastic/plastic deformation with no phase transformation. The transformation strain in this figure can be regained from either strain recovery upon heating (referring SME) or strain recovery upon unloading (referring SE). Normally, shape memory effect occurred below the Ms and superelasticity happened between the A_f and M_d. It should be noted that all these phenomena occur below the critical stress for slip. Therefore, the material has enough yield stress to achieve promising SME or SE functionality [18].

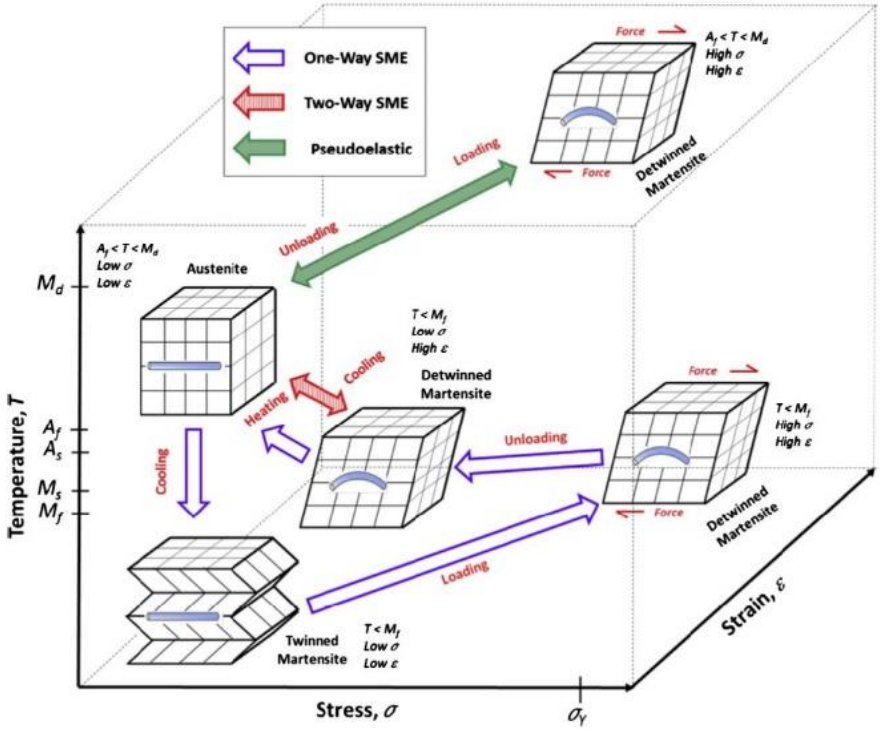

Figure 2-5 Behavior of superelastic and shape memory effect of NiTi [5].

Some other alloys also have shape memory effect and superelasticity with the same mechanisms as NiTi, however, NiTi has better mechanical properties and better strain recovery for both SE and SME in comparison with other shape memory alloys. NiTi also has a wide range of applications in the biomedical industry due to its superior corrosion resistance and biocompatibility [19].

2.2 **Importance of Welding of NiTi**

Welding and joining procedures are an inevitable part of manufacturing to provide mechanical support, electrical connection or insulation and other purposes. Fusion welding processes has been introduced around 50s by electric arc-based methods. However, as is shown in Figure 2-6 by increasing the power density the damage to workpiece would be decreased and penetration, welding speed and weld quality will be enhanced significantly[20].

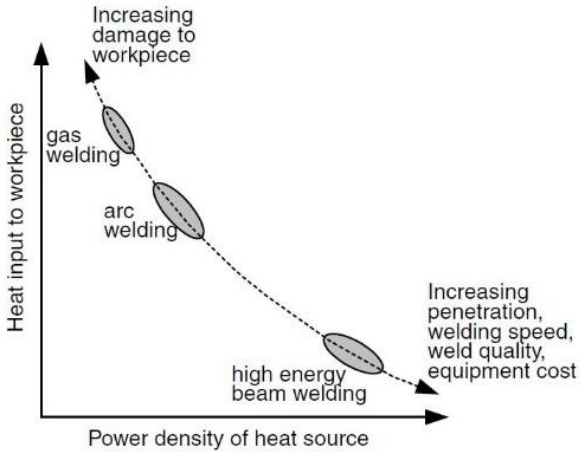

Figure 2-6 The relationship between heat input and power density of the heat source in fusion welding processes [20].

In case of NiTi shape memory alloy, aside from its many useful functional and mechanical properties, the poor workability due to high work-hardening and their increasing applications demand has resulted in numerous published investigations for suitable joining techniques to obtain complex system components. Figure 2-7 shows the number of published works relating to different types of welding and joining technologies for NiTi shape memory alloys. There are multiple fusion and solid-state welding processes available. For the former, the base materials melt and solidify in the joined area while in the latter, there is no melting of the base metals while joining by plastic deformation and/or solid-state diffusion occurs. As is seen the number of publications is rapidly growing in the recent years and solid state processes have a considerable portion of that, specially from 2020.

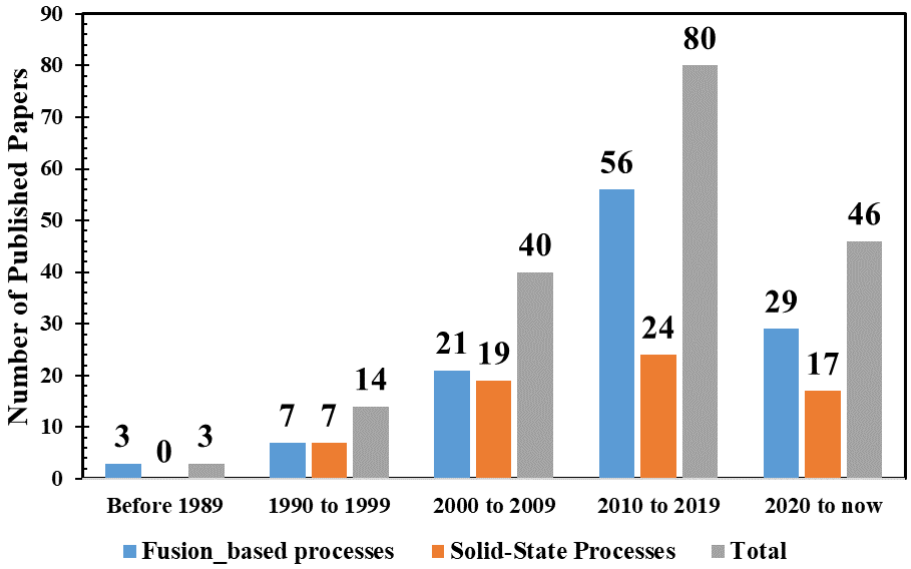

Figure 2-7 Number of published papers until now on joining processes for NiTi.

The selection of the type of these welding methods really depends on the size of the parts, the mechanical properties which are targeted and applications. So far, laser welding is the most heavily investigated welding process in the case of NiTi, due to its low heat input, reduced size of heat affected zone (HAZ) and fusion zone (FZ), no contact with heat source, high precision and high welding speed [21], as is shown in Figure 2-6. However, it has reported that the preferential volatilization of Ni due to the high energy density of the laser beam causes the formation of brittle IMCs and therefore reduces the mechanical properties of the joints.

The formation of brittle IMCs is the main concern especially in dissimilar joining of NiTi to other engineering alloys, where these IMCs can easily form and worsen the mechanical properties and functional properties of the joints. Hence, solid-state welding can be applied with no melting and solidification, and thus introduces lower IMCs content in the FZ, but it has other limitations. The aim of this work is to review fusion welding with focusing on laser welding and analyze the microstructure evolution, functional and mechanical properties and finally compare these methods in similar and dissimilar welding of NiTi. First, similar welding of NiTi will be discussed due to reduce complexity on the nature of these joints and then dissimilar welding of NiTi is conveyed thoroughly.

Table 2-1 Published works on fusion and solid-state welding of NiTi and their applications

Type of Materials	Year of Publication	Applications
NiTi/NiTi	2012[22],2016 [23–25] 2017[26–28], 2018[29–31], 2019[32], 2020 [33–35]	Aerospace, Auto industry, Construction, Medical devices (Stents, coil anchors, filters, orthopedic implants), Orthodontic archwires, Staples, Brackets
NiTi/MP35N	2014[36]	Novel medical devices such as PE wire and tubing for angioplasty and stents
NiTi/Cu	2015[37], 2017[38], 2021 [39]	Medical devices, automotive, aerospace and electronics industries
NiTi/SS 301	2020 [40]	Medical devices and civil construction Biomedical, implants materials such as artificial bones and joints
NiTi/SS 304	2011[41], 2013[42,43], 2017[44], 2018[45], 2019[46,47] , 2020 [48,49], 2021[50]	
NiTi/ SS 316	2012 [51,52], 2015 [53], 2017[54]	
NiTi/CuAlMn	2017[55]	Superelastic joints with the high electrical conductivity
NiTi/Ti6Al4V	2014[56],2016[57], 2017[58], 2020 [59–61], 2021[62–64]	High resistance to corrosion and biocompatibility properties
NiTi/ Ti	2018[65]	Various industrial segments to improve design flexibility with reduced cost

Dissimilar welding of NiTi is highly demanded since the utilization of complex multi-component systems has been growing rapidly in recent years. Table 2-1 depicts some of the researches on different joining combinations of NiTi to other materials and their potential applications [66]. This thesis is reviewing fusion-based welding of NiTi dissimilar joints. In fusion-based welding, most of the research focused on laser welding; however, resistance microwelding technique as well as gas tungsten arc welding and electron beam welding processes will be discussed as well.

2.3 **Typical welding processes of NiTi**

Figure 2-8 shows different fusion based processes applied for dissimilar materials. Figure 2-8-a depicts the laser welding of NiTi wires when Nd-YAG laser source is utilized. As is mentioned earlier, laser welding is the most interesting way for joining NiTi in the published literature due to narrow fusion and heat affected zones, good controllability over the process, precise method especially under controlled atmosphere. The details will be discussed in Section 2.4. The laser welding can be expensive and time-consuming compared with other typical welding processes. Figure 2-8-b shows the micro gas tungsten arc welding (GTAW) of NiTi and SS304 sheets when NiTi filler material is used. In this type of processes an electric arc is applied between the electrode and the base materials under an inert gas protection. The arc produces enough heat to melt the base materials and clean the interested welded area. The electrode usually made of Tungsten since it has a high thermal emissivity and high melting temperature.

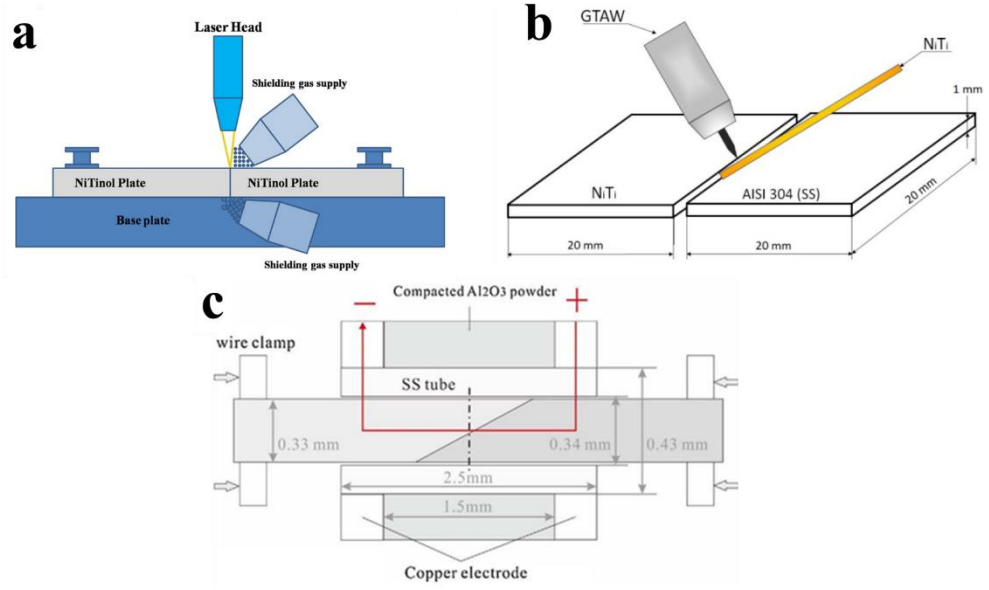

Figure 2-8 Different fusion based procedures using in NiTi dissimilar joints a) laser welding[35], b) Micro gas tungsten arc welding [47] and c) Resistance welding [44].

Finally, Figure 2-8-c demonstrates the schematic of resistance welding of NiTi and stainless steel clamped wires where they are inserted into the stainless steel tube and surrounded by Al_2O_3 compact powder. Generally, in resistance welding, high intensity electric current passed through the base materials which could be wires or sheets and due to materials resistivity, great amount of heat generated which resulted in melting the interface of base materials. Eventually, the welding occurred by applying an external force on the base materials.

2.3.1 **Gas Tungsten Arc Welding (GTAW)**

GTAW is a typical fusion welding process implemented in welding of NiTi alloys. In compare with laser welding, GTAW process is simpler and cheaper, however there are limited studies on dissimilar welding of NiTi using GTAW because of its high energy density, wide HAZ and FZ. It is reported that since NiTi and stainless steel 304 has large difference in their chemical compositions, the formation of partially diluted zone (PDZ) would be inevitable. Figure 2-9 shows this PDZ in the micro GTAW welding of NiTi to Stainless Steel 304 sheets when NiTi filler material and no post weld heat treatment (PWHT) were applied. By changing the filler material to Inconel 625 the PDZ still existed however the Ni-rich phases would be created which decreased the hardness of the PDZ of weld [47].

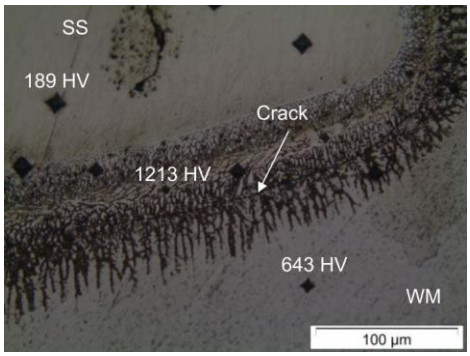

Figure 2-9 Partial diluted zone observed in micro GTAW of NiTi/SS304 with using the NiTi filler [47].

The mechanical properties and the failure regions of mentioned welded samples by NiTi filler and with/without PWHT are depicted in Table 2-2. As can be seen the best mechanical properties was the case of using Inconel 625 and after applying PWHT due to mitigation of brittle nature of NiTi/SS304 interface with thermal treatment and formation of less hard and brittle phases in their interface [47].

Table 2-2 Mechanical properties and fracture regions of NiTi/SS 304 dissimilar micro GTAW joints [47]

Filler Materials	PWHT	Elongation (%)	Fracture region
NiTi	No	0.5	SS/FZ Interface
NiTi	Yes	0.5	NiTi/FZ Interface
Inconel	No	2.0	NiTi/FZ Interface
Inconel	Yes	4.5	NiTi/FZ Interface

Overall, the GTAW process generate significant amount of heat as is mentioned earlier which could create wide FZ and HAZ resulted in deterioration of mechanical properties of the weld[67]. As is reported in the case of NiTi/SS304, applying the GTAW resulted in similar mechanical properties of joints welded using laser [68]. However, adopting GTAW is significantly more economical than most of the welding processes, and in the use of sheet geometry and by selecting optimal parameters and proper post weld heat treatments, it could be replaced with laser welding of dissimilar NiTi joints [69].

2.3.2 **Resistance Welding**

Typical applications of resistance welding involve passing a current across and the welding interface. The resistance to current flow that occurs at the interface generates enough heat to melt the weldments at the interface, fusing them together.

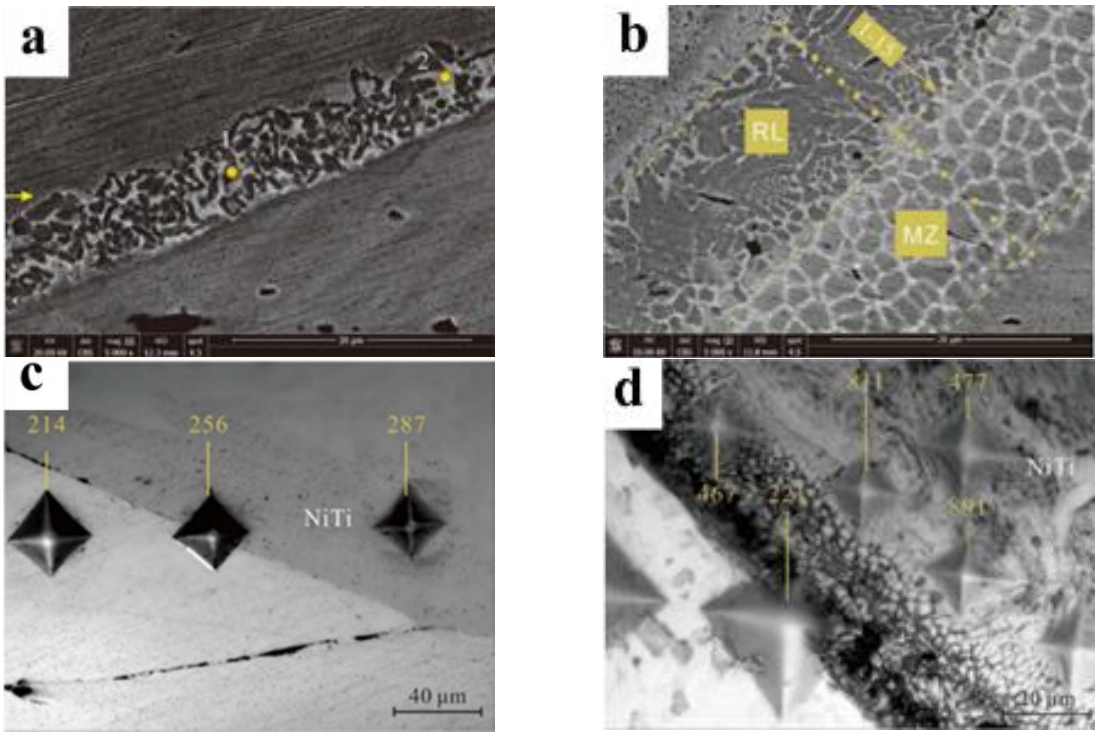

Figure 2-10 a, b) Microstructure and c, d) hardness values of the cross section of resistence welded NiTi and stainless steel using 40A and 45A current [44].

Figure 2-10 shows the microstructure of a stainless steel and NiTi joint interface applying resistance welding at two different currents (40 and 45A). In Figure 2-10-a, two distinct regions are observable in the interface: the worm-like phase, which is depicted as the darker phase within the interface, is detected as Fe_2Ti and the other phase is Fe_2Ti/(Fe, Ni)Ti/Ni_3Ti eutectic phase, which formed in very thin layer

in the interface and would have detrimental effects on the joint strength, as is discussed earlier. By increasing the current (Figure 2-10-b) different phases can be formed: the reaction layer, which is seen as light grey, is in contact with the melted zone analyzed as Ni_3Ti/(Fe, Ni)Ti eutectic phase and also Fe_2Ti/(Fe, Ni)Ti/Ni_3Ti [44]. The influence of these microstructures on the microhardness is quite evident, as shown in Figure 2-10-c and d. In lower current of resistance welding (40A), there is no high hardness value in the interface, and it seems that the interfacial layer is so thin that it cannot be detected by the hardness indenter. On the other hand, in higher current sample, which contains a reaction layer and evidence of interfacial melting and the re-solidification process, much higher hardness values (up to ~800HV) could be detected, which is a sign of the formation of hard and brittle IMCs[44].

These modified microstructures formed with low current (40A) resulted in improvement of the mechanical properties of dissimilar NiTi/SS joints. The joints failed before reaching the stress induced martensite level and therefore, the superelastic response of NiTi could not be achieved. However, as is seen in Figure 2-11, the optimum parameters of resistance welding of NiTi and stainless steel raised the mechanical response significantly and stress induced martensite formed [44].

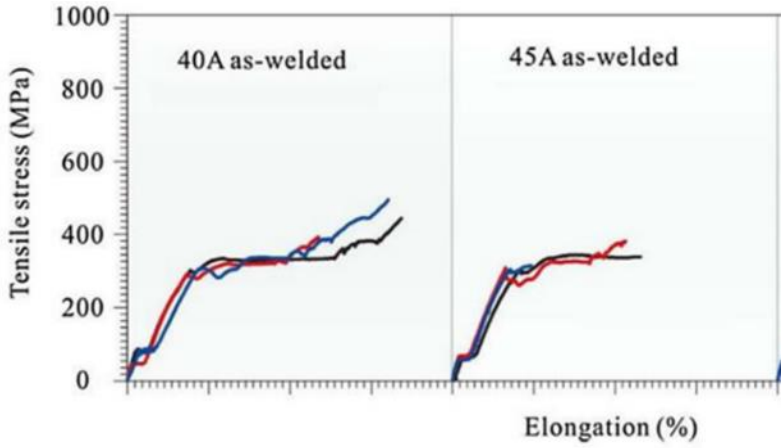

Figure 2-11 Stress strain response of NiTi/stainless steel welded by resistance welding and [44].

The reason for this improvement is due to the thinning of the diffusion layer (10μm in 40A in comparison with 40μm in 45A) between the interface[44]. This thinning effect prevents the hard and brittle intermetallic phases in the fusion zone and results in the formation of the eutectic phase, especially at the interface of NiTi and fusion zone, which provides better bonding strength at the interface. Therefore, it is expected that by applying solid state welding of dissimilar welding of NiTi, the superelastic response could accomplished again.

The other technique which is quite useful to exclude molten metal from the formation of weld after it is formed is micro resistance welding (MRW). It was employed for the first time on fine Ni wires[70]

(Figure 2-12), in which sufficient surface melting was generated and then the molten metal was squeezed out by plastic deformation to form a solid-state weld with high strength. This method requires a proper balance of high initial contact resistance and sufficiently high welding force. In the first stage of this process, there is a deformation imposed by electrodes, afterwards the interfacial resistances between top electrode and upper wire (R1), faying interface (R2) and between bottom electrode and lower wire (R3) (all are shown in Figure 2-12-a), caused heat generation, and increasing the temperature until it surpassed the solidus temperature of the wires at their interface. Finally, the electrodes squeezed out the molten material toward perimeter and the wires joined together with solid-state bonding[71]. It should be mentioned that the amount of wires deformation after the welding are reported as setdown parameter which is defined as[70]:

$$\text{Setdown} = \frac{A - B}{A} \times 100(\text{pct})$$

where A and B are defined as is shown in Figure 2-12-b. This parameter is one of the important variables which could influence on the quality and weldability of the welded samples. It is reported that, the setdown parameter is not enough to evaluate the joint strength of the welded sample however, there is an optimum condition of this parameter which resulted in highest joint strength[70].

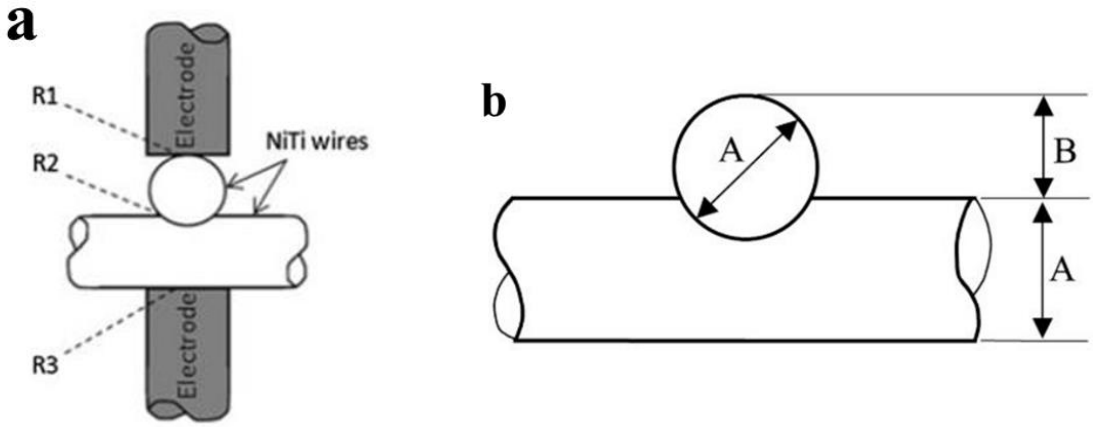

Figure 2-12 Schematic of the a) MRW process and b) definition of setdown [22,70].

It is reported that the MRW process could locally annealed the previous strain-hardened base materials and therefore resulted in modification in transformation temperature of NiTi wires. As is seen in Figure 2-13, the transformation temperature of the welded NiTi wires is quite similar to the solution treated NiTi wires. However, it is important to note that, because of MRW, the transformation temperature of NiTi wires did not change drastically and the austenite phase is predominant phase after MRW at room temperature which is crucial to have room temperature superelasticity of NiTi wires after welding process.

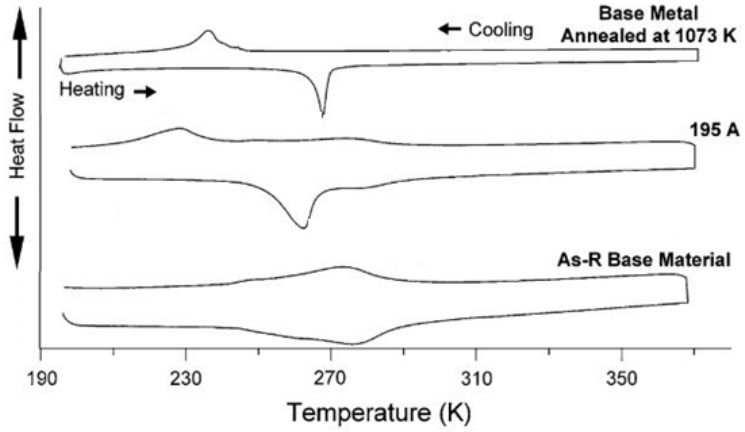

Figure 2-13 Comparison of DSC curves of as received, MRW and annealed NiTi wires (modified from Ref. [22]).

2.4 **Laser welding of NiTi**

The most investigated method of joining NiTi alloys is laser welding. Most of the applications for welding NiTi alloys focused on Ni rich alloys where superelastic behavior is expected at room temperature. However, the effect of laser welding on mechanical properties, texture, microstructure evolution and functional properties of both Ni and Ti-rich NiTi, which the superelasticity and shape memory effect occurs at room temperature, needs more understanding. In laser process, an energy source causes a light radiation emission which has several characteristics such as monochromaticity, low beam divergence, coherence and high brightness[72]. Therefore, a high density beam could be focused on a very small spot on a workpiece and generate narrow heat affected and fusion zones. Amongst different lasers, Nd-YAG laser which is a solid-state laser having Nd:$Y_3Al_5O_{15}$ garnet, is widely used in laser welding of NiTi in both pulsed and continuous welding configuration. There are some fundamental issues and challenges regarding to applying laser welding and related solutions will be reviewed below.

2.4.1 **Ni vaporization and texture evolution**

Falvo et.al [73] reported the effect of similar laser welding on shape memory and mechanical behavior of NiTi. As is shown in Figure 2-14-a strength of the welded NiTi significantly decreased in comparison with unwelded base material, and the material becomes more brittle after welding. According to the phase diagram of Ni-Ti, it is expected with variations to the Ti-side of the material, Ti_2Ni intermetallics formed [74]. As shown in Figure 2-14-b and c there is grain boundary precipitation of this hard and brittle phase and micro-cracks in the FZ also existed [75].

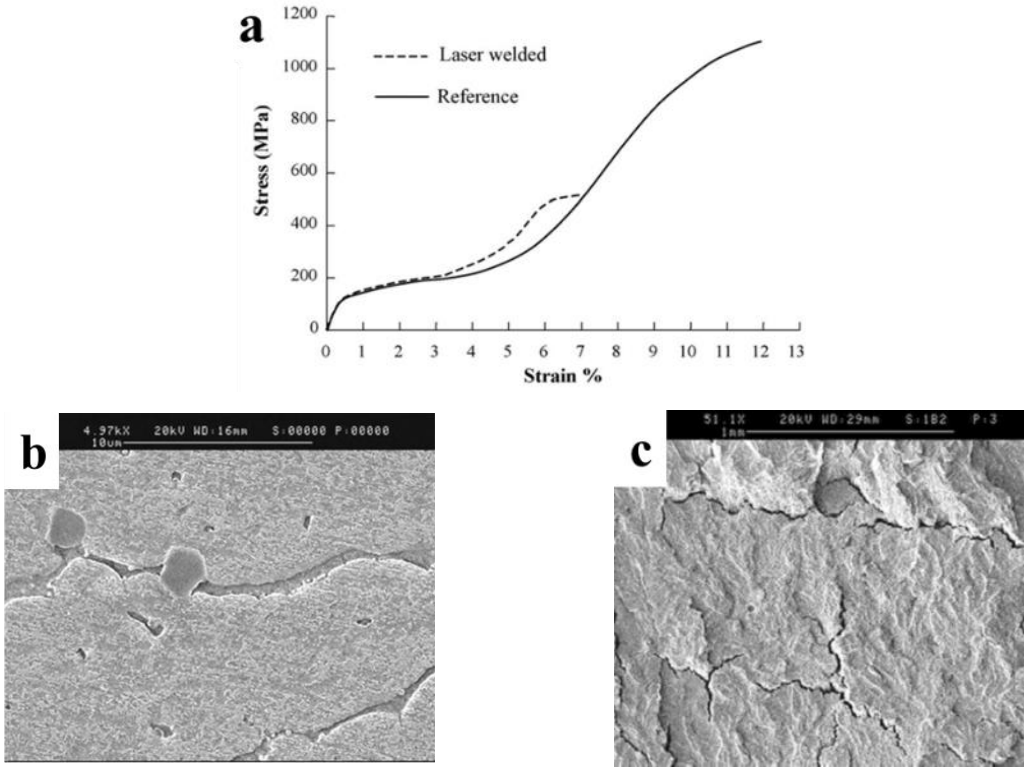

Figure 2-14 a) Mechanical response of the welded and NiTi base material after laser welding [73]. b) microstructure of similar NiTi HAZ grain boundary with Ti rich segregated compound and c) surface fracture of same weld [75].

As was mentioned, most studies discussed Ni-rich NiTi due to its wide range of applications where a superelastic response is needed (particularly in medical devices). The biggest challenge during high power density processing procedures like laser or electron beam is composition changes induced by vaporization of Ni. NiTi is one of the materials that is very sensitive to compositional changes, as is seen in Figure 2-15-a, a slight modification in chemical composition (especially in Ni-rich NiTi) could cause considerable variation in transformation temperature.

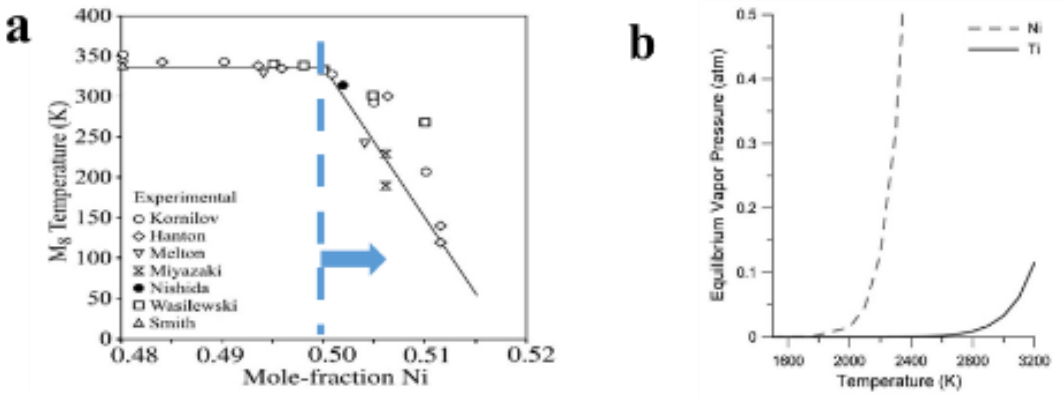

Figure 2-15 a) M_s temperature vs. Ni content for NiTi [6], and b) Ni and Ti vapor pressure vs. temperature [76].

The reason for the higher rate of vaporization of Ni in NiTi alloys is the difference in the partial vapor pressure of Ni and Ti in an equiatomic NiTi at higher temperatures[76]. In Figure 2-15-b calculated vapor pressures of these elements as a function of temperature are depicted. As seen, Ni has higher equilibrium vapor pressure in compared with Ti in the shown temperature range, and therefore easily evaporated during laser welding of NiTi which will be resulted in the changes the transformation temperature of the welded material (Figure 2-15-a).

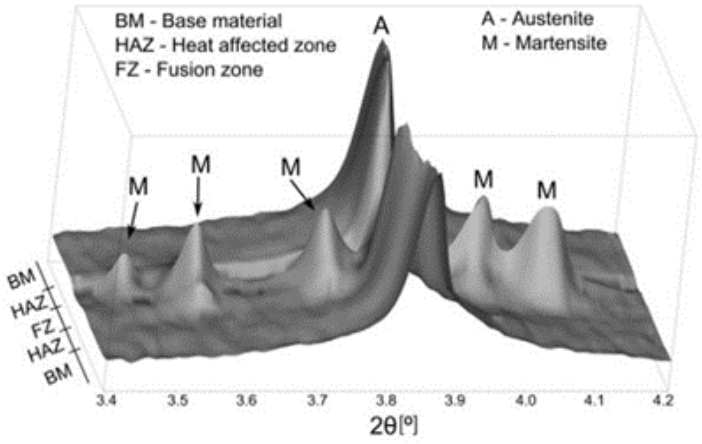

Figure 2-16 X-Ray diffraction of NiTi welded sample with presence of martensite in FZ[24].

The change in the transformation temperature causes the formation of a mixture of austenite/martensite in the fusion zone (FZ). In Figure 2-16, thermally stable martensite forms due to the preferential Ni vaporization in FZ which results in an increase of the transformation temperature, thus different amounts of martensite will coexist with some amount of retained austenite. It has been reported that higher heat input gives a larger percentage of the martensite phase in the FZ [24].

Taking a closer look at the different regions' microstructure by indexing the phases under transmission electron microscopy reveals that in the base material there is only the B2 phase (Figure 2-17-a) and the HAZ and FZ consist of a mixture of different phases. The HAZ (Figure 2-17-b) contains both of B2 and R-phase with some dislocations present. A more complex microstructure is visible in FZ (Figure 2-17-c) with B2 phase and different second particles identified as Ti_3Ni_4, Ti_2Ni and $TiNi_3$ compounds[31,74,77].

The formation of these phases, dislocations and destruction of the martensite phase due to melting and re-solidification can cause non-uniform stress fields in the HAZ and FZ and decreases the mobility of the martensite/austenite interface and hence deteriorates the superelastic and shape memory response by creating irreversible deformation [31,77]. However, post weld heat treatment is one solution to improve the superelasticity of NiTi welded samples [78].

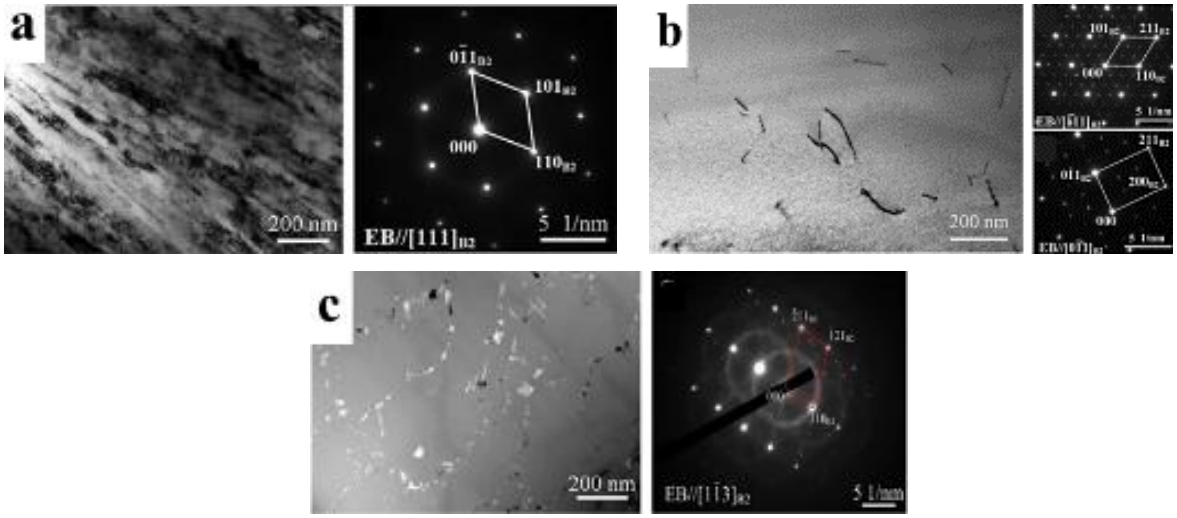

Figure 2-17 TEM images and SAD pattern of a) BM, b)HAZ and c) FZ of welded NiTi [31,77].

The other important aspect of similar laser welding of NiTi is the grain structure and texture evolution of re-solidified material in the fusion zone. The grain structure, texture orientation and inverse pole figures of welded samples in keyhole and conduction modes are shown in Figure 2-18. The base material in this study [79] was superelastic cold-drawn wire and therefore their texture was predominantly <111> type grains [14]. After welding in keyhole mode condition (Figure 2-18-a), coarse columnar grains at the centerline and finer columnar grains near the HAZ are formed due to directional solidification after welding. However, in conduction mode (Figure 2-18-b) the average grain size of FZ is smaller and more equiaxed. As expected, the easy growth direction of cubic materials after solidification is <100>-type orientation [79–81] which is visible after keyhole condition. In conduction mode (Figure 2-18-b), there are deviation from the cubic easy growth orientation due to a more rapid re-solidification.

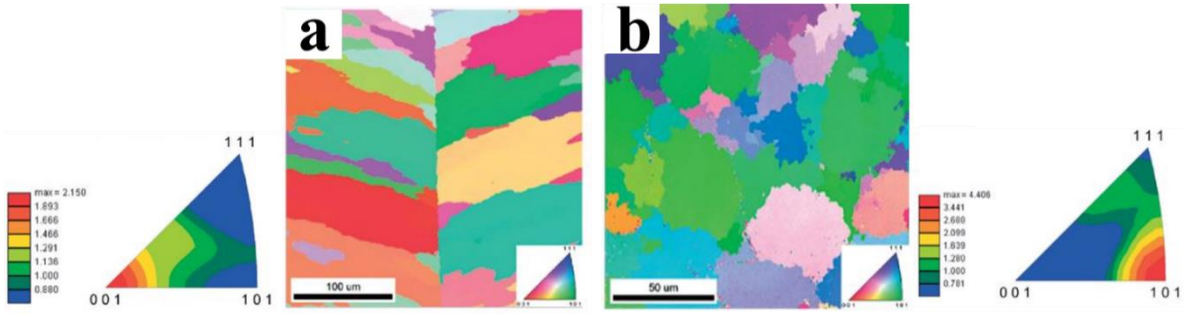

Figure 2-18 IPF images in the tensile direction of Similar NiTi in a c) Keyhole condition and b) Conduction mode and their corresponded austenite B2 inverse pole figures [79].

Figure 2-19 depicts the joint efficiency (the maximum strength ratio of the welded to the base material) of similar NiTi laser welding in the selected optimal conditions. It varies from near 30% [82] to more than 90% [83]. The justification of dropping strength of the welded NiTi/NiTi joints were mainly referred to as deviations in texture and grain size [84], formation of brittle IMCs [35,73,85] and dendritic structures within the fusion zone [86]. It should be mentioned that in all these studies, the best joint efficiency was achieved by optimizing the laser parameters(peak power of 0.15kW and 20ms pulse duration) [84], changing the heat input value (power of 1200W and speed of 6000mm/min) [35] and proper post-weld heat treatment (laser heat treatment at speed of 50mm/s, power of 2.5kW) [87].

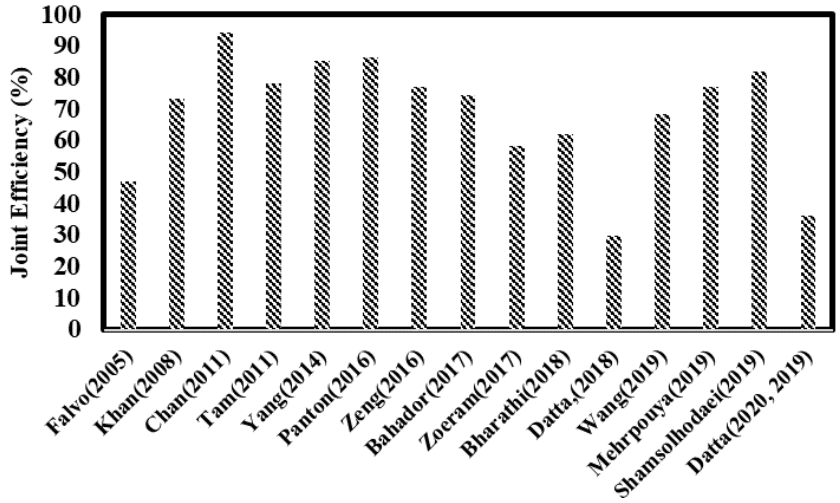

Figure 2-19 Joint Efficiency [25,27,28,35,73,81–91] on similar laser welding of NiTi.

2.4.2 **Formation of Intermetallic compounds and segregations**

In medical industry, dissimilar welding of NiTi and stainless steel is usually required in many application scenarios as shown in Table 2-1 Published works on fusion and solid-state welding of NiTi and their applications. However this joint formation is extremely sensitive to the formation of IMCs inside the fusion zone, particularly during laser welding [2]. Figure 2-20-a displays a cross-section of a typical laser welded joint, where different regions were selected for localized chemical composition analysis (Figure 2-20-b) and labeled by letters a to e in red color [41]. According to the diffusion path theory [92], it is expected that the chemical composition of the joint lies in the connected line between the two base materials (yellow line in the ternary phase diagram of Figure 2-20-b) which is NiTi with equiatomic Ni and Ti and stainless steel with 90% of Fe. From stainless steel toward NiTi, all of the shown phases in ternary phase diagram (γ-(Fe, Ni), Fe_2Ti, Ni_3Ti, (Fe, Ni)Ti, …) can be found along this grey line. Therefore, many of hard and brittle phases such as Fe_2Ti and Ti_2Ni should be avoided to form which will be discussed later.

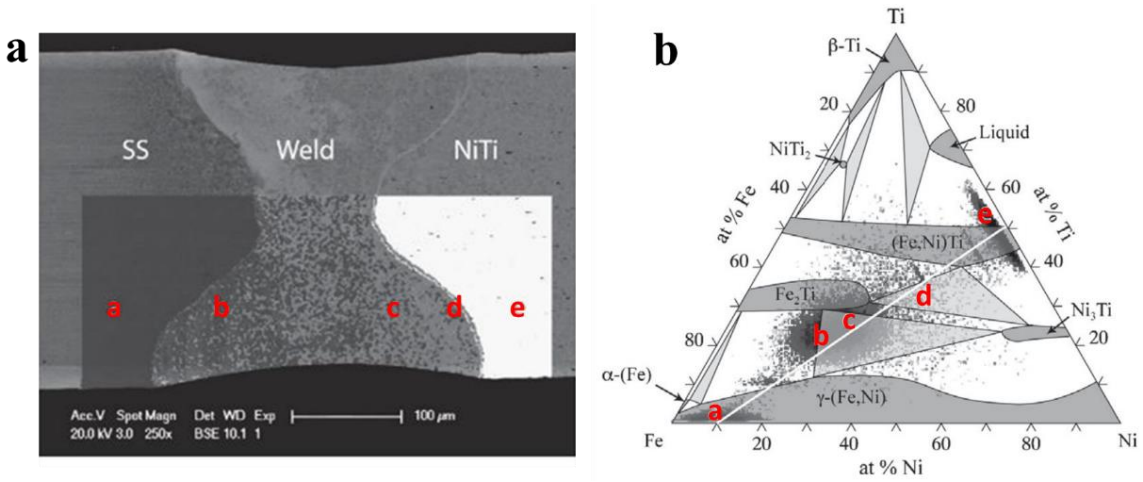

Figure 2-20 EDX chemical analysis of a) different points on SS-NiTi weld put into relation with b)the corresponding Fe-Ni-Ti ternary phase diagram[41].

For better understanding aside 2D chemical composition analysis, 3D chemical composition analysis of NiTi/SS weld joint is also presented in Figure 2-21. This figure is reconstructed from phase analysis made by focused ion beam sectioning and EDS mapping, which shows solidification routes and diffusion pathways inside the FZ [93]. With this figure, there is better understanding of diffusion pathways and possibility of hard and brittle phases formation during welding and solidification. After welding, solidification started and the first phase to form from the NiTi side of the phase diagram is (Fe, Ni)Ti, which grows epitaxially with planar, cellular and dendritic formation. The remaining liquid in interdendritic arms solidifies as a dendritic phase, Ni_3Ti. On the other side, the Fe-rich part starts to solidify as dendritic Fe_2Ti and within the dendrites Ti-poor melt forms another eutectic phase. The remaining liquids from both sides reach together and forms another complex eutectic. Therefore, the fusion zone microstructure is quite complex and contains lots of intermetallic networks. As could be compared, this information related to diffusion pathways was missed in 2D images.

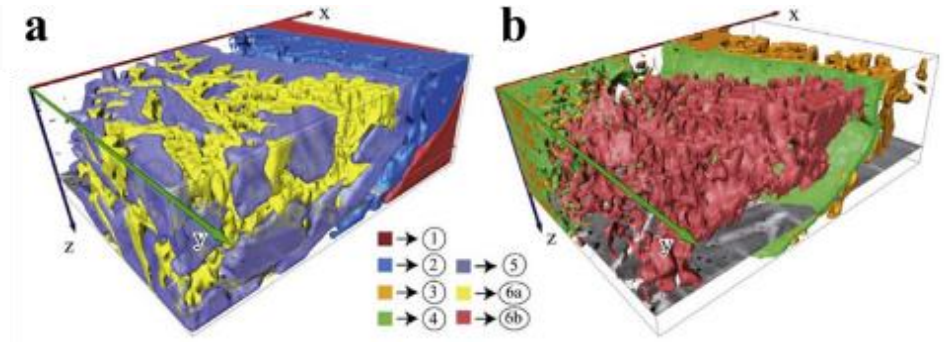

Figure 2-21 3D map reconstruction made by FIB and EDS showing different regions of SS-NiTi fusion zone: 1) NiTi base metal, 2) (Fe,Ni)Ti dendrites, 3)Ni_3Ti in eutectic, 4)remained thin region 5)Fe_2Ti dendrites, 6) dendrites made of 6-a) γ-(Fe, Ni) and 6-b)Fe_2Ti [93].

The other common dissimilar welding of NiTi using in medical application is to join it to Ti6Al4V. As it can be seen in Figure 2-22, in both partial penetration conditions (Figure 2-22-a) and full penetration conditions (Figure 2-22-b), extensive cracking is visible adjacent to the fusion line due to solidification shrinkage. As is shown in Figure 2-22-b, the different orientation of cracks follows the dendrite growth directions. This dendritic structure formed due to molten material flow after welding during solidification. The EDS analysis proved that Ni migrated and formed extreme brittle Ti_2Ni phases which is stable in a wide range of Ni, Ti and Al chemical compositions. On the other hand, in compared with NiTi/SS joint, NiTi/Ti joint has more potential in formation of Ti_2Ni hard and brittle phases due to containing more Ti in Ti alloys, therefore the extensive cracks would be visible adjacent to the fusion zone in the Ti6Al4V area (Figure 2-22) [94].

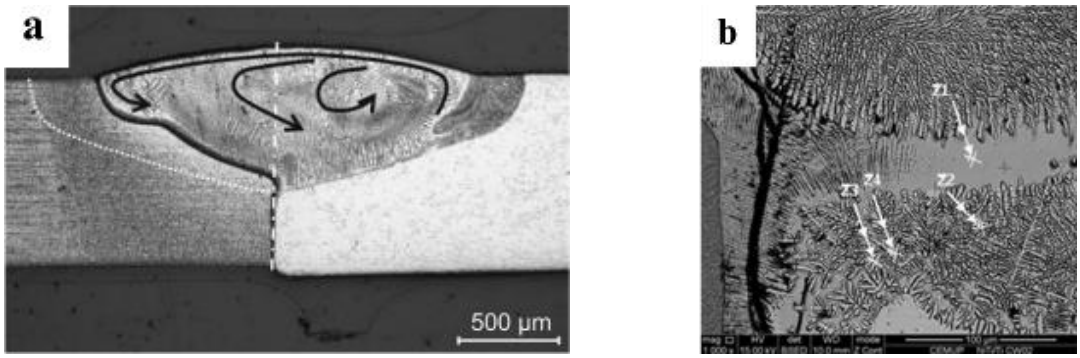

Figure 2-22 Macrograph of NiTi/Ti6Al4V showing a) partial penetration and cracking close to Ti alloy (left). Dashed lines evidence the weld asymmetries and the black arrows suggest the main NiTi-rich liquid flows in the melt pool and b) extensive cracking in higher magnification [94].

The other well documented NiTi dissimilar welding is its joining with Cu. Sun et. al. reported the segregation mechanism of NiTi/Cu laser welded [39]. As is seen in Figure 2-23, in NiTi/FZ interface, the liquidus temperature of molten fusion zone is lower than this parameter for NiTi, the stagnant layer has been formed along the fusion boundary without any sufficient mixing (Figure 2-23-a). Subsequently and due to strong convection, liquid NiTi get mixed in the molten pool and quickly solidified without any considerable mixing (Figure 2-23-b and c) and caused NiTi peninsula at the NiTi/FZ interface (Figure 2-23-d).

However, on the other side, since the liquidus temperature of fusion zone is higher than the Cu, after forming the stagnant layer at the Cu/FZ interface (Figure 2-23-e), the molten fusion zone started to solidify pushing toward stagnant layer (Figure 2-23-f). Finally, some Cu beach created due to solidify the remaining of liquid Cu in irregular shape (Figure 2-23-d). This mentioned segregation in NiTi/Cu joints has the main responsibility for poor mechanical properties in this dissimilar joint.

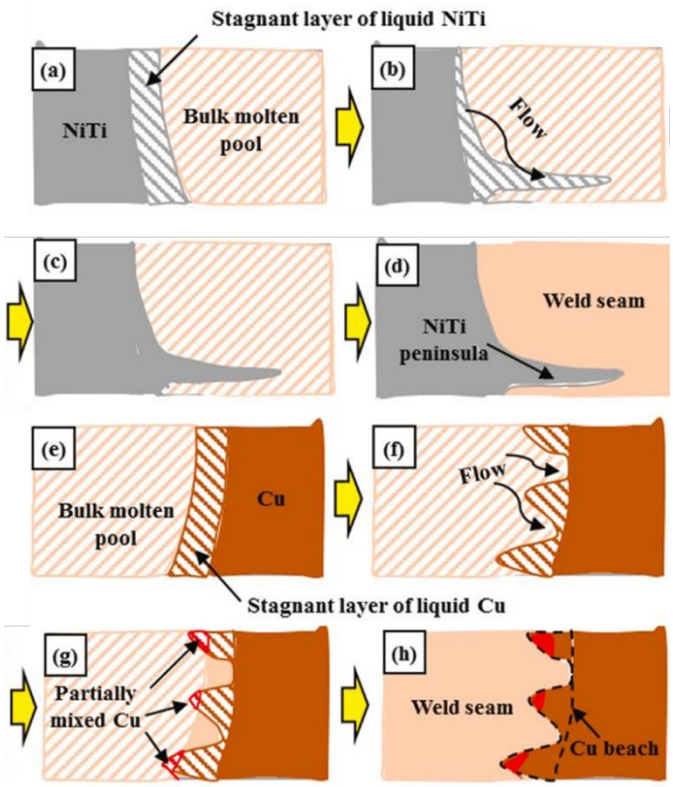

Figure 2-23 Segregation mechanism in a-d) NiTi/FZ interface and e-h) FZ/Cu interface in NiTi/Cu weld [39].

2.4.3 **Use of Interlayers**

Due to the formation of extensively wide and complex networks of hard and brittle IMCs inside the FZ of NiTi/stainless steels joints, many works adopted different materials as interlayers in order to prevent the formation of these phases and improve the joints' mechanical properties[2]. In this regard, different elements such as Ni[51,95], Co[96], Ta[53] and Cu[97] were used in order to stop the formation of hard and brittle common intermetallics between Ni, Ti and Fe or to form other less hard and brittle IMCs and modified the microstructure.

The selection of the interlayer [98] mainly contains three steps: i. thermodynamic assessment comparing formation enthalpy (ΔH) and Δ(G) of any possible IMCs to base materials, ii. mechanical assessment of formed fusion zone and if the formed IMCs are not hard phases and iii. feasibility study through trials and optimization processes. Table 2-3 shows the different interlayers used in the dissimilar fusion based welding (mostly laser welding) of NiTi to other materials. As can be seen, different interlayers have been implemented due to either form a chemical barrier (Ni, Ta, ...) and reduce the amount of IMCs content in the FZ or forming eutectic phase (Nb) in the interface of base material and fusion zone instead of hard and brittle IMCs.

Table 2-3 Interlayers used in laser welding of NiTi in published literature [47,50,51,53,54,57,60,62,96,97,99–103]

Base Materials	Type of Welding	Year	Interlayer	Strength	Ref.
NiTi/304 SS	Nd-YAG	2012	10-100µm Ni	372 MPa	[51]
NiTi/304 SS	Nd-YAG Laser	2013	20-120µm Cu	521 MPa	[97]
NiTi/304 SS	Nd-YAG Laser	2013	10-50µm Co	347 MPa	[96]
NiTi/316L SS	Fiber Laser	2015	25-100µm Ta	251 MPa	[53]
NiTi/Ti6Al4V	Nd-YAG Laser	2016	50µm Nb	300 MPa	[57]
NiTi/316L SS	Nd-YAG Laser	2017	100-150µm Cu	150 MPa	[54]
NiTiNb/Ti6Al4V	Nd-YAG Laser	2018	300µm filler Nb	740 MPa	[99]
NiTi/Ti6Al4V	Electron Beam	2019	0.45mm Nb	480 MPa	[60]
NiTi/304 SS	Micro GTAW	2019	Inconel 625 filler	286 MPa	[47]
NiTi/304 SS	Nd-YAG Laser	2020	Ni powder	300 MPa	[100]
NiTi/301 SS	Fiber Laser	2020	0.75mm Nb + 0.15mm Cu	240 MPa	[101]
NiTi/304 SS	Nd-YAG Laser	2020	0.3mm Ni	643 MPa	[102]
NiTi/316L SS	Nd-YAG Laser	2020	50µm Ni	410 MPa	[103]
NiTi/304 SS	Electron Beam	2021	0.5mm FeNi	343 MPa	[50]
NiTi/Ti6Al4V	Fiber Laser	2021	100µm Cu	353 MPa	[62]

Figure 2-24 shows the effect of a Co interlayer in transition between the base material and the fusion zone in a NiTi/SS joint where lots of IMCs could be formed without using an interlayer (Figure 2-24-a). The white structure in Figure 2-24-a indicates the of the IMCs caused many microcracks. Whereas using 20µm Co interlayer shows a better transition in NiTi/FZ interface (Figure 2-24-b), which improves the stress concentration in the fusion zone and there are no visible cracks in the joints.

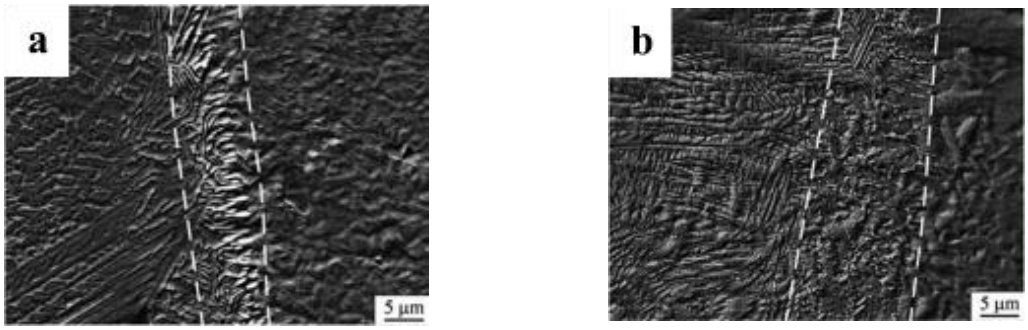

Figure 2-24 Microstructure of NiTi and fusion zone in NiTi/SS joint a) without and b) with 50µm Co interlayer [96].

The use of interlayers can promote the formation of ductile IMCs or decrease the amount of hard and brittle IMCs. Figure 2-25 demonstrates the use of Nb in NiTi/Ti6Al4V joints which leads to formation of a eutectic phase in NiTi and the fusion zone between NiTi and Nb. This eutectic formation

improves the mechanical properties of the joint by providing better bonding related to modification of transient zones between materials[57,99].

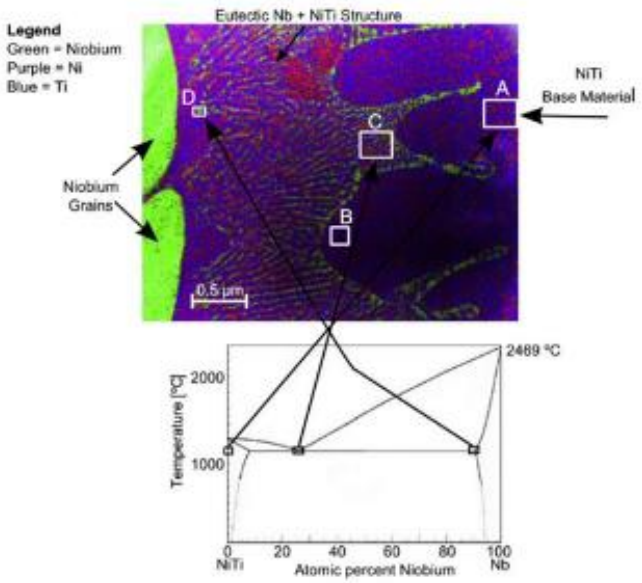

Figure 2-25 EDS map of NiTi/Nb interface in NiTi/SS joint and the correlated regions with NiTi/Nb phase diagram[57].

Formation of different phases are characterized in dissimilar welding of NiTi using XRD, an example of which is shown in Figure 2-26. In this figure, the effect of different thickness of Ni and Co interlayers on the formation of IMCs phases could be seen. In all those cases, when less interlayer is present, more detrimental phases are formed; however, with high amounts of interlayer, some new IMCs such as $TiNi_3$ (in Ni), $TiCo_2$, Ti_2Co and TiCo (in Co) are formed. It is important to note that for all these cases there is optimum amount of interlayer (visible later in Figure 2-28) for which the minimum amount of harmful intermetallics are made[51,53,96].

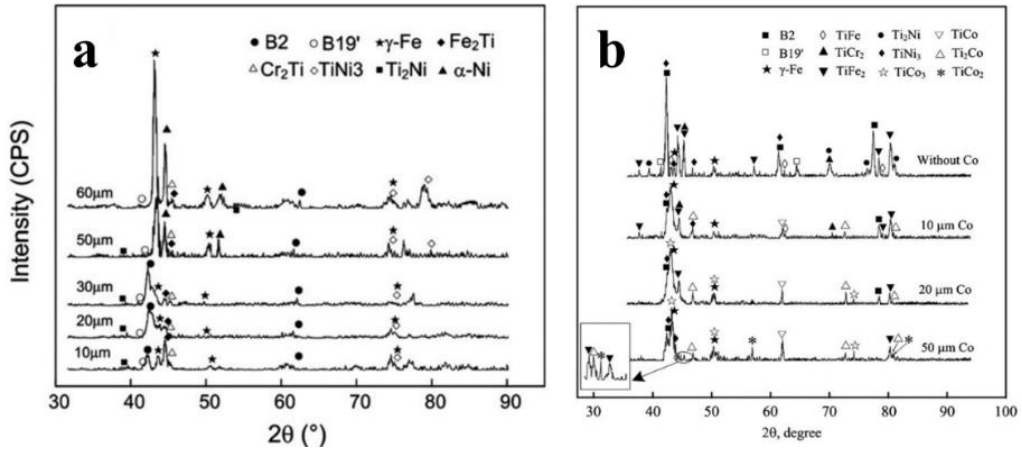

Figure 2-26 XRD pattern of NiTi/SS weld using a Ni [51] and b) Co [96].

Other than aforementioned pure metal interlayers, alloyed FeNi interlayer has been recently used in the laser welding of NiTi to Stainless Steel 304[50]. It is reported that, this specific interlayer improved the uniformity of the composition of the fusion zone. By using the EBSD (Figure 2-27), the distribution and content of IMCs are visible in the fusion zone of NiTi/SS304. By applying the Ni interlayer, the IMCs content decreased from 47% (in Figure 2-27-a) to 43% (Figure 2-27-b), whereas this number significantly decreased to just 9% (Figure 2-27-c).

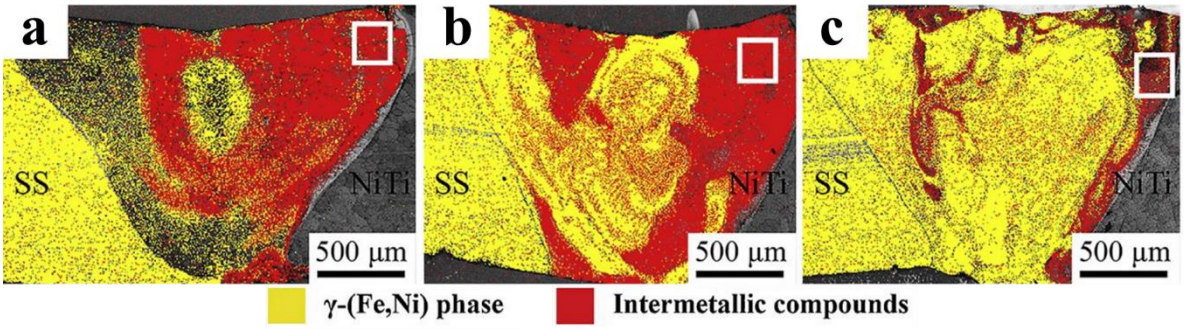

Figure 2-27 EBSD phase map on the fusion zone of NiTi/SS304 showing IMCs content in different conditions of using a) no interlayer, b) Ni interlayer and c) FeNi interlayer [50].

As is expected from different formed phase in Figure 2-26, the mechanical properties of these joints are the best in the optimum condition as can be seen in Figure 2-28. In optimum condition of Ni interlayer thickness where minimum Ti element is presented in fusion zone and Ni is not too much to form Ni_3Ti, the hardness value of the fusion zone is considerably lower than the other interlayer thicknesses (Figure 2-28-b) and therefore the tensile strength of this joint is the best (Figure 2-28-b) due to fewer preferential sites for crack initiation and propagation during the loading. It could also be seen that by using proper interlayer (FeNi instead of Ni in Figure 2-28-c), the tensile strength could be improved from 264MPa to 343MPa in the case of NiTi to Stainless Steel joint[50].

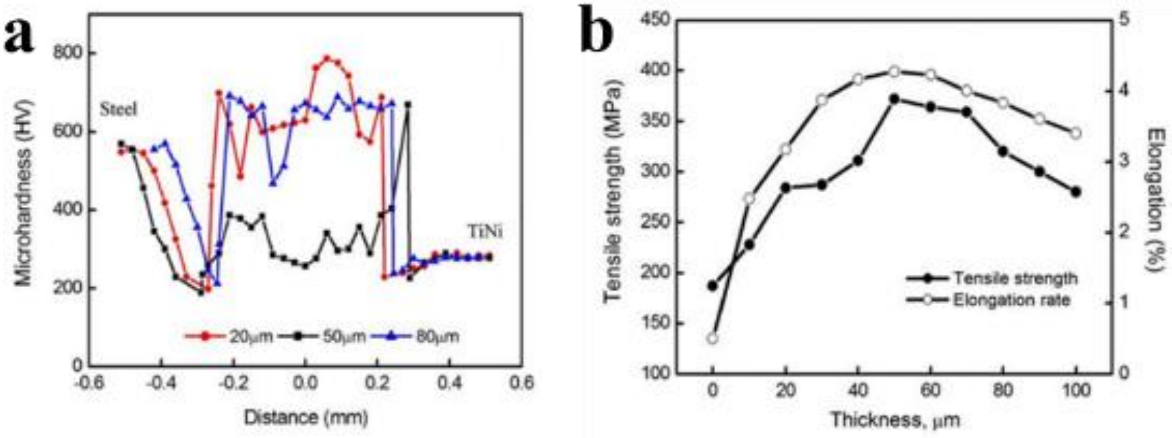

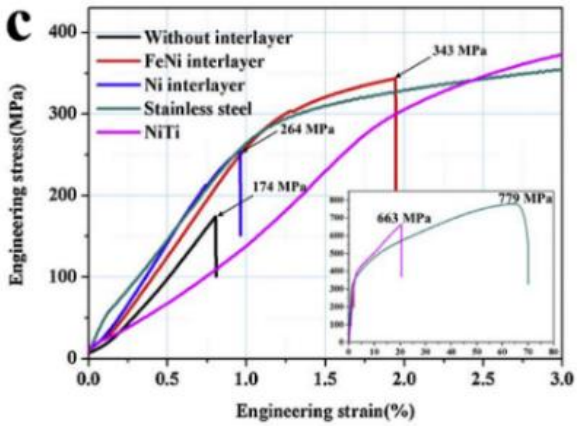

Figure 2-28- a) microhardness and b) tensile strength of NiTi/SS joint using different Ni interlayer thickness [51] and c) effect of FeNi interlayer on tensile strength of NiTi/SS joint [50].

2.4.4 **Effect of Laser power**

The other method for controlling the base materials' elements mixing is to optimize the laser process parameters and the main important one is laser power. Figure 2-29 shows the application of different laser peak powers in dissimilar laser welding between NiTi and Cu. Various regions are labeled based differentiations in contrast of microstructure and EDS measurements used to estimate the chemical composition within each region.

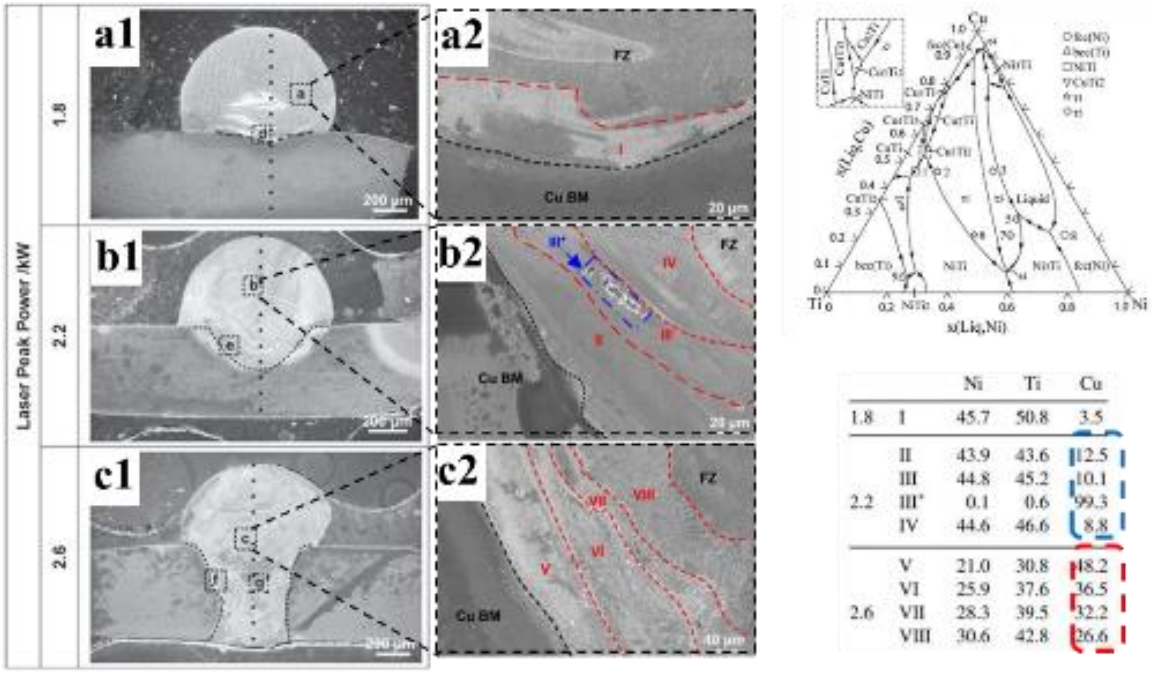

		Ni	Ti	Cu
1.8	I	45.7	50.8	3.5
2.2	II	43.9	43.6	12.5
	III	44.8	45.2	10.1
	III*	0.1	0.6	99.3
	IV	44.6	46.6	8.8
2.6	V	21.0	30.8	48.2
	VI	25.9	37.6	36.5
	VII	28.3	39.5	32.2
	VIII	30.6	42.8	26.6

Figure 2-29 Microstructures of NiTi/Cu dissimilar joints showing formation of different regions and their corresponded chemical composition gathered by EDS[104].

With the proper peak power, which is 2.2kW in this case by using pulsed Nd-YAG laser, the Cu content is lower than 10% leading to the formation of the soft and ductile NiTiCu phase. However, lower peak powers resulted in insufficient bonding strength, while higher peak powers caused high Cu content in the FZ (due to increased mixing of the element) to form possible hard and brittle CuTi, $CuTi_2$ and other brittle intermetallics.

By selecting proper parameters, the mechanical properties improved due to enhancements to the microstructure, as shown in Figure 2-30. In NiTi/Ti6Al4V joints (wires with a diameter of 300µm), the laser power of 22.4W (the highest between samples) resulted in the best tensile strength (around 82% of Ti alloy), due to better microstructure, less IMC content and reduced HAZ width in comparison with the two other parameters[99]. On the other hand, in NiTi/Cu joints, adopting 2.2 kW power (Figure 2-30-b) improved the formation of stress induced martensite because of defect-free joint and preventing the formation of brittle fusion zone, thus a stress induced martensite region in stress-strain curve of the joint appears, which could be a sign of the preserving superelasticity[38].

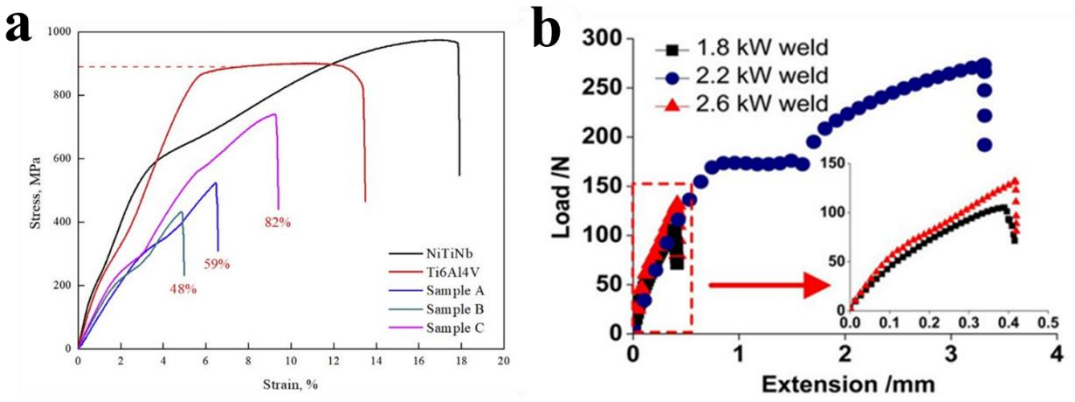

Figure 2-30 Mechanical properties of a)NiTi/Ti6Al4V joint in different laser power (from Sample A to C the laser power increased)[99], b)Cu/NiTi joint in different laser power[104].

2.4.5 **Laser Offsetting**

Another way to decrease the amount of IMCs is through applying the laser offset to the centerline of the two base materials but focused on the material which has a lower conductivity, higher melting point and less diffusivity and therefore the potential for mixing different elements together would be lower. Panton et. al [36] showed that offsetting the laser onto MP35N (Ni-Co-Cr-Mo alloy) in the laser welding of NiTi and MP35N would bring crack free joint with less porosity and less macro-segregation (Figure 2-31). The reason for this behavior is less mixing of Ti into the MP35N alloy and therefore a reduced possibility for the formation Ti_2Ni, Ti_2Co and $TiCr_2$ inside the fusion zone. Enhancement of mechanical properties by using the offsetting strategy has been demonstrated in the case of MP35N-

NiTi joints. Using offsetting onto MP35N improved the joint break force significantly from 40N to near 100N due to less mixing of Ti, formation of cracks, and porosity in fusion zone[36].

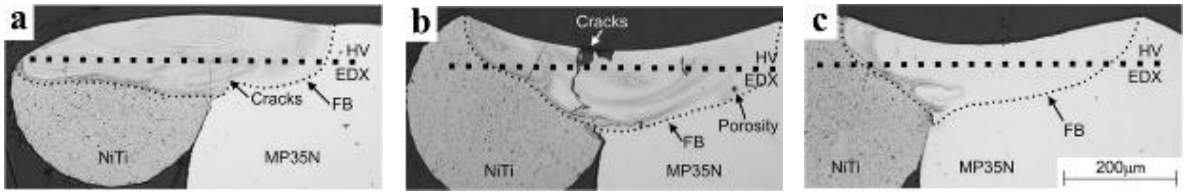

Figure 2-31 Cross section of NiTi/MP35 with a)100µm on NiTi b) centerline and c) 100µm on MP35N offset [36].

One of the recent studies [40] used hybrid of both laser offsetting and Nb and Cu interlayer foils. As observed in Figure 2-32, there are four distinct zones in this joint, namely: i. the reaction layer I formed at the NiTi/Nb interface, ii. the unmelted Nb, iii. the fusion zone (FZ) formed in the Nb interlayer, and iv. the reaction layer II formed at the Nb/Cu/301SS interface. As mentioned in section 2.4.3[57], NiTi/Nb interface formed an eutectic phase. Additionally, the pure Cu foil melts completely and causes wetting to Nb and Fe and their diffusion into the liquid phase. Therefore, three distinct metallurgical joining zones are formed based on three welding mechanisms for the NiTi and SS301 laser joint. The first metallurgical joining region is the melting zone formed within the Nb interlayer based on the fusion welding mechanism. The second metallurgical joining region is the reaction layer I based on the eutectic reaction of Nb and NiTi. The third metallurgical joining region is the reaction layer II formed at the Nb/ Cu/301SS interface based on the brazing mechanism.

However, cracks could form in Cu/Nb interface due to the high heating and cooling rates of pulsed laser welding and immiscibility between Cu and Nb. The Fe_7Nb_6 IMC is also formed at the interface of Nb/Cu/301SS. The strength and ductility of this joint with these interlayers were 240 MPa and 1.3%, respectively, which were 126% and 188% higher than the joint without these interlayers [101].

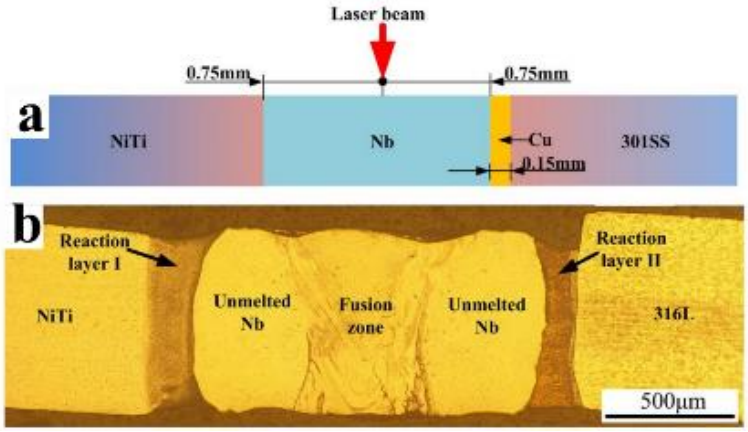

Figure 2-32 Cross section micrograph of NiTi/Ni/ 304SS joint using laser offsetting [101].

2.4.6 **Post Weld Heat Treatment**

Post weld heat treatment (PWHT) also can improve the weld microstructure by forming possible ductile phases. As reported in the dissimilar welding of NiTi and SS304 [48], by adopting a Ni interlayer, the post weld heat treatment has a great beneficial effect. The interface of NiTi and Ni is observed in three different conditions: without PWHT (Figure 2-33-a), PWHT at 650°C (Figure 2-33-b) and PWHT at 850°C (Figure 2-33-c). There are two distinct layers in fusion zone of this interface (Figure 2-33-a) and the thickness of the layer I gradually decreases as the PWHT temperature increases. Layer I is mainly a eutectic structure of NiTi and Ni_3Ti confirmed by the EDS results. Another layer, which shown as layer II, is mainly Ni_3Ti IMCs and its content increases as the PWHT temperature increases (shown by XRD). This phenomenon can be justified by the increase in the diffusion coefficient as the PWHT temperature increased, thereby promoting more inter-diffusion at the interface. Therefore, PWHT introduced some Ni_4Ti_3 phases (shown by gray in Figure 2-33-b and c) as a result of Ni dilution in the eutectic structure.

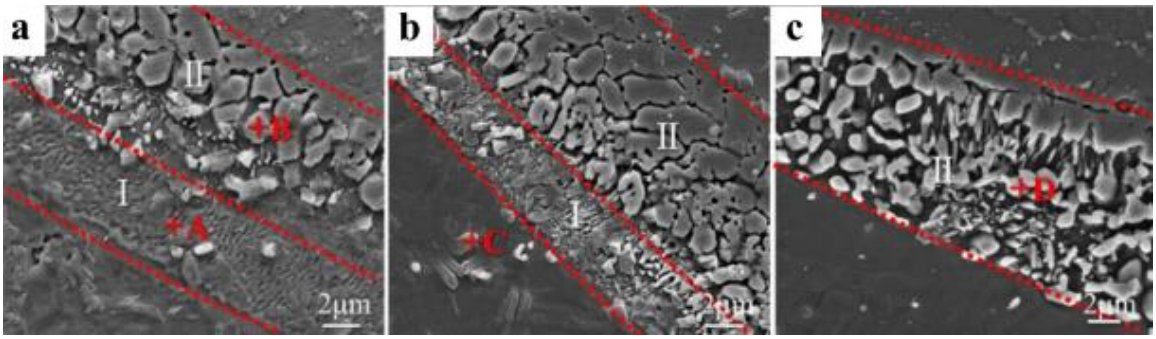

Point	Chemical compositions (at. %)				Possible phase
	Ti	Ni	Fe	Cr	
A	38.77	59.21	2.01	–	NiTi + Ni_3Ti
B	25.42	68.15	5.34	1.09	Ni_3Ti
C	49.87	50.13	–	–	Ni_4Ti_3
D	27.60	67.78	4.62		Ni_3Ti

Figure 2-33 The microstructure at the NiTi/Ni interface of the joints: (a) As-welded, (b) PWHT at 650 °C, (c) PWHT at 850 °C. EDS analysis results of the NiTi/Ni interface [48].

As shown in Figure 2-34, post weld heat treatment can increase the mechanical strength of the joint. Adopting PWHT at 100°C, 200°C and 300°C in NiTi/SS304 orthodontic arch wire joints [68] can alter the tensile strength of these joints as demonstrated in Figure 2-34-a. There is an optimum condition at 200°C due to the releasing of the residual stress in the joint, whereas at 300°C lots of brittle IMCs formed (Ni_3Ti, Ti_2Ni) causing deterioration the mechanical properties of the joint. However, as is

shown in the other study [48] higher temperatures of PWHT in the same materials joint (NiTi to Stainless Steel 304) could increase the tensile strength significantly, because it can homogenize the microstructure and form Ni_4Ti_3 precipitates. As is seen in Figure 2-34-b, while the average tensile strength of as-welded NiTi/SS304 joints is approximately 303 MPa, the 650°C of PWHT temperature increased this value up to approximately 384 MPa. By increasing the PWHT to 850 °C, the joint showed the best average tensile strength and elongation, which was about 643 MPa and 12%, which are 2.12 and 3.91 times higher than that of the as-welded joints, respectively. The tensile strength and elongation improvements may be caused by the precipitation of Ni_4Ti_3 phase [105–107] and also through the decreasing the layer I in interface of NiTi/Ni (Figure 2-33.c)[48]. Therefore, the influence of post weld heat treatment on the microstructure and mechanical properties of the welded NiTi to other materials such as stainless steel, needs further investigation by selecting different range of temperature and time of the heat treatment.

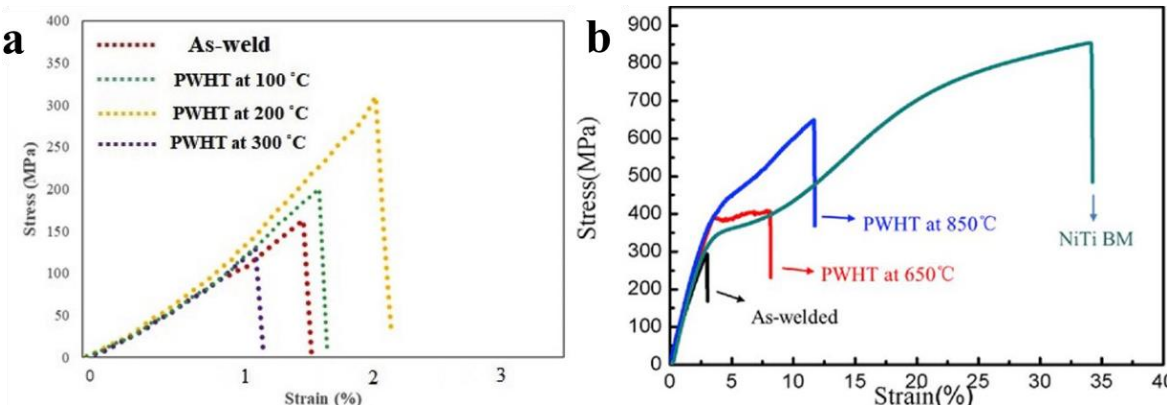

Figure 2-34 Tensile properties of the PWHT of NiTi/SS304 joint at a)100°C to 300°C [68] and b) 650°C and 850°C [48].

2.5 Ternary NiTi-based alloys

2.5.1 Introduction to HTSMAs

Despite great functional properties and biocompatibility of binary NiTi shape memory alloys, their applications are limited to the temperatures below 100°C. However, in auto and aerospace industries, it is vital to have higher temperature shape memory effect and/or superelasticity properties. Therefore, to increase the transformation temperature of shape memory alloys for high temperature shape memory alloys (HTSMAs) applications, two different approaches could be chosen. The first solution is applying plastic deformation on binary NiTi alloy to stabilize the martensite phase, however once the stabilized martensite phase heated to austenite phase the mentioned effect would be vanished [108]. The second

approach is adding some elements such as Au, Pd, Pt, Zr and Hf in the binary NiTi alloys to fabricate ternary NiTi-based HTSMAs[109–113].

The applicable transformation temperature and shape memory strain of different types of high temperature shape memory alloys have been studied and it has been showed the best performance of material in different temperature range and also where the material could preserve the 85% of its functional properties' performance. As compared, among these alloys, NiTiPt is one of the unique materials that have functional properties in a wide range of temperatures and even above 700°C which make it applicable in the variety of industrial applications.

The fabrication and production of ternary NiTi-based shape memory alloys are the same as NiTi alloys consists of casting the material from high purity Ni, Ti and the third elements using vacuum induction melting (VIM) or vacuum arc remelting (VAR) processes, following by homogenization and optimum heat treatment. Figure 2-35 shows the microstructure of the NiTiPt material after casting (Figure 2-35-a with dendritic structure), homogenization at 1050°C (Figure 2-35-b) and cold worked to 60% reduction with subsequent annealing (Figure 2-35-c)[115]. This conventional method contains time-consuming procedures and needs precise optimizing, additionally the fabricated material has lots of difficulty for any traditional forming and machining [116]. In recent years, additive manufacturing (AM) has been introduced as an effective way to fabricate high temperature shape memory alloy [117], although it also contains lots of trial and error to achieve a non-defective HTSMA[118,119].

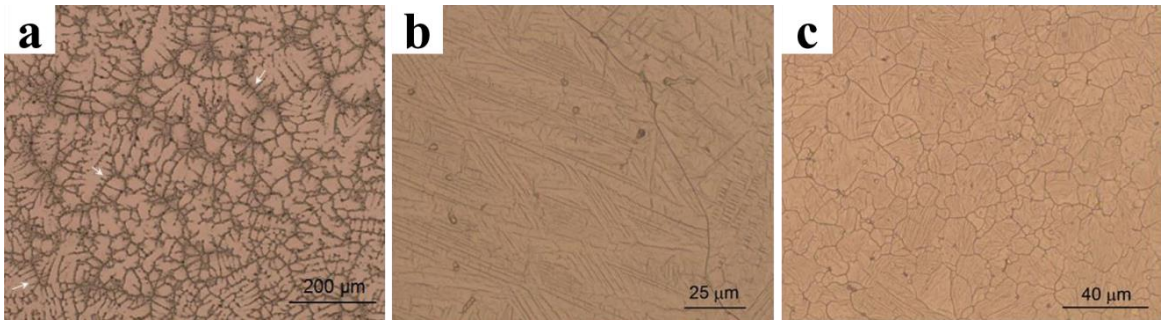

Figure 2-35 NiTiPt alloy production after a) casting showing dendritic structure, b) homogenization and c)cold working and annealing [115].

2.5.2 **Laser Welding of HTSMAs**

There are very few reports on welding and joining of HTSMAs, except some focus on the laser welding of a phase strengthened NiTiZr [120,121]. In these types of material (NiTiHf and NiTiZr), H-phase precipitates resulted in solid solution strengthening and promoting phase transformation[122]. However, as is seen in Figure 2-36-a, while the base material mainly consists of martensite and near

7% H-phase, the H-phase completely dissolve inside the fusion zone causing changes in chemical composition of the matrix and decreasing the transformation temperature. Therefore, the considerable fraction of austenite phase (near 30%) could be found inside the fusion zone. Additionally, the microhardness map of the weld (Figure 2-36-b) indicates a sharp decrease in hardness values by entering the fusion zone, due to H-phase dissolution. However, in the middle of the fusion zone, when there is significant amount of austenite phase and drop in the amount of H-phase, the hardness values increased again[121].

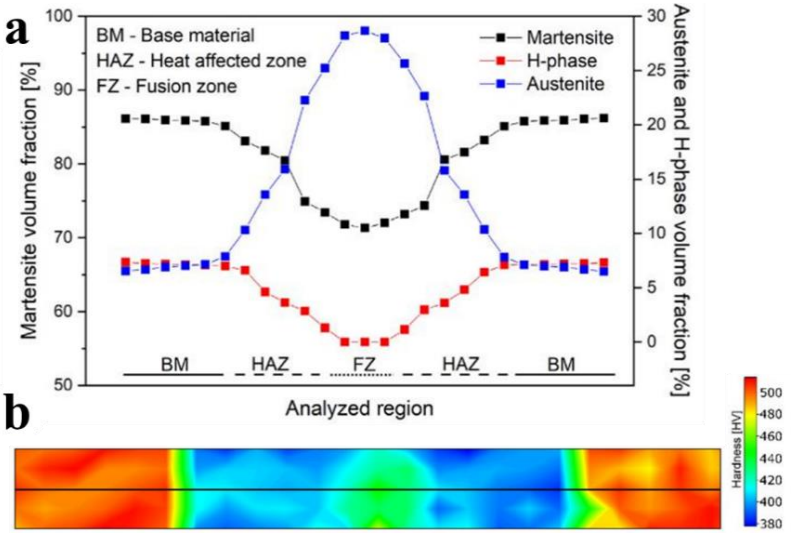

Figure 2-36 Evolution of a) different phases volume fraction and b) hardness mapping across the weld joint [121].

2.5.3 **Increasing the radiopacity**

The other important effect of the third elements in NiTi-based alloys, rather than fabricating a high temperature shape memory alloy, is increasing the radiopacity of these materials for medical application. Despite having excellent functional properties for NiTi shape memory alloys, they have radiolucent visibility under X-ray fluoroscopy. In this case, there are two well-known solutions to make the medical device (stent, guidewires, etc.) more visible under the X-ray fluoroscopy. The first one is using some markers by using some radiopaque elements, and the second option is to make the whole NiTi based medical device radiopaque by adding a third element (amongst radiopaque elements). With comparison the relevant radiopacity between different metals such as Pt, Ir, Au it can observed that they have extremely higher radiopacity in compared with Ni and Ti [123].

As is mentioned the first solution to track the radiolucent NiTi medical device inside the patient's body is welding the proper markers to NiTi. As is seen PtIr sleeve markers are applied on the

expandable stent (Fig. Figure 2-37-a) or Ta markers are welded on other types of self-expandable stents (Figure 2-37-b) [124], therefore their visibility under the x-ray could be enhanced significantly.

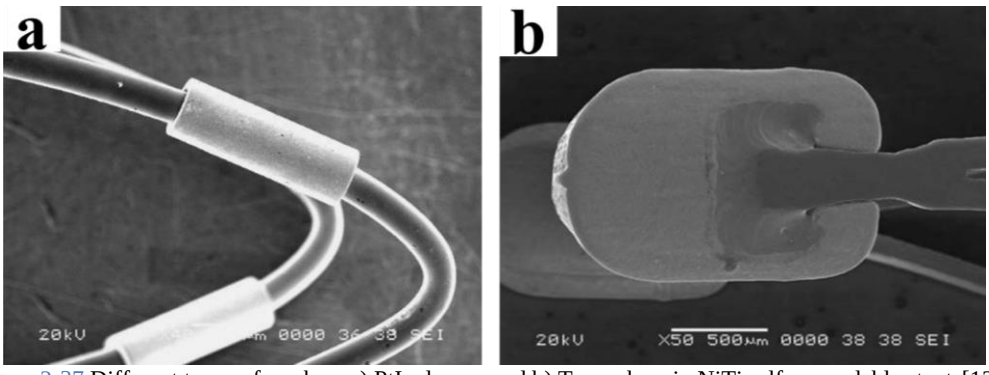

Figure 2-37 Different types of markers a) PtIr sleeves and b) Ta markers in NiTi self-expandable stents[124].

The second way to track NiTi-based medical device under the fluoroscopy is alloying the radiopaque element with NiTi and fabricating NiTiX ternary shape memory alloy to increase their x-ray visibility. The comparison between binary NiTi and ternary NiTiPt stents are shown in Figure 2-38-a, where the top 5 stents are NiTiPt, and the bottom two stents are NiTi.

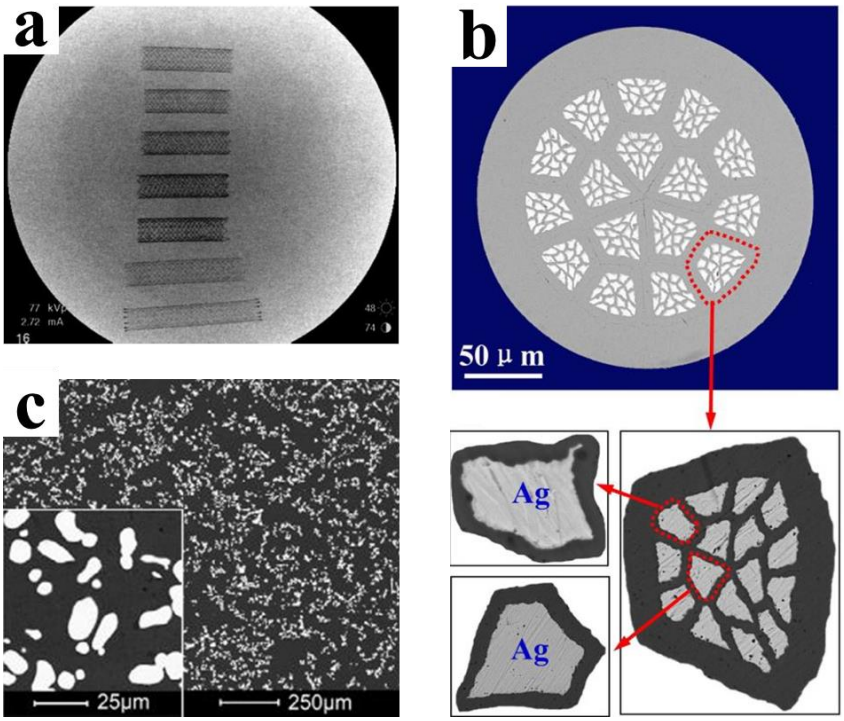

Figure 2-38 Adding third element to binary NiTi alloy using a) NiTiPt stents (top 5)[125], b) NiTi-Ag composite with hierarchical structure[126] and c) In-situ NiTi-W composite [127].

Additionally, there are some efforts to fabricate NiTi-X composite where X is the radiopaque element. Figure 2-38-b shows the cross section of hierarchical structure of the NiTi-Ag composite

manufactured by repeated assembling and wiredrawing with preserving the superelasticity of NiTi material. The other example is fabrication in-situ NiTi-W composite as its microstructure shown in Figure 2-38-c by two-step melting process. Therefore, it could be concluded that applying other creative methods to resolve the x-ray visibility issue of NiTi medical devices are needed in future.

2.6 Issues and problems in laser welding of NiTi

This chapter reviewed the most important works on fusion welding focusing on laser process of NiTi shape memory alloys. As is mentioned, there are several challenges regarding the laser welding of NiTi such as Ni vaporization and changing the transformation temperature, formation of IMCs, complex flow pattern specially in dissimilar joints with different element density and deterioration of functional properties of NiTi during welding. Next chapters are discussing these issues and suggesting solutions to overcome them using advanced characterization methods, and finally introducing capabilities of laser microwelding of NiTi in fabrication of ternary NiTi alloys.

Chapter 3 The controlling of Ni evaporation during laser welding of NiTi[1]

3.1 Introduction

The inevitable joining processes during the production of multi-component biodevices can significantly compromise the alloy's unique properties. As a rule of thumb, the formation of the HAZ and FZ typically deteriorates the mechanical properties of any welds, including laser welded material. However, laser welding has been commonly used for joining of NiTi due to narrow fusion and heat affected zones along with the desired reproducibility [21,128]. Still, the laser welding cycle destroys the previously optimized cold worked and annealed NiTi material by formation of dendrites and coarse grains [129] results in the deterioration of its superelastic response. Some studies [89,130–133] have indicated that by selecting optimal parameters obtained from design of experiments in laser welding, 75% to 86% of strength of the base material in NiTi joints can be achieved after the formation of stress induced martensite at fracture.

Additionally, one of the main challenges in laser welding of NiTi is the preferential Ni vaporization during welding which occurs due to the higher equilibrium vapor pressure of Ni in comparison with Ti [76,134]. This phenomena results in a decrease in the Ni concentration of the material and in turn the formation of Ti-rich IMCs (such as Ti2Ni) which deteriorates the mechanical properties and also increases the transformation temperature [6]. Transformation temperature changes can lead to significant microstructural changes and martensite formation which affect joint properties [23,24,135]. It is well established [136] that the superelastic response of welded samples also decreased, since aside from thermal stability of martensite, mechanical stabilization of martensite will also occurred in FZ and HAZ due to dislocations introduced during superelastic cycling of welded joints [137].

Although many efforts have been made to improve the functional behavior of laser welded NiTi alloys through changing the process parameters [2,138], eliminating of Ni vaporization during laser welding/joining of NiTi is difficult, and the evaluation of local superelastic response to Ni concentration variation across NiTi welds is still unclear. Additionally, debating is still ongoing regarding whether the superelasticity of the welded NiTi could be altered by changing the cyclic test temperature, considering the variation in the transformation temperature of the welded material.

[1] The results of these chapter are published in two journal papers: 1- **Shamsolhodaei, A.**, Y. N. Zhou, and A. Michael. *Science and Technology of Welding and Joining* 24.8 (2019): 706-712 and 2- **Shamsolhodaei, A.**, et al. *Materials Letters* 287 (2021): 129310.

In this chapter, a laser process window is designed to have a fundamental study of Ni vaporization issue in laser welding of NiTi wires; and two extreme laser conditions (the highest and lowest power within a laser processing window) are selected for further analysis. The results shows that the dominant phase at room temperature changes from austenite to a mixture of austenite and martensite under low power and high power condition, respectively, due to higher Ni loss in the high power sample. Furthermore, the high power sample has deviation from base material texture that causes deterioration in mechanical properties. Superelastic response were studied using nanoindentations and cyclic tensile tests. By adopting the possible lowest power laser condition, superelastic response in both conditions significantly enhanced.

3.2 **Experimental Procedure**

3.2.1 **Welding setup**

A superelastic NiTi wire with diameter of 400µm and 50.8at%Ni was used in this study. A dilute solution of 7.5% HF, 28.5% HNO3 and 64% H2O was used to remove the thick surface oxide from the wires. After etching, the wires were cleaned using acetone, ethanol and de-ionized water to remove any surface contaminants. Laser processing/welding on this material was performed using a Nd:YAG Miachi Unitek LW50A laser with a wavelength of 1.064µm. Laser processed/welded samples were produced using square pulsed profiles with 400µm nominal spot size diameter with pulse durations of 5, 10, 15 and 20ms included 1ms ramp up and ramp down. First, laser processing was conducted to find the full penetration processing window with a 60% pulse spot overlap and the maximum peak power before any observable breakage in wires. Thereafter, lowest power and highest power of full penetration processed window were determined to be the conditions of consequence welding of NiTi. Butt joint laser welding configuration was selected in order to evaluate the mechanical properties and superelastic response of welded wire samples. Figure 3-1 shows the schematic of the laser welding in a butt joint configuration of NiTi wires.

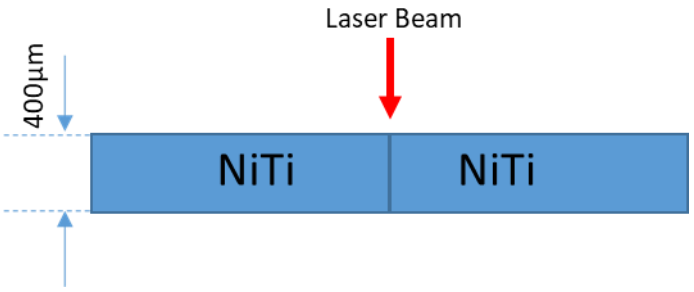

Figure 3-1 Schematic of the laser welding in a butt joint configuration

3.2.2 **Characterization**

Microstructural analysis of cross sections of welded samples were examined through conventional procedures, which is mounting in epoxy, grinding with SiC sandpaper up to number of 1200, polishing to 0.25µm diamond spray and etching with Kroll reagent (2-4%HF, 5-7%HNO3 and 89-93%water). The etched samples were observed by optical microscopy (OM). Detailed analysis of the phase map and microstructure carried out by electron backscatter diffraction (EBSD) using JEOL JSM 7000 FESEM equipped with the HKL Technology system with a step size of 1µm, working distance of about 15 mm and an accelerating voltage of 20 kV. The welded samples were prepared using oxide polishing suspension (OPS) after grinding with sandpapers up to number of 1200 and polishing to 0.25µm diamond spray. The acquisition of data was carried out by the Oxford Instruments Aztec software and collected data was post-processed by HKL Channel 5 software.

Phase transformation temperatures of welded materials were measured by Differential Scanning Calorimetry (DSC- TA Q2000) system equipped with a refrigerated cooling system. It should be mentioned that due to small size of HAZ and FZ regions, some remnant base materials existed in DSC samples. The DSC samples were first thermally pre-cycled to remove any effects of internal mechanical stress generated by the laser procedures and then DSC curves were recorded in a temperature range from -50°C to 50°C using a heating and cooling rate of 10°C/min. All required transformation temperatures were measured using TA Trios software in accord with ASTM F2004-05 Standard. Based on this standard, each DSC sample should be measured prior experiment and should be in the range of 25-40 mg. To satisfy this criteria, 4 or 5 welded samples have been used as a DSC sample.

Vickers Microhardness were adopted using Clemex CMT automated hardness tester attached to Clemex CMT 8.0 software according to ASTM E384. Microhardness measurements were captured by applying a load of 200 g for 15 seconds and 50 µm apart on the longitudinal centerline of the welds. Tensile tests of were conducted three times for each laser condition at room temperature with an Instron 5548 microtensile tester at a gauge length of 12 mm and a strain rate of 2.8×10^{-4} s^{-1} for all welded samples. Also, cyclic tests to evaluate superelasticity and were performed to a maximum strain of 10% before unloading to zero stress and repeated for 5 cycles also for 3 samples for each condition. Nanoindentations were performed by a nanoindentation platform (NHT, CSM Instruments, Switzerland), using a spherical tip, with a radius of 20 µm, a maximum indentation load of P = 100 mN, a loading/unloading rate of 200 mN/min and a dwell time equal to 15 s. Finally, the cyclic tests were performed at room temperature and 60 °C to a maximum strain of 10% before unloading to zero stress and repeated for 10cycles.

3.3 Results and Discussion

3.3.1 Laser welding parameters

Figure 3-2 shows the profile map for 400um spot size during laser processing, with the full-penetration processing window labeled. This processing window was obtained by applying different peak powers and pulse durations on a 400 µm NiTi wire. It is well known that high power (keyhole mode) causes more Ni vaporization than low power parameters due to extra keyhole vaporization and surface vaporization that is predominant in low power condition (conduction mode) [76,134]. These two mentioned criteria, labeled by green and red dotted circle for lowest and highest peak power respectively, were selected to study the effect of Ni vaporization. As displayed in Figure 3-2, both selected conditions result in full penetration condition without any retained base materials and are applicable for butt-joint welding of NiTi wires.

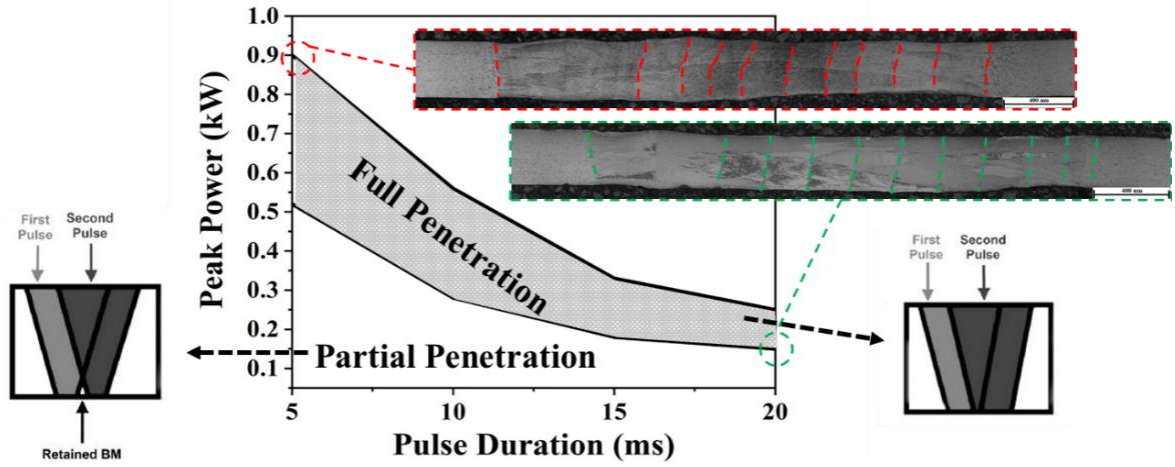

Figure 3-2 Laser pulse processing window showing full penetration condition. Green circled low power (0.15kW) condition vs. red circled high power (0.9 kW) condition in this chapter.

3.3.2 Microstructure and texture of welds

Cross section of welded samples and their corresponding phase maps are seen in Figure 3-3. In the microstructures, the location of FZ, HAZ and BM regions of welded samples are marked by dashed lines and will be discussed later. However, in the corresponding phase maps, it could be seen that the FZ region of high power (0.9 kW) sample (Figure 3-3-b) contains a considerable amount of unindexed areas (black color) which are related to martensite phase formation after welding. The low power (0.15kW) sample (Figure 3-3-a) is almost fully austenite (indexed with red color and very low amount of unindexed parts). The formation of martensite is related to more Ni vaporization at high power,

resulting in shifting the transformation temperature to higher temperatures and the appearance of martensite phase at room temperature.

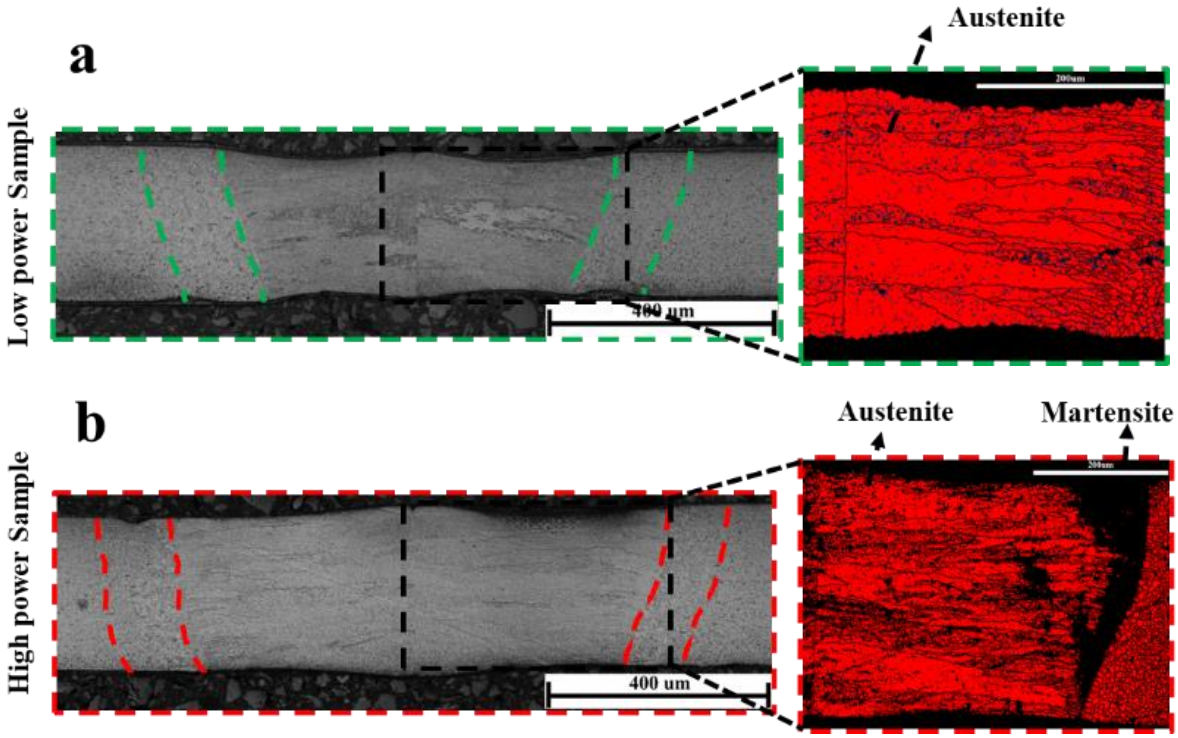

Figure 3-3 Microstructure of a) low power condition and b) High power condition laser welded samples and their corresponded phase map

The SEM overview and EBSD IPF images of the low power and high power laser welded samples are shown in Figure 3-4-a and c. The IPF image in the high power condition shows a considerable unindexed region which is attributed to the B19' martensite phase. This behavior is a direct result of Ni evaporation during high power laser processing (Figure 3-4-c). It worth to mentioned although the base material has <111> direction, the fusion zone of the high power sample (Figure 3-5-a) has directed toward <100> which is a easy-growth direction during the solidification of cubic materials whereas this region in the low power sample, contained finer and more random grains due to applying laser conduction mode (Figure 3-4-a).

To provide better insights into this observation, EPMA maps of the low and high power conditions are shown in Figure 3-4-b and d, respectively. As seen at the high power laser condition (Figure 3-4-d) more blue color is detected inside the fusion zone which means lower amounts of Ni is present inside the fusion zone. However, to quantify this variation, one region outside and two regions inside the fusion zone were selected and labeled by BM, FZ1 and FZ2.

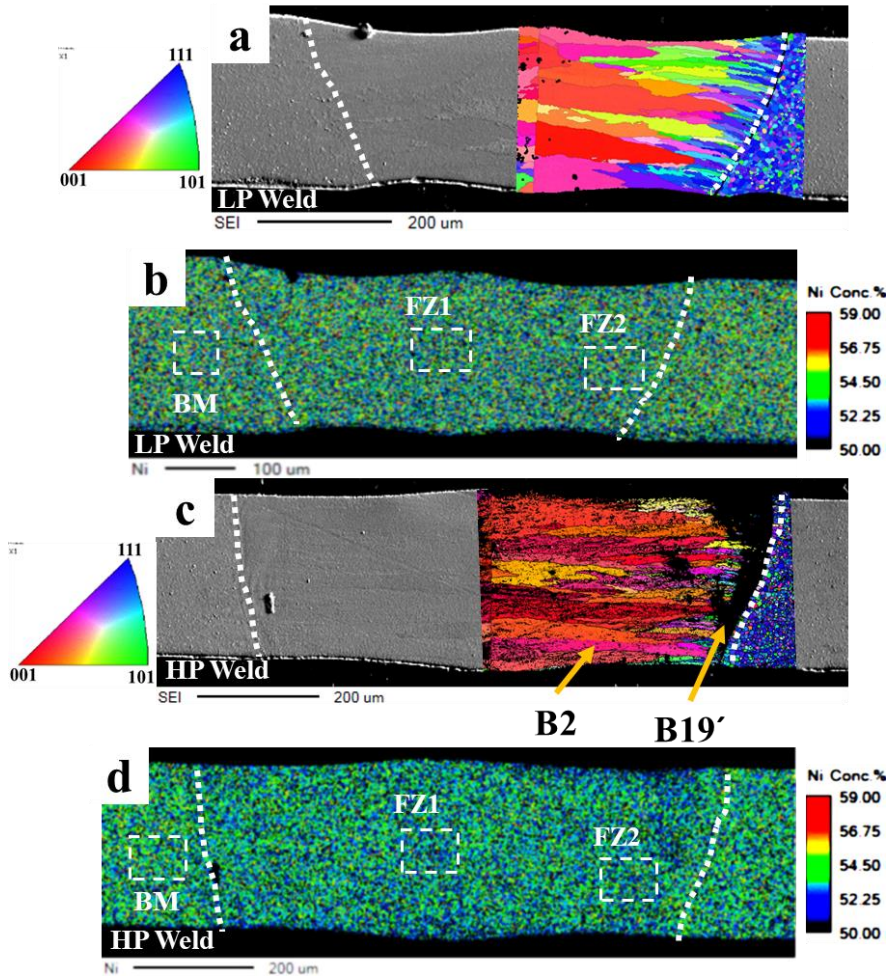

Figure 3-4 Microstructure and IPF map of a) low power (LP) welded sample, b) high power (HP) welded sample and c) the low power (LP) and d) high power (HP) welded samples' EPMA showing Ni concentration.

Detailed grain structure, texture orientation and inverse pole figures of base material and welded samples are shown in Figure 3-5. As expected, base material (Figure 3-5-a) has predominantly <111> type grains because the superelastic wire are cold drawn and subsequently heat treated to have this texture orientation to exhibit supreme superelastic response [14]. Figure 3-5-b and c illustrate coarse columnar grains at the centerline and finer columnar grains near the HAZ formed after welding due to directional solidification. It is also evident (Figure 3-5-c) that the high power sample contains coarser grains both in FZ and HAZ in comparison with low power one (Figure 3-5-c). However, a deviation in texture orientation after welding between base and weld material for both conditions exist based on the IPF maps related to these welded sample: formation of <100>-type orientation after laser welding of NiTi has been already observed [79–81], because this orientation is the preferred and easy-growth

direction for cubic materials under maximum temperature gradient and maximum heat extraction conditions. Since the NiTi has B2 (bcc order) structure, hence it is expected that the solidified grains within FZ form in this <100> direction (coloured by red). In low power sample (Figure 3-5-c), although grains are formed slightly toward <100>, they are distributed in randomly with a lower intensity. This behavior has been observed when conduction mode is in dominant [79]. Therefore, it should be mentioned that in the low power sample (Figure 3-5-b) less observed deviation from base material texture in comparison with the high power sample (Figure 3-5-c).

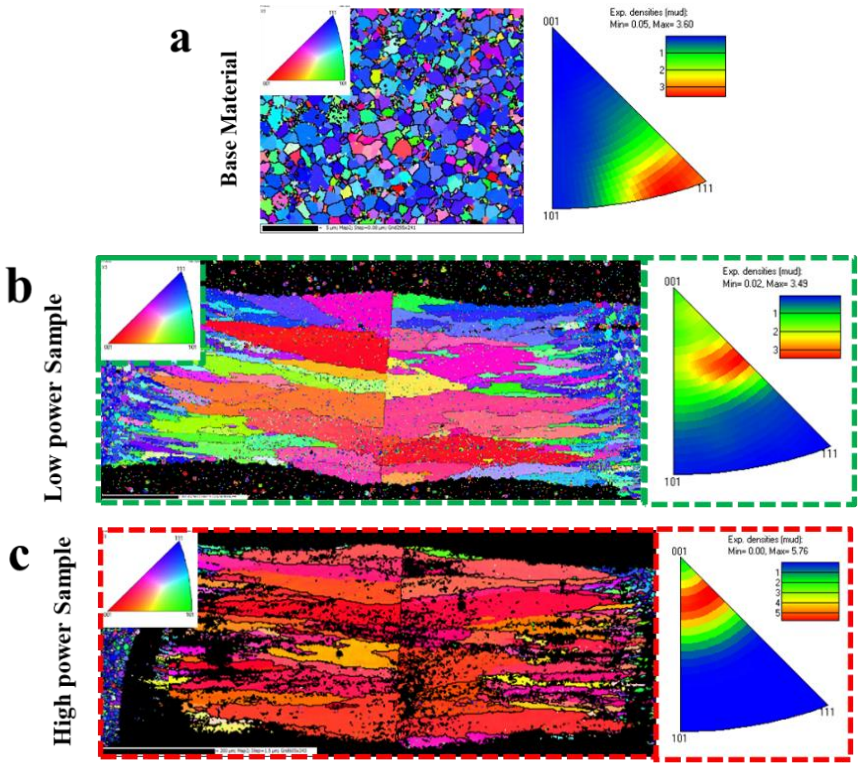

Figure 3-5 IPF images in the tensile direction of a) NiTi base material, b) HP and c) LP samples and their corresponded austenite B2 inverse pole figures showing the deviation of intensity after laser welding.

3.3.3 **Ni content and Phase transformation Temperature**

The weight percentage of Ni inside the selected regions (BM, FZ1 and FZ2 in Figure 3-4-b and d) are given in Table 3-1, where the difference of Ni concentration in BM and FZ of the low power sample is negligible. However, this difference is in the range of 0.3-0.4 wt.% between the FZ and the BM at the high power condition, which could cause a significant difference in transformation temperature of welds. Generally, the higher rate of Ni evaporation is mainly attributed to the higher vapor pressure of Ni, compared to that of Ti during laser keyhole welding of NiTi alloys [76].

Table 3-1 Ni concentration per wt.% in selected region of the laser welded samples shown in Figure 3-4

Regions	BM	FZ1	FZ2
Ni (wt%) in LP	55.04	54.98	55.12
Ni (wt%) in HP	55.69	55.38	55.31

To understand the effect of Ni evaporation, differential scanning calorimetry (DSC) of the high power and low power samples was used to characterize transformation temperature changes. Figure 3-6 indicates the variation of the transformation temperatures during heating and cooling for high power sample (red curves) and low power sample (green curves). In both samples, there are two sets of peaks: one relates to phase transformation of base material and another one relates to weld. The transformation temperature of the weld material in the high power sample increases significantly in comparison with the low power samples because of its lower Ni concentration caused by more Ni vaporization. The Ni evaporation of the material can directly shift the transformation temperature between austenite B2 and martensite B19'.

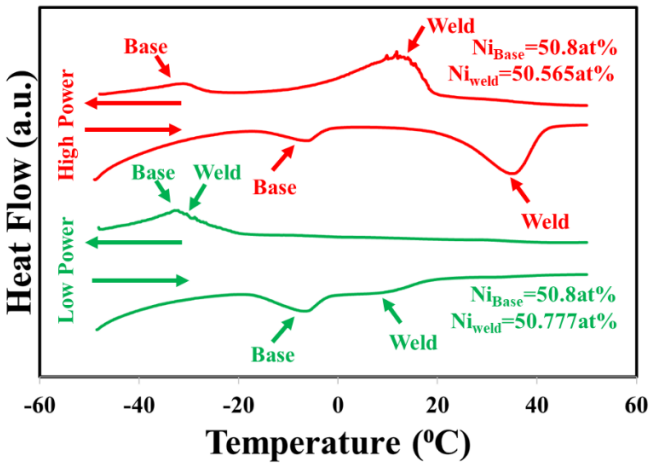

Figure 3-6 Differential Scanning Calorimetry of High Power (Red curves) and Low Power samples (Green curves) during cooling and heating showing the variation of transformation temperature due to Ni loss in both conditions.

The critical transformation temperatures of the NiTi BM, low power, and high power welding conditions were measured from DSC curves as -16, -2 and 22°C for As, -2.5, 18 and 42°C for Af, -25.5, -32 and 19.5°C for Ms and -43, -21.5 and -7°C for Mf, respectively. Therefore, the transformation temperature of weld increased; however, this increase is more significant in the high power condition due to the Ni evaporation resulting in the formation of the martensite phase which was not indexed in IPF image (Figure 3-5-c). On the other hand, the austenite transformation finish temperature (A_f) for the low power condition is still at room temperature (18°C), which was confirmed by the fully austenite microstructure in the FZ (Figure 3-5-b).

Furthermore, to approximate the Ni concentration in the welded joints, an established relationship between Ni concentration and austenite transformation temperature is recalled [134]. In this regard, the Equations 3-1 and 3-2 were used [139,140], replacing ΔT with (AP-MP) in Equation 3-2 the Ni concentration can be determined. These relationships are as follows:

$$M_P(c_{Ni}) = (2027077588.5 - 205968221.1c_{Ni} + 8370845.646{c_{Ni}}^2 - 170093.5974{c_{Ni}}^3 + 1728.050544{c_{Ni}}^4 - 7.022069029{c_{Ni}}^5)K$$ Equation 3-1

$$\begin{cases} if\ c_{Ni} > 49.8at.\%, & \Delta T = (-17.5c_{Ni} + 920.5)K \\ if\ c_{Ni} \leq 49.8at.\%, & \Delta T = 49K \end{cases}$$ Equation 3-2

where, c_{Ni} is the Ni concentration. Therefore, by extracting the austenite temperature from DSC curves, Ni concentration can easily be determined, which is mentioned in Figure 3-6. As is seen the major Ni loss (~0.23 at %) occurs when the peak power is high. On the contrary, when lower power is used, there was a negligible change in the Ni concentration (less than 0.03 at %).

3.3.4 **Mechanical Properties**

The high degree of deviation in texture between base and weld materials in high power sample (Figure 3-5-c) caused a drastic decrease in the UTS from 81% of base material strength in the low power sample to 63% in the high power sample, as is seen in Figure 3-7. It is worth to mention that in this figure, the overshoot of stress in welded samples is the result of needing extra force to create the initial martensite nuclei [141]. Moreover, due to formation of thermally stable martensite phase in the high power sample, this welded sample needs lower amount of critical resolve shear stress in plateau region rather than the low power sample which contains fully austenitic phase and also has lower young modulus in elastic region [142].

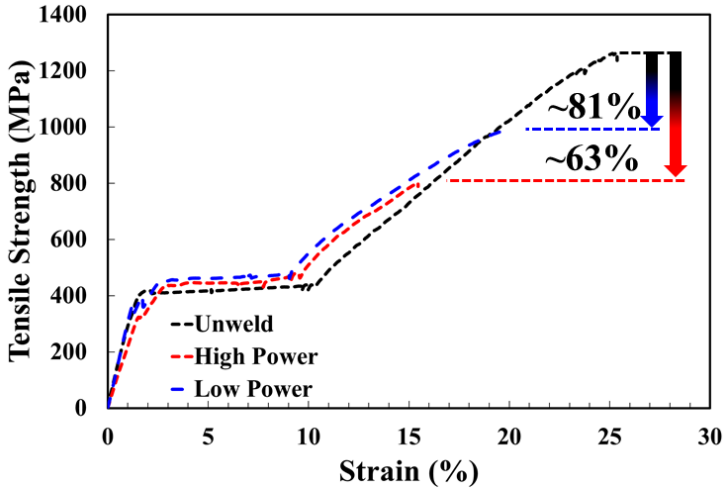

Figure 3-7 Tensile Stress-Strain curves of NiTi un-weld, high power and low power welded samples.

Figure 3-8 shows the variation of microhardness across the weld for both the high and low power samples. In both conditions the base material has a higher hardness than the FZ and HAZ due to the coarser grain size (See Figure 3-5). However, the hardness was higher in the FZ of the low power sample compared with the high power samples for two main reasons: coarser grain size in high power in compare with low power one and containing a considerable amount of martensite phase in high power sample, due to Ni vaporization, which is a softer phase in NiTi [6].

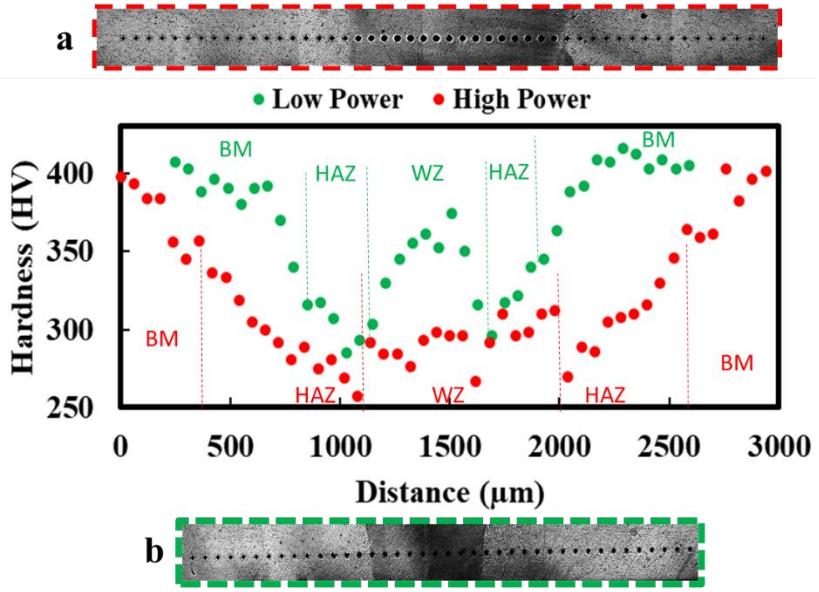

Figure 3-8 Microhardness profile of a) HP (red dots) and b) LP (green dots) welded samples.

3.3.5 **Superelasticity**

Load-unload nanoindentation across the FZ and HAZ has been applied across the fusion zone for both samples. The correspondent residual depth and dissipated energy has been calculated from the load-unload curves as seen in Figure 3-9-a and b, respectively. As observed by entering the HAZ and FZ, the residual depth and dissipated energy gradually increased after unloading. As a rule of thumb, any melting and solidification of a superelastic wire can significantly degrade the material's superelasticity, since the critical yield strength of the material could be shifted to a lower value than the critical stress for the martensitic transformation [6]. However, within the FZ of the high power condition, the mentioned parameters are higher than its low power counterpart due to the existence of martensite phase. It should be noted that most of the energy inside the FZ of the high power sample had dissipated by plastic deformation or martensite detwinning and only a small fraction of it was consumed for the strain recovery.

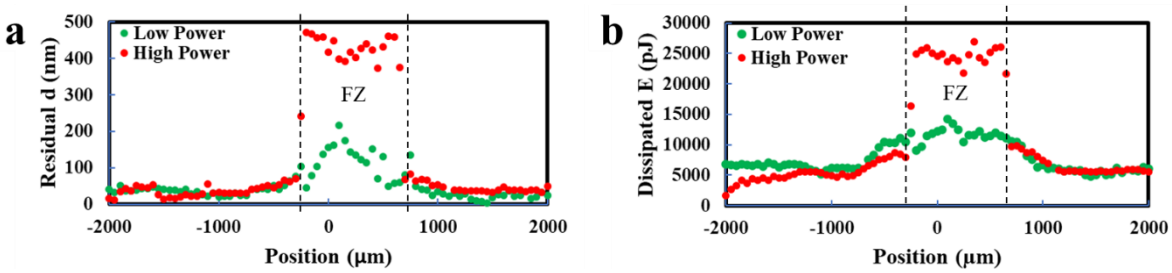

Figure 3-9 The calculated parameter from load-unload nanoindentation on LP and HP welded samples a) Residual depth after unloading and b) Dissipated energy

Nevertheless, it is worthwhile to evaluate the cyclic tensile test to evaluate the superelastic response through the whole welded wires and to the effect of different amounts of Ni loss during welding. This behavior is characterized by the residual strain after a cyclic tensile test at room temperature and at 60°C where both welded samples are in austenitic phase condition, as shown in the stress strain curves in Figure 3-10. As can be seen the formation of martensite via the stress induced phenomena occurs in several stages in the fusion zone before reaching a stress plateau level. As reported elsewhere this phenomena is related to the existence of residual stresses in the HAZ and FZ of the laser welded NiTi joints [23] and these kinks can manifest before or within the plateau [131]. Moreover, there was almost complete strain recovery with very little residual strain (0.38%) observed in low power welded wires after the first cycle, and it reaches a saturation point of 1% residual strain after 10 cycles (Figure 3-10-a), both at room temperature. However, for the high power welded samples at room temperature, the amount of residual strain is considerably higher (1.1% after first cycle and 1.9% after saturation in 10 cycles, as shown in Figure 3-10-b). It is important to note that during mechanical cycling, dislocations are introduced in the FZ and HAZ and therefore mechanical stabilization of martensite would be occurred [137]. Therefore, residual strain continues to increase with cycling until a saturation point is reached. However, rather than martensite stabilization during cycling, which is common for both welding conditions, presence of martensite in the high power sample or thermal stability of martensite in addition to relatively coarse grain in FZ and HAZ causes a reduction in the superelastic response. Since fully recoverable strain due to superelasticity is based on the B2 (austenite phase) to B19' (martensite phase) reversible transformation [6], the material must be fully in the austenite phase to obtain higher amounts of recovered strains. Overall, the low power conditions have better a superelastic response and the control of the evaporation of Ni during laser welding plays a key role in achieving this.

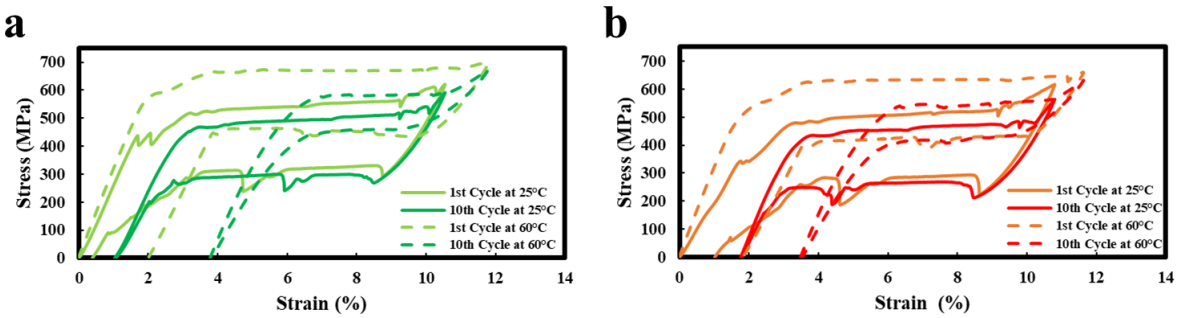

Figure 3-10 The tensile cyclic response of the a) LP and b) HP welded samples up to 10 cycles at RT and 60°C.

However, at 60°C (Above A_f of both samples), there is almost no difference between the low and high power welded samples (shown by dotted lines in Figure 3-10), even after the 10th cycle and the residual strain is near 4% for both samples. Nevertheless, the considerable residual strain in both welded conditions at 60°C is attributed to the large grains in the HAZ and the fusion zone along with the lower yield strength of the welded samples at this temperature, which resulted in more plastic strain and a lower recoverable strain [143].

3.4 **Summary**

This study examined the effect of Ni vaporization on NiTi joint performance by selecting low and high power welding parameters. It was shown that in addition to Ni vaporization and its consequences, which is changing the transformation temperature and forming martensite phase in FZ, the texture variation between fusion zone and base material has a great impact on the mechanical properties of weldments. Whereas the high power sample has mostly <001> grain type orientation, the low power sample has lower intensity in texture and was slightly rotated toward <111> which is the main orientation in base material. In this regard, the strength of the low power sample reaches 81% of ultimate tensile strength of the as-received sample, while this number drops to 63% in case of high power sample. Furthermore, the residual strain, which is a sign of superelasticity, was just 0.38% for the lower Ni loss sample which was significantly better than the higher Ni loss sample with 1.01% residual strain. This behaviour justified by formation of fraction of martensite phase and also coarser grain in HAZ and FZ of the high power sample.

The high power sample has more texturized microstructures and larger grains compared to the low power condition, in addition to the vaporization of Ni-content of the FZ. This Ni loss resulted in changing the transformation temperature, and hence, in the formation of the martensite phase within the fusion zone of the high power sample. It was shown that the presence of this unfavorable martensite

phase is the primary reason for the different superelastic response of both welded samples at room temperature. This superelastic response is shown by performing nanoindentation tests across the weld area and cyclic tests up to 10 cycles in the tensile mode. However, by increasing the tensile cyclic test temperature to 60°C (above Af temperature of the high power welded sample), the residual strain difference between high power and low power samples was eliminated and both welded samples presented similar superelastic behaviors.

With this chapter's understanding of Ni vaporization and selecting proper laser parameters, next chapter will study the formation of IMCs due to great affinity of Ti and complex flow pattern in the dissimilar laser welding of NiTi.

Chapter 4 Intermetallic compounds and flow behavior in dissimilar NiTi welds[1]

4.1 Introduction

This chapter is the starting point for entering the dissimilar laser welding of the NiTi shape memory alloys to other biomaterials. The most important one is the laser welding of NiTi to stainless steel (SS) which is quite challenging and is of great importance to design medical devices, but formation of hard and brittle IMCs results in low strength joints. The other highly demanded dissimilar welding of NiTi is its joint with Cu since its use in the production of NiTi medical devices which need high electrical conductivity (pacemakers). Therefore, these two dissimilar NiTi laser welds will be discussed in this chapter in two separate sections.

Based on NiTi/stainless steel dissimilar joints studies and also taking the ternary phase diagram of Ni-Ti-Fe into consideration [144], numerous extensive and complex networks of different hard and brittle IMCs are responsible for low strength nature and extreme brittleness of NiTi/stainless steel joints [41,93]. Therefore, different interlayers have been used to prevent the formation of these harmful IMCs and improve the joints mechanical properties [51,53,54,95–97,145]. However, the usage of interlayers needs optimization of laser parameters and a proper selection of interlayer material dissimilar laser welding.

One of the aspects of minimizing IMCs in joints is to control the degree of mixing in the fusion zone. In fact, accurate positioning of the laser spot and using of small dimension of the heat source can control the microstructural evolution within the fusion zone [36,146], especially in butt joint configuration. Laser offsetting welding (LOW) technique is another effective method to achieve sound joints [147–151], because it provides different patterns of element mixing and thus different phases in joints [152–154].

The aim of the present chapter is to adopt laser offsetting welding in a dissimilar combination of NiTi to 316L SS and to Cu. In the first section, laser offsetting welding was introduced without inserting any interlayer by shifting the laser beam 100μm into the stainless steel from the NiTi/316L stainless steel interface. It shows that the LOW could be an effective method to laser weld the NiTi/SS.

[1] The results of these chapter are published in two journal papers: 1- **Shamsolhodaei, A.**, et al. Intermetallics 116 (2020): 106656. and 2- **Shamsolhodaei, A.**, et al. Journal of Materials Engineering and Performance 29.2 (2020): 849-857.

The second section discusses the dissimilar pulsed laser welding of NiTi and Cu wires, used to investigate the effect of laser positioning on NiTi/Cu joint performance. It was shown that positioning the laser beam on the NiTi or on the centerline resulted in a better transition in microstructure that led to acceptable mechanical properties without optimizing laser parameters or inserting any interlayers. Thus, this present work may open the door for fabricating biomedical devices by studying effects of laser beam offset on the microstructure, mixing patterns and mechanical properties of NiTi/SS316L and NiTi/Cu dissimilar butt welded joints.

4.2 Experimental Procedure

4.2.1 Laser welding of NiTi/SS

A superelastic NiTi (50.2 at% Ni) wire and stainless steel AISI316 (17 at. %Cr, 12 at. %Ni, 2% at. Mo and Fe balanced) wire both with 400µm diameter were used in this work. Both sets of wires were cleaned prior to laser welding using acetone, ethanol and de-ionized water to remove any impurities and contamination. Laser welding on these dissimilar materials performed using Miyachi Unitek LW50A pulsed Nd:YAG laser, with a wavelength of 1.064 µm, the nominal spot size of 400 µm and a square shaped laser profile with a 0.9 kW peak power and width of 5 ms. Argon gas protection was employed as a shielding gas with a flow rate of 30 Cfh. Figure 4-1 depicts the schematic of the different conditions of dissimilar laser welding in a butt joint configuration: a) laser beam positioned at the interface of both materials, b) laser beam offsetting by 100 µm from centerline and c) Ni foil with 50 µm thickness inserted between two materials and the laser beam positioned at the centerline.

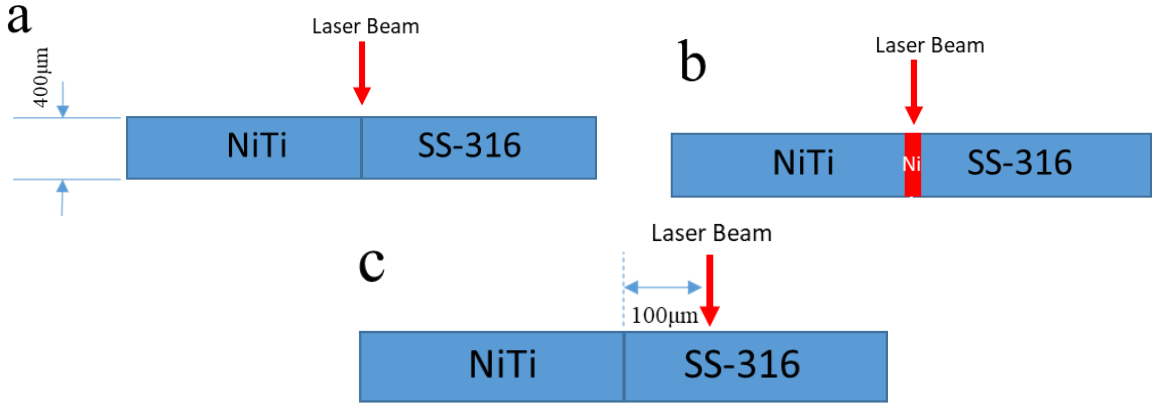

Figure 4-1 Dimensions and schematic of stainless steel 316 and NiTi in conditions: a) laser beam on centerline b) using 50µm Ni interlayer and c) laser beam offsetting 100µm from centerline.

Microstructural studies were performed on cross sections of dissimilar welded specimens prepared by mounting the welded wires in epoxy, grinding up to grit number 1200, polishing by diamond spray

down to 0.25 μm and etching with Kroll reagent (2-4%HF, 5-7%HNO_3 and 89-93% water by volume). Microstructure observation and phase map were conducted by Olympus BX51M Optical microscope (OM) and Zeiss Ultra Plus field emission scanning electron microscope (SEM) equipped with Energy dispersive spectroscopy (EDS). Synchrotron XRD performed with a Perkin Helmer 2D detector placed at 1.35 m from the sample with a wavelength of 0.1426 Å (87 keV) at beamline P07 high energy materials science (HEMS) of Helmholtz-Zentrum Geesthacht at PETRA III. A 200×200 μm pixel size of a detector with a measured accuracy of 2θ=0.0084° was used. The raw data images were treated using Fit2D [155] using the procedure described in [24]. In these experiments, the probing line started from NiTi base material and ended in SS base material perpendicular to the weld area. The distance between consecutive probed regions was of 50μm, while the X-ray beam size had 50 x 50 μm.

Vickers microhardness testing was carried out to make a series of 200 g indents with a distance of 50 μm between each indent and 10 seconds holding time using a CMT Clemex automated hardness tester according to ASTM E384. The strength of the welded samples measured by adopting an Instron 5548 micro tester at a gauge length of 12 mm which includes the FZ, the heat affected zones and the base materials. All tensile tests were performed at room temperature and a strain rate of $3\times10^{-4}s^{-1}$ and three samples for each welding condition were tested.

4.2.2 **Laser welding of NiTi/Cu**

A superelastic Ni-rich NiTi (50.2 at% Ni) wire with 400 μm diameter and commercially pure Cu (99.9 at%) wire with same diameter were used in this present study. The sample preparation and laser equipment are the same as previous part. The top-hat shaped laser profile with a 0.9 kW peak power and width of 15 ms, including 1ms upslope and 11ms downslope was used for all experiments. The laser was positioned on five different locations on the NiTi side, centerline and Cu side which are depicted in Figure 4-2. Focusing the laser on NiTi with a 100 μm offset could not make a sound joint with Cu and will not be discussed further. X-ray diffraction (XRD) measurements were taken at room temperature on a Bruker D8 diffractometer with Co source with the scanning range of 2θ = 30 to 100°.

Cross sections of welds were mounted in epoxy and then grinded with sandpaper up to number 1200 and then polished to 1 μm using diamond sprays, followed by etching with Kroll's reagent for 30 seconds. The related microstructures were observed using Olympus BX51M Optical microscope (OM) and Zeiss Ultra Plus field emission scanning electron microscope (SEM) equipped with Energy dispersive spectroscopy (EDS) to analyze the compositional changes. A Clemex CMT automated micro-Vickers hardness tester was used to make a series of 50g indents across the base materials and

FZ, 50 µm apart with a holding time of 10 seconds. Tensile testing was performed four times for each weld with a gauge length of 12mm and a strain rate of $3\times10^{-4}s^{-1}$ using an Instron 5548 micro tester.

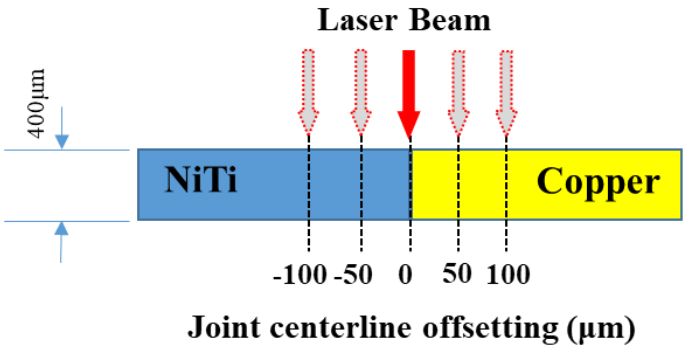

Figure 4-2 Schematic of the laser welding process with different laser offsets.

4.3 Formation of IMCs in NiTi/SS316L welds

4.3.1 Microstructural analysis

The cross-section microstructure of the laser welded sample without any offsetting is shown in Figure 4-3. Full penetration was achieved and both base materials could be distinguished as NiTi in the left side and stainless steel in the right side (Figure 4-3-a). In addition, a swirling effect occurred inside the FZ which is related to the Marangoni effect and promotes mixing of the two base materials within the fusion zone. Different densities of the base materials, rapid heating and cooling in laser welding could cause this complex pattern inside the FZ. Three different regions of the FZ: NiTi/ FZ interface, inside the FZ and in FZ/stainless steel interface are shown in Figure 4-3-b to d.

The NiTi/FZ interface in Figure 4-3-b shows the characteristics of epitaxial growth starting from planar, mainly cellular and ended with dendritic structure from base material to FZ. The cellular interface between NiTi and the FZ consists of numerous microcracks (Figure 4-3-c) which were reported elsewhere in this region due to formation of brittle phases [41]. On the FZ interface with stainless steel (Figure 4-3-e), planar, cellular and dendritic morphologies formed in a thinner region due to higher cooling rate during solidification. The microstructure of FZ in this sample (Figure 4-3-d) consists of an extensive network of intermetallic phases in the form of a dendritic structure. These IMCs are the main outcome of mixing elements, especially Ti which formed $TiFe_2$, $TiCr_2$, $TiNi_3$ and Ti_2Ni, and caused extreme brittleness and failure even under low stress conditions.

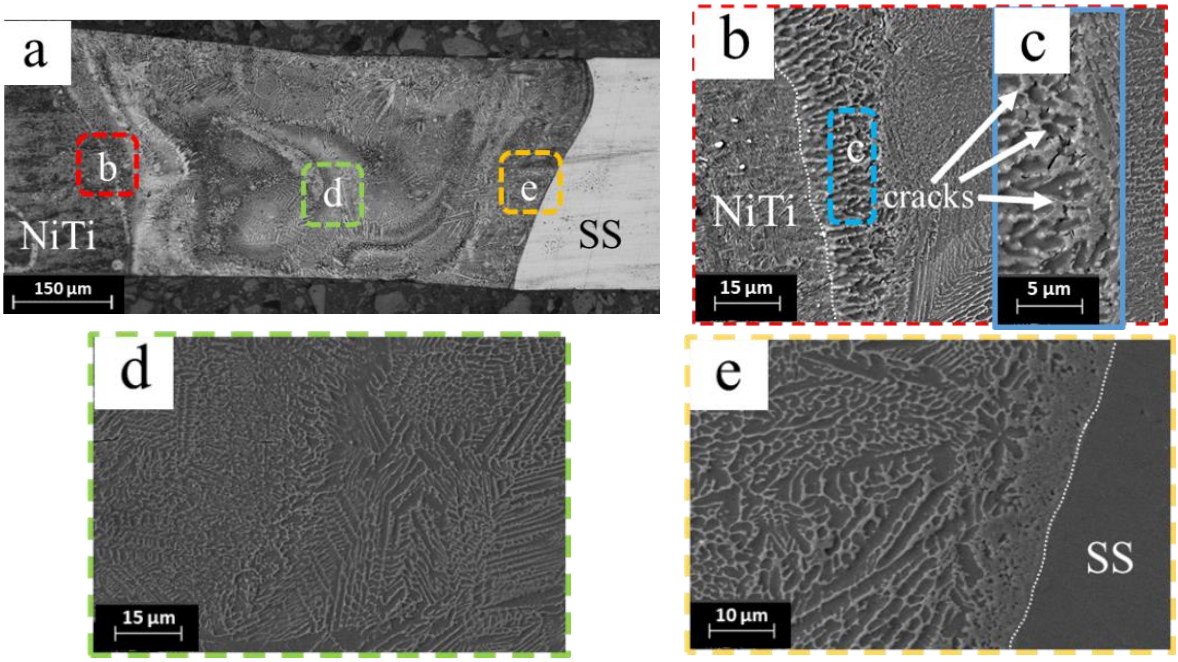

Figure 4-3 Microstructure of welded sample without laser offsetting shows a) the whole FZ area, b) interface of NiTi/FZ, c) microcracks in the interface, d) center of the FZ and e) interface of SS/FZ.

By inserting a Ni interlayer between the two base materials (Figure 4-4), a white and sharp interface formed in the interface of NiTi and the FZ (Figure 4-4-b). This interface consists mainly cellular and cellular dendrites similar as literature [51]. This white interface might be the mixture of $TiFe_2$, $TiNi_3$ and NiTi B2 phases based on the mentioned literature in Chapter 2, extending along the entire interface.

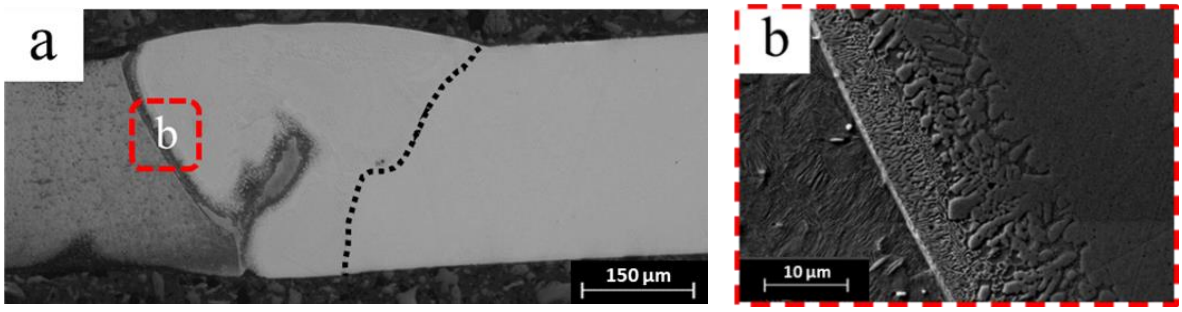

Figure 4-4 Cross section microstructure of welded sample by inserting 50µm in thickness Ni interlayer a) the whole FZ area and b) interface of NiTi and FZ.

In case of offsetting the laser beam on stainless steel (Figure 4-5-a), the FZ exhibits different characteristics. It seems that the large network of IMCs is limited to some regions inside the FZ and its amount reduced considerably. The interface of NiTi and stainless steel (Figure 4-5-b) became narrower but still consist of mainly cellular growth characteristic without visible microcracks. A dendritic structure inside the FZ is formed with finer features in some selected regions inside the FZ (Figure 4-5-c). The other important microstructural difference between the joint using the Ni interlayer and the one

obtained without laser offsetting (Figure 4-3) is the inability to identify the interface of the stainless steel/FZ. A section of the interface could be characterized (Figure 4-5-d) with very narrow and abrupt interface and very fine and modified equiaxed dendritic structure.

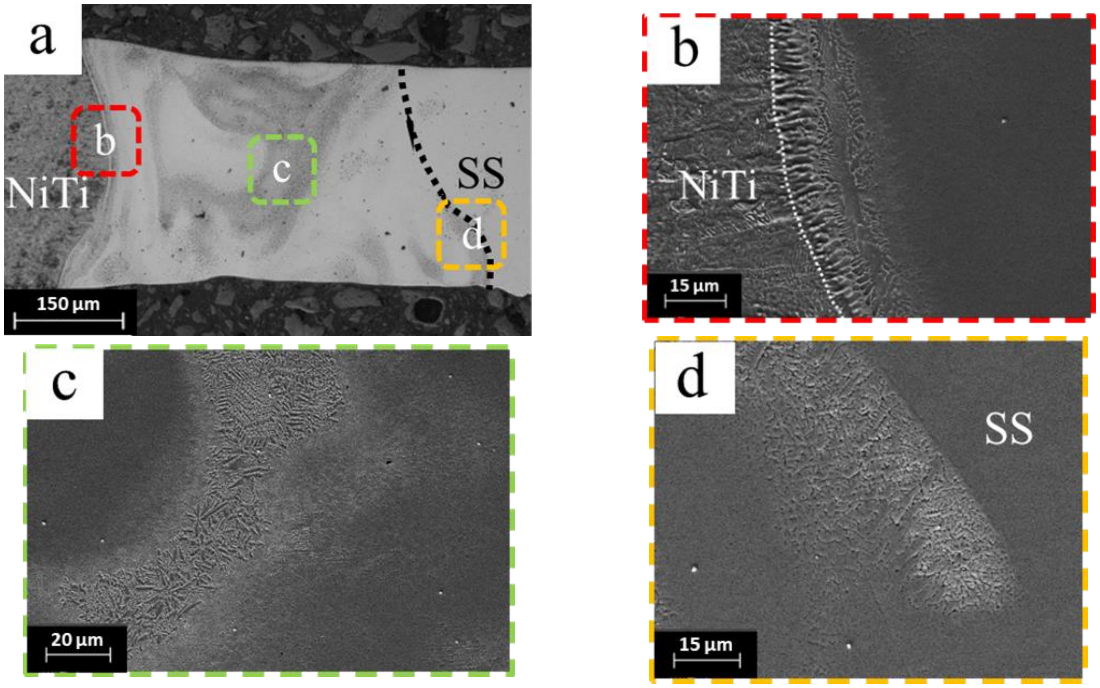

Figure 4-5 Cross section microstructure of welded sample in 100µm offsetting laser on stainless steel a) the whole FZ area, b) interface of NiTi and FZ, c) center of the FZ and e) interface of SS/FZ.

4.3.2 **Phase identification**

Figure 4-6 demonstrates the distribution of Ti, Fe and Ni elements for the different welded joint. As seen in Figure 4-6-a to c, by focusing the laser beam on the centerline of two base materials, the elements distributed uniformly (especially Ti and Fe that could form several IMCs). In the case of inserting the Ni interlayer, the amount of Fe mixing decreased inside the FZ (Figure 4-6-e) compared with the other two conditions because of the chemical barrier role of Ni between two base materials. The amount of Ni increased considerably due to the insertion of the Ni interlayer which caused the formation of Ni-based IMCs inside the FZ. By offsetting the laser beam onto the stainless steel, Ti content (Figure 4-6-g) decreased significantly and most of the FZ consisted of Fe (Figure 4-6-h) which is the result of the stainless steel melting and welding with NiTi. This decrease in mixing of Ti inside the weld pool could cause reduction in the amount of IMCs inside the FZ which will be discussed further. In general, the higher mixing of Ti and Fe inside the FZ results in more IMCs formation. When Ni content increased (using Ni interlayer), Ni-rich IMCs can be preferentially formed.

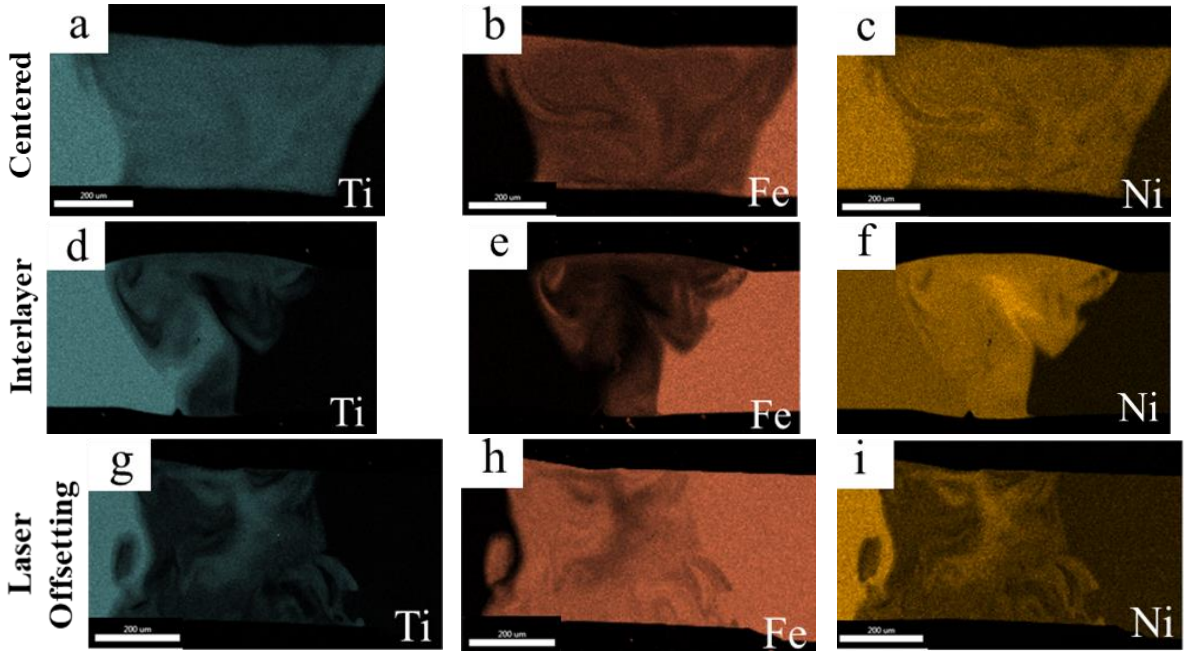

Figure 4-6 EDS mapping of a-c) centerline, d-f) inserting Ni interlayer and g-i) laser offsetting welding condition showing distribution of a, d, g) Ti, b, e, h) Fe and c, f, i) Ni element.

To identify which IMCs formed in the different welded joint, synchrotron X-ray diffraction (SXRD) was used. The superimposition of the scans performed from one base material to the other base material are plotted in Figure 4-7. Additionally, the intensity variation of one diffraction peak of each one of the IMCs found along the joints was plotted to obtain a qualitative assessment of the volume fraction of each IMC. Overall, various phases are formed inside the FZ. In weld centerline condition (Figure 4-7-a) for instance, from the NiTi base material side to stainless steel base material side, Fe_2Ti, Cr_2Ti, Fe_3Ti and Ni_3Ti are formed. These IMCs are highly brittle and detrimental for joint performance [43]. These mentioned variation in different IMCs could be better followed in Figure 4-7-b in which Cr_2Ti and Fe_3Ni have higher intensity inside the FZ when compared to the LOW or Ni interlayer insertion joints. It should be mentioned that these intensities were captured just from the main peaks of each phase and as it could be seen Fe_2Ti are highly formed within the FZ in centerline condition FZ. Inserting the Ni interlayer (Figure 4-7-c and d), however, introduced Ni-rich intermetallics compounds such as Fe_3Ni and Ni_3Ti. By offsetting the laser to the stainless steel side, a considerable decrease in IMCs intensity could be visible (Figure 4-7-e), as Fe_2Ti peaks reduced and the amount of Ti_2Ni, Ni_3Ti and Cr_2Ti also considerably decreased. The main peaks intensities of different phases are clearly visible in Figure 4-7-f, where stainless steel austenite phase possess highest intensity inside the FZ.

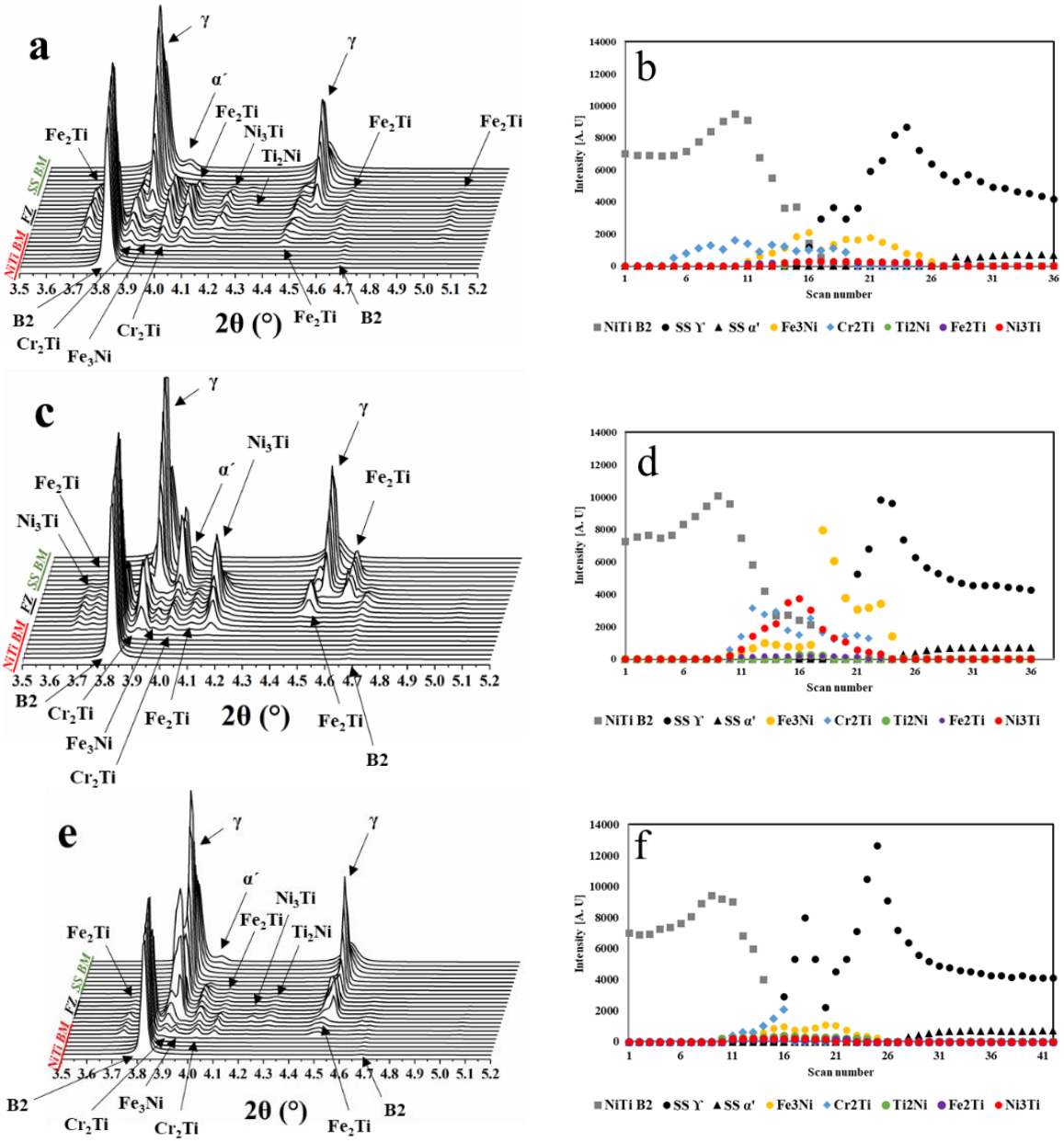

Figure 4-7 Superimposition of synchrotron x-ray diffractograms of a) centerline joint, c) Ni interlayer joint welded, e) laser offsetting joint; and b, d and f) the extracted intensity of different phases in the corresponding samples.

4.3.3 **Mechanical Properties**

The microhardness maps for each weld condition are depicted in Figure 4-8. The microhardness variations are in a good agreement with cross section microstructure and mixing element pattern (Figure 4-6). In Figure 4-8-a high microhardness values (with average ~970HV) could be visible all over the fusion zone due to homogenous distribution of elements (Figure 4-6-a to c) and the presence of hard and brittle IMCs network inside the fusion zone (Figure 4-3-a). In the case of Ni inserted sample (Figure

4-8-b), a higher content of Ti caused higher values microhardness region (red areas). By offsetting the laser beam on stainless steel (Figure 4-8-c), lower hardness values inside the FZ (570HV) can be observed. Considering the element distribution and phase identification based on SXRD results (Figure 4-7), it could be suggested that the higher amount of Ti inside the FZ (Figure 4-6-d) and also more brittle and hard phases such as Cr_2Ti and Fe_2Ti resulted in higher values of microhardness. The HAZ displayed lower values of hardness values as expected due to grain growth in the cold worked wires and destabilization of martensite in the 316L SS base material due to the experienced thermal cycles.

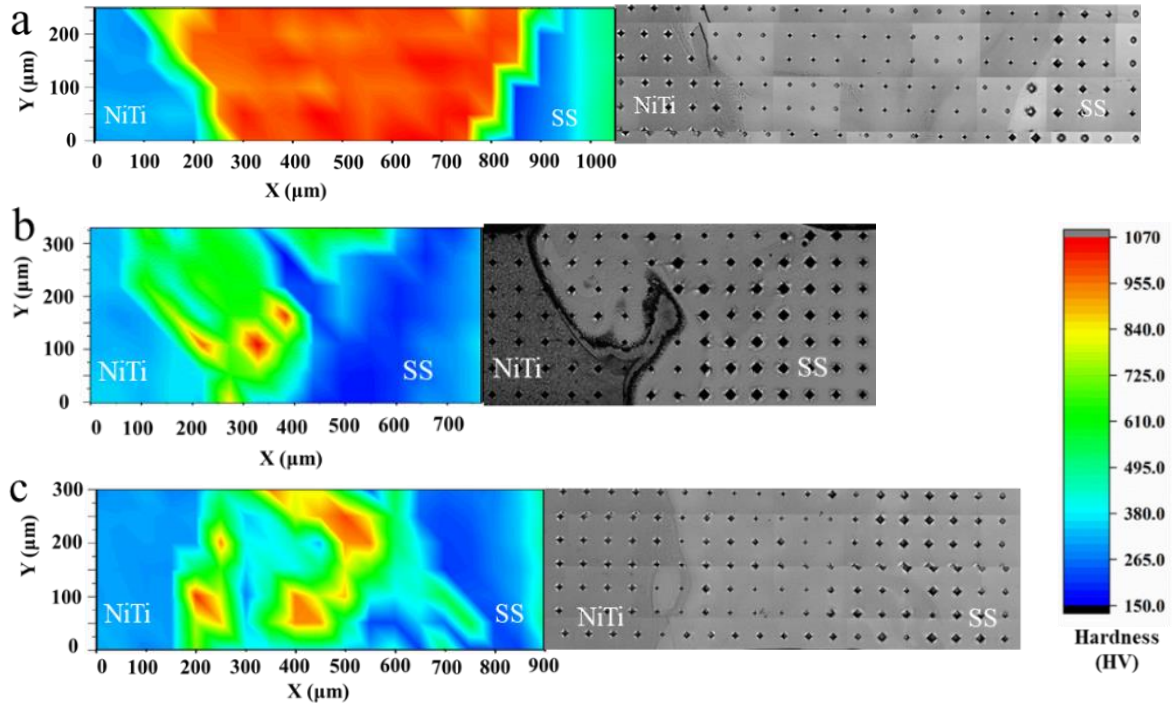

Figure 4-8 Microhardness maps for a) centerline condition, b) Ni interlayer and c) laser offsetting welded samples.

Figure 4-9 depicts the mechanical properties of welded samples and corresponded base materials. Both offsetting and insertion of the Ni interlayer increase the maximum tensile strength (Figure 4-9-a) two times. As mentioned in section 4.1, using a Ni interlayer was already an established method for improving joint performance in NiTi/stainless steel dissimilar welding. Similarly, laser offsetting welding also has the ability of enhancing mechanical properties as shown in Figure 4-9-a through hindering the formation of hard and brittle intermetallics and modifying the microstructure in the interfaces of base materials and FZ. Nevertheless, none of the samples could reach the required stress level to exhibit stress induced martensite phenomena (Figure 4-9-b) and even laser offsetting samples failed just before occurring stress induced martensite plateau region for NiTi base material.

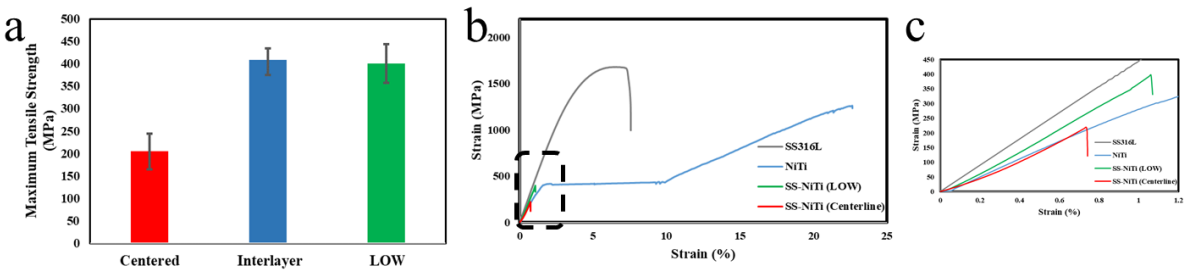

Figure 4-9 Mechanical properties of NiTi/SS welded samples in different conditions showing a) Maximum Tensile Strength of the samples and b) Stress-Strain curves for welded samples and the base materials.

Figure 4-10 shows the fracture surface of welded samples after tensile testing. All the samples exhibit sharp facets and considerable cleavages suggesting a sign of brittle nature of fracture. However, by inserting Ni interlayer (Figure 4-10-b) and laser beam offsetting (Figure 4-10-c), some dimples and tearing ridge could be observed as a sign of better ductility of these pulled samples in compare with centerline weld sample (Figure 4-10-a).

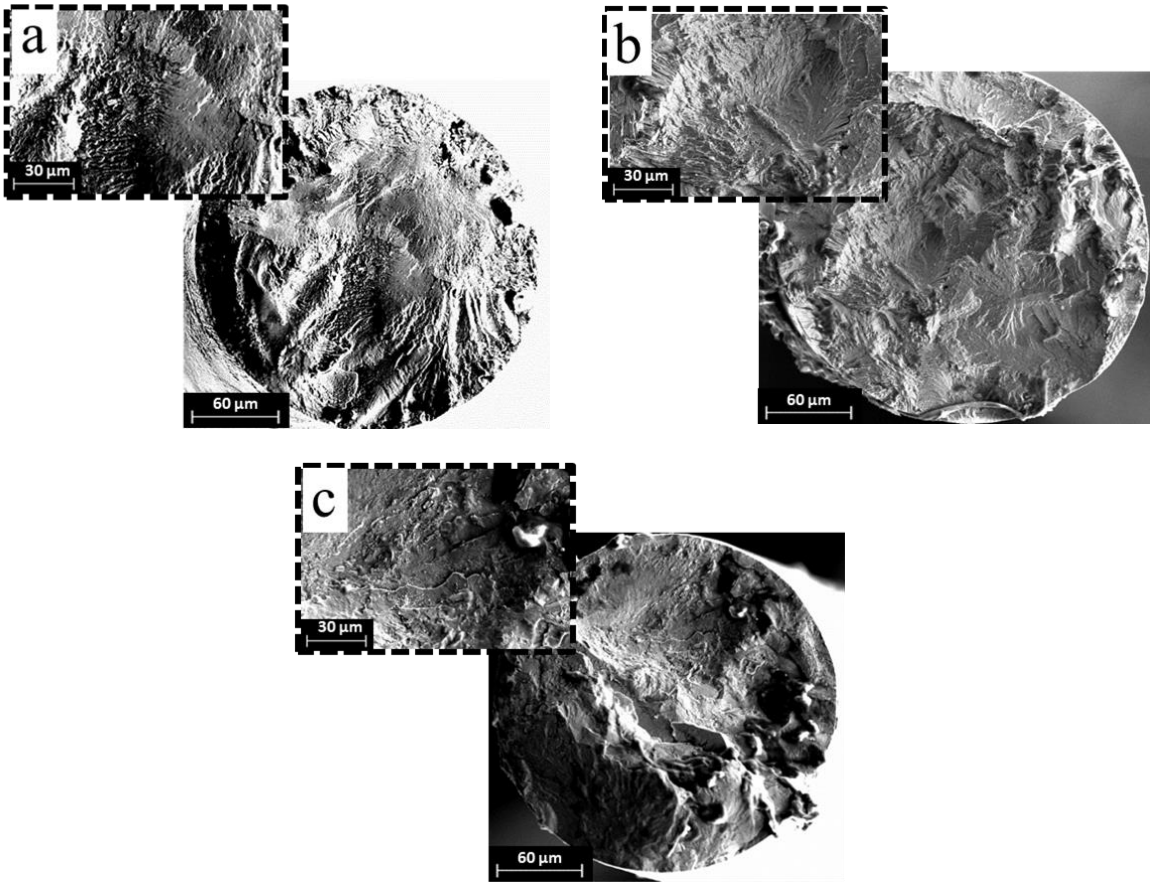

Figure 4-10 Surface Fracture of NiTi/SS Joints in a) centerline condition, b) Ni interlayer and c) laser offsetting welded samples.

4.4 Flow behavior in NiTi/Cu welds

4.4.1 Fusion zone appearance

Figure 4-11 to Figure 4-13 display the cross sections of NiTi/Cu dissimilar joints welded by different laser offset positions and their corresponding elemental distribution map. The weld width decreased when moving the laser position from NiTi to Cu and the mixing pattern inside the FZ changed significantly. The FZ in the NiTi offset and centerline welds (Figure 4-11and Figure 4-12) have uniform element mixing. The Cu offset welds (Figure 4-13) have a complex mixing pattern and elemental distribution, which will be discussed in the next section. Focusing the laser on the NiTi side (Figure 4-11-a) can result in forming of large weld width with 1150µm. As the laser was positioned towards the Cu side of the joint, the weld width decreased to 950µm (Figure 4-12-a), 500µm (Figure 4-13-a), and 375µm (Figure 4-13-e).

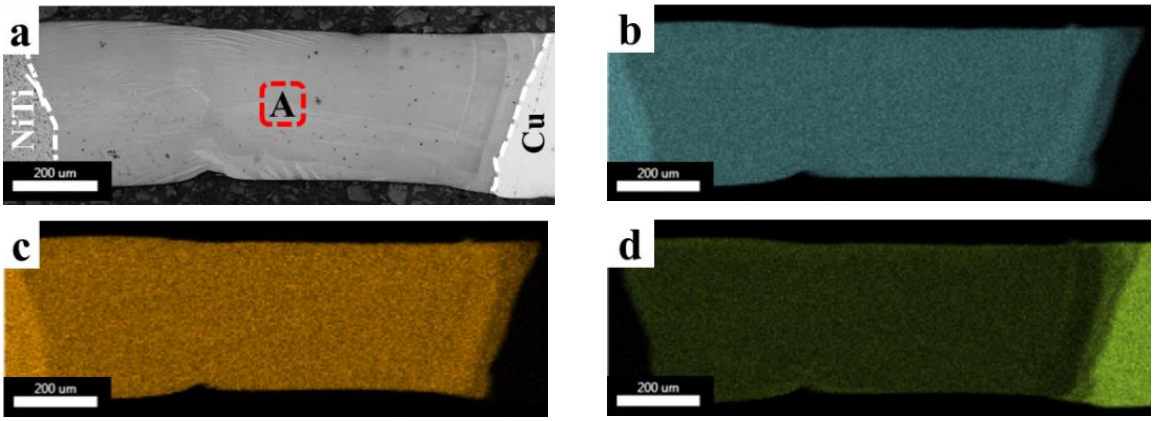

Figure 4-11 FZ microstructure of the laser focused on the NiTi (-50 µm) and its EDS map for b) Ti, c) Ni and d) Cu.

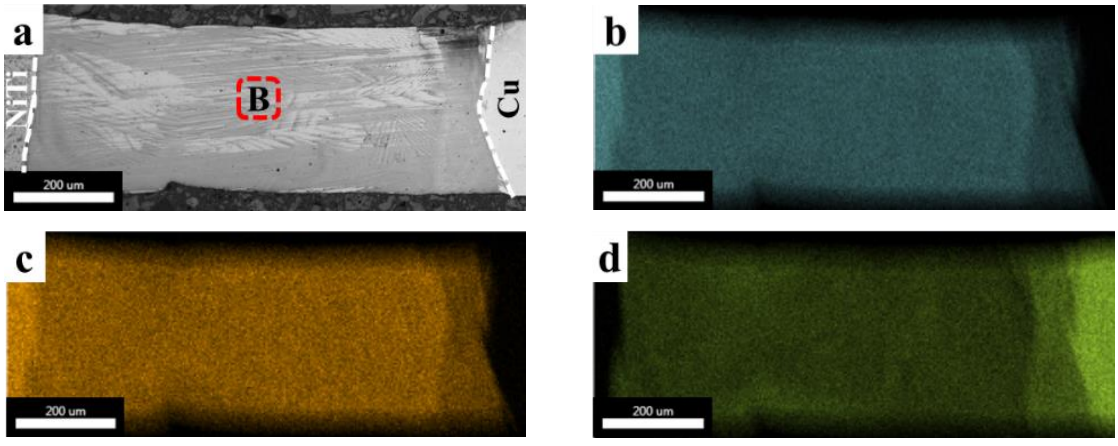

Figure 4-12 FZ microstructure of the laser focused on the centerline and its EDS map for b) Ti, c) Ni and d) Cu.

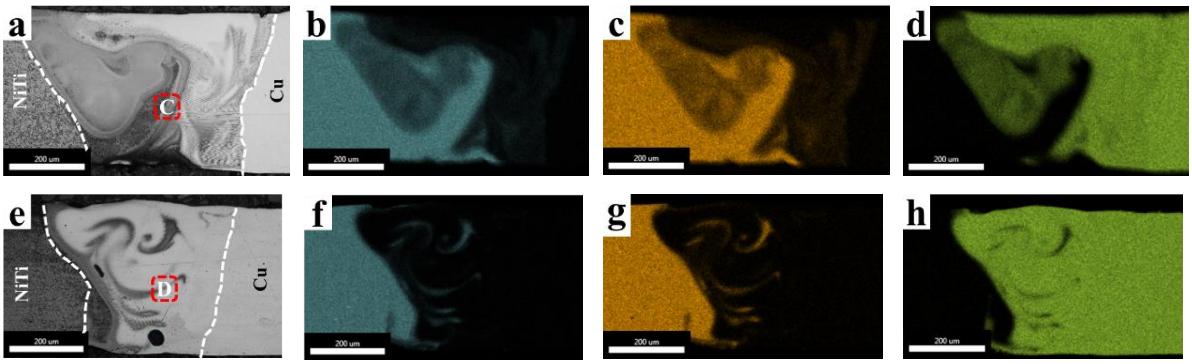

Figure 4-13 FZ microstructure of the laser focused on a) Cu (50 µm) and e) Cu (100 µm) and their EDS elemental map for b and f) Ti, c and g) Ni and d and h) Cu.

It was reported in dissimilar welding of Cu and other alloys that Cu was melted not by the welding heat source, but by heat transfer from the melted dissimilar material [153]. This is due to the high thermal conductivity, higher melting point and expansion coefficients of Cu [153,154]. In the current study NiTi has lower thermal conductivity and laser reflectivity than Cu (Table 4-1), therefore, most of the input energy for melting in joint was through laser absorption of NiTi and heat transferring into Cu. The Cu was melted by the liquid NiTi alloy [97,154]. As the laser offset changed from the NiTi to the Cu side, the energy absorption decreased, leading to a decreased FZ width.

Table 4-1 Thermo-physical properties of experimental materials at room temperature

Metal	Melting point (°C)	Conductivity (W/m ◦C)	Heat capacity (J/(kg ◦C))	Absorptivity with laser (%)
NiTi[17, 29]	1310	10	77	~35
Cu[18]	1083	401	386	3

4.4.2 **Microstructure and phase identification**

Figure 4-14 presents the magnified microstructure inside the FZ in different samples labeled by A, B, C and D in Figure 4-11 to Figure 4-13. The welds with the laser offset onto the NiTi (-50µm in Figure 4-11-a, Figure 4-14-a) and on the centerline (0µm in Figure 4-12-a, Figure 4-14-b) show columnar dendritic microstructures. This dendritic solidification microstructure is formed due to higher mixing of elements inside the FZ [37,97]. The weld with the laser offset onto the Cu exhibits a variety of microstructures with complex elemental mixing patterns (Figure 4-14-c and d). With increasing Cu content in the FZ, cellular and dendritic microstructures can be suppressed [97]. EDS point analysis was performed on the labeled points on different zones (P1 to P6 in Figure 4-14-c and P1 to P7 in Figure 4-14-d) and the results are listed in Table 4-2. The microstructures in region C (Figure 4-14-c) consists of zones I, II and III which are related to gradual changes from dendrites to lamellar

microstructures from left to right. The EDS results (Table 4-2) and Ni-Ti-Cu alloy ternary phase diagrams [156] indicate that NiTi and Ni-Ti IMCs may be present in zone I.

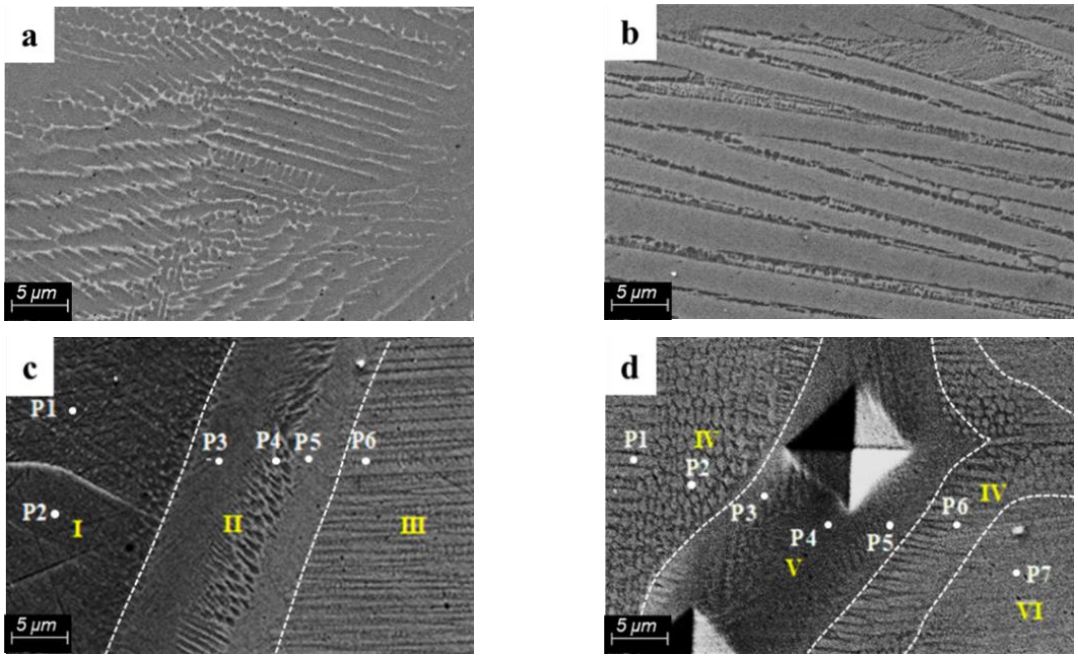

Figure 4-14 FZ microstructures from different welded conditions, laser spots pointed on a) NiTi (-50µm), A in Figure 4-11-a, b) centerline (0µm), B in Figure 4-12-a, c) Cu (50µm), C in Figure 4-13-a and d) Cu (100µm), D in Figure 4-14-a.

Thus, it can be inferred that the re-melting and solidification of NiTi base metal occurred in this region. As previously mentioned in section 4.4.1, Cu has much higher heat conductivity and reflectivity, in addition to a lower melting point. The higher conductivity, melting temperature, and reflectivity of Cu compared to NiTi increased the cooling rate of the weld resulting in the entrapment of NiTi in the FZ with insufficient time for mixing with Cu. In zone II (Figure 4-14-c), the Cu content increased from 22.74 at.% to 68.06 at.% from P3 to P5. The existing phase in this region could be a mixture of $Ni_xTi_yCu_z$ hard and brittle phase, Ni-Ti and Cu-Ti IMCs [157–159]. In zone III, because the Cu content is more than ~80 at.%, there is a potential for dissolution of Ni and Ti in Cu to form a Cu solid solution [160,161]. In the case of the 100µm offset on the Cu side (Figure 4-14-d), chemical compositions of different zones with were characterized (Table 4-2). Pure Cu was detected in the FZ (VI zone) which was not present in the former condition (50µm offset on Cu). The reason for the presence of pure Cu inside the FZ is the fact that the Cu content was greater than the other offset conditions, as well as the high thermal conductivity of Cu and laser rapid cooling rate, leading to an uneven mixing of Cu with the NiTi alloy. The chemical composition of selected points in zones VI and V shows the presence of Cu solid solution and in some extent of Ni-Ti and Cu-Ti IMCs as possible phases [97,158].

Table 4-2 Composition and possible phases in selected points in the FZ shown in Figure 4-14

Samples	Zone		Points	Cu (at.%)	Ni (at.%)	Ti (at.%)	Possible phases [31-35]
NiTi (-50µm)	A		--	21.7	39.1	39.2	NiTiCu matrix and probable $Ni_xTi_yCu_z$ IMCs
Centered (0µm)	B		--	31.4	33.0	35.6	
Cu (50µm)	C	I	P1	0	55.9	44.1	NiTi islands
			P2	0	55.9	44.1	
		II	P3	22.7	41.9	35.4	NiTiCu matrix and probable $Ni_xTi_yCu_z$ IMCs
			P4	52.5	23.8	23.8	
			P5	68.1	15.6	16.4	
		III	P6	80.3	9.5	10.2	Cu solid solution
Cu (100µm)	D	IV	P1	83.6	7.9	8.4	
			P2	75.3	12.2	12.5	
		V	P3	55.5	23.0	21.6	NiTiCu matrix and probable Cu-Ti and $Ni_xTi_yCu_z$ IMCs
			P4	35.4	34.7	29.9	
			P5	42.2	31.2	26.6	
		IV	P6	82.5	8.4	9.2	Cu solid solution
		VI	P7	100	0	0	Pure Cu

To identify the formed phases in the welds, X-ray diffraction (XRD) was adopted. The XRD graph is plotted for all the samples with different laser positions as shown in Figure 4-15. Overall, various phases are formed inside the FZ of each sample mainly consisting of NiTi, pure Cu and equiatomic NiTiCu phase in two different forms (NiTiCu and $Ni_{0.37}Ti_{0.33}Cu_{0.3}$). By positioning the laser position on Cu, a phase consisting mainly of Cu is formed inside the FZ and some NiTiCu phases are present. In the centerline condition and positioning on Ni (-50µm), most of the peaks are related to NiTi and NiTiCu phases which is in good agreement with Table 4-2.

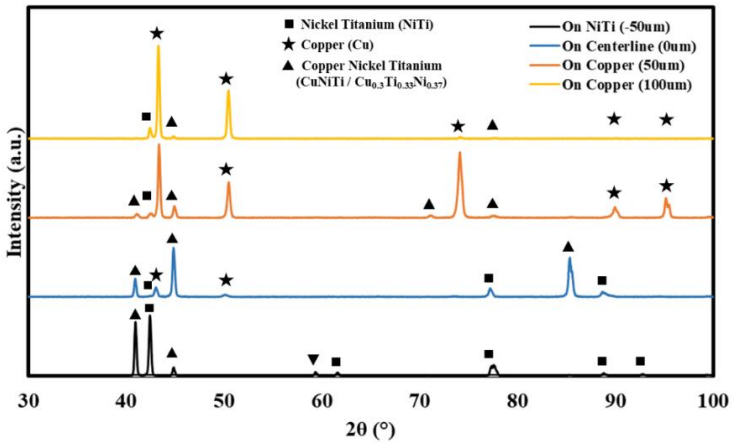

Figure 4-15 XRD of welded samples showing formed phases of the different laser positions on the NiTi/Cu joint.

4.4.3 **Mechanical properties**

Figure 4-16 presents the microhardness profile mapping of dissimilar welded samples with different laser offset. As is observed, the Cu base material has a significantly lower hardness (90HV) than NiTi

base material (~380HV). However, in almost all joints, the FZ has higher values of hardness due to mixing of different elements of the base materials and formation of new phases and hard IMCs (mainly $Ni_xTi_yCu_z$). With changing the offset from NiTi to Cu, the FZ width decreases drastically and therefore the higher hardness region decreases; the NiTi offset condition (Figure 4-16-a), has large and extensive high hardness regions and the Cu offset samples (Figure 4-16-c and d) have very small and narrow high hardness regions in the FZ.

On the other hand, positioning the laser on NiTi or on the centerline resulted in more homogenous FZ both in chemical composition and hardness values as expected from EDS maps (Figure 4-11 to Figure 4-13). Nevertheless, the hardness values inside the FZ in Cu offset samples are uneven and experienced near 80HV to 450HV in some points. Based on EDS maps and point scans, this variation in hardness is pointed to complex mixing patterns of Cu inside Ti and Ni elements which could cause the formation of pure Cu islands (indicated by the color green in Figure 4-13-d and h, Figure 4-16-c and d) in some parts and $Ni_xTi_yCu_z$ intermetallic hard phases (Table 4-2 and red color in Figure 4-16-c and d). It is worth noting that the hardness of pure Cu was measured at 105±4HV, therefore the green area (hardness less than 100HV) is a sign of softness in HAZ of Cu side [162].

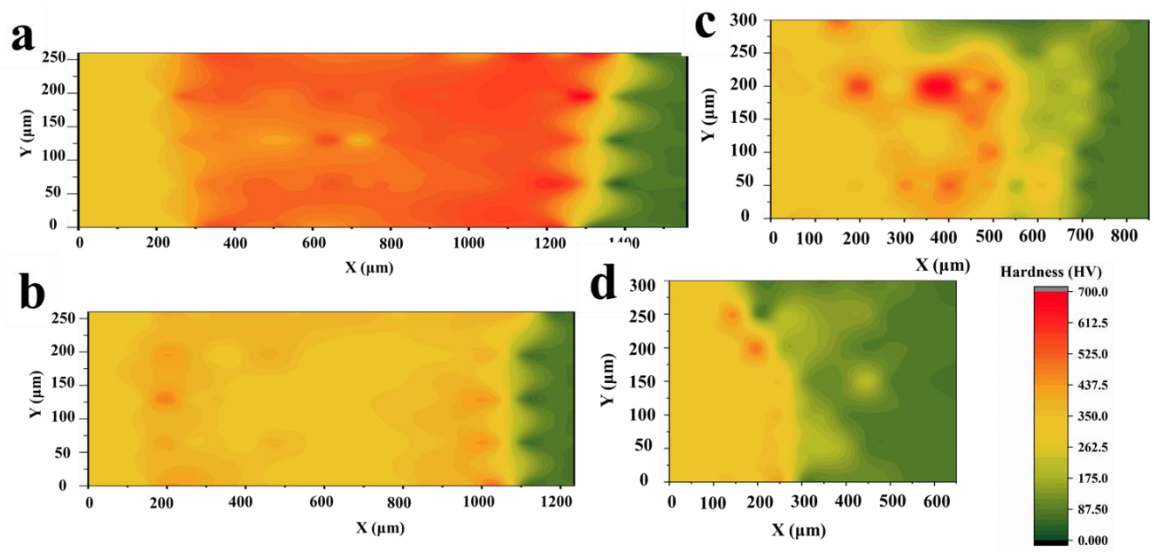

Figure 4-16 Microhardness mapping of NiTi/Cu welded joint offsetting a) 50µm on NiTi, b) on base metals centerline c) 50µm on Cu and d) 100µm on Cu.

To compare the hardness values quantitatively, the average hardness values inside the FZs are depicted in Figure 4-17. It could be observed that with changing of the offset from NiTi (-50µm) to Cu (+100µm), the average hardness values decrease from ~512 HV to ~158HV, respectively. The main reasons for higher hardness in the NiTi offset condition is due to a greater mixing of elements and an

increased possibility of the presence of $Ni_xTi_yCu_z$ which is a hard and brittle phase (especially when z is higher than 10% [157]).

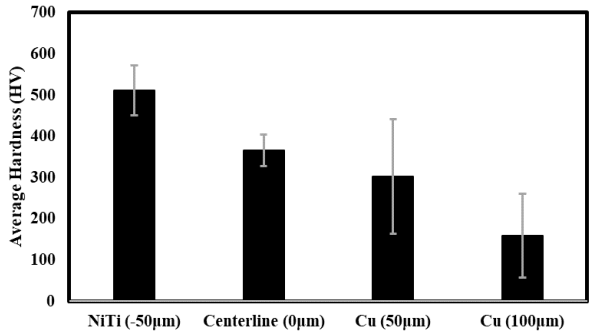

Figure 4-17 Effect of laser position offset on average hardness inside the FZ of NiTi/Cu.

By altering the focus of the laser onto the centerline and then Cu, the FZ had less Ti and more Cu content, which means the probable presence of Cu-Ti IMCs (the softer IMCs) instead of NiTiCu and Ni-Ti IMCs. Thus, it can be considered that the hardness of the FZ decreased with shifting the laser position from the NiTi side to the Cu side, although some local regions in these samples could be found with high hardness values due to Ti-rich and Cu-lean regions.

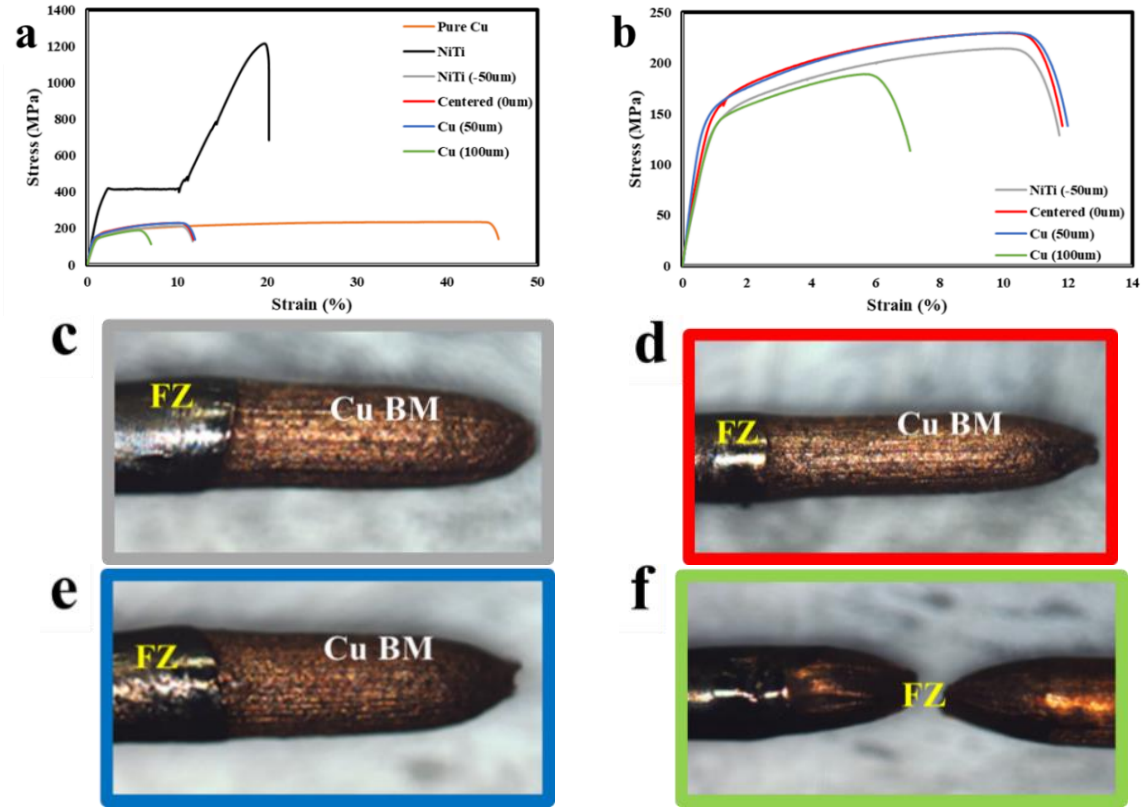

Figure 4-18 a) Stress-strain curves for all samples, b) Stress-Strain curves for welded samples and the corresponding fracture locations for c) Offset on NiTi (-50µm) d) Centerline (0µm) e) 50µm offset on Cu and f) 100µm offset on Cu.

Figure 4-18 shows the stress-strain curves and the locations of failure for all joints. The extracted mechanical properties from these stress-strain curves are shown in Table 4-3. The joints with offset onto the NiTi(-50µm) and the centerline (0µm) had the highest tensile strengths (Figure 4-18-b), and fracture occurred in the Cu heat affected zone (Figure 4-18-c and d). In comparison with these conditions, the tensile strength of the Cu (50µm) offset joint decreased slightly, but with a near similar extension and fracture location (Figure 4-18-e). On the contrary, more offset on Cu (100µm) resulted in a drastic decrease in both the tensile strength (more than 50 MPa) and the extension (6%) (Figure 4-18-b and Table 4-3). It is also visible that the fracture location in the 100µm offset sample changed from the Cu base material to the FZ of the NiTi/Cu joint (Figure 4-18-f).

Table 4-3 Mechanical properties of as received and welded samples extracted from the curves shown in Figure 4-18

Sample	YS (MPa)	UTS (MPa)	Elongation (%)
NiTi	915.1 ± 5.1	1257 ± 4.8	21.8 ± 0.3
Cu	179.1 ± 6.4	245 ± 2.4	47.5 ± 0.4
NiTi (-50µm)	136.8 ± 6	216.9 ± 3.2	11.8 ± 1.5
Centerline (0µm)	155.8 ±7.1	234.7 ± 4.1	12.1 ± 0.8
Cu (50µm)	148.8 ±6.5	229.9 ± 2.4	12.2 ± 1.2
Cu (100µm)	175.6 ± 7.2	175.6 ± 7.8	6.4 ± 1.1

It should be mentioned that compared to the Cu(100µm) joint, the mixing pattern of the Cu(50µm) joint was also not uniform, but the defect-free FZ ensured the properties of the joints and the fracture occurred in the softer Cu base metal. Moreover, as the Cu(100µm) sample absorbed more energy into the Cu side of the joint, the HAZ of the Cu would have larger grain size [162]; thus, the effect of HAZ on the deterioration of the Cu(100) strength should not be neglected.

To have a better understanding of the differences between these fracture locations, fracture surfaces of offset -50µm on NiTi (with failure from the cu base material) and the 100µm Cu joint (failure occurring at the FZ) are depicted in Figure 4-19. The other two samples (centerline and 50µm offset on Cu) have the same mechanical properties (Figure 4-18), the same fracture locations (in Cu base material) and almost the same fracture surface features. The top view and low magnification fracture surfaces of the aforementioned welded samples are depicted in Figure 4-19-a and d. Fracture surfaces of the first three mentioned samples (the candidate is NiTi -50µm in Figure 4-18-c) display many deep and equiaxed dimples in the fiber region, implying ductile fracture in the Cu base material [163,164] (shown in Figure 4-19-b and c). However, with the laser position focused on Cu at 100µm (Figure 4-19-f), the fiber region shrinks (Figure 4-19-d) and tear ridges coexist with decreasing amount of dimples and pores indicating a more brittle nature of this welded sample [163,164]. In it worth mentioning that as seen in Figure 4-19-c some precipitates could cause the dimpling of the samples while in offsetting

condition on Cu (Figure 4-19-f), there is no such precipitates. Based on previous results, the mentioned precipitates might be $Ni_xTi_yCu_z$ IMCs formed in the case of no offsetting or offsetting on NiTi.

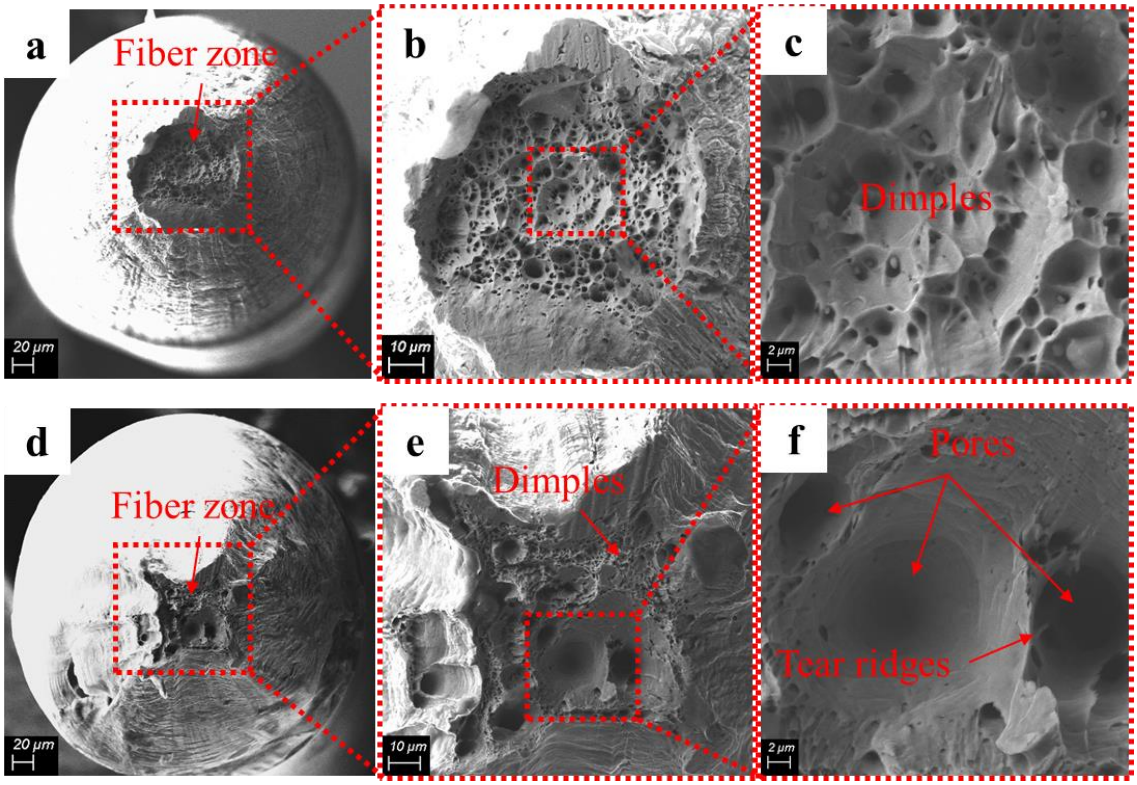

Figure 4-19 Fracture surface morphology of two different offset conditions in NiTi/Cu weld joints a), b) and c) centerline (0µm) and d), e) and f) 100µm on Cu.

The microstructure of the Cu 100µm laser offset contains cracks and pores inside the FZ as shown in Figure 4-20. Some points surrounding these defects were selected for composition analysis using EDS and the results are gathered in Table 4-4. There are sharp gradients in the composition (Table 4-4) for different sides of the crack (P1 and P2 in Figure 4-20), which could indicate that the crack was located at the interface of the Cu solid solution and probably brittle $Ni_xTi_yCu_z$ IMCs.

Previous studies showed that the formation of cracks in dissimilar NiTi welds had been attributed to both solidification cracking and brittle IMCs [36,165]. It should be mentioned that the crack appeared at the interface of Cu-lean (P1 in Figure 4-20-a) and Cu-rich (P2 in Figure 4-20-a) regions. Therefore, due to the formation of these different phases, solidification cracking has great potential to form [37,97]. Additionally, the chemical composition of P1 in Figure 4-20-a has a great potential to form $Ni_xTi_yCu_z$ hard and brittle IMCs and formation of cracks would be inevitable.

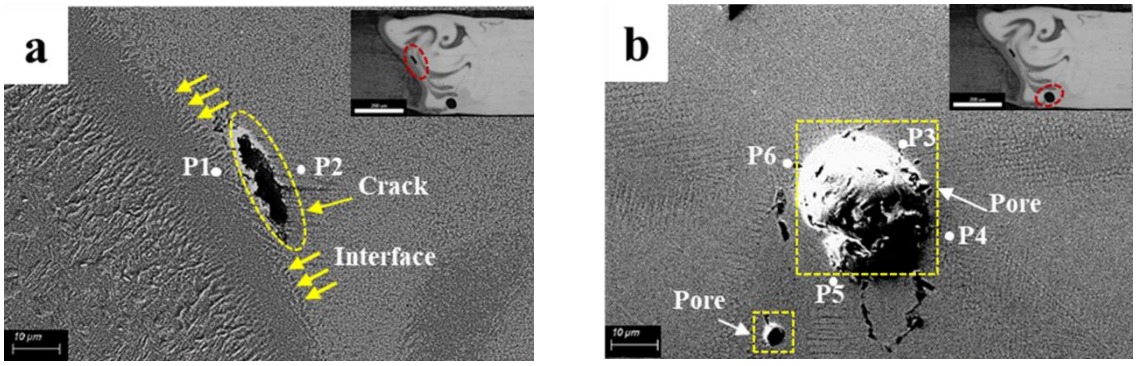

Figure 4-20 Magnified microstructure of Cu (100µm) joints showing a) cracks and b) pores inside the FZ. Different points are indicated for EDS point scan analysis in Table 4-4.

Formation of pores in the Cu offset weld sample (Figure 4-20-b) refers to the high conductivity and fluidity of Cu combined with the short cooling time of the laser process. Therefore, any created bubble inside the welding pool had no time to escape to result in pores during solidification [165]. Consequently, it can be concluded that focusing the laser on Cu increased the potential for the formation of cracks and pores inside the FZ that will deteriorate the mechanical properties of NiTi/Cu dissimilar joints.

Table 4-4 Elemental distribution around cracks and pores in the Cu(100µm) joint in selected points shown in Figure 4-20

Points	Cu (at.%)	Ni (at.%)	Ti (at.%)	Inferred phase [31-35]
P1	39.1	20.7	30.2	NiTiCu matrix with $Ni_xTi_yCu_z$ IMCs
P2	91.1	3.7	5.1	
P3	97.1	2.9	0	
P4	96.8	3.2	0	Cu solid solution
P5	97.6	2.3	0	
P6	93.2	2.4	4.5	

4.5 Summary

The current study surveyed the effect of laser offsetting welding on joint performance of NiTi/stainless steel 316L and NiTi/Cu. The enhancement of the joint performance of NiTi/SS joints was achieved by laser offset welding without using interlayer. By focusing the laser beam on the centerline of NiTi and stainless steel, extensive IMCs (such as Fe_2Ti, Cr_2Ti and Ti_2Ni) formed inside the FZ which caused high hardness because of a uniform distribution of elements. Offsetting the laser beam on stainless steel caused different element distribution and IMCs to form. Therefore, microhardness values are non-uniform and high hardness values are related to higher Ti content and the intermetallic formation inside the FZ. The same phenomena occurred when a 50µm thickness Ni interlayer was used. However, Ni interlayer resulted in many Ni-rich IMCs, such as Fe_3Ni and Ni_3Ti

inside the FZ. Finally, it is reported that offsetting strategy and inserting a Ni interlayer could both increase the mechanical response of the welded samples by suppressing the high hardness regions and extremely brittle intermetallics, changing their distribution inside the FZ and modifying the microstructure.

In the second part of the chapter, NiTi and pure Cu wires were laser welded in butt joint configuration with different laser positioning to understand the effect of laser location on the microstructure and properties of these joints. It is concluded that positioning the laser on the NiTi (50μm) and the centerline (0μm) resulted in a homogenous microstructure including the presence of $Ni_xTi_yCu_z$ IMCs. By changing the position onto the Cu (50μm and 100μm), the microstructure displayed complex flow and mixing patterns containing NiTiCu, pure NiTi, Cu solid solution and pure Cu. XRD measurements confirmed that the amount of NiTi and NiTiCu alloys decreased and pure Cu inside the FZ increased, respectively.

Hardness profile maps showed an increase in hardness with increasing mixing of NiTi and Cu in the FZ of the joints. By positioning the laser on the Cu, soft pure Cu and hard IMCs inside the FZ coexisted with a softened HAZ in the Cu side. However, the average hardness of the FZ varied from ~512 HV to ~158HV by positioning on NiTi and Cu, respectively. Only the 100μm Cu offset joint fractured in the FZ during tensile loading, while the other joints failed in the Cu base material. The 100μm Cu offset joint contained inhomogeneous microstructures, composition distributions, cracks, and pores. Therefore, it was acceptable to weld NiTi and Cu wires with a 0~50μm laser offset on the NiTi side.

Although the mechanical properties of dissimilar laser welds of NiTi to SS and Cu can be enhanced by changing the IMCs contents and flow behavior in FZ, another issue related to these dissimilar welds is the losing of their superelasticity. In the next chapter, the dissimilar laser welding of NiTi to PtIr based on the previous knowledge will be studied and the possibility of perseverance of superelasticity of NiTi in the NiTi/PtIr welds will be discussed.

Chapter 5 Laser microwelding of NiTi to PtIr[1]

5.1 Introduction

In the previous chapter, the dissimilar laser welding of NiTi to SS and Cu could be improved by adopting some techniques such as inserting interlayers and offsetting laser strategy. However, even in the modified scenario, the laser welded material could not preserve the functional properties of NiTi due to insufficient strength in the welded material. In this chapter, the laser welding of another biomedical couple, NiTi to PtIr has been surveyed.

NiTi has a wide range of applications in biomedical devices such as guidewires, stents and orthodontic archwires [5,166,167]. On the other hand, Pt-based alloys have been traditionally employed in the medical industry as electrical terminals and electrodes owing to its excellent electrical conductivity, X-ray visibility, excellent corrosion resistance and biocompatibility [168]. Nevertheless, some medical devices have complexity in design and dissimilar joining of biomaterials is not only a good solution to overcome this challenge but also allows to combine properties of the two base materials. For instance, PtIr has been used as electrode terminals in pacemakers while the interconnecting wires were made of NiTi [169]. Since NiTi stents have poor visibility under X-ray fluoroscopy, Pt-based alloys have been welded to NiTi which act as a marker for NiTi guidewires [124].

Dissimilar laser welding of PtIr is limited to joining with Ti-based alloys and stainless steels. It is reported that by increasing the laser pulse energy, dilution of Ti inside the FZ increases and Ti_3Pt and TiPt hard and brittle phases can be formed, promoting the formation of microcracks [168]. During microwelding of PtIr and stainless steel wires, selecting the optimum peak power resulted in achieving 90% of the PtIr base material tensile strength [170]. However, the preservation of superelasticity dissimilar laser welding of NiTi to other relevant engineering materials is still needed [55]. In this chapter, the microstructural and mechanical properties of dissimilar laser welded joints of NiTi to PtIr has been studied by optimizing the welding parameters.

It shows that by process optimization, it was possible to control the formation of the B2 NiTiPt, with no IMCs being formed. The NiTiPt phase inside the fusion zone had a strong metallurgical bonding with the NiTi base material due to the smooth transition of its grain orientation towards <111> B2 NiTi. The major finding of the present work is the preservation of the NiTi superelastic response in the welded

[1] The results of these chapter are published in a journal paper: 1- Shamsolhodaei, Amirali, et al. Materialia 16 (2021): 101090.

joint as evidenced by the load/unloading cycling up to 6 % strain, significantly higher than typically required for biomedical applications.

5.2 Experimental Procedure

The materials used in this study were a 50.2 at% Ni-rich NiTi and Pt-10at%Ir wires both with a diameter of 380 μm. The nominal laser spot size was 400μm and a square shaped temporal laser profile with a 0.15 kW peak power and pulse duration of 20 ms was selected. These laser parameters were reported as an optimum condition for achieving full penetration condition, while still minimizing the Ni evaporation for the same NiTi wire [84]. Microstructural observations and chemical composition analysis were conducted using a Zeiss Ultra Plus field emission scanning electron microscope (SEM) equipped with Energy dispersive spectroscopy (EDS). Detailed analysis of the grain structure, texture and phase map analysis was performed by electron backscatter diffraction (EBSD) using JEOL JSM 7000 FESEM. The step size for the EBSD measurements were 1 and 0.2 μm, using a working distance of 15 mm and an accelerating voltage of 20 kV. Data acquisition and post processing of the collected EBSD raw data was executed by Aztec and HKL channel 5 software, respectively.

Scanning transmission electron microscopy (STEM) images and electron diffraction patterns were acquired on a FEI Tecnai G2 F20 microscope at 200 kV. EDS analyses were obtained using an EDAX super ultra-thin window (SUTW) X-ray detector. Quantification was performed using the Pt M_α, Ti K_α and Ni K_α signals with FEI TEM Imaging and Analysis (TIA) software. Phase identification has been done via synchrotron X-ray diffraction using a 2D Perkin Elmer detector. A 200×200μm pixel size of a detector with a measured accuracy of $2\theta = 0.0084°$ was used. The raw data images were treated using Fit2D [171] using the procedure described in [24]. In this study, the probing line started from NiTi BM and ended in PtIr BM perpendicular to the weld area. The distance between consecutive probed regions was of 50 μm, while the X-ray beam size was of 50×50 μm.

Vickers microhardness testing was conducted to make a series of 50 g indents with a distance of 50 μm between each indent vertically and horizontally with 10 s for holding time using a CMT Clemex automated hardness tester according to ASTM E384. The strength of the welded samples measured by adopting an Instron 5548 micro tester at a gauge length of 15 mm which includes the fusion zone, the heat affected zones and the BMs. All tensile tests were performed at room temperature and at a strain rate of 3×10^{-4} s^{-1} and three samples for the selected welding condition were tested. To evaluate superelasticity and residual strain upon each full load/unload cycle, cyclic tests performed at room temperature up to a maximum strain of 6% before unloading to a zero stress condition. The cyclic tests

for the welded samples were continued until fracture occurred and to differentiate the BMs effect on cyclic response, both BMs were also tested for a total of 50 cycles.

5.3 Results and Discussion

5.3.1 Microstructure and phase of welds

The microstructure of NiTi/PtIr laser butt weld joint is depicted in in Figure 5-1. The NiTi BM (left side), the PtIr BM (on the right side) and the FZ can be clearly observed in Figure 5-1-a. There were not any visible cracks or detectable gas porosity inside the FZ and a full penetration condition was achieved. The presence of relatively high-density elements (Pt, Ir) and the high heating and cooling rates during the laser welding cause Marangoni currents resulting in a visible mixing pattern inside the FZ. The BMs/FZ interfaces are selected in Figure 5-1-a and b (blue and red boxes) and have been magnified to have better understanding of the microstructure evolution in Figure 5-1-b and c.

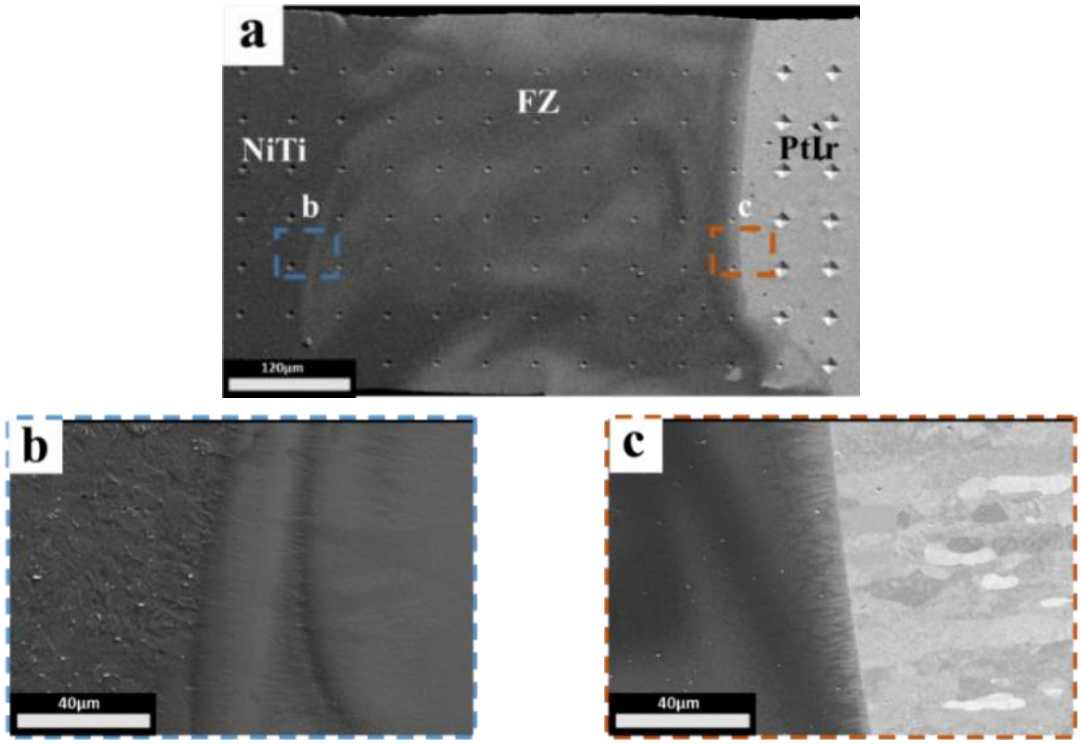

Figure 5-1 Microstructure of NiTi/PtIr welded sample shows a) the whole cross section microstructure, b) interface of NiTi/FZ and c) interface of PtIr/FZ.

In the adjacent of NiTi/FZ interface (Figure 5-1-b), the grain growth of the NiTi heat affected zone is visible and the grains are connected to the epitaxial grains of the fusion zone. This phenomenon can also be seen at the PtIr/FZ interface (Figure 5-1-c). It should be mentioned that the thermal conductivity

of PtIr (31 $W.m^{-1}K^{-1}$) is higher than that of NiTi (10 $W.m^{-1}K^{-1}$), therefore it is expected that cellular and planar structures in the PtIr side become thinner in comparison to those of the NiTi side.

Figure 5-2 shows the elemental distribution inside the FZ and across the dissimilar interfaces. The line scan was performed from the NiTi to the PtIr base materials on the marked green line seen in Figure 5-2-a. The concentration of Pt inside the FZ is less than 15at. % all over the analyzed line; while inside the FZ/PtIr interface the amount of Pt reaches higher values (up to 40 at. %). To understand the overall distribution of Pt inside the FZ, EDS mapping was performed as shown in Figure 5-2-b and Figure 5-2-c. This EDS map reveals that, the Pt content is very low (Figure 5-2-c) in comparison to the Ni content (Figure 5-2-b).

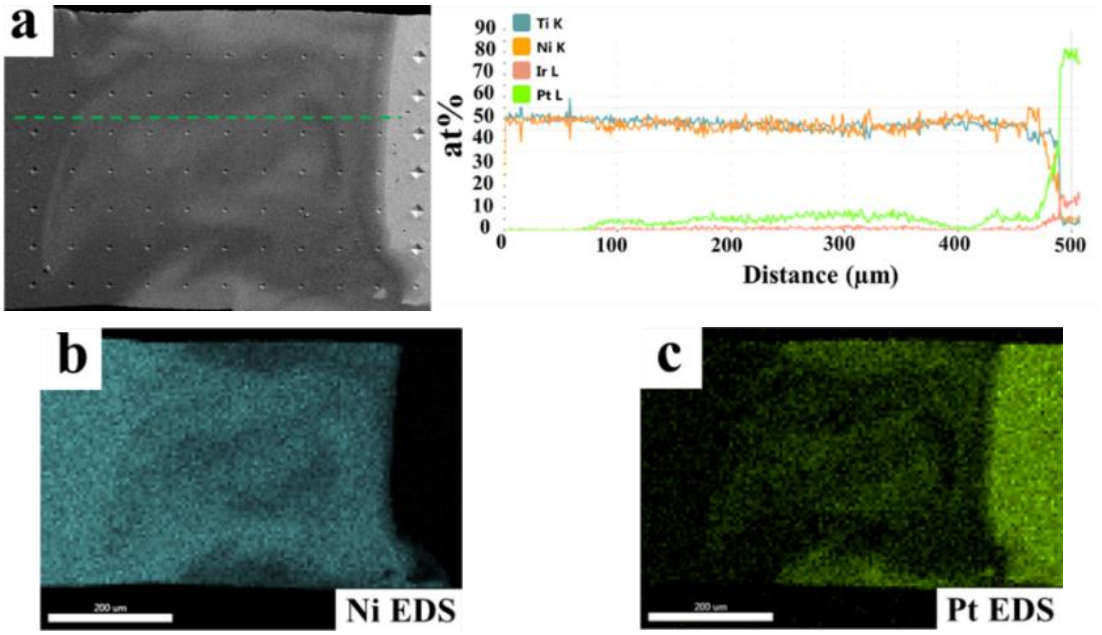

Figure 5-2 The EDS scan of FZ showing a) line scan showing elements variation b) Ni map and c) Pt map.

The reason for lower dilution of Pt and Ir inside the FZ is related to the higher melting point of PtIr (about 1800º) and higher laser reflectivity of PtIr (near 80% at room temperature) when compared to NiTi (1310ºC and 60% at room temperature, respectively). Therefore, during laser welding of these materials, a lower amount of PtIr was melted and diluted inside the FZ, resulting in the composition of Pt not exceeding 20at.% [172,173]. The elemental distribution is not homogenous inside the FZ due to incomplete mixing as a result of the short duration of the laser pulse, and the different densities of the alloys (6.45 g / cm^3 for NiTi vs 21.56 g / cm^3 for PtIr) [55,103]. This swirling pattern inside the FZ has brighter areas which corresponds to higher Pt/Ir content, while the darker areas correspond to a higher concentration of Ni/Ti. These variations are visible in EDS line and maps depicted in Figure 5-2.

To see the details of grain structure and possible precipitation in the welded sample, TEM analysis was performed (refer to Figure 5-3). The NiTi BM contains the B2 austenite phase (confirmed with a selected area diffraction, SAD, pattern) with equiaxed nanosized grains (Figure 5-3-a) due to prior cold drawing and annealing process. In the FZ, relatively large grains with the B2 NiTiPt crystal structure (indexed with a SAD pattern) were observed, and dislocations pile up (labelled by black arrows in Figure 5-3-b) are depicted. This is an example of substructured grains which will be discussed in IPF images in Figure 5-5-c. They are related to some distortion in NiTi crystal structure due to dissolution of relatively high amount of Pt entrapped in the B2 crystal structure. In other parts of the FZ, nanoscale precipitates can be observed in the grain boundaries of the NiTiPt phase (Figure 5-3-c). Chemical analysis of this precipitate is shown in Figure 5-3-c. The precipitate has more than 40 at. % Pt and has less than 20 at. % Ni. Therefore, this phase is related to (Ni+Pt)-rich precipitates which were reported in a previous study of NiTiPt ternary alloys [174].

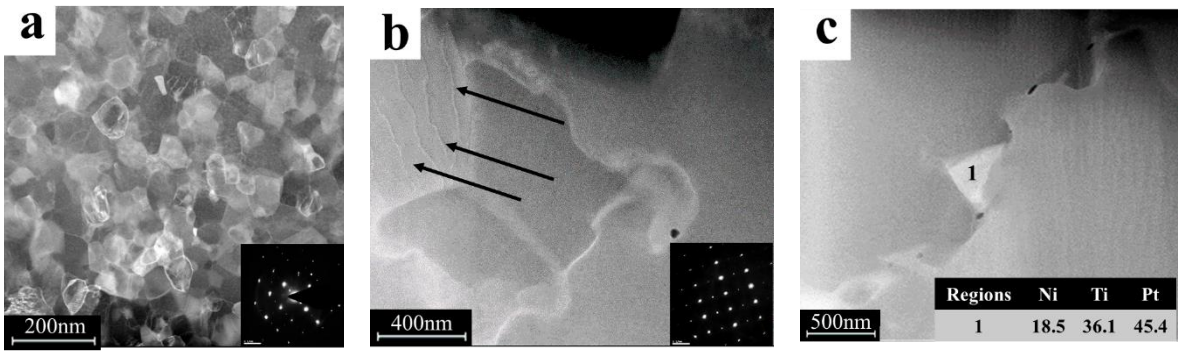

Figure 5-3 TEM images of different region of NiTi/PtIr welded sample showing the grain structure a) in NiTi BM/HAZ b) inside the FZ near to NiTi containing some dislocations (labelled by arrows) and c) in the center of the FZ and chemical composition (per at%) in selected regions labelled by numbers.

Figure 5-4 illustrates the superimposition of the synchrotron X-ray diffraction patterns from one base material to the other passing through the fusion and heat affected zones. As is seen in Figure 5-4-a, the series of peaks related to NiTi BM and PtIr BM were detected and there are some microstructural changes inside the FZ. For the sake of clarity, the indexed phases from each region (NiTi BM, FZ and PtIr BM) are shown in Figure 5-4-b to Figure 5-4-d. All diffraction peaks in the NiTi BM corresponding to the B2 austenitic phase (Figure 5-4-b) while on the PtIr BM only diffraction peaks corresponding to the cubic PtIr phase are observed (Figure 5-4-c). Inside the FZ (Figure 5-4-d), multiple diffraction peaks corresponding to both austenite and martensite phase of NiTi as well as PtIr and NiTiPt are observed. It seems that Ni vaporization shifts the transformation temperatures to higher value, promoting the formation of martensite inside the FZ [175,176]. On the other hand, the dilution of Pt inside the FZ

promoted the formation of ternary NiTiPt with the same crystal structure, but different lattice parameters, of NiTi B2 austenite. It should be mentioned that, since the concentration of Pt inside the FZ was low, there were no detectable IMC compounds inside the FZ.

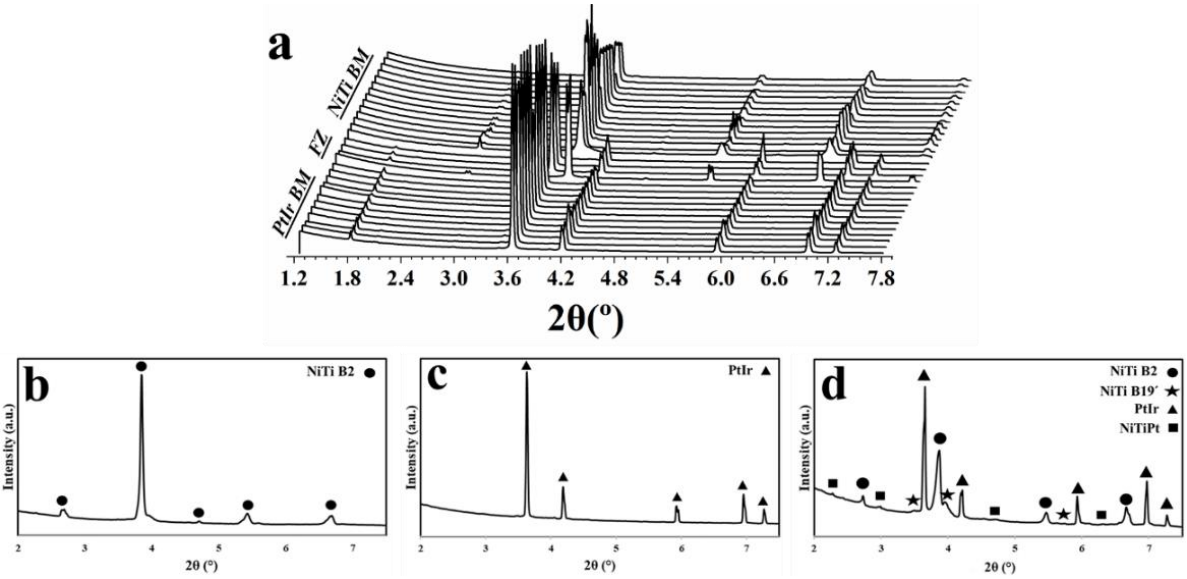

Figure 5-4 superimposition of synchrotron XRD for the welded sample showing a) whole sample consisting of FZ and both BM, b) NiTi BM, c) PtIr BM and d) FZ.

5.3.2 **Grain orientations and texture**

The inverse pole figure (IPF) images of the grain structure and grain orientation distribution across the FZ and BMs are depicted in Figure 5-5. The NiTi BM (left side in Figure 5-5) was previously cold drawn and annealed, therefore most of its grains were rotated toward the <111> direction in order to enhance the alloy superelastic properties [14]. The PtIr BM was also cold drawn and annealed and most of its grains are distributed toward <111> and <100>. By entering to the FZ, the epitaxial structure is clearly seen at both interfaces with the BMs. However, these structures are smaller in size at the PtIr interface due to the higher thermal conductivity of the PtIr alloy in comparison to NiTi. In the central region of the FZ, the existing different colors of the grains indicate the formation of a random texture inside the FZ, which is also presented in the IPF triangle.

Nevertheless, the important issue here is the way of transition of grain orientations from random texture toward the predominant texture of the BMs [177]. From NiTi BM side toward FZ the grain orientation (IPF images in Figure 5-5) is gradually changed and the interface of NiTi/FZ exhibits almost the same orientation of NiTi BM. On the contrary, the interface of FZ/PtIr has great variation of grain

orientation in comparison with FZ and PtIr BM. The reason behind these variations and their consequences will be discussed later.

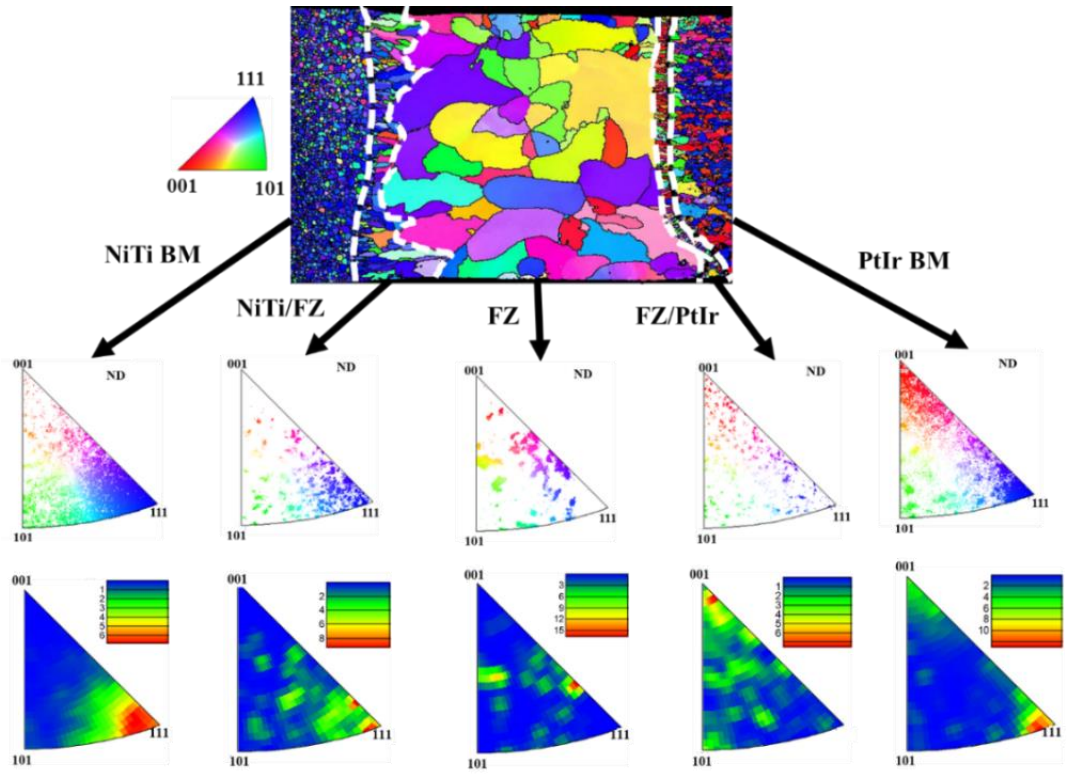

Figure 5-5 Microstructure, grain orientation distribution and IPF maps of different regions (NiTi BM, NiTi/FZ interface, FZ, FZ/PtIr BM and PtIr BM) of butt weld NiTi-PtIr joint.

The EBSD phase map, Kernel Average Misorientation (KAM) map and the fraction of recrystallized grains of the joint are depicted in Figure 5-6. The phase map (Figure 5-6.a) indicates that the FZ is indexed as a NiTi B2 crystal structure as well as in NiTi BM which was also confirmed previously in the SXRD experiments (Figure 5-4). The reason behind the indexing FZ with B2 crystal structure is the fact that NiTi can dissolve up to 20 at.% of Pt without changing its crystal structure [178]. The Pt concentration across the FZ (except at FZ/PtIr interface) is lower than 15 at.%. The PtIr BM is indexed with as FCC structure as labeled in red in the EBSD phase map (right side in Figure 5-6-a). KAM is the measurement of the misorientation of every single point of the map related to its neighboring point and is observed in Figure 5-6-b. As was shown in Figure 5-5, both BMs contained small grain size and therefore their local misorientation is not negligible. However, the melted and solidified FZ has low value of KAM as blue color indicated in Figure 5-6-b. It should be also pointed out that the smooth distribution change of KAM values between FZ and BM is an indication of lower amount of residual

strain [179,180] as is observed here between NiTi BM and FZ. This transition between FZ and PtIr BM shows the presence of residual strain at this interface after welding. Figure 5-6-c depicts the degree of recrystallization of the grains inside the FZ and in both BMs. As mentioned, the BMs were in the cold drawn and annealed condition. Therefore, the mixture of deformed and recrystallized grains could be detected in NiTi and PtIr BMs. However, after laser welding, the FZ consisted mostly of substructured (in yellow color) and recrystallized grains (in blue color). The presence of some substructured grains inside the FZ was due to the higher amount of Pt (based on EDS map in Figure 5-2.c). As detailed in section5.3.1, Pt can dissolve into the NiTi crystal structure and change its lattice structure, therefore the corresponding formed grains could be indexed as substructured grains due to the presence of dislocations caused substructured grain evolution [181,182].

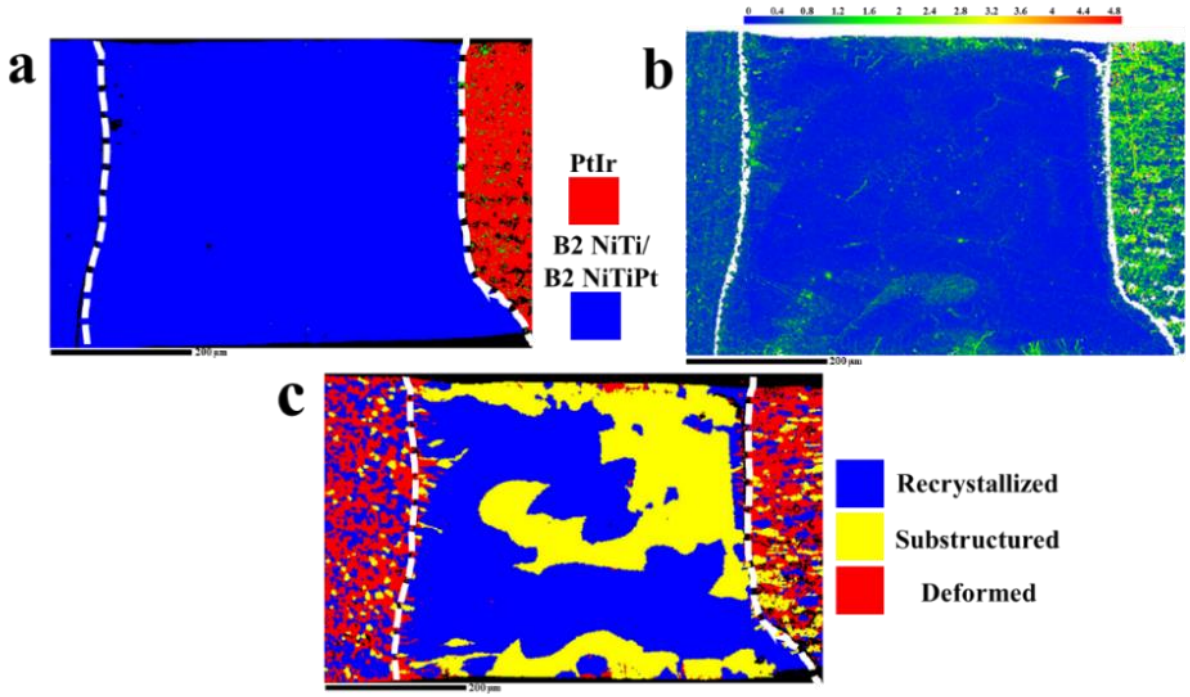

Figure 5-6 EBSD images of welded sample showing a) IPF image in the tensile direction b) corresponded phase map and c) recrystallized, substructured and deformed grains.

The high magnified EBSD images in the interface of FZ and both BMs are depicted in Figure 5-7. The IPF image of NiTi/FZ interface shows epitaxial grains and this kind of growth is visible by maintaining the orientation of the HAZ grain structure (toward <111>) at the mentioned interface. This behavior occurs due to a crystal structure matching between the BM and FZ [20] and in the present study both of these regions were indexed with a B2 crystal structure as seen in Figure 5-7-b. At the PtIr/FZ interface (Figure 5-7-c), there are also epitaxial grains, however the grain orientation of FZ and

HAZ of PtIr are not the same. Based on Figure 5-7-d, there is a thin layer of NiTiPt with B19 orthorhombic crystal structure between the B2 FZ and FCC PtIr BM. This phase is formed when the concentration of Pt inside NiTi surpasses 20 at. % [183].

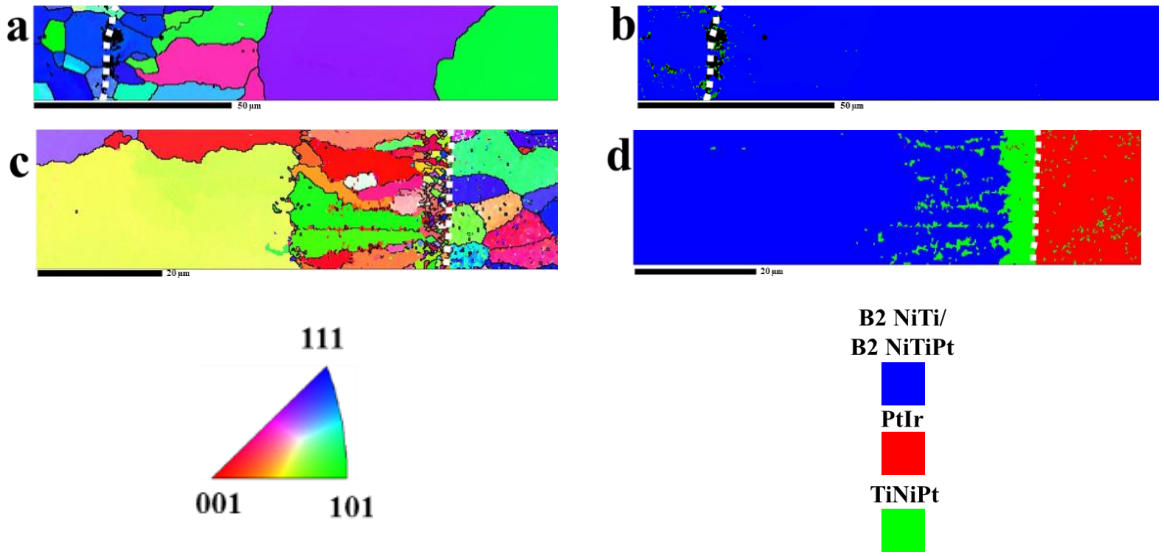

Figure 5-7 The EBSD images at the interfaces of FZ and BMs shows a) IPF image and b) phase map of NiTi/FZ interface and c) the IPF image and d) the phase map of PtIr/FZ interface.

5.3.3 **Mechanical Properties**

The joint microhardness map is depicted in Figure 5-8. In Figure 5-8-a, the hardness profile map is superimposed with an actual image of the FZ microstructure after indentation. The variation of hardness inside the FZ (Figure 5-8-a) is in good agreement with the variation of the Pt concentration as depicted in Figure 5-2-c. That is to say that the higher amount of Pt inside NiTi and, therefore, more dilution of Pt can promote an increase in hardness due to solid solution strengthening mechanism as well as precipitation hardening owing to mentioned NiTiPt precipitates.

This hardness increase is further evidenced in profile lines from show in Figure 5-8.b. It has been reported that NiTiPt alloys can present high hardness due to solid solution hardening for high Pt contents (typically above 10 at. %) and the elemental variation of Pt strongly affects the alloy hardness. However, with further increasing of the Pt concentration rather than solid solution hardening second phases can form in order to maintain the stoichiometry of NiTiPt phase [174]. This correlates with the higher hardness in the region adjacent to the PtIr/FZ interface (Figure 5-8-b), where the Pt content is at a maximum level. Another important observation in the line profile hardness in Figure 5-8-b is the slight decreasing in hardness in the HAZ of NiTi and PtIr due to grain coarsening.

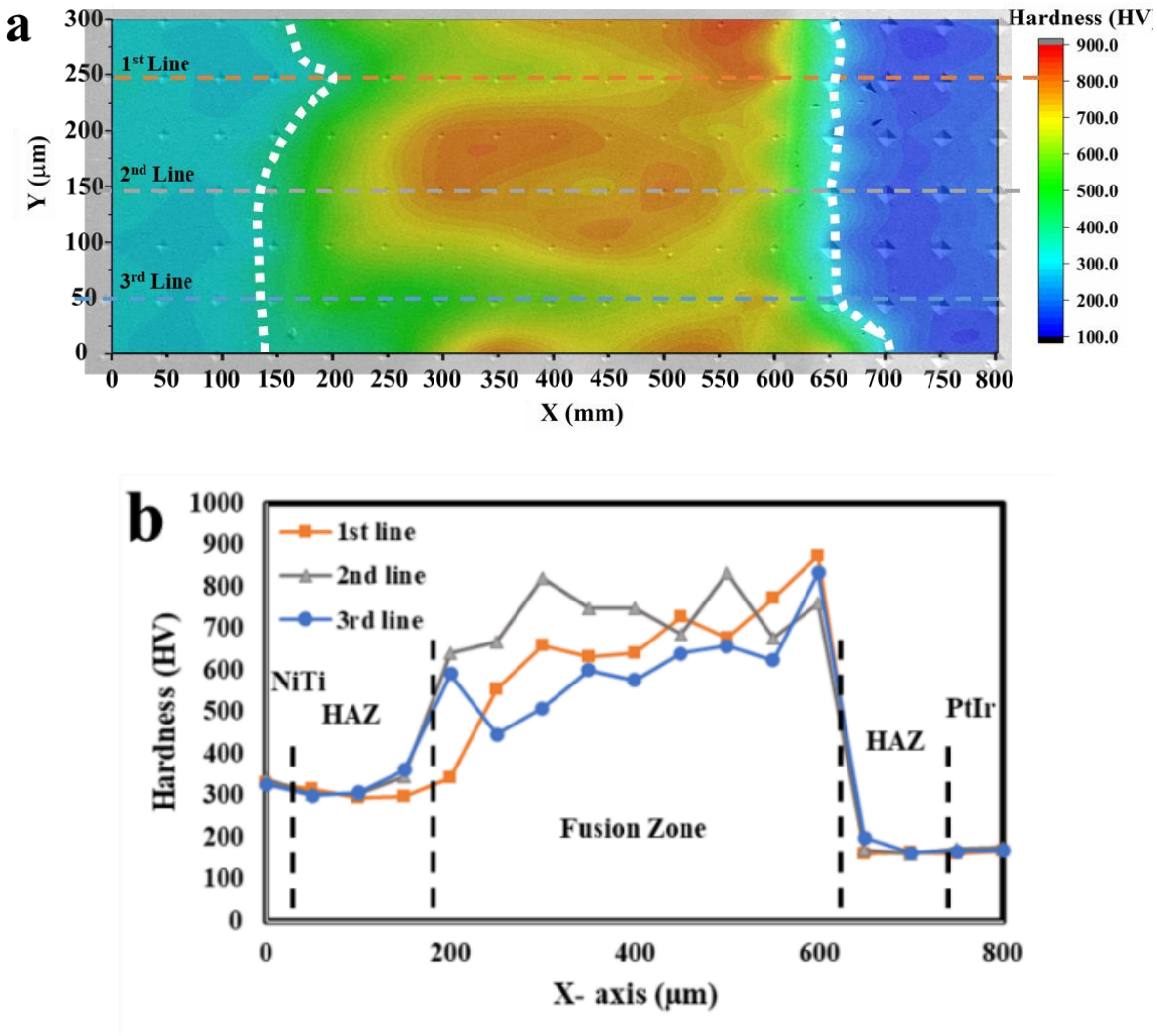

Figure 5-8 Microhardness evaluation of NiTi/PtIr laser dissimilar welds showing a) microhardness map and b) line profile hardness in 3 selected lines marked in Figure 5-3-a.

Figure 5-9-a shows the stress-strain response of both the BMs wires and the welded sample during uniaxial tensile tests. The NiTi BM shows a constant stress plateau condition up to 10% strain and fracture at 25% strain, whereas the annealed PtIr shows little strain hardening after yielding and fractured at around 12% strain. The welded sample fractured after an external imposed strain of 7% after a semi plateau region at a higher stress level than the stress plateau region of NiTi. In a higher magnification, a kink is visible before reaching to load-free condition which could be related to existence of residual stresses within the HAZ and/or FZ of the welded sample [23].

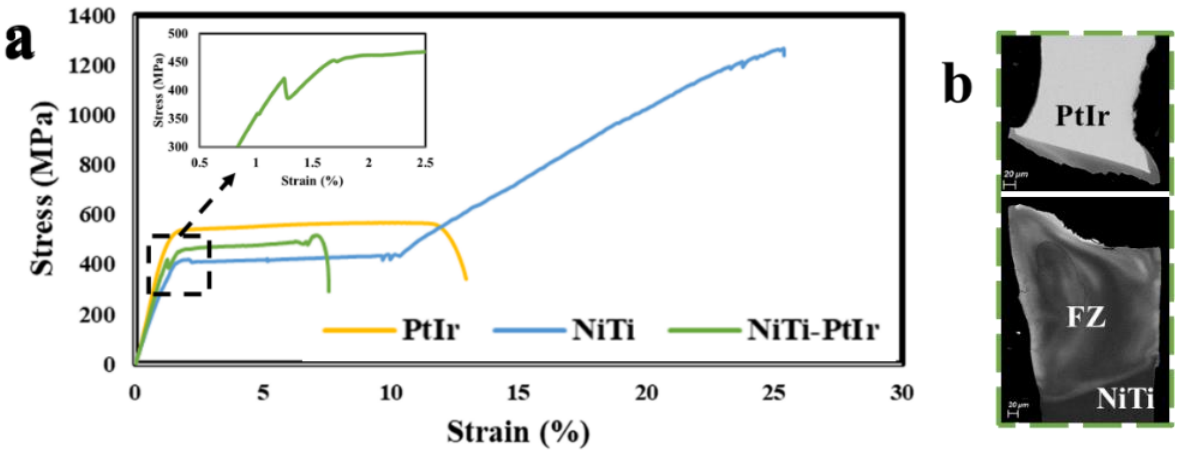

Figure 5-9 a) Stress-strain curve of two BMs and dissimilar welds between NiTi/PtIr joint and b) the cross section of fractured welded sample after tensile test.

The welded joint fractured at the PtIr/FZ interface as displayed in Figure 5-9-b. This can be attributed to the fact that the NiTi/FZ interface has an epitaxial growth and the same texture as the adjacent NiTi HAZ (Figure 5-6), leading a strong metallurgical bonding since epitaxial growth the molten material inside the FZ through solidifying from the lattice site of the NiTi BM. However, in the PtIr/FZ there is a crystal structure mismatch between PtIr and the FZ and higher concentration of residual strain (based on KAM in Figure 5-6-b) resulting in a weaker metallurgical bonding. It should be mentioned that, since the welded sample evidences a semi-plateau stress region in the stress-strain curve during loading, this dissimilar joint possibility exhibits superelastic response.

5.3.4 **Cyclic Response**

Based on the observation in Figure 5-9-a, it is worthwhile to examine the potential existence of superelasticity in NiTi/PtIr dissimilar joint. In this regard, cyclic tests were performed on both BMs and the dissimilar joint up to 6% (before fracture of welded sample) to differentiate the possible superelastic response. As expected, the NiTi BM wire (Figure 5-10-a) displayed almost full recovery and reached to a saturated condition of superelasticity after multiple cycles. Also, the PtIr had no recoverable strain and yielded around 1.5% strain (Figure 5-10-b). However, the welded sample showed superelastic response (Figure 5-10-c) with a residual strain of around 0.5% after a first cycle and this cyclic behavior is comparable to that of NiTi similar joints obtained by laser welding [84].

The cyclic load-unload test of the welded sample continued until fracture occurred after 263 cycles which is a great achievement in dissimilar laser welding of NiTi shape memory alloys. As observed in Figure 5-10-d after 263 cycles the welded sample almost reached to a saturated strain of 1.2%, which is the double of that obtained for the NiTi BM (0.6%). This means that the dissimilar laser welding of

NiTi/PtIr could preserve the superelasticity of NiTi shape memory alloy BM to a great extent. Except for the increase in residual strain, the cyclic response characteristics of the welded joints are similar to that of the NiTi BM and in both cases the stress plateau level decreased with increasing the number of cycles. Therefore, it could be concluded that with achieving acceptable strength in the welded sample the NiTi BM could preserve its functional behavior. The increase in the residual strain is a direct consequence of the large and recrystallized grains inside the FZ, as well as the contribution of the PtIr BM to the irrecoverable strain in the first load/unload cycle.

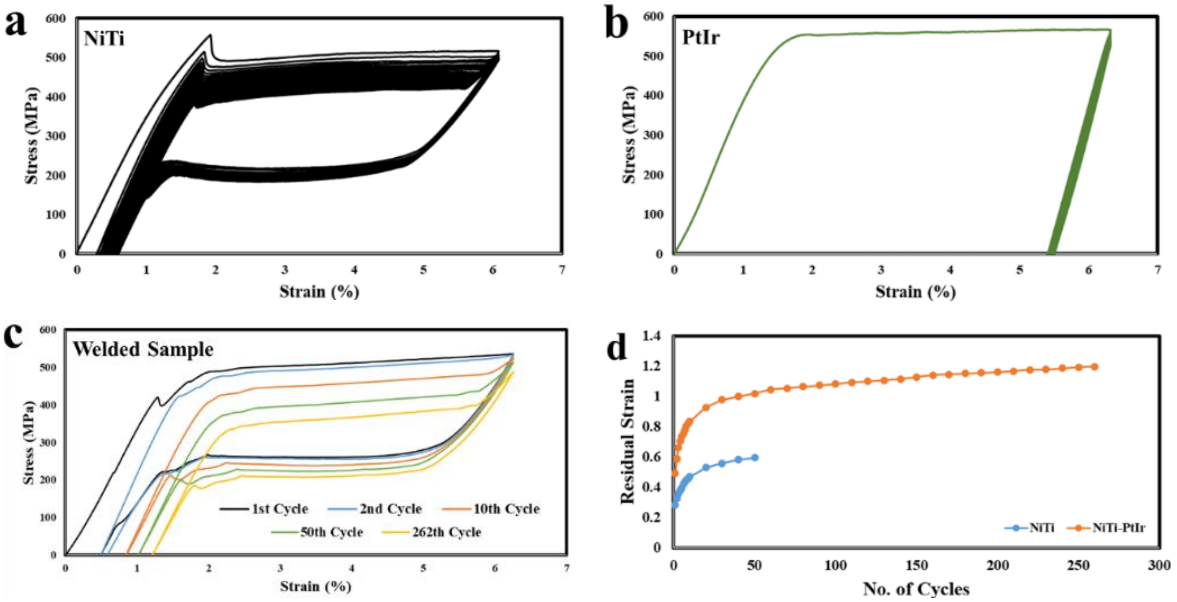

Figure 5-10 Cyclic response of a) NiTi BM, b) PtIr BM, c) NiTi/PtIr welds up to 263 cycles where 1st, 2nd, 10th, 50th and last cycles are selected and d) residual strain of NiTi BM and NiTi/PtIr welds after cyclic tests.

Fracture surfaces of NiTi/PtIr dissimilar joint on both NiTi BM and PtIr BM sides were observed after the tensile test and cycling test. As mentioned in section 5.3.3, the welded sample fractured at the interface of PtIr/FZ because the residual strain and the weak metallurgical bonding. Based on Figure 5-9-b, the fracture occurred after necking indicating ductile fracture. It is in good agreement with Figure 5-11-a and b where dimples are visible. However, in the PtIr side (Figure 5-11-b) some tear ridges are also due to brittle fracture. After cyclic test up to 263 and subsequent fracture (Figure 5-11-c and d), the tear dimples became smaller and changed to microvoids suggesting a ductile-like fracture while a quasi-cleavage fracture mode is also visible in the adjacent region (right side of Figure 5-11-c). The interesting point here especially in the PtIr fracture side (Figure 5-11-d) is formation of corrugated pattern which is a sign of fatigue fracture. Therefore, it could be concluded that the weakest region of

the joint was responsible for the fracture after 263 cycles due to accumulation of plastic deformation in each cycle and fatigue occurrence.

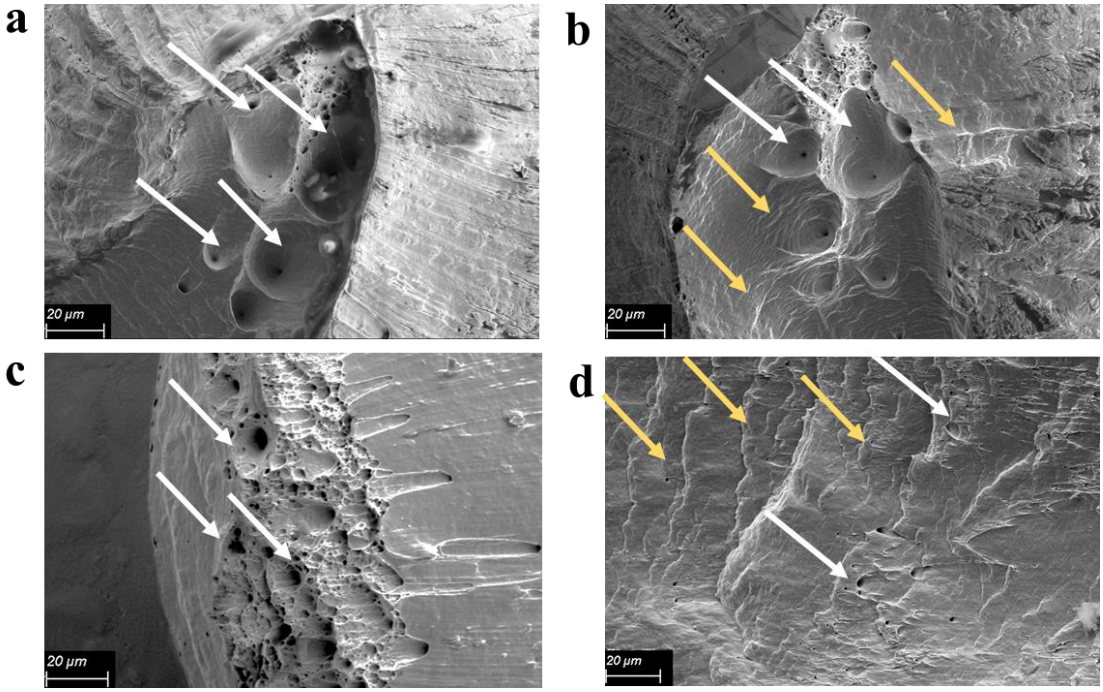

Figure 5-11 Fracture morphology of NiTi/PtTi dissimilar laser welds after a) tensile test- NiTi side, b) tensile test- PtIr side c) 263 cycles- NiTi side and d)263 cycles- PtIr side. White arrows show dimples and yellow arrows show tear ridges and corrugated patterns.

5.4 **Summary**

This study focused on laser welding of dissimilar NiTi and PtIr wires. A comprehensive microstructure and mechanical characterization along with the analysis of the functional behavior of the joint was performed. The major conclusions of this chapter are summarized as follows:

The solute Pt inside the FZ (up to 15 at. %) caused the formation of ternary NiTiPt with the same crystal structure of B2 NiTi. Nonetheless, based on the synchrotron X-ray diffraction measurements, there were no detectable IMCs inside the FZ. The grain orientation of NiTi BM gradually transitioned toward FZ and the NiTi/FZ interface exhibits almost the same orientation of NiTi BM due to their similar B2 crystal structure. On the contrary, this transition is completely abrupt at the interface of FZ/PtIr.Some precipitates were observed under TEM at the grain boundaries of the NiTiPt phase which were related to (Ni+Pt)-rich precipitates. Formation of substructured grains inside the FZ was related to the dislocation pile ups occurred owing to the dissolution of Pt into the NiTi crystal structure.

Microhardness mapping of the joint is in good agreement with the variation of Pt concentration. In particular, more dilution of Pt promoted higher hardness due to solid solution hardening. The fusion zone has stronger bonding with NiTi BM in compared with PtIr BM. It was also shown that the residual strain was higher in the interface of PtIr BM/FZ due to crystallographic and textural mismatch after the welding, therefore the fracture during tensile tests occurred in this interface.

As a result of achieving acceptable strength in the welded sample, the NiTi BM preserved its functional superelastic behavior (up to 263 cycles with 6 % imposed strain before failure). The incremental increasing in the residual strain after each cycle was a consequence of large and recrystallized grains inside the FZ.

The formed NiTiPt phase inside the FZ is a type of high temperature shape memory. Therefore, in the next chapter, the possibility of fabricating of this high temperature shape memory alloy using laser microwelding concept will be discussed. In case of succession, it would be a straightforward and applicable method to fabricate these kinds of materials.

Chapter 6 Laser microwelding enabled alloying to fabricate NiTiPt [1]

6.1 Introduction

Using laser welding of NiTi to PtIr, high temperature shape memory alloy namely NiTiPt has been formed inside the fusion zone. Therefore, it opened a door to fabricate the mentioned high temperature alloy. In current chapter, this proof of concept will be surveyed by dissimilar laser welding of PtIr wire inside NiTi tube in a single pulse and afterwards multiple pulses to fabricate the NiTiPt high temperature shape memory wire which will be discussed in two sections, separately.

The operating temperatures of binary NiTi alloys are generally limited to room temperature. in some industries such as auto, aerospace and actuators, there is a great demand for using the mentioned functional properties at relatively higher temperature (100 to 400°C) [10,184]. On the other hand, in medical industries, NiTi implants and guidewires have poor visibility under X-ray fluoroscopy. Hence, the addition of alloying elements have a twofold effect: the development of shape memory alloys with higher transformation temperatures as well as an increasing radiopacity of binary NiTi which increases visibility under x-ray imaging [124,185]. Among these elements, Pt was found to be more beneficial due to create a narrower transformation hysteresis and better dimensional stability[186,187].

Alongside the previously stated advantages, the addition of Pt to NiTi alloys results in complexities in the microstructure of the shape memory alloys. For instance, As a consequence of forming $Ti_2(Ni, Pt)_3$ precipitates, the matrix is depleted of Ni and the transformation temperature is increased, the same behavior as Ni_4Ti_3 in binary NiTi alloys [188]. It is worth mentioning that the $Ti_2(Ni, Pt)_3$ and P-phase precipitates are one of the main characteristic of NiTiPt and their presence is strong evidence for showing the fabrication of NiTiPt HTSMAs [115,189].

So far, most of the HTSMA fabrication methods are limited to conventional or additive manufacturing except some attempts adopting MEMS [190] (NiTi thin film covered by Ta patterns) or assembling NiTi/Ag composite [126]. The conventional methods include casting the material from high purity Ti, Ni and third element in a vacuum furnace, homogenization, and finally optimal thermomechanical processing similar as that of NiTi which all needs expensive facilities as well as precise optimization of the equipment [178,186]. It is reported [191,192] that some inherently problems are associated with fabrication of NiTiPt and optimizing their thermomechanical process parameters is quite challenging. Rios et. al [174] produced NiTiPt in different chemical composition using vacuum,

[1] The results of these chapter are published in a journal paper: 1- **Shamsolhodaei, A.**, et al. Metallurgical and Materials Transactions A (2021): 1-11.

non-consumable-arc melting by a cooled Cu crucible. They did vacuum arc remelting for multiple time in addition to 72 hours heat treatment in vacuum furnace at 1050°C for having homogenous bulk material, since the Ni, Ti and Pt elements have complete difference density.

To overcome these challenges, many alternatives (e.g., additive manufacturing[193–196]) have been introduced. It was shown that by selecting optimal parameters (the dominant one is laser power) the density could be increased and the amount of pores and the Ni loss of fabricated NiTiHf and NiTiCu could be decreased [118,197,198]. Currently, there are some studies focus on laser surface alloying on NiTi substrate with Nb or Cu elements to enhance its corrosion or wear resistivity [199,200]. If fabricating of HTSMA using laser alloying method can be realized, it will greatly simplify the process. Therefore, the objective of this chapter is to fabricate NiTiPt HTSMA using dissimilar laser alloying of NiTi and PtIr alloys. To this end, knowledge regarding laser processing of NiTi and its advanced characterizations will be applied to verify the assembly of the desired material.

In the first section, four different peak powers (from 1.0kW to 2.5kW) in a single pulse were implemented on PtIr inserted into the NiTi tube to study their effects on NiTiPt laser fabricated materials. It was found that the formed phase inside the mixed zone shifted the critical transformation temperature more than 200°C which is a sign of fabrication of high temperature shape memory alloy. In the second section, a NiTiPt high temperature shape memory alloy (HTSMA) was fabricated using the mentioned microwelding procedure. The results showed that the fabricated NiTiPt material has considerable functional properties at 250°C with just 0.7% residual strain after heat treatment due to formation of $Ni_4(Ti, Pt)_3$. Adopting microwelding enabled laser alloying for fabrication of NiTiPt could open a door for straightforward method of producing HTSMAs.

6.2 Experimental procedure

6.2.1 Single pulse laser welding

A superelastic NiTi (50.2 at% Ni) tube (inner diameter (ID)= 400 μm, outer diameter (OD)= 600 μm) and a Pt-10%Ir 400 μm OD wire were used in this study. Both sets of materials were cleaned prior to laser mixing using acetone, ethanol and de-ionized water to remove any impurities and contamination. Laser mixing was performed using a Miyachi Unitek LW50A pulsed Nd:YAG laser, with a wavelength of 1.064 μm and a nominal spot size of 400 μm. The top hat shape laser profile with peak powers ranging from 1.0 kW to 2.5 kW with a pulse width of 5 ms, which included a 1ms upslope and downslope, were selected. Argon gas protection was employed as a shielding gas with a flow rate of 14 L/min. Figure 6-1 illustrates the schematic of the laser welding procedure, where PtIr wire was

inserted into the NiTi tube. Thereafter, the laser beam was pointed on the NiTi tube and the FZ formed as is shown in the schematic. Microstructural studies were executed on cross sections of the specimen, which were prepared by mounting the sample in epoxy, grinding up to grit number 1200, polishing by diamond spray down to 0.25 μm and etching with a Kroll reagent (4%HF, 7%HNO3 and 89% water by volume). Microstructural observations and chemical composition analysis were conducted with an Olympus BX51 M Optical microscope (OM) and a Zeiss Ultra Plus field emission Scanning Electron Microscope (SEM) equipped with Energy Dispersive Spectroscopy (EDS), respectively.

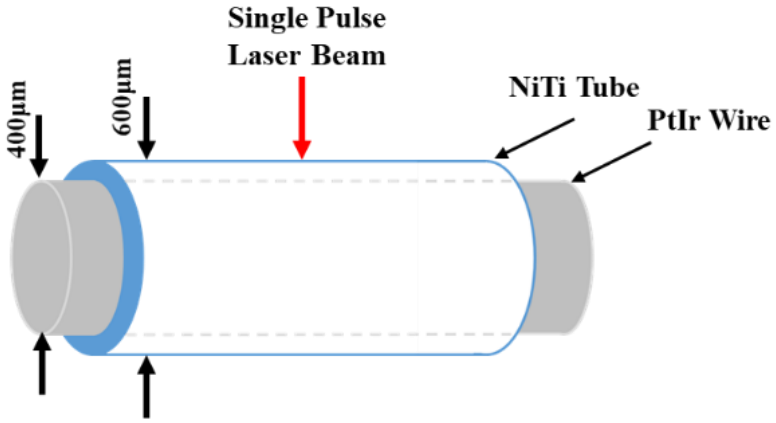

Figure 6-1 Schematic of NiTi wire and PtIr tube configuration during laser welding.

Detailed analysis of the phase map and IPF image microstructure was carried out by Electron Backscattered Diffraction (EBSD) using a JEOL JSM 7000 FESEM equipped with the HKL Technology system using a step size of 1 μm and 0.2 μm, at a working distance of about 15 mm, with an accelerating voltage of 20 kV and 70° for the incline angle of the sample. The sample was prepared using oxide-polishing suspension after grinding with sandpaper up to the number of 1200 and polishing to 0.25 μm diamond spray. The acquisition of data was carried out by the Oxford Instruments Aztec software and the collected data were post-processed by the HKL Channel 5 software. Transmission Electron Microscopy (TEM) analysis was completed using a JEOL 2010F operated at 200 kV. Cross-sectional TEM samples were prepared by the focused Ion Beam (FIB) lift-out technique using Thermo Scientific Helios G4 UXe Dual Beam Plasma FIB in a selected region inside the mixed zone. TEM analysis was carried out by employing an FEI Tecnai Osiris Scanning Transmission Electron Microscope (STEM) at an operating voltage of 200 kV.

X-ray diffraction (XRD) measurement in both mixed laser samples were carried out with a Bruker D8 Discover X-ray Diffractometer using Cu kα radiation in a range of 30-60º 2θ with 0.01º step size. The XRD results were analyzed with DIFRAC.EVA V3.0 software. The microhardness testing was

performed using a CMT Clemex automated Vickers hardness tester according to ASTM E384. In order to have a hardness map a series of 50 g indents with a distance of 50µm between each indent vertically and horizontally with 10 s for holding time have been conducted. Phase transformation temperatures of materials were measured by the differential scanning calorimetry (DSC-TA Q2000) system equipped with a refrigerated cooling system. The DSC sample was first thermally pre-cycled to remove any effects of internal mechanical stress generated by the laser procedures and then DSC curves were recorded in a temperature range from −50°C to 300 °C using a heating and cooling rate of 10 °Cmin^{-1}. All required transformation temperatures were measured using TA Trios software in accord with ASTMF2004-05 Standard. As is mentioned in Chapter 3, some processed samples have been measured to be in the correct weight range for a DSC sample.

6.2.2 **Multi pulse laser welding**

A simple dissimilar laser welding on the NiTi and Pt alloys can be introduced as a novel method to fabricate NiTiPt HTMSA. In this regard, a PtIr wire with 400µm diameter has been inserted into a NiTi tube (ID=400µm and OD=720µm) and laser processing has been conducted using multiple pulses on the sample. An Nd-YAG Miyachi pulse laser with 400µm spot size and 1.064µm wavelength has been used to perform the laser pulsation with considering the 60% overlap for subsequent laser spots to ensure the processing the materials. Based on the previous section, two laser powers of 1.5kW and 2.0kW has been selected to do the laser processing. Figure 6-2 shows the schematic of the process. The as-fabricated material was homogenized at 1050°C for 6hrs following 1hr aging process at 450°C for strengthening the alloy by introducing Ni-rich precipitates.

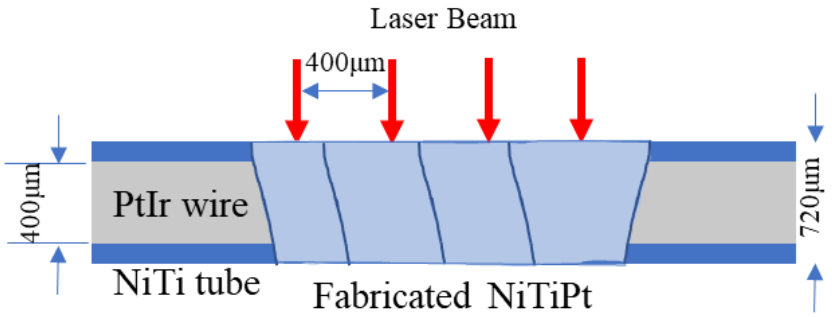

Figure 6-2 The schematic of NiTiPt fabrication using microwelding of NiTi tube with PtIr wire.

The 3D microstructure of fabricated materials was thoroughly characterized using X-ray computed tomography (XCT). The scans were acquired employing a Zeiss Versa 520 x-ray microscope with a 120 kV accelerating voltage. The angular increments of 0.12° between -180 to 180° were used to

collected 2000 projected scans. A pixel size of 0.4 µm up to 1 µm was achieved with an exposure time of 1s per projections. Finally, the 3D reconstruction from the acquired 2D projection was generated after using smoothing filtering, vertical artifacts removing and using phase retrieval to enhance the contrast at the boundary of constituent phases.

A TA Q2000 differential scanning calorimetry (DSC) system equipped with a refrigerated cooling system was utilized to measure the transformation temperatures. The DSC curves were recorded in a temperature range from 150 °C to 300 °C using a heating and cooling rate of 10°Cmin^{-1}. Microstructural studies were executed on cross sections of the specimen, which were prepared by mounting the sample in epoxy, grinding up to grit number 1200, polishing by diamond spray down to 0.25µm and etching with a Kroll reagent (4%HF, 7%HNO3 and 89% water by volume). Microstructural observation was conducted with a Zeiss Ultra Plus field emission Scanning Electron Microscope (SEM). Transmission Electron Microscopy (TEM) analysis was completed using a JEOL 2010F operated at 200 kV. Cross-sectional TEM samples were prepared by the focused Ion Beam (FIB) lift-out technique using Thermo Scientific Helios G4 UXe Dual Beam Plasma FIB in a selected region inside the mixed zone. TEM analysis was carried out by employing an FEI Tecnai Osiris Scanning Transmission Electron Microscope (STEM) at an operating voltage of 200 kV.

6.3 Single Pulse Laser Alloying of PtIr to NiTi

6.3.1 Weld Appearance

The overview of applying different laser power on the NiTi tube and PtIr wire can be observed in Figure 6-3. As seen the 1 kW (Figure 6-3-a) laser power did not result in sufficient mixing region and there is interfacial bonding between the two materials. The 2.5 kW (Figure 6-3-d) laser power resulted in significant through the laser mixed sample due to thermal shock. Therefore, to study the effect of laser alloying of NiTi into the PtIr wire two intermediary powers of 1.5 kW (Figure 6-3-b) and 2.0 kW (Figure 6-3-c) have been selected for further investigation. In these selected laser mixed samples, some boxes have been marked and their detailed microstructure will be discussed later. For simplicity, the 1.5 kW and 2.0 kW peak powers were named low and high laser powers, respectively. In these two laser conditions (Figure 6-3-b and c), the mixed region contains a sound and defect-free laser process (i.e., no voids or other internal defects). The darker base material (top right corner of Figure 6-3-b and c) and the brighter base material (bottom half of Figure 6-3-b and c) correspond to the NiTi tube and PtIr wire, respectively. Evidently, the varying mixture of the different elements within the mixed zone (MZ) has caused the appearance of different contrasts in the backscattered SEM images: the areas

enriched with heavier elements (Pt and Ir) are brighter. Moreover, there are two different interfaces related to NiTi/MZ (marked by the yellow box) and PtIr/MZ (marked by the green box). It should be mentioned that presence of dark and bright areas inside the mixing zone of the low power sample (Figure 6-3-b) is a sign of non-homogeneity inside the mixed zone; whereas, this zone is observed to be larger and more homogenous after applying the high power condition (Figure 6-3-c).

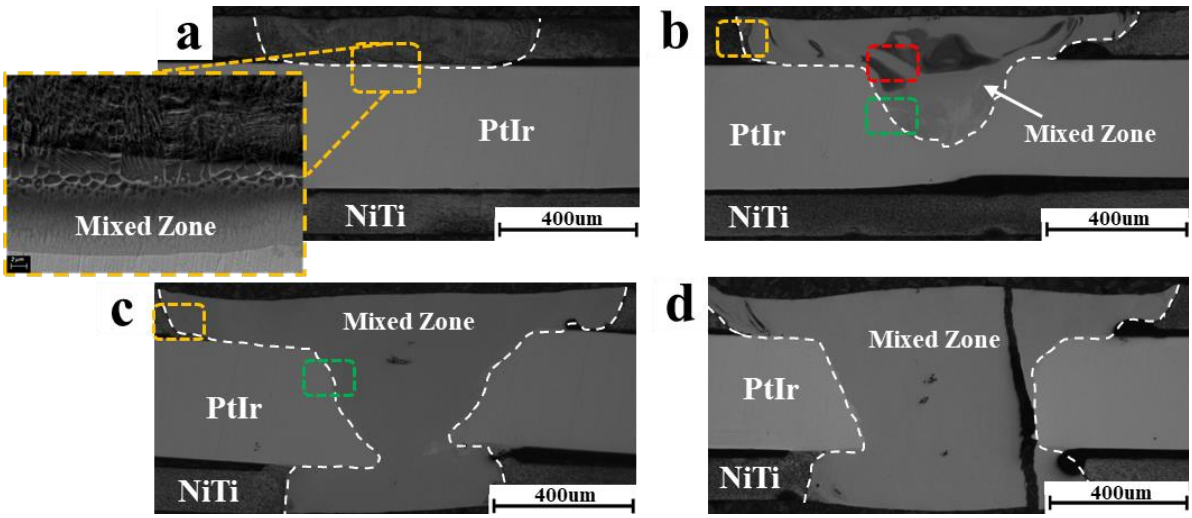

Figure 6-3 The cross section of laser mixed NiTiPt samples using a)1.0kW, b)1.5kW, c)2.0kW and d)2.5kW. The marked colored boxes are magnified in Figure 6-4 and Figure 6-6 (interfaces of the mixed zone and base materials are marked by dashed white lines).

To quantify the mixed zone geometry based on the peak power applied, several attributes of the MZ are evaluated and summarized in Table 6-1. These include the width of the MZ adjacent to the NiTi wire (labeled by upper NiTi and lower NiTi), the width in the center of the MZ adjacent to the PtIr wire and the area of the MZ as shown in Figure 6-3. Although increasing the peak power can widen the mixed zone, applied peak power from 2.0 kW to 2.5 kW can maintain the upper width of the mixed zone (1311.9 vs. 1314.1µm) but cause a larger central and a lower width of the mixed zone (415.1 vs. 560.1 µm and 596.2 vs 804.8 µm). This might be the indication of entering the keyhole mode in the laser, where the penetration of the laser in the material becomes greater than the width of melt pool.

Table 6-1 The width and area of the mixed zone (MZ) from applying different peak powers as shown in Figure 6-3

Peak Power	1.0 kW	1.5 kW	2.0 kW	2.5 kW
Width of MZ (Upper NiTi)	731.4 µm	1086.9 µm	1311.9 µm	1314.1 µm
Width of MZ (PtIr)	-	323.3 µm	415.1µm	560.1 µm
Width of MZ (Lower NiTi)	-	-	596.2µm	804.8 µm
Area of MZ	884.1 μm^2	1347.3μm^2	2085.6 μm^2	2116.8 μm^2

6.3.2 **Microstructure analysis**

Figure 6-4 show higher magnification of the red, yellow and green boxes which were marked in Figure 6-3.b. An epitaxial like structure is observed to formed in the interface of the base materials and mixed zone (Figure 6-4.a and Figure 6-4.b). These epitaxial features are finer in the interface of NiTi/MZ (Figure 6-4-a) compared to the PtIr/MZ interface (Figure 6-4-b). The possible reason for this could be from lower heat dissipation in the PtIr wire confined inside the NiTi tube, which would result in a lower solidification rate and thus cause the formation of coarser columnar features in the PtIr/MZ interface (Figure 6-4-e and f) [103,168]. The specified region adjacent to NiTi/MZ (marked by the blue box in Figure 6-4-a) will be discussed later.

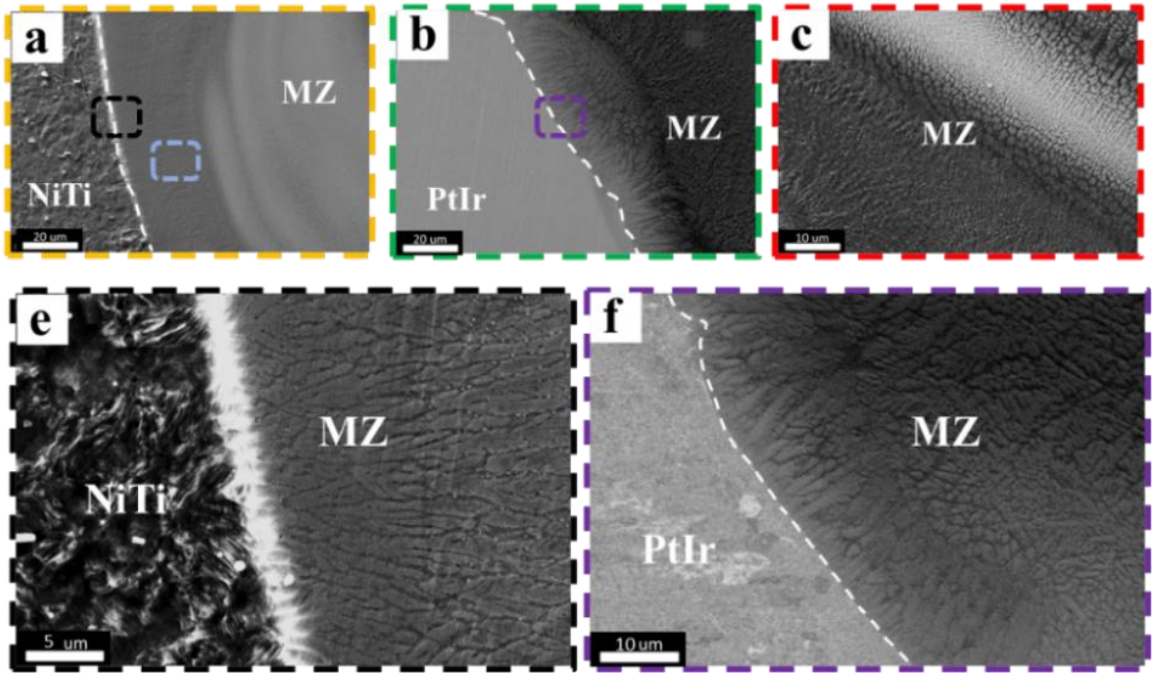

Figure 6-4 The cross section microstructure of the low power sample mixed zone showing a) the interface of the NiTi tube and the mixed zone, b) the interface of the PtIr wire and the mixed zone and c) a selected region marked in Figure 6-5-b inside the mixed zone, higher magnification of the e) NiTi/MZ and the f) PtIr/MZ interface showing dendritics.

A greater magnification of the interfaces in the MZ within the NiTi tube and PtIr wire which were marked by yellow and red box in high power sample (Figure 6-3-c) are shown in Figure 6-6-a and Figure 6-6-b, respectively. As can be seen, another difference of this sample with the low power condition, in addition to the prior mentioned change in homogeneity, is the decreased size of cellular and epitaxial features in the interface of the MZ and base materials. This is due to the lower heat dissipation of the PtIr wire inside the NiTi tube, resulting in a lower solidification rate to cause the formation of a coarser columnar structure in the interface of the MZ and PtIr (Figure 6-6-c and d).

However, in the case of the high power relatively high input energy resulted in a higher heat dissipation and finer final structure.

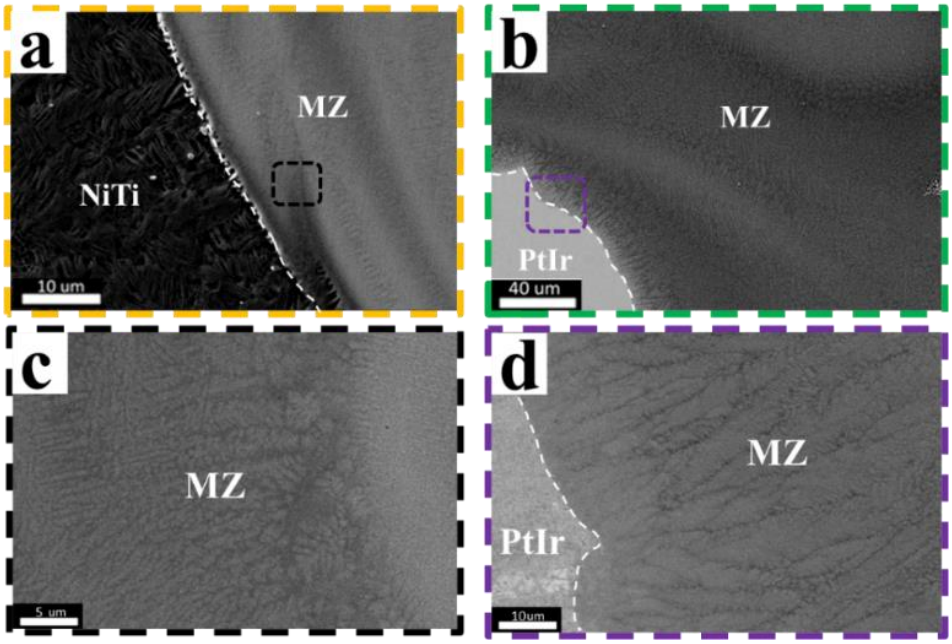

Figure 6-6 The cross section microstructure of the high power sample mixed zone showing a) the interface of the NiTi tube and the mixed zone, b) the interface of the PtIr wire and the mixed zone, higher magnification of the c) NiTi/MZ and the d) PtIr/MZ interface showing dendritic structures.

The overview of the grain structure in the low power laser mixed sample is evident in Figure 6-7-a where the IPF image of the mixed zone is depicted. The details of the interfaces of the mixed zone with both base materials are shown in Figure 6-7-b and c. As was observed earlier in Figure 6-4, the NiTi/MZ interface has equiaxed grains related to the heat affected zone, which change to elongated grains inside the mixed zone. This directional growth of the grains is prominent in the PtIr/MZ interface (Figure 6-7-c). However, the center of the mixed zone contains large grains with random orientations. It should be mentioned that both base materials are highly texturized due to the initial cold work in the manufacturing processes.

The phase map of the same region is shown in Figure 6-7-d with only the B2 phase indexed inside the mixed zone. This phase is a result of the NiTiPt material containing mostly less than 20at% Pt. However, by magnifying and decreasing the step size of the EBSD (to 0.2μm) on the interface of PtIr/NiTi (Figure 6-7-e) where the Pt-concentration should be higher than 20at%, the B19 phase could be indexed. The appearance of this phase is related to the high content of the Pt element, resulting in the formation of the B19 martensite phase of NiTiPt. Therefore, raising the Pt-content inside the mixed zone can promote the formation of the B19 martensite phase in larger quantity; where decreasing the

step size and increasing the magnification, these phases could be indexed by EBSD phase map imaging. It should be noted that the PtIr wire is in the FCC phase condition, which is the same as pure platinum [201]. Due to the high concentration of the B19' martensite phase in the high power sample, most of the regions of the fabricated sample were not indexed in EBSD, therefore the EBSD of the high power sample was not discussed.

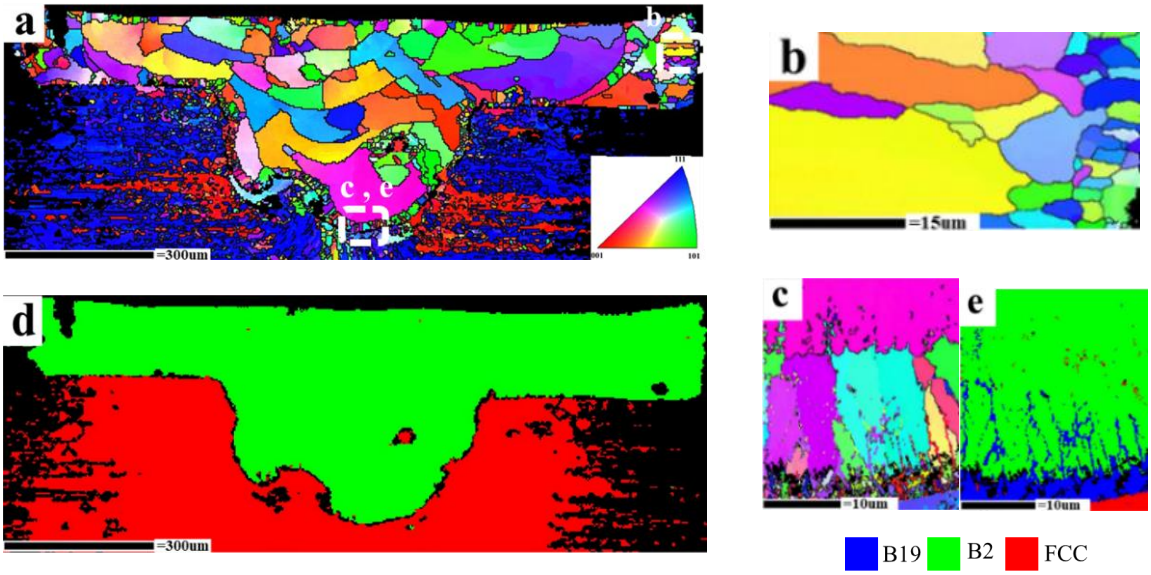

Figure 6-7 The EBSD images of the mixed zone showing the : a) IPF image of the whole sample, b) IPF image of the interface of the NiTi tube and mixed zone, c) IPF image of the interface of PtIr wire and mixed zone, d) phase map image of whole mixed region and e) phase map image of the interface of the PtIr wire and the mixed zone.

6.3.3 **Chemical analysis and phase identification**

In order to study the element distribution of low and high power laser mixed samples, the EDS map of Ti and EDS line scans of these samples were used as shown in Figure 6-8 and Figure 6-9, respectively. From the EDS maps (Figure 6-8-c and Figure 6-9-c) it is apparent that the element distribution is more homogenous in the high power sample, due to the higher mixing degrees of elements. By evaluating the Ni and Ti content in selected line scans of the low power sample (Figure 6-8-a and b), Ti and Ni are seen to approximately have the same composition along the top surface of the mixed area, whereas in the bottom surface the Ni concentration is somewhat higher than Ti. On the top surface, the laser intensity is higher and the mixed area is in the molten state for a longer period compared to the bottom region; therefore, Ni has more time to vaporize from the surface and Ti has a longer time to be mixed in molten zone overcoming the Marangoni effect owing to its lower weight density [91]. Although this Ni vaporization also occurred in the high power sample (Figure 6-9-a), due

to the higher degree of element mixing, an almost equal distribution could be observed in the whole mixed zone area. Specifically, in the bottom region of the mixed zone in the low power sample, the higher cooling rate results in diminished time, which is not enough for an equal distribution of Ni and Ti elements. Nevertheless, the degree of all elements intermixing between NiTi and PtIr is governed by both the Marangoni effect and convection flow created by the rectangular laser profile[202].

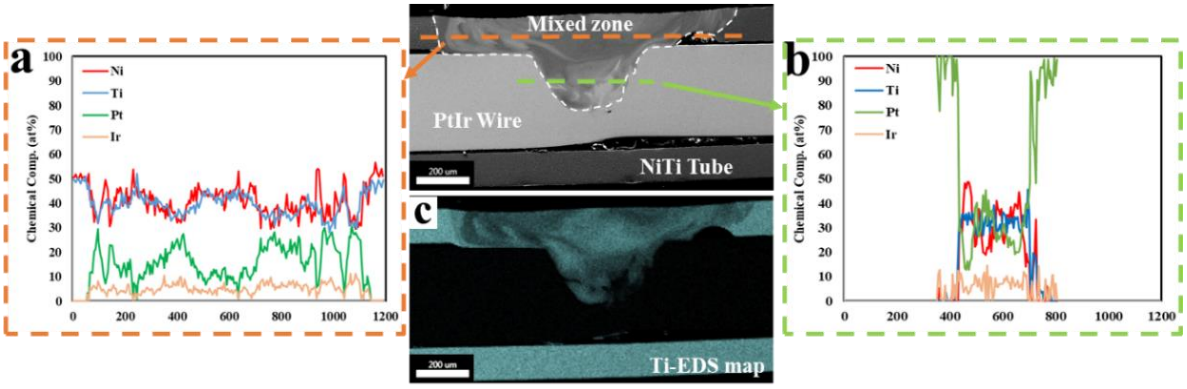

Figure 6-8 Backscattered image of the mixed zone of the high power sample and two selected line scan EDS measurement from a) the NiTi tube base material through the mixed zone , b) the PtIr wire base material through the mixed zone consisting of Ni, Ti, Pt and Ir elements (at%) and c) the Ti-EDS map for the whole region.

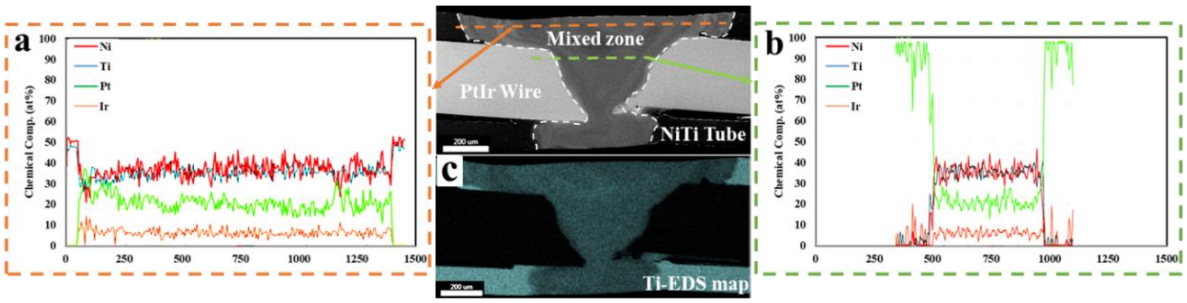

Figure 6-9 Backscattered image of the mixed zone of the low power sample and two selected line scan EDS measurement from a) the NiTi tube base material through the mixed zone, b) the PtIr wire base material through the mixed zone consisting of Ni, Ti, Pt and Ir elements (at%) and c) the Ti-EDS map for the whole region.

Based on these different variations and concentrations of Pt, there is a great possibility to form NiTiPt in both the austenite and martensite phases, either Ni or Ti rich. It should be mentioned that the crystal structure for the ternary NiTiPt structure is B2, the same as binary NiTi. When the Pt content is less that 20at%, much of the mixed zone of the low power sample (Figure 6-8) has the same parent phase as the NiTi tube base material. However, it is expected that some regions could contain the B19 martensite phase where the Pt-content is higher than 20at% due to the expected change in transformation temperatures, as seen predominantly in the high power sample (Figure 6-9) [178]. On the other hand, by having less than 5% Pt in the mixed zone (in the interface of NiTi/MZ and in some

part of the low power sample), a solid state solution of NiTi could be formed [174]. These mentioned Pt rich and lean regions can be seen throughout the mixed zone by the change of contrast in Figure 6-3-b and c.

It is also worth mentioning that in the Marangoni effect, different phase densities, surface tension gradients and temperature gradients produce flow mixing liquid metals outward from the center of the pool which is the main reason for fluid flow inside the mixed zone as well as the increased width of the melt pool at the surface [203]. On the contrary for the high power sample, the higher input energy resulted in enough time for elements to intermix, therefore homogenous NiTiPt mixed zones were fabricated. Also, in the low power sample, owing to the higher cooling rate in the bottom part of the mixed region and the fact that the PtIr wire is located at the bottom of the melt pool, there is not enough time for enough mixing and homogeneity in the mixed zone (comparing Figure 6-8-a and b).

X-ray diffraction (XRD) of these two samples is provided in Figure 6-10. Both the martensite and austenite phases of NiTiPt, in addition to some binary intermetallic phases, could be indexed in the mixed zone of both samples. As expected, most of the MZ of the low power sample is the austenite phase of NiTi and NiTiPt, because of less than 30%Pt from the line scan result (Figure 6-8). It should be mentioned that the location of the NiTi austenite and NiTiPt austenite are very close together, therefore the higher content of NiTiPt in the B2 phase and residue NiTi in the XRD sample, resulted in a wider peak in the low power sample (Figure 6-10). Additionally, as shown in the line scans of the high power sample (Figure 6-9), the higher Pt content of the MZ (slightly above 30%) could cause higher content of the NiTiPt in the martensite phase. It was also observed that the high content of Pt due to the greater mixing in the high power sample resulted in the formation of some binary intermetallics such as Pt_3Ti.

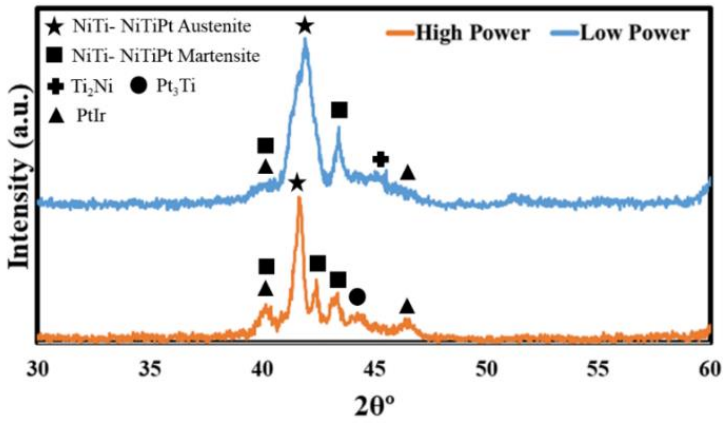

Figure 6-10 X-ray Diffraction pattern of high and low power laser mixed samples indicating presence of NiTiPt alloy in both martensite and austenite phases.

6.3.4 **Microhardness analysis**

Microhardness maps of low and high power samples inside the MZ and its surrounding are shown in Figure 6-11-a and b, respectively. The variations inside the mixed zones are in good agreement with the elements distribution as depicted in Figure 6-8 and Figure 6-9. The higher concentration of Ti and Ni content inside the mixed zone resulted in lower amounts of microhardness due to the lower possibility for the formation of ternary Ni-Ti-Pt IMCs and less solid solution strengthening related to the presence of Pt inside the NiTi structure [174].

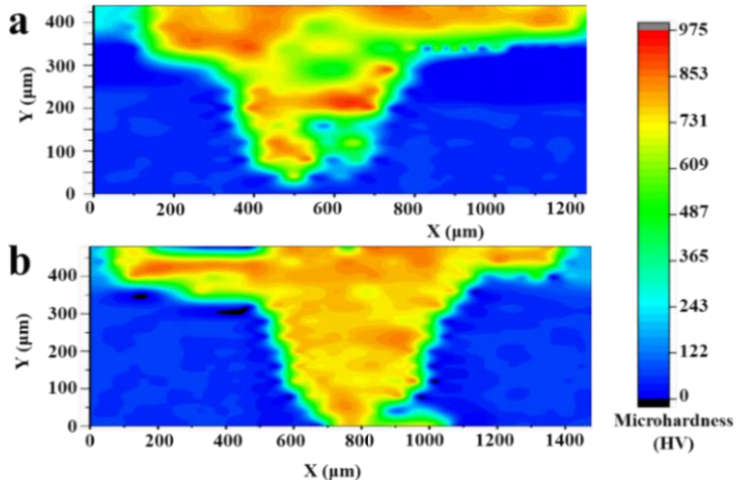

Figure 6-11 Microhardness maps of the laser mixed regions and its surroundings after adopting the a) low power and b) high power conditions.

6.3.5 **Precipitation's characteristic**

As mentioned in section 6.3.3, there are possibilities for the presence the Ni, Ti, Pt precipitates and IMCs. Figure 6-12-a is a higher magnification of the region marked with a blue box in Figure 6-4-a inside the mixed zone, adjacent to the NiTi/MZ interface. Fine nano-size precipitates are visible in inter-dendritic space of the solidified NiTiPt. TEM image in Figure 6-12-b also shows these precipitates. A higher magnification micrograph is presented in Figure 6-12-c where the captured SAD pattern confirms the presence of the B2 phase in the matrix.

To characterize the precipitates, the SAD taken from the precipitates reveals that they are P-phase particles (Figure 6-12-d), which can be commonly formed in the NiTiPt alloys. The light ring feature of the SAD pattern suggests the transition from a crystalline structure to the amorphous nature of P-phase precipitates. Normally, P-phase has a monoclinic structure that has a tendency to be amorphous under certain conditions [183]. These nano-size precipitates were formed during rapid solidification after laser alloying without enough crystallization time. However, since the formed ring-pattern is not diffused enough, the P-phase is not completely amorphous.

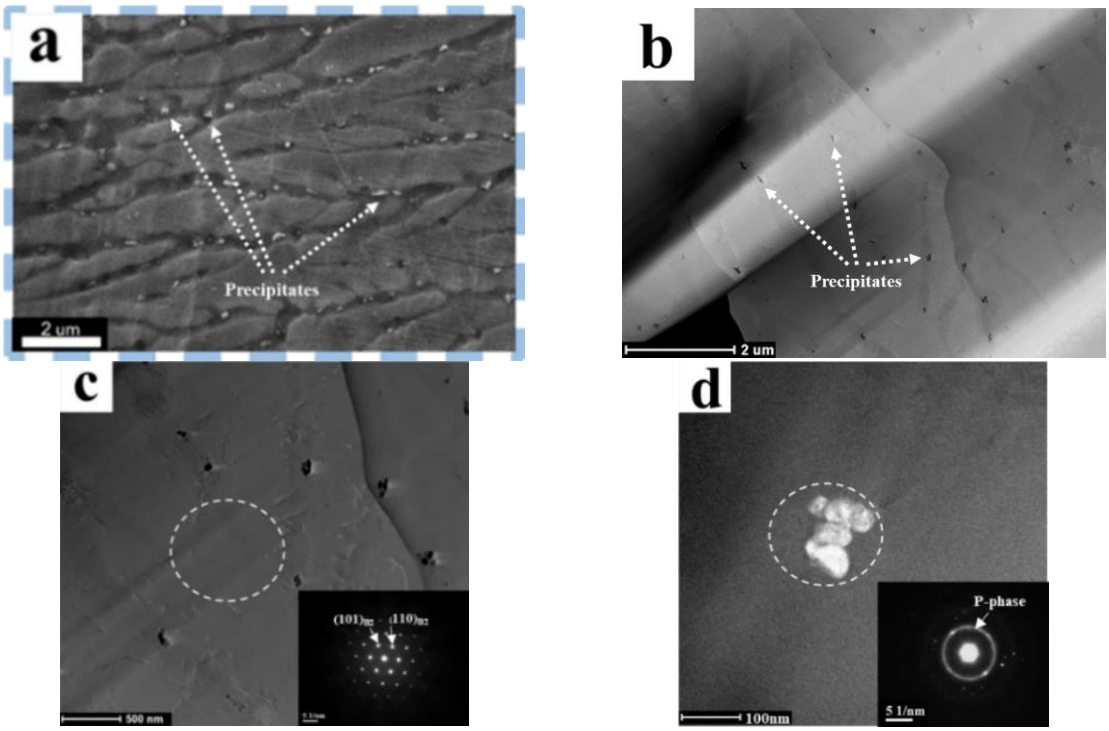

Figure 6-12 Nanoscale precipitates in the mixed zone of the low power sample a)in the interdendritic space shown by SEM micrograph, b) the same region at a higher magnification using TEM, c) SAD pattern under [111] zone axis of matrix showing B2 structure, d) SAD pattern of precipitates showing the ring-like pattern of P-phase.

The existence of P-phase in the mixed zone of the fabricated NiTiPt is confirmed with EDS analysis on these precipitates, as shown in Figure 6-13. The results are summarized in Table 6-2. The precipitates contained ~15at% Pt, near 50at% Ti and the balance is Ni. This chemical composition is in excellent agreement with the Ti11Ni9Pt4 P-phase in similar alloys [188,204]. Therefore, the existence of these precipitates is a confirmation of the fabrication of a ternary NiTiPt alloy using the laser alloying of NiTi and PtIr alloys.

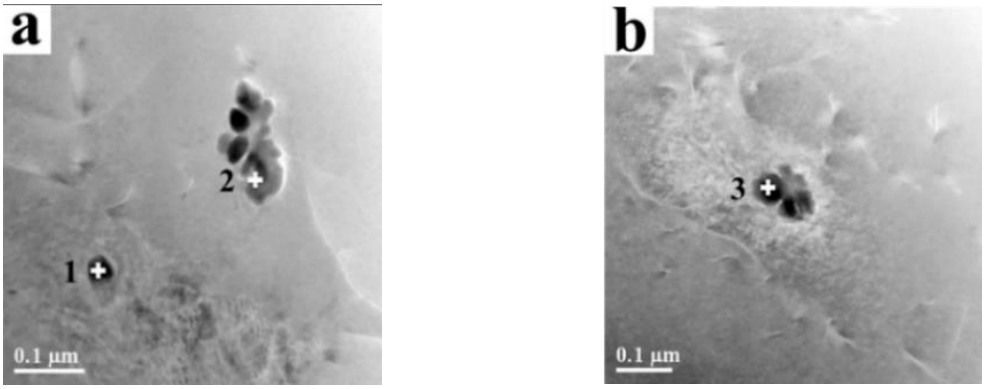

Figure 6-13 Three different spots for evaluating the chemical analysis of precipitates using EDS in the low power sample. The results are shown in Table 6-2.

Table 6-2 The chemical composition (per at%) of selected points on the precipitate presented in Figure 6-13.

Elements	Ti	Ni	Pt
Point 1	48.35	38.43	13.23
Point 2	43.21	40.04	16.75
Point 3	50.48	33.68	15.85

6.3.6 **Phase Transformation**

Figure 6-14 shows the transformation temperature variation of the sample. The results show two distinct sets of peaks both in the cooling and heating regime: the biggest peaks are in good agreement with transformation temperature of the as-received NiTi tube (As=-11, Af=-1, Ms=-25 and Mf=-33°C) which is in the B2 condition at room temperature (marked by NiTi tube in Figure 6-14-a). The other peaks located over 200°C are critical transformation temperatures of A_s=207, A_f=258, M_s=249 and M_f=202°C as magnified in Figure 6-14-b and c. These peaks are related to the mixed region where the NiTiPt phase formed as is reported elsewhere [186,205]. It should be noted that the DSC sample contained residual NiTi base material in HAZ and MZ, therefore the corresponding NiTi tube peaks are still visible. The presence of the transformation temperature related to NiTiPt is another proof for the formation of this high temperature shape memory alloy in the mixed zone.

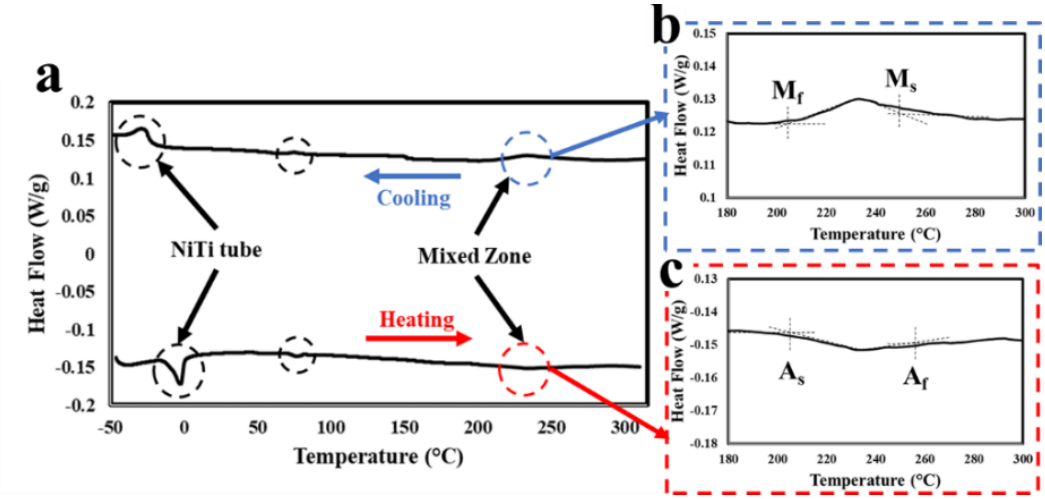

Figure 6-14 a) Differential scanning calorimetry of the laser mixed sample during cooling and heating cycles showing the shifting of the transformation temperature of the mixed region to higher temperatures during b) cooling and c) heating at around 250°C.

Moreover, there are another small set of peaks appear around 80°C both in the cooling and heating regimes (Figure 6-8-a). There could be two possible explanations: a. selective evaporation of Ni due to its higher equilibrium vapor pressure compared to Ti [76], causing a shift in transformation temperatures [84]; and b. the formation of high temperature shape memory alloys with lower transformation temperature which is distinct from the previous mentioned sets of peaks.

6.4 **Multi Pulse Laser Alloying of NiTi to PtIr**

6.4.1 **3D microstructure**

The 3D x-ray tomography image of fabricated materials is shown in Figure 6-15 where the NiTi tube and PtIr wire are indicated by green and red colors. With 1.5kW laser power (Figure 6-15-a and c), PtIr base material cannot be fully melted. However, increasing the peak power to 2.0kW, the fabricated material does not have any residue initial materials and full penetration has been achieved. Therefore, the rest of characterization will be performed just on the latter fabricated material.

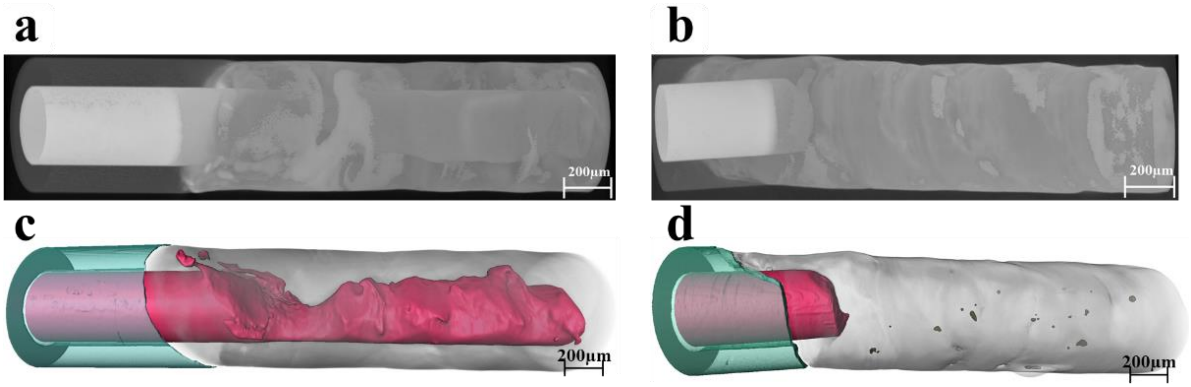

Figure 6-15 X-ray tomography and segmented of fabricated material using a and c) 1.5kW and b and d) 2.0kW laser peak power. Red color and green color are indication of PtIr and NiTi base materials.

As illustrated in Figure 6-16, there are some microporosities inside the fabricated material. Two general shapes of these porosity, irregular and spherical due to lack of fusion and gas entrapment, could be found (Figure 6-16-b). The former is reported in additive manufacturing processes, where large and irregular porosity could be formed due to lack of fusion and incomplete melting during the process [206]. The latter is a consequence of keyhole laser mode which encourage the bubble formation and bubble merging [207].

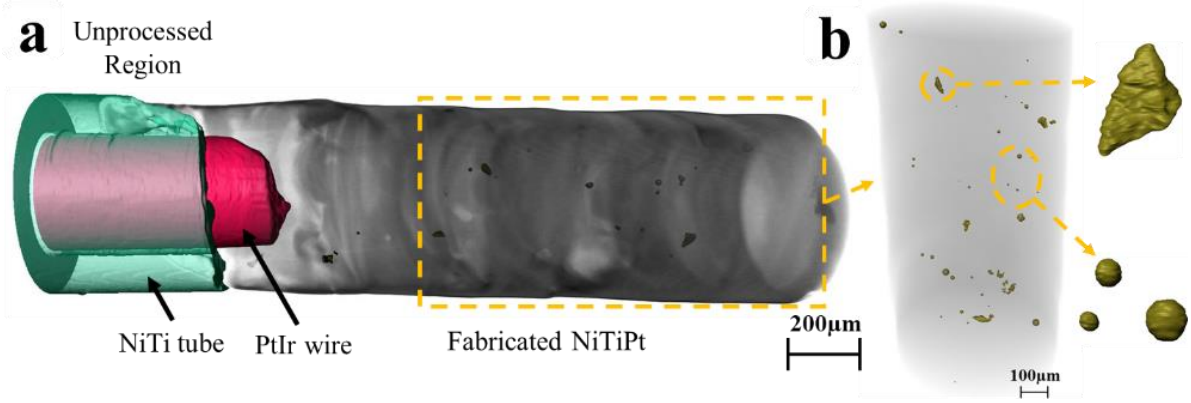

Figure 6-16 a) 3D microstructure of fabricated NiTiPt material and b) its magnified image showing microporosities with different shapes.

6.4.2 **Effect of heat treatment**

The microstructure of the as-fabricated material shows (Figure 6-17-a) the fully dendritic structure and the darker region versus bright region are represented the two different phases. The microstructure can be modified after homogenizing and aging processes (Figure 6-17-b), in which some nanoprecipitates are observed as marked by arrows. However, fully homogenization of this material needs more heat treatment time [174]. The DSC curves show the transformation temperature before and after annealing process. After annealing the curves become narrower with sharper peaks. The transformation temperatures are measured as, M_s=226°C, A_s= 174°C and M_f=182°C. Therefore, above A_f temperature, fully austenitic structure is dominant.

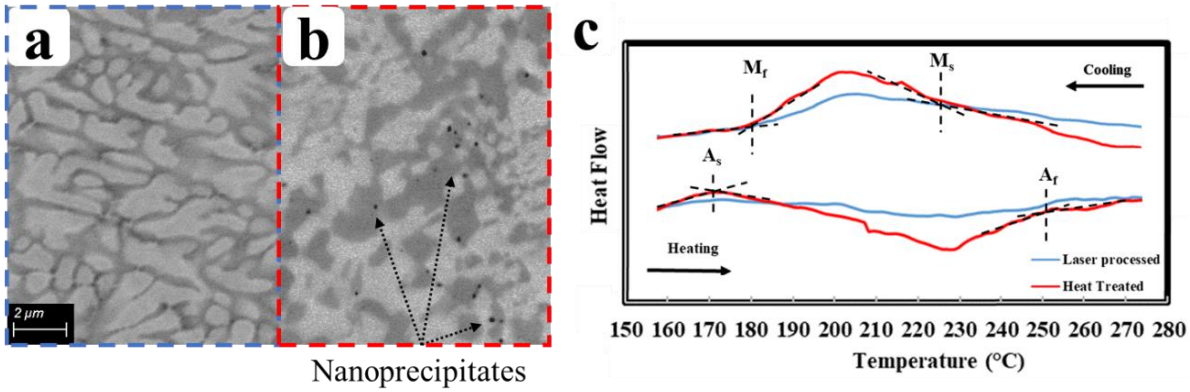

Figure 6-17 a) microstructure of as-fabricated material, b) microstructure of homogenized and aged fabricated material and c) DSC curves of fabricated material before and after heat treatment showing transformation temperatures.

The load-unload test at 250°C (above A_f temperature) exhibits a significant superelastic response at 250°C with around 0.7% residual strain from a total strain of 5% as shown in Figure 6-18.

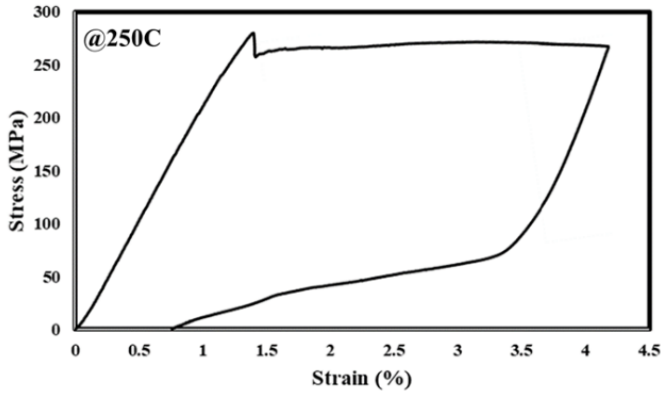

Figure 6-18 Load-unload tensile test of the fabricated material shows significant superelasticity at 250°C.

6.4.3 **Elements distribution**

Figure 6-19-a depicts the STEM image of a selected region in the fabricated sample prepared by focused ion beam. The overview of the microstructure shows a dark grain between lighter grains containing twin martensite structure. For better quantitative measurement, chemical composition of the marked area (yellow dotted circles) of Figure 6-19-a is given in Table 6-3. EDS map of this region (Figure 6-19-c to f) reveals the higher Ni content and lower Pt content in the mentioned grain.

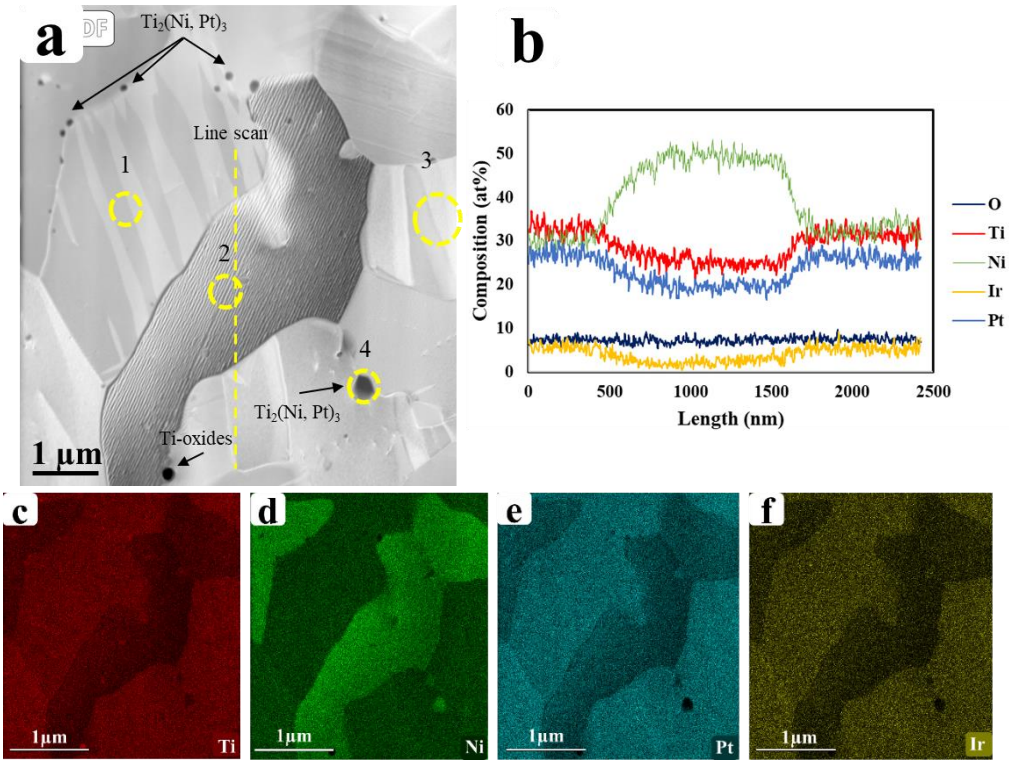

Figure 6-19 a) STEM microstructure of NiTiPt fabricated material consisting EDS map of c) Ni, d) Ti, e) Pt and f) Ir elements and b) variation of these elements in a selected line scan. The chemical composition of marked points is mentioned in Table 1.

The dominant low Ni matrix consist ~25at% of Pt which is in good agreement with formation of B19 NiTiPt when the Pt is higher than 18.75at%[187]. The amount of Pt inside the dark region (~16at%) is not high enough to switch the B19'(monoclinic) structure to B19 (Orthorhombic) martensite structure [208], nevertheless this needs further characterization. On the other hand, the chemical composition of marked precipitates in Figure 6-19 matches the stoichiometry of $Ti_2(Ni, Pt)_3$ which has been reported for introducing superelasticity in these materials [204]. It is worth mentioning that, due to oxygen entrapment during the laser processing and great affinity of Ti to absorb oxygen[209], some Ti-oxide has been detected as marked in Figure 6-19.

Table 6-3 Chemical composition (at%) and possible phase of selected regions shown in Figure 6-19-a (marked by dotted circles)

Elements	Point 1	Point 2	Point 3	Point 4
O	2.71	0.95	2.78	2.33
Ti	37.88	25.45	37.65	35.49
Ni	30.11	54.41	29.44	41.85
Ir	4.28	2.22	4.16	2.89
Pt	25.02	16.97	25.97	17.45
Phases	B19 NiTiPt	B19' NiTiPt	B19 NiTiPt	Ti_2 $(Ni, Pt)_3$

6.4.4 **Twin-based B19 and B19' martensite**

To detect the formed phase inside each of the mentioned regions in the matrix, TEM image (Figure 6-20-a) and related SAD patterns of the similar region were provided, where the interface of Ni rich and Ni lean grains is magnified (Figure 6-20-c). The SAD patterns of these regions indicate that the Ni rich grain has B19' NiTiPt martensite structure, while Ni lean region has B19 orthorhombic martensite crystal structure. B19 and B19' are shear structures of B2 austenite phase and in NiTiPt materials the B19' switches to B19 structure at higher Pt content [174].

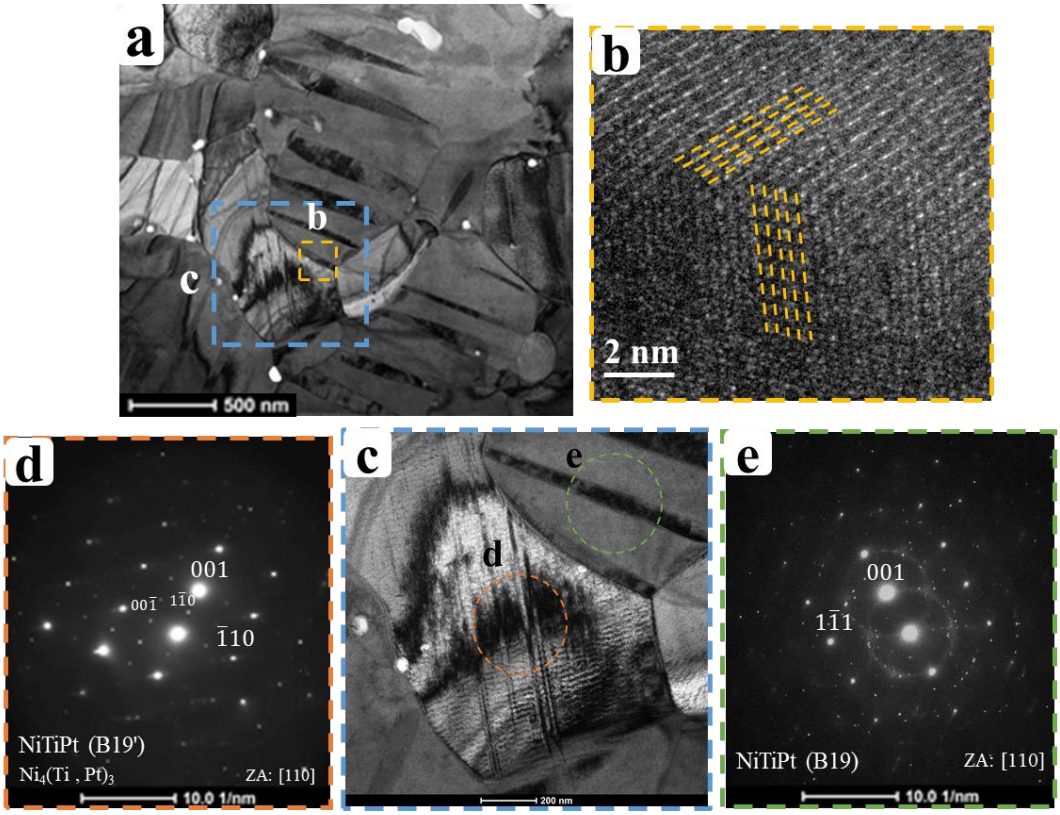

Figure 6-20 a) The TEM observation of the fabricated NiTiPt b) the HRTEM image of the interface of Ni-rich and Ni-lean grains, c) the magnified TEM image of the interface, e and f) SAD patterns of marked area of designated regions.

Therefore, the low Pt concentration in Ni rich area resulted in the presence of B19' martensite structure, whereas in other areas the high content of Pt caused the formation of B19 martensite structure. The twinned martensite structure of each type of martensite (B19 and B19') is visible in Figure 6-20-d and e. Other than presence of B19' is the designated area, the SAD pattern in Figure 6-20-d also revealed the existence of $Ni_4(Ti, Pt)_3$ precipitates due to higher concentration of Ni in this region, in addition to some dislocation pile-ups in this grain (Figure 6-20-c). These features are a probable explanation for having a 0.7% residual strain in load-unload of the fabricated material at 250°C.

6.5 Summary

In this chapter, laser alloying has been implemented during laser microwelding on the dissimilar joint between NiTi tube and PtIr wire. It was shown that the NiTi tube and PtIr wire could form a microstructurally sound mixing region and due to Marangoni effect, there is dilution of the Pt-content throughout the mixed zone, though with varied composition. However, by increasing the peak power, a more homogenous fabricated NiTiPt was achieved. The findings demonstrated that the laser alloying resulted in the successful fabrication of ternary NiTiPt shape memory alloys and by changing the laser parameters, the characteristics of the fabricated material could be affected. The key findings of this section could be summarized as follows.

Chemical analysis of the mixed zone confirmed the possibility of forming different phases based on the dilution of Pt inside the mixed zone using a low peak power condition whereas a more homogenous NiTiPt with lower element variation could be formed inside the MZ by adopting a high peak power condition. The phase map image captured by the EBSD technique and XRD patterns displayed the formation of mainly B2 and a small fraction of B19 phases of NiTiPt inside the mixed zone of the low power sample and a higher fraction of martensitic NiTiPt in addition to binary intermetallics in the high-power sample.

The microhardness evaluation inside the mixed zones and their surrounding approved the higher homogeneity by adopting higher power condition. Using TEM and STEM equipped with SAD pattern, the nanosized precipitates inside the mixed zone were indexed as P-phase precipitates. These precipitates are one of the main characteristics of ternary NiTiPt alloys. Finally, the appearing the transformation temperatures related to NiTiPt formed phase inside the mixed zone is a strong proof of formation of high temperature shape memory alloy.

By adding Pt content to NiTi base material, the transformation temperature of fabricated material increased to above 200°C and it showed significant superelasticity at 250°C. However, the

microstructure of fabricated material has microporosity. The changes in Pt concentration resulted in transition between two type of martensite structure of NiTiPt (B2 and B19') and the presence of $Ni_4(Pt, Ti)_3$ nanoprecipitates. Existed dislocations caused some irrecoverable strain in superelastic response.

Chapter 7 Conclusions and Future Works

7.1 Conclusions

In conclusion, the current thesis shed a light on the understanding of laser microwelding of NiTi shape memory alloys, adopting it in welding of similar and dissimilar materials and also fabrication of ternary high temperature shape memory alloys. The detailed conclusions are as follows:

i. One of the main issues regarding the NiTi wire similar welds is Ni vaporization. In order to study this, two different laser parameters have been applied. The high power welds have more texturized microstructures and larger grains compared to the low power condition. In addition, the vaporization of Ni-content resulted in the formation of the martensite phase at room temperature. The results at room temperature showed better superelasticity for the low power sample. However, above the A_f temperature of the high power welded sample, both welded samples presented similar superelastic behaviors.

ii. The effects of laser offset on joint performance of NiTi/stainless steel 316L and NiTi/Cu have been surveyed. In the case of NiTi/SS316L, the offsetting strategy could increase the mechanical response of the welded samples by suppressing the high hardness regions and extremely brittle intermetallics and changing their distribution inside the FZ. On the other hand, laser offsetting on NiTi/Cu showed that positioning the laser on the NiTi and the centerline resulted in a homogenous microstructure including the presence of $Ni_xTi_yCu_z$ IMCs. While laser offsetting onto the Cu, the fusion zone displayed complex flow and mixing patterns containing NiTiCu, pure NiTi, Cu solid solution and pure Cu. The microstructural analysis and phase identification suggested that an acceptable NiTi/Cu weld can be achieved with a 0~50 μm laser offset on the NiTi side.

iii. Dissimilar NiTi/PtIr wire welds without detectable IMCs inside the FZ were fabricated with laser welding. The grain orientation of NiTi BM gradually transitioned toward FZ and the NiTi/FZ interface, exhibiting almost the same orientation of NiTi BM due to their similar B2 crystal structure. However, this transition was completely abrupt at the interface of FZ/PtIr, resulting in large residual strain due to crystallographic and textural mismatch after the welding. Therefore, fracture during the tensile tests occurred in this interface. In successful NiTi/PtIr welds with acceptable tensile strength, the NiTi BM preserved its functional superelastic behavior (up to 263 cycles with 6 % imposed strain before failure).

iv. Laser alloying has been implemented during laser microwelding on the dissimilar joint between NiTi tube and PtIr wire. A single laser pulse can result in the successful fabrication of ternary NiTiPt shape memory alloys and by changing the laser parameters, the chemical composition, homogeneity

and microstructure of the fabricated material could be affected. The appearance of the additional peaks on DSC curves is a strong proof of formation of high temperature shape memory alloy. Consequently, the procedure has been used for fabricating NiTiPt wire, which has significant superelasticity at 250°C. It is shown that, the fabricated material consists of NiTiPt B19 and B19' due to different Pt content in two different phases. As a conclusion, laser welding enabled this alloying process and can introduce a unique fabrication method to rapidly develop ternary shape memory alloys.

7.2 Recommendations and opportunities for future work

Although the present thesis work provids insights into the microwelding of NiTi shape memory alloys using in medical devices, there is a great need to focus more on the process-microstructure-properties of welded NiTi joints. The future studies, in one hand, should have deep analysis of weld appearance and microstructure of microwelded samples considering the flow behavior, the porosity, and quantifying IMCs phases; on the other hand, the applying of solid state processes could be an interesting topic to overcome melting and subsequent solidification, which causes dendritic structure, IMCs formation and complex flow pattern. These studies would be providing a universal map of microwelding of NiTi alloys used in the medical sector.

As mentioned in the third chapter, changing the laser mode from keyhole to conduction mode has a great influence on texture and grain orientation of the welded material. Additionally, in the keyhole mode Ni evaporation accelerated resulting in drastically changing the transformation temperature. However, in the future studies the formation of porosity using 3D characterization technique could open a door for differentiating the types of porosity caused by Ni evaporation and/or keyhole laser mode. Furthermore, adopting a solid state method such as using optimal parameters in resistance microwelding could change the welding characteristic completely and overcome these mentioned challenges.

In the dissimilar laser microwelding between NiTi and stainless steel, interconnected IMCs network could cause embrittlement without preserving any functional properties of the NiTi. Therefore, there is a great opportunity to study other laser parameters (defocusing, adopting other interlayers, changing the laser head angle, laser profile, etc.) in addition to applying resistance microwelding to fabricate acceptable NiTi weld joints with preserved NiTi functional properties. The same studies could be surveyed in NiTi/Cu where the different density of the elements causes complex flow behavior inside the fusion zone.

Finally, fabricating NiTiPt high temperature shape memory alloy by microwelding is in the initial stage. Therefore, different methods can be investigated in the future to optimize the microstructure (through increasing the homogenization time, applying different laser parameters, different aging time and temperature) and control the different phases and precipitates. In this regard studying the shape memory effect of these fabricated materials (NiTiPt) and their relationship with characteristics of martensite would be interesting. It should be mentioned that, in the current research Pt-10Ir material was selected due to its application in the medical industry; however, in order to minimize the complexity or study the Ir influence, pure Pt could be used in the future studies.

References

[1] Industry profile of Medical devices, Gov. Canada. (n.d.). https://www.ic.gc.ca/eic/site/lsg-pdsv.nsf/eng/h_hn01736.html (accessed July 14, 2021).

[2] J.P. Oliveira, R.M. Miranda, F.M. Braz Fernandes, Welding and Joining of NiTi Shape Memory Alloys: A Review, Prog. Mater. Sci. 88 (2017) 412–466. https://doi.org/10.1016/j.pmatsci.2017.04.008.

[3] W. Huang, On the selection of shape memory alloys for actuators, Mater. Des. 23 (2002) 11–19. https://doi.org/10.1016/s0261-3069(01)00039-5.

[4] K.E. Wilkes, P.K. Liaw, Fatigue behavior of shape-memory alloys, Jom. 52 (2000) 45–51. https://doi.org/10.1007/s11837-000-0083-3.

[5] J. Mohd Jani, M. Leary, A. Subic, M.A. Gibson, A review of shape memory alloy research, applications and opportunities, Mater. Des. 56 (2014) 1078–1113. https://doi.org/10.1016/j.matdes.2013.11.084.

[6] K. Otsuka, X. Ren, Physical metallurgy of Ti-Ni-based shape memory alloys, Prog. Mater. Sci. 50 (2005) 511–678. https://doi.org/10.1016/j.pmatsci.2004.10.001.

[7] G.B. Kaufmann, I. Mayo, The Story of Nitinol: The Serendipitous Discovery of the Memory Metal and Its Applications, Chem. Educ. 2 (1997) 1–21. https://doi.org/10.1007/s00897970111a.

[8] G.F. Andreasen, T.B. Hilleman, An evaluation of 55 cobalt substituted Nitinol wire for use in orthodontics, J. Am. Dent. Assoc. 82 (1971) 1373–1375.

[9] N.B. Morgan, Medical shape memory alloy applications - The market and its products, Mater. Sci. Eng. A. 378 (2004) 16–23. https://doi.org/10.1016/j.msea.2003.10.326.

[10] D.J. Hartl, D.C. Lagoudas, Aerospace applications of shape memory alloys, Proc. Inst. Mech. Eng. Part G J. Aerosp. Eng. 221 (2007) 535–552. https://doi.org/10.1243/09544100JAERO211.

[11] P. Motzki, S. Seelecke, Industrial Applications for Shape Memory Alloys, Ref. Modul. Mater. Sci. Mater. Eng. (2019) 0–13. https://doi.org/10.1016/b978-0-12-803581-8.11723-0.

[12] W. Predki, B. Bauer, Concept of a start-up clutch with nickel-titanium shape memory alloys, Forsch. Im Ingenieurwesen/Engineering Res. 74 (2010) 41–47. https://doi.org/10.1007/s10010-010-0114-3.

[13] C.R. Knick, G.L. Smith, C.J. Morris, H.A. Bruck, Rapid and low power laser actuation of sputter-deposited NiTi shape memory alloy (SMA) MEMS thermal bimorph actuators, Sensors Actuators, A Phys. 291 (2019) 48–57. https://doi.org/10.1016/j.sna.2019.03.016.

[14] K. Gall, H. Sehitoglu, Y.I. Chumlyakov, I. V. Kireeva, Tension-compression asymmetry of the stress-strain response in aged single crystal and polycrystalline NiTi, Acta Mater. 47 (1999) 1203–1217. https://doi.org/10.1016/S1359-6454(98)00432-7.

[15] D.A. Porter, K.E. Easterling, M. Sherif, Phase Transformations in Metals and Alloys, (Revised Reprint), CRC press, 2009.

[16] D.C. Lagoudas, Shape memory alloys: Modelling and Engineering Applications, Springer, 2008. https://doi.org/10.1007/978-3-319-03188-0_1.

[17] A.P. Stebner, S.C. Vogel, R.D. Noebe, T.A. Sisneros, B. Clausen, D.W. Brown, A. Garg, L.C. Brinson, Micromechanical quantification of elastic, twinning, and slip strain partitioning exhibited by polycrystalline, monoclinic nickel-titanium during large uniaxial deformations measured via in-situ neutron diffraction, J. Mech.

Phys. Solids. 61 (2013) 2302–2330. https://doi.org/10.1016/j.jmps.2013.05.008.

[18] J. Seo, Y.C. Kim, J.W. Hu, Pilot study for investigating the cyclic behavior of slit damper systems with recentering shape memory alloy (SMA) bending bars used for seismic restrainers, Appl. Sci. 5 (2015) 187–208. https://doi.org/10.3390/app5030187.

[19] Y.K. Kim, Alloys, Shape Memory, 2006. https://doi.org/10.1002/0471732877.emd002.

[20] S. Kou, Welding metallurgy, New Jersey, USA. (2003) 431–446.

[21] K.Y. Benyounis, A.G. Olabi, M.S.J. Hashmi, Effect of laser welding parameters on the heat input and weld-bead profile, J. Mater. Process. Technol. 164–165 (2005) 978–985. https://doi.org/10.1016/j.jmatprotec.2005.02.060.

[22] B. Tam, A. Pequegnat, M.I. Khan, Y. Zhou, Resistance microwelding of Ti-55.8 wt pct ni nitinol wires and the effects of pseudoelasticity, Metall. Mater. Trans. A Phys. Metall. Mater. Sci. 43 (2012) 2969–2978. https://doi.org/10.1007/s11661-012-1115-7.

[23] J.P. Oliveira, F.M.B. Fernandes, R.M. Miranda, N. Schell, J.L. Ocaña, Residual stress analysis in laser welded NiTi sheets using synchrotron X-ray diffraction, Mater. Des. 100 (2016) 180–187. https://doi.org/10.1016/j.matdes.2016.03.137.

[24] J.P. Oliveira, F.M. Braz Fernandes, R.M. Miranda, N. Schell, J.L. Ocaña, Effect of laser welding parameters on the austenite and martensite phase fractions of NiTi, Mater. Charact. 119 (2016) 148–151. https://doi.org/10.1016/j.matchar.2016.08.001.

[25] Z.. b Zeng, M.. Yang, J.P.. P. Oliveira, D.. Song, B.. b Peng, Laser welding of NiTi shape memory alloy wires and tubes for multi-functional design applications, Smart Mater. Struct. 25 (2016). https://doi.org/10.1088/0964-1726/25/8/085001.

[26] S.S.M. Prabu, H.C. Madhu, C.S. Perugu, K. Akash, P.A. Kumar, Microstructure , mechanical properties and shape memory behaviour of friction stir welded nitinol, Mater. Sci. Eng. A. 693 (2017) 233–236. https://doi.org/10.1016/j.msea.2017.03.101.

[27] A. Bahador, E. Hamzah, K. Kondoh, Y. Kawahito, U. Junko, T.A.A. Bakar, Mechanical and superelastic properties of laser welded Ti–Ni shape-memory alloys produced by powder metallurgy, J. Mater. Process. Technol. 248 (2017) 198–206. https://doi.org/10.1016/j.jmatprotec.2017.05.019.

[28] A.S. Zoeram, A. Rahmani, S.A.A. Akbari Mousavi, Characterization the microstructure of pulsed Nd:YAG welding method in low frequencies; Correlation with tensile and fracture behavior in laser-welded nitinol joints, Smart Mater. Struct. 26 (2017). https://doi.org/10.1088/1361-665X/aa65be.

[29] Q. Li, Y. Zhu, Impact butt welding of NiTi and stainless steel- An examination of impact speed effect, J. Mater. Process. Technol. 255 (2018) 434–442. https://doi.org/10.1016/j.jmatprotec.2017.12.046.

[30] W. Zhang, S.S. Ao, J.P. Oliveira, Z. Zeng, Z. Luo, Z.Z. Hao, Effect of ultrasonic spot welding on the mechanical behaviour of NiTi shape memory alloys, Smart Mater. Struct. 27 (2018). https://doi.org/10.1088/1361-665X/aacfeb.

[31] P. Dong, H. Li, W. Wang, J. Zhou, Microstructural characterization of laser micro-welded Nitinol wires, Mater. Charact. 135 (2018) 40–45. https://doi.org/10.1016/j.matchar.2017.11.022.

[32] S.S. Mani Prabu, C.S. Perugu, H.C. Madhu, A. Jangde, S. Khan, S. Jayachandran, M. Manikandan, P.A. Kumar, S. V. Kailas, I.A. Palani, Exploring the functional and corrosion behavior of friction stir welded NiTi shape memory alloy, J. Manuf. Process. 47 (2019) 119–128. https://doi.org/10.1016/j.jmapro.2019.09.017.

[33] W. Zhang, S. Ao, J.P. Oliveira, C. Li, Z. Zeng, A. Wang, Z. Luo, On the metallurgical joining mechanism during

ultrasonic spot welding of NiTi using a Cu interlayer, Scr. Mater. 178 (2020) 414–417. https://doi.org/10.1016/j.scriptamat.2019.12.012.

[34] H. Deng, Y. Chen, S. Li, C. Chen, T. Zhang, M. Xu, D. Ji, Microstructure, mechanical properties and transformation behavior of friction stir welded Ni50.7Ti49.3 alloy, Mater. Des. 189 (2020) 1–10. https://doi.org/10.1016/j.matdes.2020.108491.

[35] S. Datta, M.S. Raza, A.K. Das, P. Saha, D.K. Pratihar, Experimental investigations and parametric optimization of laser beam welding of NiTinol sheets by metaheuristic techniques and desirability function analysis, Opt. Laser Technol. 124 (2020) 105982. https://doi.org/10.1016/j.optlastec.2019.105982.

[36] B. Panton, A. Pequegnat, Y.N. Zhou, Dissimilar laser joining of NiTi SMA and MP35N wires, Metall. Mater. Trans. A Phys. Metall. Mater. Sci. 45 (2014) 3533–3544. https://doi.org/10.1007/s11661-014-2280-7.

[37] Z. Zeng, B. Panton, J.P. Oliveira, A. Han, Y.N. Zhou, Dissimilar laser welding of NiTi shape memory alloy and copper, Smart Mater. Struct. 24 (2015) 125036. https://doi.org/10.1088/0964-1726/24/12/125036.

[38] Z. Zeng, J.P. Oliveira, M. Yang, D. Song, B. Peng, Functional fatigue behavior of NiTi-Cu dissimilar laser welds, Mater. Des. 114 (2017) 282–287. https://doi.org/10.1016/j.matdes.2016.11.023.

[39] Q. Sun, J. Chen, X. Wang, F. Gu, C. Tan, A. Shamsolhodaei, L. Sun, Y.N. Zhou, Study on weld formation and segregation mechanism for dissimilar pulse laser welding of NiTi and Cu wires, Opt. Laser Technol. 140 (2021).

[40] X.L. Gao, X.Q. Wang, J. Liu, L. kun Li, A novel laser welding method for the reliable joining of NiTi/301SS, Mater. Lett. 268 (2020) 127573. https://doi.org/10.1016/j.matlet.2020.127573.

[41] J. Vannod, M. Bornert, J.E. Bidaux, L. Bataillard, A. Karimi, J.M. Drezet, M. Rappaz, A. Hessler-Wyser, Mechanical and microstructural integrity of nickel-titanium and stainless steel laser joined wires, Acta Mater. 59 (2011) 6538–6546. https://doi.org/10.1016/j.actamat.2011.06.031.

[42] R. Hahnlen, G. Fox, M.J. Dapino, Fusion welding of nickel-titanium and 304 stainless steel tubes: Part I: Laser welding, J. Intell. Mater. Syst. Struct. 24 (2013) 945–961. https://doi.org/10.1177/1045389X12461075.

[43] G.R. Mirshekari, A. Saatchi, A. Kermanpur, S.K. Sadrnezhaad, Laser welding of NiTi shape memory alloy: Comparison of the similar and dissimilar joints to AISI 304 stainless steel, Opt. Laser Technol. 54 (2013) 151–158. https://doi.org/10.1016/j.optlastec.2013.05.014.

[44] Q. Li, Y. Zhu, J. Guo, Microstructure and mechanical properties of resistance-welded NiTi/stainless steel joints, J. Mater. Process. Technol. 249 (2017) 538–548. https://doi.org/10.1016/j.jmatprotec.2017.07.001.

[45] S. Hellberg, S. Wagner, D. Martin, S. Bohm, Micro Electron Beam Welding of the hybrid material combination Nitinol and stainless steel without filler material Micro Electron Beam Welding of the hybrid material combination Nitinol and stainless steel without filler material, IOP Conf. Ser. J. Phys. 1089 (2018) 7–16.

[46] C. Grande, Nickel-Titanium Alloys Welding of Thin Sheets Using GTAW : Comparative Study Between Similar and Dissimilar Welding with AISI 304 Stainless Steel, 22 (2019) 1–8.

[47] M.J.C. Oliveira, R.H.F. Melo, T.M. Maciel, C.J. de Araújo, Microstructural evaluation and mechanical behaviour of dissimilar niti-stainless steel joints welded by micro gas tungsten arc welding, Mater. Chem. Phys. 224 (2019) 137–147. https://doi.org/10.1016/j.matchemphys.2018.12.013.

[48] Y. Chen, S. Sun, T. Zhang, X. Zhou, S. Li, Effects of post-weld heat treatment on the microstructure and mechanical properties of laser-welded NiTi/304SS joint with Ni filler, Mater. Sci. Eng. A. 771 (2020) 138545. https://doi.org/10.1016/j.msea.2019.138545.

[49] L. Liu, J. Du, C. Zhou, Welding performance of the dissimilar joints of Fe-Mn-Si alloy and 304 stainless steel, IOP Conf. Ser. Mater. Sci. Eng. 729 (2020). https://doi.org/10.1088/1757-899X/729/1/012100.

[50] H. Niu, H.C. Jiang, M.J. Zhao, L.J. Rong, Effect of interlayer addition on microstructure and mechanical properties of NiTi/stainless steel joint by electron beam welding, J. Mater. Sci. Technol. 61 (2021) 16–24. https://doi.org/10.1016/j.jmst.2020.05.043.

[51] H.M. Li, D.Q. Sun, X.L. Cai, P. Dong, W.Q. Wang, Laser welding of TiNi shape memory alloy and stainless steel using Ni interlayer, Mater. Des. 39 (2012) 285–293. https://doi.org/10.1016/j.matdes.2012.02.031.

[52] J. Pouquet, R.M. Miranda, L. Quintino, S. Williams, Dissimilar laser welding of NiTi to stainless steel, Int. J. Adv. Manuf. Technol. 61 (2012) 205–212. https://doi.org/10.1007/s00170-011-3694-7.

[53] C.H. Ng, E.S.H. Mok, H.C. Man, Effect of Ta interlayer on laser welding of NiTi to AISI 316L stainless steel, J. Mater. Process. Technol. 226 (2015) 69–77. https://doi.org/10.1016/j.jmatprotec.2015.06.039.

[54] A. Shojaei Zoeram, A. Rahmani, S.A.A. Akbari Mousavi, Microstructure and properties analysis of laser-welded Ni–Ti and 316l sheets using copper interlayer, J. Manuf. Process. 26 (2017) 355–363. https://doi.org/10.1016/j.jmapro.2017.02.005.

[55] J.P. Oliveira, Z. Zeng, C. Andrei, F.M. Braz Fernandes, R.M. Miranda, A.J. Ramirez, T. Omori, N. Zhou, Dissimilar laser welding of superelastic NiTi and CuAlMn shape memory alloys, Mater. Des. 128 (2017) 166–175. https://doi.org/10.1016/j.matdes.2017.05.011.

[56] A. Shojaei Zoeram, S.A.A. Akbari Mousavi, Laser welding of Ti-6Al-4V to Nitinol, Mater. Des. 61 (2014) 185–190. https://doi.org/10.1016/j.matdes.2014.04.078.

[57] J.P. Oliveira, B. Panton, Z. Zeng, C.M. Andrei, Y. Zhou, R.M. Miranda, F.M.B. Fernandes, Laser joining of NiTi to Ti6Al4V using a Niobium interlayer, Acta Mater. 105 (2016) 9–15. https://doi.org/10.1016/j.actamat.2015.12.021.

[58] C. Yuhua, M. Yuqing, L. Weiwei, H. Peng, Investigation of welding crack in micro laser welded NiTiNb shape memory alloy and Ti6Al4V alloy dissimilar metals joints, Opt. Laser Technol. 91 (2017) 197–202. https://doi.org/10.1016/j.optlastec.2016.12.028.

[59] R. Prasad, D.T. Waghmare, K. Kumar, M. Masanta, Effect of overlapping condition on large area NiTi layer deposited on Ti-6Al-4V alloy by TIG cladding technique, Surf. Coatings Technol. 385 (2020) 125417. https://doi.org/10.1016/j.surfcoat.2020.125417.

[60] Z. Zhan, Y. Chen, S. Wang, Y. Huang, Y. Mao, Prevention of Crack Formation in Electron-Beam Welded Joints of Dissimilar Metal Compounds (TiNi/Ti6Al4V), Met. Sci. Heat Treat. 61 (2019) 373–378. https://doi.org/10.1007/s11041-019-00432-z.

[61] A.J. Cavaleiro, A.S. Ramos, F.M. Braz Fernandes, N. Schell, M.T. Vieira, Follow-up structural evolution of Ni/Ti reactive nano and microlayers during diffusion bonding of NiTi to Ti6Al4V in a synchrotron beamline, J. Mater. Process. Technol. 275 (2020) 116354. https://doi.org/10.1016/j.jmatprotec.2019.116354.

[62] S. Chatterjee, S.S. Mahapatra, A.K. Pandey, K.S. Arora, T.A. Nguyen, R.K. Gupta, A. Behera, Joining of NiTi/Ti6Al4V alloys using copper intermediate thin layer using fiber laser technology, J. Alloys Compd. (2021) 158916. https://doi.org/10.1016/j.jallcom.2021.158916.

[63] H. Deng, Y. Chen, Y. Jia, Y. Pang, T. Zhang, S. Wang, L. Yin, Microstructure and mechanical properties of dissimilar NiTi / Ti6Al4V joints via back-heating assisted friction stir welding, J. Manuf. Process. 64 (2021) 379–391. https://doi.org/10.1016/j.jmapro.2021.01.024.

[64] J. Xie, Y. Chen, L. Yin, T. Zhang, S. Wang, L. Wang, Microstructure and mechanical properties of ultrasonic spot welding TiNi / Ti6Al4V dissimilar materials using pure Al coating, 64 (2021) 473–480.

[65] S. Datta, M.S. Raza, S. Kumar, P. Saha, Exploring the possibility of dissimilar welding of NiTi to Ti using Yb-fiber laser Exploring the possibility of dissimilar welding of NiTi to Ti using Yb-fiber laser, Adv. Mater. Process. Technol. 0698 (2018) 1–12. https://doi.org/10.1080/2374068X.2018.1486533.

[66] M. Mehrpouya, A. Gisario, M. Barletta, S. Natali, F. Veniali, Dissimilar Laser Welding of NiTi Wires, Lasers Manuf. Mater. Process. 6 (2019) 99–112. https://doi.org/10.1007/s40516-019-00084-0.

[67] J.N. DuPont, A.R. Marder, Thermal efficiency of arc welding processes, Weld. J. (Miami, Fla). 74 (1995) 406-s.

[68] S. Asadi, T. Saeid, A. Valanezhad, I. Watanabe, J. Khalil-Allafi, The effect of annealing temperature on microstructure and mechanical properties of dissimilar laser welded superelastic NiTi to austenitic stainless steels orthodontic archwires, J. Mech. Behav. Biomed. Mater. 109 (2020) 103818. https://doi.org/10.1016/j.jmbbm.2020.103818.

[69] R.H.F. de Melo, M.J.C. de Oliveira, P.Í.V. de Oliveira, M.S.F. de Lima, T.M. Maciel, C.J. de Araújo, Mechanical properties of niti shape memory alloys welded joints: A comparative study between the gtaw, paw and lbw processes, Mater. Sci. Forum. 930 MSF (2018) 526–531. https://doi.org/10.4028/www.scientific.net/MSF.930.526.

[70] S. Fukumoto, Y. Zhou, Mechanism of resistance microwelding of crossed fine nickel wires, Metall. Mater. Trans. A Phys. Metall. Mater. Sci. 35 A (2004) 3165–3176. https://doi.org/10.1007/s11661-004-0061-4.

[71] S. Fukumoto, H. Tsubakino, Y. Zhou, Heat input and deformation control in resistance microwelding of fine nickel wires, Weld. Int. 20 (2006) 692–697. https://doi.org/10.1533/wint.2006.3632.

[72] W.W. Duley, Laser processing and analysis of materials, Springer Science & Business Media, 2012.

[73] A. Falvo, F.M. Furgiuele, C. Maletta, Laser welding of a NiTi alloy: Mechanical and shape memory behaviour, Mater. Sci. Eng. A. 412 (2005) 235–240. https://doi.org/10.1016/j.msea.2005.08.209.

[74] M. Mehrpouya, A. Gisario, M. Elahinia, Laser welding of NiTi shape memory alloy: A review, J. Manuf. Process. 31 (2018) 162–186. https://doi.org/10.1016/j.jmapro.2017.11.011.

[75] A. Tuissi, P. Bassani, M. Gerosa, D. Mauri, M. Pini, E. Capello, B. Previtali, M. Vedani, CO2 laser welding of NiTi/Ni-based alloys, in: Proc. Int. Conf. Shape Mem. Superelastic Technol, 2004: pp. 229–238.

[76] M.I. Khan, A. Pequegnat, Y.N. Zhou, Multiple memory shape memory alloys, Adv. Eng. Mater. 15 (2013) 386–393. https://doi.org/10.1002/adem.201200246.

[77] R. Yao, P. Dong, P.K. Liaw, J. Zhou, W. Wang, Microstructure and shape memory effect of laser welded Nitinol wires, Mater. Lett. 238 (2019) 1–5. https://doi.org/10.1016/j.matlet.2018.11.141.

[78] X. Yan, Y. Ge, Influence of Post-Weld Annealing on Transformation Behavior and Mechanical Properties of Laser-Welded NiTi Alloy Wires, J. Mater. Eng. Perform. 23 (2014) 3474–3479. https://doi.org/10.1007/s11665-014-1156-8.

[79] A. Bahador, E. Hamzah, K. Kondoh, S. Tsutsumi, J. Umeda, T.A.A. Bakar, F. Yusof, Heat-conduction-type and keyhole-type laser welding of TiNi shape-memory alloys processed by spark-plasma sintering, Mater. Trans. 59 (2018) 835–842. https://doi.org/10.2320/matertrans.M2017387.

[80] Y.T. Hsu, Y.R. Wang, S.K. Wu, C. Chen, Effect of CO2laser welding on the shape-memory and corrosion characteristics of TiNi alloys, Metall. Mater. Trans. A Phys. Metall. Mater. Sci. 32 (2001) 569–576. https://doi.org/10.1007/s11661-001-0073-2.

[81] D. Yang, H.C. Jiang, M.J. Zhao, L.J. Rong, Microstructure and mechanical behaviors of electron beam welded NiTi shape memory alloys, Mater. Des. 57 (2014) 21–25. https://doi.org/10.1016/j.matdes.2013.12.039.

[82] S. Datta, M.S. Raza, P. Saha, D.K. Pratihar, Effects of line energy on mechanical properties, corrosion and shape memory behavior of laser-welded NiTinol joints, ASME 2018 13th Int. Manuf. Sci. Eng. Conf. MSEC 2018. 4 (2018) 1–9. https://doi.org/10.1115/MSEC2018-6537.

[83] C.W. Chan, H.C. Man, T.M. Yue, Effects of process parameters upon the shape memory and pseudo-elastic behaviors of laser-welded NiTi thin foil, Metall. Mater. Trans. A Phys. Metall. Mater. Sci. 42 (2011) 2264–2270. https://doi.org/10.1007/s11661-011-0623-1.

[84] A. Shamsolhodaei, Y.N. Zhou, A. Michael, Enhancement of mechanical and functional properties of welded NiTi by controlling nickel vapourisation, Sci. Technol. Weld. Join. 24 (2019) 706–712. https://doi.org/10.1080/13621718.2019.1595926.

[85] M. Mehrpouya, A. Gisario, G.B. Broggiato, M. Puopolo, S. Vesco, M. Barletta, Effect of welding parameters on functionality of dissimilar laser-welded NiTi superelastic (SE) to shape memory effect (SME) wires, Int. J. Adv. Manuf. Technol. 103 (2019) 1593–1601. https://doi.org/10.1007/s00170-019-03514-7.

[86] M.I. Khan, S.K. Panda, Y. Zhou, Effects of welding parameters on the mechanical performance of laser welded nitinol, Mater. Trans. 49 (2008) 2702–2708. https://doi.org/10.2320/matertrans.MRA2008243.

[87] T.D. Bharathi, K. Raju, P.P. Sathiya, A comparison of the effect of different heat treatment processes on laser - welded NiTinol sheets, J. Brazilian Soc. Mech. Sci. Eng. 40 (2018) 1–11. https://doi.org/10.1007/s40430-018-1481-1.

[88] W. Wang, H. Li, The weldability of Shape Memory Alloy, J. Phys. Conf. Ser. 1168 (2019). https://doi.org/10.1088/1742-6596/1168/2/022076.

[89] B. Panton, J.P. Oliveira, Z. Zeng, Y.N. Zhou, M.I. Khan, Thermomechanical fatigue of post-weld heat treated NiTi shape memory alloy wires, Int. J. Fatigue. 92 (2016) 1–7. https://doi.org/10.1016/j.ijfatigue.2016.06.012.

[90] B. Tam, M.I. Khan, Y. Zhou, Mechanical and functional properties of laser-welded Ti-55.8 Wt Pct Ni nitinol wires, Metall. Mater. Trans. A Phys. Metall. Mater. Sci. 42 (2011) 2166–2175. https://doi.org/10.1007/s11661-011-0639-6.

[91] S. Datta, M.S. Raza, P. Saha, D.K. Pratihar, S. Datta, Effects of process parameters on the quality aspects of weld-bead in laser welding of NiTinol sheets Effects of process parameters on the quality aspects of weld-bead in laser welding, Mater. Manuf. Process. 00 (2019) 1–12. https://doi.org/10.1080/10426914.2019.1566608.

[92] J.S. Kirkaldy, L.C. Brown, Diffusion behaviour in ternary, multiphase systems, Can. Metall. Q. 2 (1963) 89–115.

[93] P. Burdet, J. Vannod, A. Hessler-Wyser, M. Rappaz, M. Cantoni, Three-dimensional chemical analysis of laser-welded NiTi-stainless steel wires using a dual-beam FIB, Acta Mater. 61 (2013) 3090–3098. https://doi.org/10.1016/j.actamat.2013.01.069.

[94] R.M. Miranda, E. Assunção, R.J.C. Silva, J.P. Oliveira, L. Quintino, Fiber laser welding of NiTi to Ti-6Al-4V, Int. J. Adv. Manuf. Technol. 81 (2015) 1533–1538. https://doi.org/10.1007/s00170-015-7307-8.

[95] S. Fukumoto, T. Inoue, S. Mizuno, K. Okita, T. Tomita, A. Yamamoto, Friction welding of TiNi alloy to stainless steel using Ni interlayer, Sci. Technol. Weld. Join. 15 (2010) 124–130. https://doi.org/10.1179/136217109X12577814486692.

[96] H. Li, D. Sun, X. Cai, P. Dong, X. Gu, Laser welding of TiNi shape memory alloy and stainless steel using Co filler

metal, Opt. Laser Technol. 45 (2013) 453–460. https://doi.org/10.1016/j.optlastec.2012.06.010.

[97] H. Li, D. Sun, X. Gu, P. Dong, Z. Lv, Effects of the thickness of Cu filler metal on the microstructure and properties of laser-welded TiNi alloy and stainless steel joint, Mater. Des. 50 (2013) 342–350. https://doi.org/10.1016/j.matdes.2013.03.014.

[98] L.H. Shah, A. Gerlich, Y. Zhou, Design guideline for intermetallic compound mitigation in Al-Mg dissimilar welding through addition of interlayer, Int. J. Adv. Manuf. Technol. 94 (2018) 2667–2678. https://doi.org/10.1007/s00170-017-1038-y.

[99] X. Zhou, Y. Chen, Y. Huang, Y. Mao, Y. Yu, Effects of niobium addition on the microstructure and mechanical properties of laser-welded joints of NiTiNb and Ti6Al4V alloys, J. Alloys Compd. 735 (2018) 2616–2624. https://doi.org/10.1016/j.jallcom.2017.11.307.

[100] S. Asadi, T. Saeid, A. Valanezhad, I. Watanabe, J. Khalil-Allafi, Effects of Ni powder addition on microstructure and mechanical properties of NiTi to AISI 304 stainless steel archwire dissimilar laser welds, J. Manuf. Process. 55 (2020) 13–21. https://doi.org/10.1016/j.jmapro.2020.03.041.

[101] X. Gao, X. Wang, J. Liu, L. Li, A novel laser welding method for the reliable joining of NiTi/301SS, Mater. Lett. (2020) 127573. https://doi.org/10.1016/j.matlet.2020.127573.

[102] Y. Chen, S. Sun, T. Zhang, X. Zhou, S. Li, Effects of post-weld heat treatment on the microstructure and mechanical properties of laser-welded NiTi/304SS joint with Ni filler, Mater. Sci. Eng. A. 771 (2020) 138545. https://doi.org/10.1016/j.msea.2019.138545.

[103] A. Shamsolhodaei, J.P. Oliveira, N. Schell, E. Maawad, B. Panton, Y.N. Zhou, Controlling intermetallic compounds formation during laser welding of NiTi to 316L stainless steel, Intermetallics. 116 (2020). https://doi.org/10.1016/j.intermet.2019.106656.

[104] Z. Zeng, B. Panton, J.P. Oliveira, A. Han, Y.N. Zhou, Dissimilar laser welding of NiTi shape memory alloy and copper, Smart Mater. Struct. 24 (2015). https://doi.org/10.1088/0964-1726/24/12/125036.

[105] C.W. Chan, H.C. Man, Reduction of environmentally induced cracking of laser-welded shape memory NiTi wires via post-weld heat-treatment, Mater. Sci. Eng. A. 588 (2013) 388–394. https://doi.org/10.1016/j.msea.2013.09.051.

[106] X.J. Yan, D.Z. Yang, M. Qi, Rotating-bending fatigue of a laser-welded superelastic NiTi alloy wire, Mater. Charact. 57 (2006) 58–63. https://doi.org/10.1016/j.matchar.2005.12.009.

[107] C.W. Chan, H.C. Man, T.M. Yue, Effect of postweld heat treatment on the microstructure and cyclic deformation behavior of laser-welded niti-shape memory wires, Metall. Mater. Trans. A Phys. Metall. Mater. Sci. 43 (2012) 1956–1965. https://doi.org/10.1007/s11661-011-1062-8.

[108] J. Zhang, T. Chen, W. Li, J. Bednarcik, A.C. Dippel, High temperature superelasticity realized in equiatomic Ti-Ni conventional shape memory alloy by severe cold rolling, Mater. Des. 193 (2020) 108875. https://doi.org/10.1016/j.matdes.2020.108875.

[109] H.O. Tugrul, H.H. Saygili, B. Kockar, Influence of limiting the actuation strain on the functional fatigue behavior of Ni50.3Ti29.7Hf20 high temperature shape memory alloy, J. Intell. Mater. Syst. Struct. 32 (2021) 219–227. https://doi.org/10.1177/1045389X20953610.

[110] O. Karakoc, K.C. Atli, A. Evirgen, J. Pons, R. Santamarta, O. Benafan, R.D. Noebe, I. Karaman, Effects of training on the thermomechanical behavior of NiTiHf and NiTiZr high temperature shape memory alloys, Mater. Sci. Eng. A. 794 (2020) 139857. https://doi.org/10.1016/j.msea.2020.139857.

[111] Y. Tong, A. Shuitcev, Y. Zheng, Recent Development of TiNi-Based Shape Memory Alloys with High Cycle Stability and High Transformation Temperature, Adv. Eng. Mater. 22 (2020) 1–15. https://doi.org/10.1002/adem.201900496.

[112] O. Benafan, D.J. Gaydosh, R.D. Noebe, S. Qiu, R. Vaidyanathan, In Situ Neutron Diffraction Study of NiTi–21Pt High-Temperature Shape Memory Alloys, Shape Mem. Superelasticity. 2 (2016) 337–346. https://doi.org/10.1007/s40830-016-0095-7.

[113] A.N. Bucsek, G.A. Hudish, G.S. Bigelow, R.D. Noebe, A.P. Stebner, Composition, Compatibility, and the Functional Performances of Ternary NiTiX High-Temperature Shape Memory Alloys, Shape Mem. Superelasticity. 2 (2016) 62–79. https://doi.org/10.1007/s40830-016-0052-5.

[114] J. Ma, I. Karaman, R.D. Noebe, High temperature shape memory alloys, Int. Mater. Rev. 55 (2010) 257–315. https://doi.org/10.1179/095066010X12646898728363.

[115] K. V. Ramaiah, C.N. Saikrishna, M. Sujata, M. Madan, S.K. Bhaumik, NiTiPt shape memory alloy: microstructure and transformation behaviour, ISSS J. Micro Smart Syst. 8 (2019) 81–88. https://doi.org/10.1007/s41683-019-00039-9.

[116] J.N. Lemke, F. Gallino, M. Cresci, A. Coda, Achieving improved workability and competitive high temperature shape memory performance by Nb addition to Ni-Ti-Hf alloys, Scr. Mater. 191 (2021) 161–166. https://doi.org/10.1016/j.scriptamat.2020.09.032.

[117] M. Elahinia, N. Shayesteh Moghaddam, A. Amerinatanzi, S. Saedi, G.P. Toker, H. Karaca, G.S. Bigelow, O. Benafan, Additive manufacturing of NiTiHf high temperature shape memory alloy, Scr. Mater. 145 (2018) 90–94. https://doi.org/10.1016/j.scriptamat.2017.10.016.

[118] M. Nematollahi, G. Toker, S.E. Saghaian, J. Salazar, M. Mahtabi, O. Benafan, H. Karaca, M. Elahinia, Additive Manufacturing of Ni-Rich NiTiHf20: Manufacturability, Composition, Density, and Transformation Behavior, Shape Mem. Superelasticity. 5 (2019) 113–124. https://doi.org/10.1007/s40830-019-00214-9.

[119] M. Mehrpouya, A. Gisario, M. Nematollahi, A. Rahimzadeh, K.S. Baghbaderani, M. Elahinia, The prediction model for additively manufacturing of NiTiHf high-temperature shape memory alloy, Mater. Today Commun. 26 (2021) 102022. https://doi.org/10.1016/j.mtcomm.2021.102022.

[120] J.P. Oliveira, N. Schell, N. Zhou, L. Wood, O. Benafan, Laser welding of precipitation strengthened Ni-rich NiTiHf high temperature shape memory alloys: Microstructure and mechanical properties, Mater. Des. 162 (2019) 229–234. https://doi.org/10.1016/j.matdes.2018.11.053.

[121] J.P. Oliveira, J. Shen, J.D. Escobar, C.A.F. Salvador, N. Schell, N. Zhou, O. Benafan, Laser welding of H-phase strengthened Ni-rich NiTi-20Zr high temperature shape memory alloy, Mater. Des. 202 (2021) 109533. https://doi.org/10.1016/j.matdes.2021.109533.

[122] H.E. Karaca, S.M. Saghaian, G. Ded, H. Tobe, B. Basaran, H.J. Maier, R.D. Noebe, Y.I. Chumlyakov, Effects of nanoprecipitation on the shape memory and material properties of an Ni-rich NiTiHf high temperature shape memory alloy, Acta Mater. 61 (2013) 7422–7431. https://doi.org/10.1016/j.actamat.2013.08.048.

[123] D. Mackiewicz, Z.C. Lin, Laser welding binary nitinol to NiTiPt radiopaque nitinol., in: SMST-2004 Proc. Int. Conf. Shape Mem. Superelastic Technol., ASM International, 2006: pp. 295–300.

[124] D. Stoeckel, A. Pelton, T. Duerig, Self-expanding Nitinol stents: Material and design considerations, Eur. Radiol. 14 (2004) 292–301. https://doi.org/10.1007/s00330-003-2022-5.

[125] Z. Lin, H.M. Hsiao, D. Mackiewicz, B. Anukhin, K. Pike, Anisotropic behavior of radiopaque NiTiPt hypotube for biomedical applications, Adv. Eng. Mater. 11 (2009). https://doi.org/10.1002/adem.200800403.

[126] S. Hao, L. Cui, J. Jiang, F. Guo, X. Xiao, D. Jiang, C. Yu, Z. Chen, H. Zhou, Y. Wang, Y. Liu, D.E. Brown, Y. Ren, A novel multifunctional NiTi/Ag hierarchical composite, Sci. Rep. 4 (2014). https://doi.org/10.1038/srep05267.

[127] S. Wang, F.M. Guo, D.Q. Jiang, Y. Liu, L.S. Cui, In situ W-NiTi shape memory alloy composite of high radiopacity, Scr. Mater. 81 (2014) 4–7. https://doi.org/10.1016/j.scriptamat.2014.02.002.

[128] S. Tsirkas, P. Papanikos, T. Kermanidis, Numerical simulation of the laser welding process in butt-joint specimens, J. Mater. Process. Technol. 134 (2003) 59–69. https://doi.org/10.1016/S0924-0136(02)00921-4.

[129] A.M. El-Batahgy, Effect of laser welding parameters on fusion zone shape and solidification structure of austenitic stainless steels, Mater. Lett. 32 (1997) 155–163. https://doi.org/10.1016/S0167-577X(97)00023-2.

[130] P. Schlossmacher, T. Haas, A. Schüssler, Laser-Welding of a Ni-Rich TiNi Shape Memory Alloy: Mechanical Behavior, J. Phys. IV Fr. 7 (1997) 251–256.

[131] H. Gugel, A. Schuermann, W. Theisen, Laser welding of NiTi wires, Mater. Sci. Eng. A. 481–482 (2008) 668–671. https://doi.org/10.1016/j.msea.2006.11.179.

[132] A. Tuissi, S. Besseghini, T. Ranucci, F. Squatrito, M. Pozzi, Effect of Nd-YAG laser welding on the functional properties of the Ni-49.6at.%Ti, Mater. Sci. Eng. A. 273–275 (1999) 813–817. https://doi.org/10.1016/s0921-5093(99)00422-0.

[133] C. Maletta, A. Falvo, F. Furgiuele, G. Barbieri, M. Brandizzi, Fracture behaviour of nickel-titanium laser welded joints, J. Mater. Eng. Perform. 18 (2009) 569–574.

[134] A. Michael, Laser Processing and Modelling of Multiple Memory Shape Memory Alloys by, (2018).

[135] J.P. Oliveira, R.M. Miranda, N. Schell, F.M.B. Fernandes, High strain and long duration cycling behavior of laser welded NiTi sheets, Int. J. Fatigue. 83 (2016) 195–200. https://doi.org/10.1016/j.ijfatigue.2015.10.013.

[136] J.P. Oliveira, F.M.B. Fernandes, N. Schell, R.M. Miranda, Martensite stabilization during superelastic cycling of laser welded NiTi plates, Mater. Lett. 171 (2016) 273–276. https://doi.org/10.1016/j.matlet.2016.02.107.

[137] P. Sedmák, P. Šittner, J. Pilch, C. Curfs, Instability of cyclic superelastic deformation of NiTi investigated by synchrotron X-ray diffraction, Acta Mater. 94 (2015) 257–270. https://doi.org/10.1016/j.actamat.2015.04.039.

[138] M. Mehrpouya, A. Gisario, H. Huang, A. Rahimzadeh, M. Elahinia, Numerical study for prediction of optimum operational parameters in laser welding of NiTi alloy, Opt. Laser Technol. 118 (2019) 159–169. https://doi.org/10.1016/j.optlastec.2019.05.010.

[139] J. Khalil-Allafi, A. Dlouhy, G. Eggeler, Ni4Ti3-precipitation during aging of NiTi shape memory alloys and its influence on martensitic phase transformations, Acta Mater. 50 (2002) 4255–4274. https://doi.org/10.1016/S1359-6454(02)00257-4.

[140] J. Frenzel, E.P. George, A. Dlouhy, C. Somsen, M.F.X. Wagner, G. Eggeler, Influence of Ni on martensitic phase transformations in NiTi shape memory alloys, Acta Mater. 58 (2010) 3444–3458. https://doi.org/10.1016/j.actamat.2010.02.019.

[141] H. Tobushi, Y. Shimeno, T. Hachisuka, K. Tanaka, Influence of strain rate on superelastic properties of TiNi shape memory alloy, Mech. Mater. 30 (1998) 141–150. https://doi.org/10.1016/S0167-6636(98)00041-6.

[142] O. Benafan, R.D. Noebe, S.A. Padula, D.J. Gaydosh, B.A. Lerch, A. Garg, G.S. Bigelow, K. An, R. Vaidyanathan, Temperature-dependent behavior of a polycrystalline NiTi shape memory alloy around the transformation regime,

Scr. Mater. 68 (2013) 571–574. https://doi.org/10.1016/j.scriptamat.2012.11.042.

[143] Z. Zeng, M. Yang, J.P. Oliveira, D. Song, B. Peng, Laser welding of NiTi shape memory alloy wires and tubes for multi-functional design applications, Smart Mater. Struct. 25 (2016). https://doi.org/10.1088/0964-1726/25/8/085001.

[144] G. Cacciamani, J. De Keyzer, R. Ferro, U.E. Klotz, J. Lacaze, P. Wollants, Critical evaluation of the Fe-Ni, Fe-Ti and Fe-Ni-Ti alloy systems, Intermetallics. 14 (2006) 1312–1325. https://doi.org/10.1016/j.intermet.2005.11.028.

[145] C. Zhang, S. Zhao, X. Sun, D. Sun, X. Sun, Corrosion of laser-welded NiTi shape memory alloy and stainless steel composite wires with a copper interlayer upon exposure to fluoride and mechanical stress, Corros. Sci. 82 (2014) 404–409. https://doi.org/10.1016/j.corsci.2014.01.040.

[146] D. Ruhlig, H. Gugel, A. Schulte, W. Theisenb, W. Schuhmann, Visualization of local electrochemical activity and local nickel ion release on laser-welded NiTi/steel joints using combined alternating current mode and stripping mode SECM, Analyst. 133 (2008) 1700–1706. https://doi.org/10.1039/b804718a.

[147] Z. Zhu, W. Wang, Y. Li, H. Chen, Effect of laser-arc offset and laser-deviation angle on the control of a Ti-Al interlayer, J. Mater. Process. Technol. 271 (2019) 336–345. https://doi.org/10.1016/j.jmatprotec.2019.04.010.

[148] H.C. Chen, A.J. Pinkerton, L. Li, Fibre laser welding of dissimilar alloys of Ti-6Al-4V and Inconel 718 for aerospace applications, Int. J. Adv. Manuf. Technol. 52 (2011) 977–987. https://doi.org/10.1007/s00170-010-2791-3.

[149] Z. Song, K. Nakata, A. Wu, J. Liao, Interfacial microstructure and mechanical property of Ti6Al4V/A6061 dissimilar joint by direct laser brazing without filler metal and groove, Mater. Sci. Eng. A. 560 (2013) 111–120. https://doi.org/10.1016/j.msea.2012.09.044.

[150] I. Tomashchuk, P. Sallamand, E. Cicala, P. Peyre, D. Grevey, Direct keyhole laser welding of aluminum alloy AA5754 to titanium alloy Ti6Al4V, J. Mater. Process. Technol. 217 (2015) 96–104. https://doi.org/10.1016/j.jmatprotec.2014.10.025.

[151] G. Casalino, P. Guglielmi, V.D. Lorusso, M. Mortello, P. Peyre, D. Sorgente, Laser offset welding of AZ31B magnesium alloy to 316 stainless steel, J. Mater. Process. Technol. 242 (2017) 49–59. https://doi.org/10.1016/j.jmatprotec.2016.11.020.

[152] Z. Li, G. Fontana, M. Penasa, Autogenous laser welding of austenitic stainless steel to copper alloy, Sci. Technol. Weld. Join. 3 (2014) 81–87. https://doi.org/10.1179/stw.1998.3.2.81.

[153] S. Chen, J. Huang, J. Xia, X. Zhao, S. Lin, Influence of processing parameters on the characteristics of stainless steel/copper laser welding, J. Mater. Process. Technol. 222 (2015) 43–51. https://doi.org/10.1016/j.jmatprotec.2015.03.003.

[154] S. Chen, J. Huang, J. Xia, H. Zhang, X. Zhao, Microstructural characteristics of a stainless steel/copper dissimilar joint made by laser welding, Metall. Mater. Trans. A Phys. Metall. Mater. Sci. 44 (2013) 3690–3696. https://doi.org/10.1007/s11661-013-1693-z.

[155] A.P. Hammersley, S.O. Svensson, M. Hanfland, A.N. Fitch, D. Hausermann, Two-dimensional detector software: From real detector to idealised image or two-theta scan, High Press. Res. 14 (2007) 235–248. https://doi.org/10.1080/08957959608201408.

[156] W.J. Zhu, L.I. Duarte, C. Leinenbach, Experimental study and thermodynamic assessment of the Cu-Ni-Ti system, Calphad Comput. Coupling Phase Diagrams Thermochem. 47 (2014) 9–22. https://doi.org/10.1016/j.calphad.2014.06.002.

[157] H. Du, Y. Fu, Deposition and characterization of Ti1− x (Ni, Cu) x shape memory alloy thin films, Surf. Coatings Technol. 176 (2004) 182–187. https://doi.org/10.1016/S0257-8972(03)00625-X.

[158] D.S. Zhao, J.C. Yan, C.W. Wang, Y. Wang, S.Q. Yang, Interfacial structure and mechanical properties of hot roll bonded joints between titanium alloy and stainless steel using copper interlayer, Sci. Technol. Weld. Join. 13 (2008) 765–768. https://doi.org/10.1179/136217108X329304.

[159] S. Alkan, H. Sehitoglu, Plastic flow resistance of NiTiCu shape memory alloy-theory and experiments, Acta Mater. 163 (2019) 173–188. https://doi.org/10.1016/j.actamat.2018.09.063.

[160] M. Morakabati, S. Kheirandish, M. Aboutalebi, A.K. Taheri, S.M. Abbasi, The effect of Cu addition on the hot deformation behavior of NiTi shape memory alloys, J. Alloys Compd. 499 (2010) 57–62. https://doi.org/10.1016/j.jallcom.2010.01.124.

[161] T. Nam, T. Saburi, K. Shimizu, Cu-content dependence of shape memory characteristics in Ti–Ni–Cu alloys, Mater. Trans. Jim. 31 (1990) 959–967. https://doi.org/10.2320/matertrans1989.31.959.

[162] S. V. Kuryntsev, A.E. Morushkin, A.K. Gilmutdinov, Fiber laser welding of austenitic steel and commercially pure copper butt joint, Opt. Lasers Eng. 90 (2017) 101–109. https://doi.org/10.1016/j.optlaseng.2016.10.008.

[163] C. Pandey, M.M. Mahapatra, P. Kumar, S. Sirohi, Fracture behaviour of crept P91 welded sample for different post weld heat treatments condition, Eng. Fail. Anal. 95 (2019) 18–29. https://doi.org/10.1016/j.engfailanal.2018.08.029.

[164] C. Pandey, N. Saini, M.M. Mahapatra, P. Kumar, Study of the fracture surface morphology of impact and tensile tested cast and forged (C&F) Grade 91 steel at room temperature for different heat treatment regimes, Eng. Fail. Anal. 71 (2017) 131–147. https://doi.org/10.1016/j.engfailanal.2016.06.012.

[165] E. Biro, D.C. Weckman, Y. Zhou, Pulsed Nd : YAG Laser Welding of Copper Using Oxygenated Assist Gases, 33 (2019) 2019–2030.

[166] P.J. Høl, N.R. Gjerdet, T. Jonung, Corrosion and metal release from overlapping arterial stents under mechanical and electrochemical stress – An experimental study, J. Mech. Behav. Biomed. Mater. 93 (2019) 31–35. https://doi.org/10.1016/j.jmbbm.2019.02.001.

[167] S. Shabalovskaya, J. Anderegg, J. Van Humbeeck, Critical overview of Nitinol surfaces and their modifications for medical applications, Acta Biomater. 4 (2008) 447–467. https://doi.org/10.1016/j.actbio.2008.01.013.

[168] N.J. Noolu, H.W. Kerr, Y. Zhou, J. Xie, Laser weldability of Pt and Ti alloys, Mater. Sci. Eng. A. 397 (2005) 8–15. https://doi.org/10.1016/j.msea.2004.12.044.

[169] D.S. Levi, N. Kusnezov, G.P. Carman, Smart materials applications for pediatric cardiovascular devices, Pediatr. Res. 63 (2008) 552–558. https://doi.org/10.1203/PDR.0b013e31816a9d18.

[170] G.S. Zou, Y.D. Huang, A. Pequegnat, X.G. Li, M.I. Khan, Y. Zhou, Crossed-wire laser microwelding of Pt-10 pct Ir to 316 low-carbon vacuum melted stainless steel: Part I. Mechanism of joint formation, Metall. Mater. Trans. A Phys. Metall. Mater. Sci. 43 (2012) 1223–1233. https://doi.org/10.1007/s11661-011-0763-3.

[171] A.P. Hammersley, S.O. Svensson, M. Hanfland, A.N. Fitch, D. Häusermann, Two-dimensional detector software: From real detector to idealised image or two-theta scan, High Press. Res. 14 (1996) 235–248. https://doi.org/10.1080/08957959608201408.

[172] J. Mao, Y. Huang, P. He, Study on joint formation evolution in laser microwelding of Pt-10%Ir and 316 LVM SS crossed wiresCrossed wire, Laser microwelding, Simulation, Joint formation, 93 (2016) 11–16. https://doi.org/10.2991/ismems-16.2016.3.

[173] Z. Chen, Joint formation mechanism and strength in resistance microwelding of 316L stainless steel to Pt wire, J. Mater. Sci. 42 (2007) 5756–5765. https://doi.org/10.1007/s10853-006-0671-x.

[174] O. Rios, R. Noebe, T. Biles, A. Garg, A. Palczer, D. Scheiman, H.J. Seifert, M. Kaufman, Characterization of ternary NiTiPt high-temperature shape memory alloys, Smart Struct. Mater. 2005 Act. Mater. Behav. Mech. 5761 (2005) 376. https://doi.org/10.1117/12.599608.

[175] A. Michael, Y.N. Zhou, M. Yavuz, M.I. Khan, Modelling the alloy element composition change in NiTi achieved through laser induced vaporization, Mater. Chem. Phys. 231 (2019) 87–94. https://doi.org/10.1016/j.matchemphys.2019.04.015.

[176] J.P. Oliveira, F.M. Braz Fernandes, R.M. Miranda, N. Schell, On the Mechanisms for Martensite Formation in YAG Laser Welded Austenitic NiTi, Shape Mem. Superelasticity. 2 (2016) 114–120. https://doi.org/10.1007/s40830-016-0058-z.

[177] R. Sokkalingam, V. Muthupandi, K. Sivaprasad, K.G. Prashanth, Dissimilar welding of Al0.1CoCrFeNi high-entropy alloy and AISI304 stainless steel, J. Mater. Res. (2019). https://doi.org/10.1557/jmr.2019.186.

[178] B. Lin, K. Gall, H.J. Maier, R. Waldron, Structure and thermomechanical behavior of NiTiPt shape memory alloy wires, Acta Biomater. 5 (2009) 257–267. https://doi.org/10.1016/j.actbio.2008.07.015.

[179] J. Kangazian, M. Shamanian, Micro-texture and corrosion behavior of dissimilar joints of UNS S32750 stainless steel/UNS N08825 Ni-based superalloy, Mater. Charact. 155 (2019) 109802. https://doi.org/10.1016/j.matchar.2019.109802.

[180] H. Ming, Z. Zhang, J. Wang, E.H. Han, P. Wang, Z. Sun, Microstructure of a safe-end dissimilar metal weld joint (SA508-52-316L) prepared by narrow-gap GTAW, Mater. Charact. 123 (2017) 233–243. https://doi.org/10.1016/j.matchar.2016.11.029.

[181] R. Kirchheim, Reducing grain boundary, dislocation line and vacancy formation energies by solute segregation. I. Theoretical background, Acta Mater. 55 (2007) 5129–5138. https://doi.org/10.1016/j.actamat.2007.05.047.

[182] P. Trivedi, D.P. Field, H. Weiland, Alloying effects on dislocation substructure evolution of aluminum alloys, Int. J. Plast. 20 (2004) 459–476. https://doi.org/10.1016/S0749-6419(03)00097-4.

[183] L. Kovarik, F. Yang, A. Garg, D. Diercks, M. Kaufman, R.D. Noebe, M.J. Mills, Structural analysis of a new precipitate phase in high-temperature TiNiPt shape memory alloys, Acta Mater. 58 (2010) 4660–4673. https://doi.org/10.1016/j.actamat.2010.04.039.

[184] M. Moshref-Javadi, M. Belbasi, S.H. Seyedein, M.T. Salehi, Fabrication of (Ti,Hf)-rich NiTiHf alloy using graphitic mold and crucible, J. Mater. Sci. Technol. 30 (2014) 280–284. https://doi.org/10.1016/j.jmst.2013.10.001.

[185] D. Chovan, A. Gandhi, J. Butler, S.A.M. Tofail, Static magnetic susceptibility of radiopaque NiTiPt and NiTiEr, J. Magn. Magn. Mater. 452 (2018) 451–457. https://doi.org/10.1016/j.jmmm.2017.12.090.

[186] T.E. Buchheit, D.F. Susan, J.E. Massad, J.R. McElhanon, R.D. Noebe, Mechanical and Functional Behavior of High-Temperature Ni-Ti-Pt Shape Memory Alloys, Metall. Mater. Trans. A Phys. Metall. Mater. Sci. 47 (2016) 1587–1599. https://doi.org/10.1007/s11661-016-3324-y.

[187] D. Chovan, M. Nolan, S.A.M. Tofail, First principles simulations of elastic properties of radiopaque NiTiPt, J. Alloys Compd. 630 (2015) 54–59. https://doi.org/10.1016/j.jallcom.2014.12.185.

[188] A.C. Coppa, M. Kapoor, R. Noebe, G.B. Thompson, The compositional stability of the P-phase in Ni-Ti-Pd shape memory alloys, Intermetallics. 67 (2015) 56–62. https://doi.org/10.1016/j.intermet.2015.07.014.

[189] Y. Gao, N. Zhou, F. Yang, Y. Cui, L. Kovarik, N. Hatcher, R. Noebe, M.J. Mills, Y. Wang, P-phase precipitation and its effect on martensitic transformation in (Ni,Pt)Ti shape memory alloys, Acta Mater. 60 (2012) 1514–1527. https://doi.org/10.1016/j.actamat.2011.11.043.

[190] C. Bechtold, R. Lima de Miranda, C. Chluba, C. Zamponi, E. Quandt, Method for Fabricating Miniaturized NiTi Self-Expandable Thin Film Devices with Increased Radiopacity, Shape Mem. Superelasticity. 2 (2016) 391–398. https://doi.org/10.1007/s40830-016-0086-8.

[191] K. V Ramaiah, C.N. Saikrishna, M. Sujata, S.K. Bhaumik, Ni30 Ti50 Pt20 High Temperature Shape Memory Alloy (HTSMA) Wires : Processing Related Issues, J. ISSS. 2 (2013) 1–9.

[192] L. O'Donoghue, A.A. Gandhi, J. Butler, W. Redington, P. Tiernan, T. McGloughlin, J.C. Carlson, S. Lavelle, S.A.M. Tofail, X-ray and microstructural investigation of NiTiPt alloys homogenised at intermediate to high temperatures, Nucl. Instruments Methods Phys. Res. Sect. B Beam Interact. with Mater. Atoms. 268 (2010) 287–290. https://doi.org/10.1016/j.nimb.2009.07.015.

[193] M. Elahinia, N. Shayesteh Moghaddam, M. Taheri Andani, A. Amerinatanzi, B.A. Bimber, R.F. Hamilton, Fabrication of NiTi through additive manufacturing: A review, Prog. Mater. Sci. 83 (2016) 630–663. https://doi.org/10.1016/j.pmatsci.2016.08.001.

[194] S. Parvizi, S.M. Hashemi, F. Asgarinia, M. Nematollahi, M. Elahinia, Effective parameters on the final properties of NiTi-based alloys manufactured by powder metallurgy methods: A review, Prog. Mater. Sci. 117 (2021) 100739. https://doi.org/10.1016/j.pmatsci.2020.100739.

[195] J. Van Humbeeck, Additive Manufacturing of Shape Memory Alloys, Shape Mem. Superelasticity. 4 (2018) 309–312. https://doi.org/10.1007/s40830-018-0174-z.

[196] A.N. Alagha, S. Hussain, W. Zaki, Additive manufacturing of shape memory alloys: A review with emphasis on powder bed systems, Mater. Des. 204 (2021) 109654. https://doi.org/10.1016/j.matdes.2021.109654.

[197] G.P. Toker, M. Nematollahi, S.E. Saghaian, K.S. Baghbaderani, O. Benafan, M. Elahinia, H.E. Karaca, Shape memory behavior of NiTiHf alloys fabricated by selective laser melting, Scr. Mater. 178 (2020) 361–365. https://doi.org/10.1016/j.scriptamat.2019.11.056.

[198] S. Shiva, N. Yadaiah, I.A. Palani, C.P. Paul, K.S. Bindra, Thermo mechanical analyses and characterizations of TiNiCu shape memory alloy structures developed by laser additive manufacturing, J. Manuf. Process. 48 (2019) 98–109. https://doi.org/10.1016/j.jmapro.2019.11.003.

[199] C.T. Kwok, P.K. Wong, H.C. Man, Enhancement in corrosion and electrical wear resistance of copper via laser surface alloying with NiTi, Surf. Coatings Technol. 408 (2021) 126804. https://doi.org/10.1016/j.surfcoat.2020.126804.

[200] K.W. Ng, H.C. Man, T.M. Yue, Characterization and corrosion study of NiTi laser surface alloyed with Nb or Co, Appl. Surf. Sci. 257 (2011) 3269–3274. https://doi.org/10.1016/j.apsusc.2010.10.154.

[201] Y. Yamabe-Mitarai, T. Aoyagi, T. Abe, An investigation of phase separation in the Ir-Pt binary system, J. Alloys Compd. 484 (2009) 327–334. https://doi.org/10.1016/j.jallcom.2009.04.105.

[202] K.C. Mills, B.J. Keene, R.F. Brooks, A. Shirali, Marangoni effects in welding, Philos. Trans. R. Soc. A Math. Phys. Eng. Sci. 356 (1998) 911–925. https://doi.org/10.1098/rsta.1998.0196.

[203] R. Indhu, S. Soundarapandian, L. Vijayaraghavan, Yb: YAG laser welding of dual phase steel to aluminium alloy, J. Mater. Process. Technol. 262 (2018) 411–421. https://doi.org/10.1016/j.jmatprotec.2018.05.022.

[204] F. Yang, R.D. Noebe, M.J. Mills, Precipitates in a near-equiatomic (Ni + Pt)-rich TiNiPt alloy, Scr. Mater. 69 (2013) 713–715. https://doi.org/10.1016/j.scriptamat.2013.08.002.

[205] O. Benafan, D.J. Gaydosh, R.D. Noebe, S. Qiu, R. Vaidyanathan, In Situ Neutron Diffraction Study of NiTi–21Pt High-Temperature Shape Memory Alloys, Shape Mem. Superelasticity. 2 (2016) 337–346. https://doi.org/10.1007/s40830-016-0095-7.

[206] R. Esmaeilizadeh, A. Keshavarzkermani, U. Ali, Y. Mahmoodkhani, B. Behravesh, H. Jahed, A. Bonakdar, E. Toyserkani, Customizing mechanical properties of additively manufactured Hastelloy X parts by adjusting laser scanning speed, J. Alloys Compd. 812 (2020) 152097. https://doi.org/10.1016/j.jallcom.2019.152097.

[207] J. Xu, Y. Rong, Y. Huang, P. Wang, C. Wang, Keyhole-induced porosity formation during laser welding, J. Mater. Process. Technol. 252 (2018) 720–727. https://doi.org/10.1016/j.jmatprotec.2017.10.038.

[208] S. Shiva, I.A. Palani, C.P. Paul, S.K. Mishra, B. Singh, Investigations on phase transformation and mechanical characteristics of laser additive manufactured TiNiCu shape memory alloy structures, J. Mater. Process. Technol. 238 (2016) 142–151. https://doi.org/10.1016/j.jmatprotec.2016.07.012.

[209] J.L. Smialek, A. Garg, R.B. Rogers, R.D. Noebe, Oxide scales formed on NiTi and NiPtTi shape memory alloys, Metall. Mater. Trans. A Phys. Metall. Mater. Sci. 43 (2012) 2325–2341. https://doi.org/10.1007/s11661-011-1036-x.

Appendix A
Letters of Copyright Permission

The first two pages of each material's copyright permission are added to this appendix section. The whole documents will be provided upon request.

ELSEVIER LICENSE
TERMS AND CONDITIONS

Dec 07, 2021

This Agreement between Dr. Amirali Shamsolhodaei ("You") and Elsevier ("Elsevier") consists of your license details and the terms and conditions provided by Elsevier and Copyright Clearance Center.

License Number	5203841438621
License date	Dec 07, 2021
Licensed Content Publisher	Elsevier
Licensed Content Publication	Progress in Materials Science
Licensed Content Title	Physical metallurgy of Ti–Ni-based shape memory alloys
Licensed Content Author	K. Otsuka,X. Ren
Licensed Content Date	Jul 1, 2005
Licensed Content Volume	50
Licensed Content Issue	5
Licensed Content Pages	168
Start Page	511
End Page	678
Type of Use	reuse in a thesis/dissertation
Portion	figures/tables/illustrations

Number of figures/tables/illustrations	2
Format	both print and electronic
Are you the author of this Elsevier article?	No
Will you be translating?	No
Title	Dissimilar laser welding of NiTi shape memory alloys
Institution name	University of Waterloo
Expected presentation date	Dec 2021
Portions	Figure 2, Figure 76
Requestor Location	Dr. Amirali Shamsolhodaei 200 University Avenue West Waterloo, ON N2L 3G Canada Attn: Dr. Amirali Shamsolhodaei
Publisher Tax ID	GB 494 6272 12
Total	0.00 CAD
Terms and Conditions	

INTRODUCTION

1. The publisher for this copyrighted material is Elsevier. By clicking "accept" in connection with completing this licensing transaction, you agree that the following terms and conditions apply to this transaction (along with the Billing and Payment terms and conditions established by Copyright Clearance Center, Inc. ("CCC"), at the time that you opened your Rightslink account and that are available at any time at http://myaccount.copyright.com).

GENERAL TERMS

ELSEVIER LICENSE
TERMS AND CONDITIONS

Dec 07, 2021

This Agreement between Dr. Amirali Shamsolhodaei ("You") and Elsevier ("Elsevier") consists of your license details and the terms and conditions provided by Elsevier and Copyright Clearance Center.

License Number	5203851312498
License date	Dec 07, 2021
Licensed Content Publisher	Elsevier
Licensed Content Publication	Materials Science and Engineering: A
Licensed Content Title	Medical shape memory alloy applications—the market and its products
Licensed Content Author	N.B Morgan
Licensed Content Date	Jul 25, 2004
Licensed Content Volume	378
Licensed Content Issue	1-2
Licensed Content Pages	8
Start Page	16
End Page	23
Type of Use	reuse in a thesis/dissertation
Portion	figures/tables/illustrations

Number of figures/tables/illustrations	1
Format	both print and electronic
Are you the author of this Elsevier article?	No
Will you be translating?	No
Title	Dissimilar laser welding of NiTi shape memory alloys
Institution name	University of Waterloo
Expected presentation date	Dec 2021
Portions	Figure 2
Requestor Location	Dr. Amirali Shamsolhodaei 200 University Avenue West Waterloo, ON N2L 3G Canada Attn: Dr. Amirali Shamsolhodaei
Publisher Tax ID	GB 494 6272 12
Total	0.00 CAD

Terms and Conditions

INTRODUCTION

1. The publisher for this copyrighted material is Elsevier. By clicking "accept" in connection with completing this licensing transaction, you agree that the following terms and conditions apply to this transaction (along with the Billing and Payment terms and conditions established by Copyright Clearance Center, Inc. ("CCC"), at the time that you opened your Rightslink account and that are available at any time at http://myaccount.copyright.com).

GENERAL TERMS

2. Elsevier hereby grants you permission to reproduce the aforementioned material subject to the terms and conditions indicated.

3. Acknowledgement: If any part of the material to be used (for example, figures) has appeared in our publication with credit or acknowledgement to another source, permission

ELSEVIER LICENSE
TERMS AND CONDITIONS

Dec 07, 2021

This Agreement between Dr. Amirali Shamsolhodaei ("You") and Elsevier ("Elsevier") consists of your license details and the terms and conditions provided by Elsevier and Copyright Clearance Center.

License Number	5203860024972
License date	Dec 07, 2021
Licensed Content Publisher	Elsevier
Licensed Content Publication	Elsevier Books
Licensed Content Title	Encyclopedia of Smart Materials
Licensed Content Author	Paul Motzki,Stefan Seelecke
Licensed Content Date	Jan 1, 2022
Licensed Content Pages	13
Start Page	254
End Page	266
Type of Use	reuse in a thesis/dissertation
Portion	figures/tables/illustrations
Number of figures/tables/illustrations	1
Format	both print and electronic
Are you the author of this Elsevier	No

chapter?	
Will you be translating?	No
Title	Dissimilar laser welding of NiTi shape memory alloys
Institution name	University of Waterloo
Expected presentation date	Dec 2021
Portions	Figure 11
Requestor Location	Dr. Amirali Shamsolhodaei 200 University Avenue West Waterloo, ON N2L 3G Canada Attn: Dr. Amirali Shamsolhodaei
Publisher Tax ID	GB 494 6272 12
Total	0.00 CAD
Terms and Conditions	

INTRODUCTION

1. The publisher for this copyrighted material is Elsevier. By clicking "accept" in connection with completing this licensing transaction, you agree that the following terms and conditions apply to this transaction (along with the Billing and Payment terms and conditions established by Copyright Clearance Center, Inc. ("CCC"), at the time that you opened your Rightslink account and that are available at any time at http://myaccount.copyright.com).

GENERAL TERMS

2. Elsevier hereby grants you permission to reproduce the aforementioned material subject to the terms and conditions indicated.

3. Acknowledgement: If any part of the material to be used (for example, figures) has appeared in our publication with credit or acknowledgement to another source, permission must also be sought from that source. If such permission is not obtained then that material may not be included in your publication/copies. Suitable acknowledgement to the source must be made, either as a footnote or in a reference list at the end of your publication, as follows:

"Reprinted from Publication title, Vol /edition number, Author(s), Title of article / title of chapter, Pages No., Copyright (Year), with permission from Elsevier [OR APPLICABLE

SPRINGER NATURE LICENSE
TERMS AND CONDITIONS

Dec 07, 2021

This Agreement between Dr. Amirali Shamsolhodaei ("You") and Springer Nature ("Springer Nature") consists of your license details and the terms and conditions provided by Springer Nature and Copyright Clearance Center.

License Number	5203860267095
License date	Dec 07, 2021
Licensed Content Publisher	Springer Nature
Licensed Content Publication	Forschung im Ingenieurwesen
Licensed Content Title	Concept of a start-up clutch with nickel-titanium shape memory alloys
Licensed Content Author	W. Predki et al
Licensed Content Date	Feb 24, 2010
Type of Use	Thesis/Dissertation
Requestor type	academic/university or research institute
Format	print and electronic
Portion	figures/tables/illustrations
Number of figures/tables/illustrations	1
Will you be translating?	no
Circulation/distribution	1 - 29

Author of this Springer Nature content	no
Title	Dissimilar laser welding of NiTi shape memory alloys
Institution name	University of Waterloo
Expected presentation date	Dec 2021
Portions	Figure 4
Requestor Location	Dr. Amirali Shamsolhodaei 200 University Avenue West Waterloo, ON N2L 3G Canada Attn: Dr. Amirali Shamsolhodaei
Total	0.00 CAD

Terms and Conditions

Springer Nature Customer Service Centre GmbH
Terms and Conditions

This agreement sets out the terms and conditions of the licence (the **Licence**) between you and **Springer Nature Customer Service Centre GmbH** (the **Licensor**). By clicking 'accept' and completing the transaction for the material (**Licensed Material**), you also confirm your acceptance of these terms and conditions.

1. Grant of License

1. 1. The Licensor grants you a personal, non-exclusive, non-transferable, world-wide licence to reproduce the Licensed Material for the purpose specified in your order only. Licences are granted for the specific use requested in the order and for no other use, subject to the conditions below.

1. 2. The Licensor warrants that it has, to the best of its knowledge, the rights to license reuse of the Licensed Material. However, you should ensure that the material you are requesting is original to the Licensor and does not carry the copyright of another entity (as credited in the published version).

1. 3. If the credit line on any part of the material you have requested indicates that it was reprinted or adapted with permission from another source, then you should also seek permission from that source to reuse the material.

2. Scope of Licence

ELSEVIER LICENSE
TERMS AND CONDITIONS

Dec 07, 2021

This Agreement between Dr. Amirali Shamsolhodaei ("You") and Elsevier ("Elsevier") consists of your license details and the terms and conditions provided by Elsevier and Copyright Clearance Center.

License Number	5203881178513
License date	Dec 07, 2021
Licensed Content Publisher	Elsevier
Licensed Content Publication	Materials & Design
Licensed Content Title	A review of shape memory alloy research, applications and opportunities
Licensed Content Author	Jaronie Mohd Jani,Martin Leary,Aleksandar Subic,Mark A. Gibson
Licensed Content Date	Apr 1, 2014
Licensed Content Volume	56
Licensed Content Issue	n/a
Licensed Content Pages	36
Start Page	1078
End Page	1113
Type of Use	reuse in a thesis/dissertation
Portion	figures/tables/illustrations

Number of figures/tables/illustrations	2
Format	both print and electronic
Are you the author of this Elsevier article?	No
Will you be translating?	No
Title	Dissimilar laser welding of NiTi shape memory alloys
Institution name	University of Waterloo
Expected presentation date	Dec 2021
Portions	Figure 1 and Figure 18
Requestor Location	Dr. Amirali Shamsolhodaei 200 University Avenue West Waterloo, ON N2L 3G Canada Attn: Dr. Amirali Shamsolhodaei
Publisher Tax ID	GB 494 6272 12
Total	0.00 CAD

Terms and Conditions

INTRODUCTION

1. The publisher for this copyrighted material is Elsevier. By clicking "accept" in connection with completing this licensing transaction, you agree that the following terms and conditions apply to this transaction (along with the Billing and Payment terms and conditions established by Copyright Clearance Center, Inc. ("CCC"), at the time that you opened your Rightslink account and that are available at any time at http://myaccount.copyright.com).

GENERAL TERMS

2. Elsevier hereby grants you permission to reproduce the aforementioned material subject to the terms and conditions indicated.

3. Acknowledgement: If any part of the material to be used (for example, figures) has appeared in our publication with credit or acknowledgement to another source, permission

ELSEVIER LICENSE
TERMS AND CONDITIONS

Dec 07, 2021

This Agreement between Dr. Amirali Shamsolhodaei ("You") and Elsevier ("Elsevier") consists of your license details and the terms and conditions provided by Elsevier and Copyright Clearance Center.

License Number	5203860463876
License date	Dec 07, 2021
Licensed Content Publisher	Elsevier
Licensed Content Publication	Sensors and Actuators A: Physical
Licensed Content Title	Rapid and low power laser actuation of sputter-deposited NiTi shape memory alloy (SMA) MEMS thermal bimorph actuators
Licensed Content Author	Cory R. Knick,Gabriel L. Smith,Christopher J. Morris,Hugh A. Bruck
Licensed Content Date	Jun 1, 2019
Licensed Content Volume	291
Licensed Content Issue	n/a
Licensed Content Pages	10
Start Page	48
End Page	57
Type of Use	reuse in a thesis/dissertation

Portion	figures/tables/illustrations
Number of figures/tables/illustrations	1
Format	both print and electronic
Are you the author of this Elsevier article?	No
Will you be translating?	No
Title	Dissimilar laser welding of NiTi shape memory alloys
Institution name	University of Waterloo
Expected presentation date	Dec 2021
Portions	Figure 1
Requestor Location	Dr. Amirali Shamsolhodaei 200 University Avenue West Waterloo, ON N2L 3G Canada Attn: Dr. Amirali Shamsolhodaei
Publisher Tax ID	GB 494 6272 12
Total	0.00 CAD
Terms and Conditions	

INTRODUCTION

1. The publisher for this copyrighted material is Elsevier. By clicking "accept" in connection with completing this licensing transaction, you agree that the following terms and conditions apply to this transaction (along with the Billing and Payment terms and conditions established by Copyright Clearance Center, Inc. ("CCC"), at the time that you opened your Rightslink account and that are available at any time at http://myaccount.copyright.com).

GENERAL TERMS

ELSEVIER LICENSE
TERMS AND CONDITIONS

Dec 07, 2021

This Agreement between Dr. Amirali Shamsolhodaei ("You") and Elsevier ("Elsevier") consists of your license details and the terms and conditions provided by Elsevier and Copyright Clearance Center.

License Number	5203860541409
License date	Dec 07, 2021
Licensed Content Publisher	Elsevier
Licensed Content Publication	Journal of the Mechanics and Physics of Solids
Licensed Content Title	Micromechanical quantification of elastic, twinning, and slip strain partitioning exhibited by polycrystalline, monoclinic nickel–titanium during large uniaxial deformations measured via in-situ neutron diffraction
Licensed Content Author	A.P. Stebner,S.C. Vogel,R.D. Noebe,T.A. Sisneros,B. Clausen,D.W. Brown,A. Garg,L.C. Brinson
Licensed Content Date	Nov 1, 2013
Licensed Content Volume	61
Licensed Content Issue	11
Licensed Content Pages	29
Start Page	2302
End Page	2330
Type of Use	reuse in a thesis/dissertation

Portion	figures/tables/illustrations
Number of figures/tables/illustrations	2
Format	both print and electronic
Are you the author of this Elsevier article?	No
Will you be translating?	No
Title	Dissimilar laser welding of NiTi shape memory alloys
Institution name	University of Waterloo
Expected presentation date	Dec 2021
Portions	Figure 1 and Figure 2
Requestor Location	Dr. Amirali Shamsolhodaei 200 University Avenue West Waterloo, ON N2L 3G Canada Attn: Dr. Amirali Shamsolhodaei
Publisher Tax ID	GB 494 6272 12
Total	0.00 CAD
Terms and Conditions	

INTRODUCTION

1. The publisher for this copyrighted material is Elsevier. By clicking "accept" in connection with completing this licensing transaction, you agree that the following terms and conditions apply to this transaction (along with the Billing and Payment terms and conditions established by Copyright Clearance Center, Inc. ("CCC"), at the time that you opened your Rightslink account and that are available at any time at http://myaccount.copyright.com).

GENERAL TERMS

JOHN WILEY AND SONS LICENSE
TERMS AND CONDITIONS

Dec 07, 2021

This Agreement between Dr. Amirali Shamsolhodaei ("You") and John Wiley and Sons ("John Wiley and Sons") consists of your license details and the terms and conditions provided by John Wiley and Sons and Copyright Clearance Center.

License Number	5203860648380
License date	Dec 07, 2021
Licensed Content Publisher	John Wiley and Sons
Licensed Content Publication	Wiley Books
Licensed Content Title	Welding Metallurgy, 3rd Edition
Licensed Content Author	Sindo Kou
Licensed Content Date	Oct 1, 2020
Licensed Content Pages	1
Type of use	Dissertation/Thesis
Requestor type	University/Academic
Format	Print and electronic
Portion	Figure/table
Number of figures/tables	1
Will you be translating?	No
Title	Dissimilar laser welding of NiTi shape memory alloys

Institution name	University of Waterloo
Expected presentation date	Dec 2021
Portions	Figure 1-1
Requestor Location	Dr. Amirali Shamsolhodaei 200 University Avenue West Waterloo, ON N2L 3G Canada Attn: Dr. Amirali Shamsolhodaei
Publisher Tax ID	EU826007151
Total	0.00 CAD

Terms and Conditions

TERMS AND CONDITIONS

This copyrighted material is owned by or exclusively licensed to John Wiley & Sons, Inc. or one of its group companies (each a"Wiley Company") or handled on behalf of a society with which a Wiley Company has exclusive publishing rights in relation to a particular work (collectively "WILEY"). By clicking "accept" in connection with completing this licensing transaction, you agree that the following terms and conditions apply to this transaction (along with the billing and payment terms and conditions established by the Copyright Clearance Center Inc., ("CCC's Billing and Payment terms and conditions"), at the time that you opened your RightsLink account (these are available at any time at http://myaccount.copyright.com).

Terms and Conditions

- The materials you have requested permission to reproduce or reuse (the "Wiley Materials") are protected by copyright.
- You are hereby granted a personal, non-exclusive, non-sub licensable (on a stand-alone basis), non-transferable, worldwide, limited license to reproduce the Wiley Materials for the purpose specified in the licensing process. This license, **and any CONTENT (PDF or image file) purchased as part of your order,** is for a one-time use only and limited to any maximum distribution number specified in the license. The first instance of republication or reuse granted by this license must be completed within two years of the date of the grant of this license (although copies prepared before the end date may be distributed thereafter). The Wiley Materials shall not be used in any other manner or for any other purpose, beyond what is granted in the license. Permission is granted subject to an appropriate acknowledgement given to the author, title of the material/book/journal and the publisher. You shall also duplicate the copyright notice that appears in the Wiley publication in your use of the Wiley

ELSEVIER LICENSE
TERMS AND CONDITIONS

Dec 09, 2021

This Agreement between Dr. Amirali Shamsolhodaei ("You") and Elsevier ("Elsevier") consists of your license details and the terms and conditions provided by Elsevier and Copyright Clearance Center.

License Number	5205030747321
License date	Dec 09, 2021
Licensed Content Publisher	Elsevier
Licensed Content Publication	Optics & Laser Technology
Licensed Content Title	Experimental investigations and parametric optimization of laser beam welding of NiTinol sheets by metaheuristic techniques and desirability function analysis
Licensed Content Author	Susmita Datta,Mohammad Shahid Raza,Amit Kumar Das,Partha Saha,Dilip Kumar Pratihar
Licensed Content Date	Apr 1, 2020
Licensed Content Volume	124
Licensed Content Issue	n/a
Licensed Content Pages	1
Start Page	105982
End Page	0
Type of Use	reuse in a thesis/dissertation

Portion	figures/tables/illustrations
Number of figures/tables/illustrations	1
Format	both print and electronic
Are you the author of this Elsevier article?	No
Will you be translating?	No
Title	Dissimilar laser welding of NiTi shape memory alloys
Institution name	University of Waterloo
Expected presentation date	Dec 2021
Portions	Figure 1
Requestor Location	Dr. Amirali Shamsolhodaei 200 University Avenue West Waterloo, ON N2L 3G Canada Attn: Dr. Amirali Shamsolhodaei
Publisher Tax ID	GB 494 6272 12
Total	0.00 CAD
Terms and Conditions	

INTRODUCTION

1. The publisher for this copyrighted material is Elsevier. By clicking "accept" in connection with completing this licensing transaction, you agree that the following terms and conditions apply to this transaction (along with the Billing and Payment terms and conditions established by Copyright Clearance Center, Inc. ("CCC"), at the time that you opened your Rightslink account and that are available at any time at http://myaccount.copyright.com).

GENERAL TERMS

ELSEVIER LICENSE
TERMS AND CONDITIONS

Dec 07, 2021

This Agreement between Dr. Amirali Shamsolhodaei ("You") and Elsevier ("Elsevier") consists of your license details and the terms and conditions provided by Elsevier and Copyright Clearance Center.

License Number	5203860902907
License date	Dec 07, 2021
Licensed Content Publisher	Elsevier
Licensed Content Publication	Materials Chemistry and Physics
Licensed Content Title	Microstructural evaluation and mechanical behaviour of dissimilar niti-stainless steel joints welded by micro gas tungsten arc welding
Licensed Content Author	M.J.C. Oliveira,R.H.F. Melo,T.M. Maciel,C.J. de Araújo
Licensed Content Date	Feb 15, 2019
Licensed Content Volume	224
Licensed Content Issue	n/a
Licensed Content Pages	11
Start Page	137
End Page	147
Type of Use	reuse in a thesis/dissertation

Portion	figures/tables/illustrations
Number of figures/tables/illustrations	4
Format	both print and electronic
Are you the author of this Elsevier article?	No
Will you be translating?	No
Title	Dissimilar laser welding of NiTi shape memory alloys
Institution name	University of Waterloo
Expected presentation date	Dec 2021
Portions	Table 5, Table 6, Figure 1, Figure 6
Requestor Location	Dr. Amirali Shamsolhodaei 200 University Avenue West Waterloo, ON N2L 3G Canada Attn: Dr. Amirali Shamsolhodaei
Publisher Tax ID	GB 494 6272 12
Total	0.00 CAD
Terms and Conditions	

INTRODUCTION

1. The publisher for this copyrighted material is Elsevier. By clicking "accept" in connection with completing this licensing transaction, you agree that the following terms and conditions apply to this transaction (along with the Billing and Payment terms and conditions established by Copyright Clearance Center, Inc. ("CCC"), at the time that you opened your Rightslink account and that are available at any time at http://myaccount.copyright.com).

GENERAL TERMS

ELSEVIER LICENSE
TERMS AND CONDITIONS

Dec 07, 2021

This Agreement between Dr. Amirali Shamsolhodaei ("You") and Elsevier ("Elsevier") consists of your license details and the terms and conditions provided by Elsevier and Copyright Clearance Center.

License Number	5203861027261
License date	Dec 07, 2021
Licensed Content Publisher	Elsevier
Licensed Content Publication	Journal of Materials Processing Technology
Licensed Content Title	Microstructure and mechanical properties of resistance-welded NiTi/stainless steel joints
Licensed Content Author	Qiao Li,Yuanxiang Zhu,Jialin Guo
Licensed Content Date	Nov 1, 2017
Licensed Content Volume	249
Licensed Content Issue	n/a
Licensed Content Pages	11
Start Page	538
End Page	548
Type of Use	reuse in a thesis/dissertation
Portion	figures/tables/illustrations

Number of figures/tables/illustrations	5
Format	both print and electronic
Are you the author of this Elsevier article?	No
Will you be translating?	No
Title	Dissimilar laser welding of NiTi shape memory alloys
Institution name	University of Waterloo
Expected presentation date	Dec 2021
Portions	Figure 1, Figure 3, Figure 5, Figure 10 and Figure 11
Requestor Location	Dr. Amirali Shamsolhodaei 200 University Avenue West Waterloo, ON N2L 3G Canada Attn: Dr. Amirali Shamsolhodaei
Publisher Tax ID	GB 494 6272 12
Total	0.00 CAD

Terms and Conditions

INTRODUCTION

1. The publisher for this copyrighted material is Elsevier. By clicking "accept" in connection with completing this licensing transaction, you agree that the following terms and conditions apply to this transaction (along with the Billing and Payment terms and conditions established by Copyright Clearance Center, Inc. ("CCC"), at the time that you opened your Rightslink account and that are available at any time at http://myaccount.copyright.com).

GENERAL TERMS

2. Elsevier hereby grants you permission to reproduce the aforementioned material subject to the terms and conditions indicated.

3. Acknowledgement: If any part of the material to be used (for example, figures) has appeared in our publication with credit or acknowledgement to another source, permission

SPRINGER NATURE LICENSE
TERMS AND CONDITIONS

Dec 07, 2021

This Agreement between Dr. Amirali Shamsolhodaei ("You") and Springer Nature ("Springer Nature") consists of your license details and the terms and conditions provided by Springer Nature and Copyright Clearance Center.

License Number	5203861276617
License date	Dec 07, 2021
Licensed Content Publisher	Springer Nature
Licensed Content Publication	Metallurgical and Materials Transactions A
Licensed Content Title	Resistance Microwelding of Ti-55.8 wt pct Ni Nitinol Wires and the Effects of Pseudoelasticity
Licensed Content Author	Billy Tam et al
Licensed Content Date	Mar 17, 2012
Type of Use	Thesis/Dissertation
Requestor type	academic/university or research institute
Format	print and electronic
Portion	figures/tables/illustrations
Number of figures/tables/illustrations	2
Will you be translating?	no

Circulation/distribution	1 - 29
Author of this Springer Nature content	no
Title	Dissimilar laser welding of NiTi shape memory alloys
Institution name	University of Waterloo
Expected presentation date	Dec 2021
Portions	Figure 1, Figure 10
Requestor Location	Dr. Amirali Shamsolhodaei 200 University Avenue West Waterloo, ON N2L 3G Canada Attn: Dr. Amirali Shamsolhodaei
Total	0.00 CAD

Terms and Conditions

Springer Nature Customer Service Centre GmbH
Terms and Conditions

This agreement sets out the terms and conditions of the licence (the **Licence**) between you and **Springer Nature Customer Service Centre GmbH** (the **Licensor**). By clicking 'accept' and completing the transaction for the material (**Licensed Material**), you also confirm your acceptance of these terms and conditions.

1. Grant of License

1. 1. The Licensor grants you a personal, non-exclusive, non-transferable, world-wide licence to reproduce the Licensed Material for the purpose specified in your order only. Licences are granted for the specific use requested in the order and for no other use, subject to the conditions below.

1. 2. The Licensor warrants that it has, to the best of its knowledge, the rights to license reuse of the Licensed Material. However, you should ensure that the material you are requesting is original to the Licensor and does not carry the copyright of another entity (as credited in the published version).

1. 3. If the credit line on any part of the material you have requested indicates that it was reprinted or adapted with permission from another source, then you should also

SPRINGER NATURE LICENSE
TERMS AND CONDITIONS

Dec 07, 2021

This Agreement between Dr. Amirali Shamsolhodaei ("You") and Springer Nature ("Springer Nature") consists of your license details and the terms and conditions provided by Springer Nature and Copyright Clearance Center.

License Number	5203861356823
License date	Dec 07, 2021
Licensed Content Publisher	Springer Nature
Licensed Content Publication	Metallurgical and Materials Transactions A
Licensed Content Title	Mechanism of resistance microwelding of crossed fine nickel wires
Licensed Content Author	S. Fukumoto et al
Licensed Content Date	Jan 1, 2004
Type of Use	Thesis/Dissertation
Requestor type	academic/university or research institute
Format	print and electronic
Portion	figures/tables/illustrations
Number of figures/tables/illustrations	1
Will you be translating?	no
Circulation/distribution	1 - 29

Author of this Springer Nature content	no
Title	Dissimilar laser welding of NiTi shape memory alloys
Institution name	University of Waterloo
Expected presentation date	Dec 2021
Portions	Figure 3
Requestor Location	Dr. Amirali Shamsolhodaei 200 University Avenue West Waterloo, ON N2L 3G Canada Attn: Dr. Amirali Shamsolhodaei
Total	0.00 CAD

Terms and Conditions

Springer Nature Customer Service Centre GmbH
Terms and Conditions

This agreement sets out the terms and conditions of the licence (the **Licence**) between you and **Springer Nature Customer Service Centre GmbH** (the **Licensor**). By clicking 'accept' and completing the transaction for the material (**Licensed Material**), you also confirm your acceptance of these terms and conditions.

1. Grant of License

1. 1. The Licensor grants you a personal, non-exclusive, non-transferable, world-wide licence to reproduce the Licensed Material for the purpose specified in your order only. Licences are granted for the specific use requested in the order and for no other use, subject to the conditions below.

1. 2. The Licensor warrants that it has, to the best of its knowledge, the rights to license reuse of the Licensed Material. However, you should ensure that the material you are requesting is original to the Licensor and does not carry the copyright of another entity (as credited in the published version).

1. 3. If the credit line on any part of the material you have requested indicates that it was reprinted or adapted with permission from another source, then you should also seek permission from that source to reuse the material.

2. Scope of Licence

ELSEVIER LICENSE
TERMS AND CONDITIONS

Dec 07, 2021

This Agreement between Dr. Amirali Shamsolhodaei ("You") and Elsevier ("Elsevier") consists of your license details and the terms and conditions provided by Elsevier and Copyright Clearance Center.

License Number	5203861423282
License date	Dec 07, 2021
Licensed Content Publisher	Elsevier
Licensed Content Publication	Materials Science and Engineering: A
Licensed Content Title	Laser welding of a NiTi alloy: Mechanical and shape memory behaviour
Licensed Content Author	A. Falvo,F.M. Furgiuele,C. Maletta
Licensed Content Date	Dec 5, 2005
Licensed Content Volume	412
Licensed Content Issue	1-2
Licensed Content Pages	6
Start Page	235
End Page	240
Type of Use	reuse in a thesis/dissertation
Portion	figures/tables/illustrations

Number of figures/tables/illustrations	1
Format	both print and electronic
Are you the author of this Elsevier article?	No
Will you be translating?	No
Title	Dissimilar laser welding of NiTi shape memory alloys
Institution name	University of Waterloo
Expected presentation date	Dec 2021
Portions	Figure 7
Requestor Location	Dr. Amirali Shamsolhodaei 200 University Avenue West Waterloo, ON N2L 3G Canada Attn: Dr. Amirali Shamsolhodaei
Publisher Tax ID	GB 494 6272 12
Total	0.00 CAD

Terms and Conditions

INTRODUCTION

1. The publisher for this copyrighted material is Elsevier. By clicking "accept" in connection with completing this licensing transaction, you agree that the following terms and conditions apply to this transaction (along with the Billing and Payment terms and conditions established by Copyright Clearance Center, Inc. ("CCC"), at the time that you opened your Rightslink account and that are available at any time at http://myaccount.copyright.com).

GENERAL TERMS

2. Elsevier hereby grants you permission to reproduce the aforementioned material subject to the terms and conditions indicated.

3. Acknowledgement: If any part of the material to be used (for example, figures) has appeared in our publication with credit or acknowledgement to another source, permission

CCC Marketplace™

Order Confirmation

Thank you, your order has been placed. An email confirmation has been sent to you. Your order license details and printable licenses will be available within 24 hours. Please access Manage Account for final order details.

This is not an invoice. Please go to manage account to access your order history and invoices.

CUSTOMER INFORMATION

Payment by invoice: You can cancel your order until the invoice is generated by contacting customer service.

Billing Address

Dr. Amirali Shamsolhodaei
200 University Avenue West
Waterloo, ON N2L 3G1
Canada

+1 (519) 888-4567
ashamsol@uwaterloo.ca

Customer Location

Dr. Amirali Shamsolhodaei
200 University Avenue West
Waterloo, ON N2L 3G1
Canada

PO Number (optional)

N/A

Payment options

Invoice

PENDING ORDER CONFIRMATION

Confirmation Number: Pending

Order Date: 09-Dec-2021

1. SMST-2003 : Proceedings

0.00 CAD

Article: CO~2 Laser Welding of NiTi/Ni-Based Alloys

Order License ID	Pending	**Publisher**	ASM International
ISBN-13	9780966050837	**Portion**	Chart/graph/table/ figure
Type of Use	Republish in a thesis/dissertation		

LICENSED CONTENT

Publication Title	SMST-2003 : Proceedings	**Publication Type**	Book
Article Title	CO~2 Laser Welding of NiTi/Ni-Based Alloys	**Start Page**	229
		End Page	238
Date	01/01/2003	**Volume**	2003; 2003; YEAR

Country	United States of America
Rightsholder	ASM International

REQUEST DETAILS

Portion Type	Chart/graph/table/figure	Distribution	Canada
Number of charts / graphs / tables / figures requested	2	Translation	Original language of publication
Format (select all that apply)	Print, Electronic	Copies for the disabled?	No
		Minor editing privileges?	No
Who will republish the content?	Academic institution	Incidental promotional use?	No
Duration of Use	Life of current and all future editions	Currency	CAD
Lifetime Unit Quantity	Up to 499		
Rights Requested	Main product		

NEW WORK DETAILS

Title	Dissimilar laser welding of NiTi shape memory alloys	Institution name	University of Waterloo
		Expected presentation date	2021-12-07
Instructor name	Prof. Norman Zhou, Prof. Peng Peng		

ADDITIONAL DETAILS

Order reference number	N/A	The requesting person / organization to appear on the license	Amirali Shamsolhodaei

REUSE CONTENT DETAILS

Title, description or numeric reference of the portion(s)	CO~2 Laser Welding of NiTi/Ni-Based Alloys	Title of the article/chapter the portion is from	CO~2 Laser Welding of NiTi/Ni-Based Alloys
Editor of portion(s)	Tuissi, A.; Gerosa, M.; Bassani, P.; Vedani, M.; Previtali, B.; Capello, E.; Pini, M.; Mauri, D.	Author of portion(s)	Tuissi, A.; Gerosa, M.; Bassani, P.; Vedani, M.; Previtali, B.; Capello, E.; Pini, M.; Mauri, D.
Volume of serial or monograph	2003; 2003; YEAR	Issue, if republishing an article from a serial	N/A
Page or page range of portion	231 and 233 (Figure 1 and Figure 4)	Publication date of portion	2003-01-01

Total Items: 1 **Total Due: 0.00 CAD**

Accepted: All Publisher and CCC Terms and Conditions

JOHN WILEY AND SONS LICENSE
TERMS AND CONDITIONS

Dec 07, 2021

This Agreement between Dr. Amirali Shamsolhodaei ("You") and John Wiley and Sons ("John Wiley and Sons") consists of your license details and the terms and conditions provided by John Wiley and Sons and Copyright Clearance Center.

License Number	5203890472009
License date	Dec 07, 2021
Licensed Content Publisher	John Wiley and Sons
Licensed Content Publication	Advanced Engineering Materials
Licensed Content Title	Multiple Memory Shape Memory Alloys
Licensed Content Author	Y. Norman Zhou, Andrew Pequegnat, Mohammad Ibraheem Khan
Licensed Content Date	Feb 15, 2013
Licensed Content Volume	15
Licensed Content Issue	5
Licensed Content Pages	8
Type of use	Dissertation/Thesis
Requestor type	University/Academic
Format	Print and electronic
Portion	Figure/table

Number of figures/tables	1
Will you be translating?	No
Title	Dissimilar laser welding of NiTi shape memory alloys
Institution name	University of Waterloo
Expected presentation date	Dec 2021
Portions	Figure 1
Requestor Location	Dr. Amirali Shamsolhodaei 200 University Avenue West Waterloo, ON N2L 3G Canada Attn: Dr. Amirali Shamsolhodaei
Publisher Tax ID	EU826007151
Total	0.00 CAD

Terms and Conditions

TERMS AND CONDITIONS

This copyrighted material is owned by or exclusively licensed to John Wiley & Sons, Inc. or one of its group companies (each a"Wiley Company") or handled on behalf of a society with which a Wiley Company has exclusive publishing rights in relation to a particular work (collectively "WILEY"). By clicking "accept" in connection with completing this licensing transaction, you agree that the following terms and conditions apply to this transaction (along with the billing and payment terms and conditions established by the Copyright Clearance Center Inc., ("CCC's Billing and Payment terms and conditions"), at the time that you opened your RightsLink account (these are available at any time at http://myaccount.copyright.com).

Terms and Conditions

- The materials you have requested permission to reproduce or reuse (the "Wiley Materials") are protected by copyright.
- You are hereby granted a personal, non-exclusive, non-sub licensable (on a stand-alone basis), non-transferable, worldwide, limited license to reproduce the Wiley Materials for the purpose specified in the licensing process. This license, **and any CONTENT (PDF or image file) purchased as part of your order,** is for a one-time use only and limited to any maximum distribution number specified in the license.

ELSEVIER LICENSE
TERMS AND CONDITIONS

Dec 07, 2021

This Agreement between Dr. Amirali Shamsolhodaei ("You") and Elsevier ("Elsevier") consists of your license details and the terms and conditions provided by Elsevier and Copyright Clearance Center.

License Number	5203890557689
License date	Dec 07, 2021
Licensed Content Publisher	Elsevier
Licensed Content Publication	Materials Characterization
Licensed Content Title	Effect of laser welding parameters on the austenite and martensite phase fractions of NiTi
Licensed Content Author	J.P. Oliveira,F.M. Braz Fernandes,R.M. Miranda,N. Schell,J.L. Ocaña
Licensed Content Date	Sep 1, 2016
Licensed Content Volume	119
Licensed Content Issue	n/a
Licensed Content Pages	4
Start Page	148
End Page	151
Type of Use	reuse in a thesis/dissertation
Portion	figures/tables/illustrations

Number of figures/tables/illustrations	1
Format	both print and electronic
Are you the author of this Elsevier article?	No
Will you be translating?	No
Title	Dissimilar laser welding of NiTi shape memory alloys
Institution name	University of Waterloo
Expected presentation date	Dec 2021
Portions	Figure 1
Requestor Location	Dr. Amirali Shamsolhodaei 200 University Avenue West Waterloo, ON N2L 3G Canada Attn: Dr. Amirali Shamsolhodaei
Publisher Tax ID	GB 494 6272 12
Total	0.00 CAD

Terms and Conditions

INTRODUCTION

1. The publisher for this copyrighted material is Elsevier. By clicking "accept" in connection with completing this licensing transaction, you agree that the following terms and conditions apply to this transaction (along with the Billing and Payment terms and conditions established by Copyright Clearance Center, Inc. ("CCC"), at the time that you opened your Rightslink account and that are available at any time at http://myaccount.copyright.com).

GENERAL TERMS

2. Elsevier hereby grants you permission to reproduce the aforementioned material subject to the terms and conditions indicated.

3. Acknowledgement: If any part of the material to be used (for example, figures) has appeared in our publication with credit or acknowledgement to another source, permission

ELSEVIER LICENSE
TERMS AND CONDITIONS

Dec 07, 2021

This Agreement between Dr. Amirali Shamsolhodaei ("You") and Elsevier ("Elsevier") consists of your license details and the terms and conditions provided by Elsevier and Copyright Clearance Center.

License Number	5203890645739
License date	Dec 07, 2021
Licensed Content Publisher	Elsevier
Licensed Content Publication	Materials Characterization
Licensed Content Title	Microstructural characterization of laser micro-welded Nitinol wires
Licensed Content Author	Peng Dong,Hongmei Li,Wenxian Wang,Jun Zhou
Licensed Content Date	Jan 1, 2018
Licensed Content Volume	135
Licensed Content Issue	n/a
Licensed Content Pages	6
Start Page	40
End Page	45
Type of Use	reuse in a thesis/dissertation
Portion	figures/tables/illustrations

Number of figures/tables/illustrations	1
Format	both print and electronic
Are you the author of this Elsevier article?	No
Will you be translating?	No
Title	Dissimilar laser welding of NiTi shape memory alloys
Institution name	University of Waterloo
Expected presentation date	Dec 2021
Portions	Figure 4
Requestor Location	Dr. Amirali Shamsolhodaei 200 University Avenue West Waterloo, ON N2L 3G Canada Attn: Dr. Amirali Shamsolhodaei
Publisher Tax ID	GB 494 6272 12
Total	0.00 CAD

Terms and Conditions

INTRODUCTION

1. The publisher for this copyrighted material is Elsevier. By clicking "accept" in connection with completing this licensing transaction, you agree that the following terms and conditions apply to this transaction (along with the Billing and Payment terms and conditions established by Copyright Clearance Center, Inc. ("CCC"), at the time that you opened your Rightslink account and that are available at any time at http://myaccount.copyright.com).

GENERAL TERMS

2. Elsevier hereby grants you permission to reproduce the aforementioned material subject to the terms and conditions indicated.

3. Acknowledgement: If any part of the material to be used (for example, figures) has appeared in our publication with credit or acknowledgement to another source, permission

ELSEVIER LICENSE
TERMS AND CONDITIONS

Dec 07, 2021

This Agreement between Dr. Amirali Shamsolhodaei ("You") and Elsevier ("Elsevier") consists of your license details and the terms and conditions provided by Elsevier and Copyright Clearance Center.

License Number	5203890712828
License date	Dec 07, 2021
Licensed Content Publisher	Elsevier
Licensed Content Publication	Materials Letters
Licensed Content Title	Microstructure and shape memory effect of laser welded Nitinol wires
Licensed Content Author	Runhua Yao,Peng Dong,Peter K. Liaw,Jun Zhou,Wenxian Wang
Licensed Content Date	Mar 1, 2019
Licensed Content Volume	238
Licensed Content Issue	n/a
Licensed Content Pages	5
Start Page	1
End Page	5
Type of Use	reuse in a thesis/dissertation
Portion	figures/tables/illustrations

Number of figures/tables/illustrations	1
Format	both print and electronic
Are you the author of this Elsevier article?	No
Will you be translating?	No
Title	Dissimilar laser welding of NiTi shape memory alloys
Institution name	University of Waterloo
Expected presentation date	Dec 2021
Portions	Figure 4
Requestor Location	Dr. Amirali Shamsolhodaei 200 University Avenue West Waterloo, ON N2L 3G Canada Attn: Dr. Amirali Shamsolhodaei
Publisher Tax ID	GB 494 6272 12
Total	0.00 CAD

Terms and Conditions

INTRODUCTION

1. The publisher for this copyrighted material is Elsevier. By clicking "accept" in connection with completing this licensing transaction, you agree that the following terms and conditions apply to this transaction (along with the Billing and Payment terms and conditions established by Copyright Clearance Center, Inc. ("CCC"), at the time that you opened your Rightslink account and that are available at any time at http://myaccount.copyright.com).

GENERAL TERMS

2. Elsevier hereby grants you permission to reproduce the aforementioned material subject to the terms and conditions indicated.

3. Acknowledgement: If any part of the material to be used (for example, figures) has appeared in our publication with credit or acknowledgement to another source, permission

To : The Japan Institute of Metals and Materials

Request for Permission to Reproduce Copyrighted Publication

I am preparing an article entitled: Dissimilar Laser Welding of NiTi Shape Memory alloys

Reuse in : Doctoral Thesis which will be published by : University of Waterloo

Expected publication date : December 2021 Language : English

Format : both print and electronic

Price: free Circulation : 1

I wish to have your permission to include in my article the following publication.

Title of Journal / Book : Materials Transactions

Paper Title : Heat-Conduction-Type and Keyhole-Type Laser Welding of Ti-Ni Shape-Memory Alloys Processed by Spark-Plasma Sintering

Author(s) : Abdollah Bahador, Esah Hamzah, Katsuyoshi Kondoh, Seiichiro Tsutsumi, Junko Umeda, Tuty Asma Abu Bakar and Farazila Yusof

Year : 2018 Vol : 59 No.: 5 Page : 835-842

Figure(s)/Table(s) : Figure 10 and Figure 11

If permission is granted for the use of this publication, the author(s) and your publication will be credited as the original source.

I would greatly appreciate it if you could indicate your agreement by signing and returning this form.

Thank you for your cooperation.

Sincerely yours,

Name : Amirali Shamsolhodaei

Affiliation : University of Waterloo

Address : 200 University Ave. West, Waterloo, ON, Canada N2l5G1

E-mail : ashamsol@uwaterloo.ca

TEL : +1 519 888 4567 FAX :

****

I/We hereby grant permission for the use of the publication requested above.

Date: December 9, 2021

Signed: Hideaki Yamamura

Copyright Holder : The Japan Institute of Metals and Materials

1-14-32, Ichibancho, Aoba-Ku, Sendai 980-8544, Japan

ELSEVIER LICENSE
TERMS AND CONDITIONS

Dec 07, 2021

This Agreement between Dr. Amirali Shamsolhodaei ("You") and Elsevier ("Elsevier") consists of your license details and the terms and conditions provided by Elsevier and Copyright Clearance Center.

License Number	5203891246849
License date	Dec 07, 2021
Licensed Content Publisher	Elsevier
Licensed Content Publication	Acta Materialia
Licensed Content Title	Mechanical and microstructural integrity of nickel–titanium and stainless steel laser joined wires
Licensed Content Author	J. Vannod,M. Bornert,J.-E. Bidaux,L. Bataillard,A. Karimi,J.-M. Drezet,M. Rappaz,A. Hessler-Wyser
Licensed Content Date	Oct 1, 2011
Licensed Content Volume	59
Licensed Content Issue	17
Licensed Content Pages	9
Start Page	6538
End Page	6546
Type of Use	reuse in a thesis/dissertation

Portion	figures/tables/illustrations
Number of figures/tables/illustrations	1
Format	both print and electronic
Are you the author of this Elsevier article?	No
Will you be translating?	No
Title	Dissimilar laser welding of NiTi shape memory alloys
Institution name	University of Waterloo
Expected presentation date	Dec 2021
Portions	Figure 7
Requestor Location	Dr. Amirali Shamsolhodaei 200 University Avenue West Waterloo, ON N2L 3G Canada Attn: Dr. Amirali Shamsolhodaei
Publisher Tax ID	GB 494 6272 12
Total	0.00 CAD

Terms and Conditions

INTRODUCTION

1. The publisher for this copyrighted material is Elsevier. By clicking "accept" in connection with completing this licensing transaction, you agree that the following terms and conditions apply to this transaction (along with the Billing and Payment terms and conditions established by Copyright Clearance Center, Inc. ("CCC"), at the time that you opened your Rightslink account and that are available at any time at http://myaccount.copyright.com).

GENERAL TERMS

2. Elsevier hereby grants you permission to reproduce the aforementioned material subject to the terms and conditions indicated.

ELSEVIER LICENSE
TERMS AND CONDITIONS

Dec 07, 2021

This Agreement between Dr. Amirali Shamsolhodaei ("You") and Elsevier ("Elsevier") consists of your license details and the terms and conditions provided by Elsevier and Copyright Clearance Center.

License Number	5203891311507
License date	Dec 07, 2021
Licensed Content Publisher	Elsevier
Licensed Content Publication	Acta Materialia
Licensed Content Title	Three-dimensional chemical analysis of laser-welded NiTi–stainless steel wires using a dual-beam FIB
Licensed Content Author	P. Burdet,J. Vannod,A. Hessler-Wyser,M. Rappaz,M. Cantoni
Licensed Content Date	May 1, 2013
Licensed Content Volume	61
Licensed Content Issue	8
Licensed Content Pages	9
Start Page	3090
End Page	3098
Type of Use	reuse in a thesis/dissertation
Portion	figures/tables/illustrations

Number of figures/tables/illustrations	1
Format	both print and electronic
Are you the author of this Elsevier article?	No
Will you be translating?	No
Title	Dissimilar laser welding of NiTi shape memory alloys
Institution name	University of Waterloo
Expected presentation date	Dec 2021
Portions	Figure 12
Requestor Location	Dr. Amirali Shamsolhodaei 200 University Avenue West Waterloo, ON N2L 3G Canada Attn: Dr. Amirali Shamsolhodaei
Publisher Tax ID	GB 494 6272 12
Total	0.00 CAD

Terms and Conditions

INTRODUCTION

1. The publisher for this copyrighted material is Elsevier. By clicking "accept" in connection with completing this licensing transaction, you agree that the following terms and conditions apply to this transaction (along with the Billing and Payment terms and conditions established by Copyright Clearance Center, Inc. ("CCC"), at the time that you opened your Rightslink account and that are available at any time at http://myaccount.copyright.com).

GENERAL TERMS

2. Elsevier hereby grants you permission to reproduce the aforementioned material subject to the terms and conditions indicated.

SPRINGER NATURE LICENSE
TERMS AND CONDITIONS

Dec 07, 2021

This Agreement between Dr. Amirali Shamsolhodaei ("You") and Springer Nature ("Springer Nature") consists of your license details and the terms and conditions provided by Springer Nature and Copyright Clearance Center.

License Number	5203891395802
License date	Dec 07, 2021
Licensed Content Publisher	Springer Nature
Licensed Content Publication	The International Journal of Advanced Manufacturing Technology
Licensed Content Title	Fiber laser welding of NiTi to Ti-6Al-4V
Licensed Content Author	R. M. Miranda et al
Licensed Content Date	May 26, 2015
Type of Use	Thesis/Dissertation
Requestor type	academic/university or research institute
Format	print and electronic
Portion	figures/tables/illustrations
Number of figures/tables/illustrations	2
Will you be translating?	no
Circulation/distribution	1 - 29

Author of this Springer Nature content	no
Title	Dissimilar laser welding of NiTi shape memory alloys
Institution name	University of Waterloo
Expected presentation date	Dec 2021
Portions	Figure 1, Figure 3
Requestor Location	Dr. Amirali Shamsolhodaei 200 University Avenue West Waterloo, ON N2L 3G Canada Attn: Dr. Amirali Shamsolhodaei
Total	0.00 CAD

Terms and Conditions

Springer Nature Customer Service Centre GmbH
Terms and Conditions

This agreement sets out the terms and conditions of the licence (the **Licence**) between you and **Springer Nature Customer Service Centre GmbH** (the **Licensor**). By clicking 'accept' and completing the transaction for the material (**Licensed Material**), you also confirm your acceptance of these terms and conditions.

1. Grant of License

1. 1. The Licensor grants you a personal, non-exclusive, non-transferable, world-wide licence to reproduce the Licensed Material for the purpose specified in your order only. Licences are granted for the specific use requested in the order and for no other use, subject to the conditions below.

1. 2. The Licensor warrants that it has, to the best of its knowledge, the rights to license reuse of the Licensed Material. However, you should ensure that the material you are requesting is original to the Licensor and does not carry the copyright of another entity (as credited in the published version).

1. 3. If the credit line on any part of the material you have requested indicates that it was reprinted or adapted with permission from another source, then you should also seek permission from that source to reuse the material.

2. Scope of Licence

ELSEVIER LICENSE
TERMS AND CONDITIONS

Dec 07, 2021

This Agreement between Dr. Amirali Shamsolhodaei ("You") and Elsevier ("Elsevier") consists of your license details and the terms and conditions provided by Elsevier and Copyright Clearance Center.

License Number	5203860375613
License date	Dec 07, 2021
Licensed Content Publisher	Elsevier
Licensed Content Publication	Materials & Design
Licensed Content Title	A review of shape memory alloy research, applications and opportunities
Licensed Content Author	Jaronie Mohd Jani,Martin Leary,Aleksandar Subic,Mark A. Gibson
Licensed Content Date	Apr 1, 2014
Licensed Content Volume	56
Licensed Content Issue	n/a
Licensed Content Pages	36
Start Page	1078
End Page	1113
Type of Use	reuse in a thesis/dissertation
Portion	figures/tables/illustrations

Number of figures/tables/illustrations	2
Format	both print and electronic
Are you the author of this Elsevier article?	No
Will you be translating?	No
Title	Dissimilar laser welding of NiTi shape memory alloys
Institution name	University of Waterloo
Expected presentation date	Dec 2021
Portions	Figure 1, Figure 18
Requestor Location	Dr. Amirali Shamsolhodaei 200 University Avenue West Waterloo, ON N2L 3G Canada Attn: Dr. Amirali Shamsolhodaei
Publisher Tax ID	GB 494 6272 12
Total	0.00 CAD

Terms and Conditions

INTRODUCTION

1. The publisher for this copyrighted material is Elsevier. By clicking "accept" in connection with completing this licensing transaction, you agree that the following terms and conditions apply to this transaction (along with the Billing and Payment terms and conditions established by Copyright Clearance Center, Inc. ("CCC"), at the time that you opened your Rightslink account and that are available at any time at http://myaccount.copyright.com).

GENERAL TERMS

2. Elsevier hereby grants you permission to reproduce the aforementioned material subject to the terms and conditions indicated.

3. Acknowledgement: If any part of the material to be used (for example, figures) has appeared in our publication with credit or acknowledgement to another source, permission

ELSEVIER LICENSE
TERMS AND CONDITIONS

Dec 07, 2021

This Agreement between Dr. Amirali Shamsolhodaei ("You") and Elsevier ("Elsevier") consists of your license details and the terms and conditions provided by Elsevier and Copyright Clearance Center.

License Number	5203900044075
License date	Dec 07, 2021
Licensed Content Publisher	Elsevier
Licensed Content Publication	Optics & Laser Technology
Licensed Content Title	Laser welding of TiNi shape memory alloy and stainless steel using Co filler metal
Licensed Content Author	Hongmei Li,Daqian Sun,Xiaolong Cai,Peng Dong,Xiaoyan Gu
Licensed Content Date	Feb 1, 2013
Licensed Content Volume	45
Licensed Content Issue	n/a
Licensed Content Pages	8
Start Page	453
End Page	460
Type of Use	reuse in a thesis/dissertation
Portion	figures/tables/illustrations

Number of figures/tables/illustrations	2
Format	both print and electronic
Are you the author of this Elsevier article?	No
Will you be translating?	No
Title	Dissimilar laser welding of NiTi shape memory alloys
Institution name	University of Waterloo
Expected presentation date	Dec 2021
Portions	Figure 5, Figure 7
Requestor Location	Dr. Amirali Shamsolhodaei 200 University Avenue West Waterloo, ON N2L 3G Canada Attn: Dr. Amirali Shamsolhodaei
Publisher Tax ID	GB 494 6272 12
Total	0.00 CAD

Terms and Conditions

INTRODUCTION

1. The publisher for this copyrighted material is Elsevier. By clicking "accept" in connection with completing this licensing transaction, you agree that the following terms and conditions apply to this transaction (along with the Billing and Payment terms and conditions established by Copyright Clearance Center, Inc. ("CCC"), at the time that you opened your Rightslink account and that are available at any time at http://myaccount.copyright.com).

GENERAL TERMS

2. Elsevier hereby grants you permission to reproduce the aforementioned material subject to the terms and conditions indicated.

3. Acknowledgement: If any part of the material to be used (for example, figures) has appeared in our publication with credit or acknowledgement to another source, permission

ELSEVIER LICENSE
TERMS AND CONDITIONS

Dec 07, 2021

This Agreement between Dr. Amirali Shamsolhodaei ("You") and Elsevier ("Elsevier") consists of your license details and the terms and conditions provided by Elsevier and Copyright Clearance Center.

License Number	5203900117215
License date	Dec 07, 2021
Licensed Content Publisher	Elsevier
Licensed Content Publication	Acta Materialia
Licensed Content Title	Laser joining of NiTi to Ti6Al4V using a Niobium interlayer
Licensed Content Author	J.P. Oliveira,B. Panton,Z. Zeng,C.M. Andrei,Y. Zhou,R.M. Miranda,F.M. Braz Fernandes
Licensed Content Date	Feb 15, 2016
Licensed Content Volume	105
Licensed Content Issue	n/a
Licensed Content Pages	7
Start Page	9
End Page	15
Type of Use	reuse in a thesis/dissertation
Portion	figures/tables/illustrations

Number of figures/tables/illustrations	1
Format	both print and electronic
Are you the author of this Elsevier article?	No
Will you be translating?	No
Title	Dissimilar laser welding of NiTi shape memory alloys
Institution name	University of Waterloo
Expected presentation date	Dec 2021
Portions	Figure 6
Requestor Location	Dr. Amirali Shamsolhodaei 200 University Avenue West Waterloo, ON N2L 3G Canada Attn: Dr. Amirali Shamsolhodaei
Publisher Tax ID	GB 494 6272 12
Total	0.00 CAD

Terms and Conditions

INTRODUCTION

1. The publisher for this copyrighted material is Elsevier. By clicking "accept" in connection with completing this licensing transaction, you agree that the following terms and conditions apply to this transaction (along with the Billing and Payment terms and conditions established by Copyright Clearance Center, Inc. ("CCC"), at the time that you opened your Rightslink account and that are available at any time at http://myaccount.copyright.com).

GENERAL TERMS

2. Elsevier hereby grants you permission to reproduce the aforementioned material subject to the terms and conditions indicated.

3. Acknowledgement: If any part of the material to be used (for example, figures) has appeared in our publication with credit or acknowledgement to another source, permission

ELSEVIER LICENSE
TERMS AND CONDITIONS

Dec 07, 2021

This Agreement between Dr. Amirali Shamsolhodaei ("You") and Elsevier ("Elsevier") consists of your license details and the terms and conditions provided by Elsevier and Copyright Clearance Center.

License Number	5203900181897
License date	Dec 07, 2021
Licensed Content Publisher	Elsevier
Licensed Content Publication	Materials & Design
Licensed Content Title	Laser welding of TiNi shape memory alloy and stainless steel using Ni interlayer
Licensed Content Author	H.M. Li,D.Q. Sun,X.L. Cai,P. Dong,W.Q. Wang
Licensed Content Date	Aug 1, 2012
Licensed Content Volume	39
Licensed Content Issue	n/a
Licensed Content Pages	9
Start Page	285
End Page	293
Type of Use	reuse in a thesis/dissertation
Portion	figures/tables/illustrations

Number of figures/tables/illustrations	3
Format	both print and electronic
Are you the author of this Elsevier article?	No
Will you be translating?	No
Title	Dissimilar laser welding of NiTi shape memory alloys
Institution name	University of Waterloo
Expected presentation date	Dec 2021
Portions	Figure 5, Figure 10 and Figure 11
Requestor Location	Dr. Amirali Shamsolhodaei 200 University Avenue West Waterloo, ON N2L 3G Canada Attn: Dr. Amirali Shamsolhodaei
Publisher Tax ID	GB 494 6272 12
Total	0.00 CAD

Terms and Conditions

INTRODUCTION

1. The publisher for this copyrighted material is Elsevier. By clicking "accept" in connection with completing this licensing transaction, you agree that the following terms and conditions apply to this transaction (along with the Billing and Payment terms and conditions established by Copyright Clearance Center, Inc. ("CCC"), at the time that you opened your Rightslink account and that are available at any time at http://myaccount.copyright.com).

GENERAL TERMS

2. Elsevier hereby grants you permission to reproduce the aforementioned material subject to the terms and conditions indicated.

3. Acknowledgement: If any part of the material to be used (for example, figures) has appeared in our publication with credit or acknowledgement to another source, permission

ELSEVIER LICENSE
TERMS AND CONDITIONS

Dec 07, 2021

This Agreement between Dr. Amirali Shamsolhodaei ("You") and Elsevier ("Elsevier") consists of your license details and the terms and conditions provided by Elsevier and Copyright Clearance Center.

License Number	5203900260288
License date	Dec 07, 2021
Licensed Content Publisher	Elsevier
Licensed Content Publication	Journal of Material Science & Technology
Licensed Content Title	Effect of interlayer addition on microstructure and mechanical properties of NiTi/stainless steel joint by electron beam welding
Licensed Content Author	H. Niu,H.C. Jiang,M.J. Zhao,L.J. Rong
Licensed Content Date	Jan 20, 2021
Licensed Content Volume	61
Licensed Content Issue	n/a
Licensed Content Pages	9
Start Page	16
End Page	24
Type of Use	reuse in a thesis/dissertation
Portion	figures/tables/illustrations

Number of figures/tables/illustrations	2
Format	both print and electronic
Are you the author of this Elsevier article?	No
Will you be translating?	No
Title	Dissimilar laser welding of NiTi shape memory alloys
Institution name	University of Waterloo
Expected presentation date	Dec 2021
Portions	Figure 4 and Figure 7
Requestor Location	Dr. Amirali Shamsolhodaei 200 University Avenue West Waterloo, ON N2L 3G Canada Attn: Dr. Amirali Shamsolhodaei
Publisher Tax ID	GB 494 6272 12
Total	0.00 CAD

Terms and Conditions

INTRODUCTION

1. The publisher for this copyrighted material is Elsevier. By clicking "accept" in connection with completing this licensing transaction, you agree that the following terms and conditions apply to this transaction (along with the Billing and Payment terms and conditions established by Copyright Clearance Center, Inc. ("CCC"), at the time that you opened your Rightslink account and that are available at any time at http://myaccount.copyright.com).

GENERAL TERMS

2. Elsevier hereby grants you permission to reproduce the aforementioned material subject to the terms and conditions indicated.

ELSEVIER LICENSE
TERMS AND CONDITIONS

Dec 09, 2021

This Agreement between Dr. Amirali Shamsolhodaei ("You") and Elsevier ("Elsevier") consists of your license details and the terms and conditions provided by Elsevier and Copyright Clearance Center.

License Number	5205040613833
License date	Dec 09, 2021
Licensed Content Publisher	Elsevier
Licensed Content Publication	Journal of Alloys and Compounds
Licensed Content Title	Effects of niobium addition on the microstructure and mechanical properties of laser-welded joints of NiTiNb and Ti6Al4V alloys
Licensed Content Author	Xingwen Zhou,Yuhua Chen,Yongde Huang,Yuqing Mao,Yangyang Yu
Licensed Content Date	Feb 25, 2018
Licensed Content Volume	735
Licensed Content Issue	n/a
Licensed Content Pages	9
Start Page	2616
End Page	2624
Type of Use	reuse in a thesis/dissertation

Portion	figures/tables/illustrations
Number of figures/tables/illustrations	1
Format	both print and electronic
Are you the author of this Elsevier article?	No
Will you be translating?	No
Title	Dissimilar laser welding of NiTi shape memory alloys
Institution name	University of Waterloo
Expected presentation date	Dec 2021
Portions	Figure 7
Requestor Location	Dr. Amirali Shamsolhodaei 200 University Avenue West Waterloo, ON N2L 3G Canada Attn: Dr. Amirali Shamsolhodaei
Publisher Tax ID	GB 494 6272 12
Total	0.00 CAD

Terms and Conditions

INTRODUCTION

1. The publisher for this copyrighted material is Elsevier. By clicking "accept" in connection with completing this licensing transaction, you agree that the following terms and conditions apply to this transaction (along with the Billing and Payment terms and conditions established by Copyright Clearance Center, Inc. ("CCC"), at the time that you opened your Rightslink account and that are available at any time at http://myaccount.copyright.com).

GENERAL TERMS

CCC Marketplace™

Order Confirmation

Thank you, your order has been placed. An email confirmation has been sent to you. Your order license details and printable licenses will be available within 24 hours. Please access Manage Account for final order details.

This is not an invoice. Please go to manage account to access your order history and invoices.

CUSTOMER INFORMATION

Payment by invoice: You can cancel your order until the invoice is generated by contacting customer service.

Billing Address

Dr. Amirali Shamsolhodaei
200 University Avenue West
Waterloo, ON N2L 3G1
Canada

+1 (519) 888-4567
ashamsol@uwaterloo.ca

Customer Location

Dr. Amirali Shamsolhodaei
200 University Avenue West
Waterloo, ON N2L 3G1
Canada

PO Number (optional)

N/A

Payment options

Invoice

PENDING ORDER CONFIRMATION

Confirmation Number: Pending

Order Date: 07-Dec-2021

1. Smart Materials and Structures

0.00 CAD

Order License ID	Pending	**Publisher**	IOP Publishing
ISSN	1361-665X	**Portion**	Chart/graph/table/ figure
Type of Use	Republish in a thesis/dissertation		

LICENSED CONTENT

Publication Title	Smart Materials and Structures	**Country**	United Kingdom of Great Britain and Northern Ireland
Author/Editor	Institute of Physics (Great Britain)	**Rightsholder**	IOP Publishing, Ltd
Date	01/01/1992	**Publication Type**	e-Journal
Language	English		

		URL	http://iopscience.iop.org/0964-1726

REQUEST DETAILS

Portion Type	Chart/graph/table/figure	Distribution	Canada
Number of charts / graphs / tables / figures requested	4	Translation	Original language of publication
Format (select all that apply)	Print, Electronic	Copies for the disabled?	No
		Minor editing privileges?	No
Who will republish the content?	Academic institution	Incidental promotional use?	No
Duration of Use	Life of current and all future editions	Currency	CAD
Lifetime Unit Quantity	Up to 499		
Rights Requested	Main product		

NEW WORK DETAILS

Title	Dissimilar laser welding of NiTi shape memory alloys	Institution name	University of Waterloo
		Expected presentation date	2021-12-07
Instructor name	Prof. Norman Zhou, Prof. Peng Peng		

ADDITIONAL DETAILS

Order reference number	N/A	The requesting person / organization to appear on the license	Amirali Shamsolhodaei

REUSE CONTENT DETAILS

Title, description or numeric reference of the portion(s)	Dissimilar laser welding of NiTi shape memory alloy and copper	Title of the article/chapter the portion is from	Dissimilar laser welding of NiTi shape memory alloy and copper
Editor of portion(s)	N/A	Author of portion(s)	Institute of Physics (Great Britain)
Volume of serial or monograph	24	Issue, if republishing an article from a serial	12
Page or page range of portion	3, 4, 6	Publication date of portion	2015-09-21

RIGHTSHOLDER TERMS AND CONDITIONS

These special terms and conditions are in addition to the standard terms and conditions for CCC's Republication Service and, together with those standard terms and conditions, govern the use of the Works. As the User you will make all reasonable efforts to contact the author(s) of the article which the Work is to be reused from, to seek consent for your intended use. Contacting one author who is acting expressly as authorised agent for their co-author(s) is acceptable. User will reproduce the following wording prominently alongside the Work: the source of the Work, including author, article title, title of journal, volume number, issue number (if relevant), page range (or first page if this is the only information available) and date of first publication; and a link back to the article (via DOI); and if practicable, and IN ALL CASES for new works published under any of the Creative Commons licences, the words "© IOP Publishing. Reproduced with permission. All rights reserved" Without the express permission of the author(s) and the Rightsholder of the article from which the Work is

SPRINGER NATURE LICENSE
TERMS AND CONDITIONS

Dec 07, 2021

This Agreement between Dr. Amirali Shamsolhodaei ("You") and Springer Nature ("Springer Nature") consists of your license details and the terms and conditions provided by Springer Nature and Copyright Clearance Center.

License Number	5203900861502
License date	Dec 07, 2021
Licensed Content Publisher	Springer Nature
Licensed Content Publication	Metallurgical and Materials Transactions A
Licensed Content Title	Dissimilar Laser Joining of NiTi SMA and MP35N Wires
Licensed Content Author	Boyd Panton et al
Licensed Content Date	Apr 15, 2014
Type of Use	Thesis/Dissertation
Requestor type	academic/university or research institute
Format	print and electronic
Portion	figures/tables/illustrations
Number of figures/tables/illustrations	1
Will you be translating?	no
Circulation/distribution	1 - 29

Author of this Springer Nature content	no
Title	Dissimilar laser welding of NiTi shape memory alloys
Institution name	University of Waterloo
Expected presentation date	Dec 2021
Portions	Figure 3
Requestor Location	Dr. Amirali Shamsolhodaei 200 University Avenue West Waterloo, ON N2L 3G Canada Attn: Dr. Amirali Shamsolhodaei
Total	0.00 CAD

Terms and Conditions

Springer Nature Customer Service Centre GmbH
Terms and Conditions

This agreement sets out the terms and conditions of the licence (the **Licence**) between you and **Springer Nature Customer Service Centre GmbH** (the **Licensor**). By clicking 'accept' and completing the transaction for the material (**Licensed Material**), you also confirm your acceptance of these terms and conditions.

1. Grant of License

1. 1. The Licensor grants you a personal, non-exclusive, non-transferable, world-wide licence to reproduce the Licensed Material for the purpose specified in your order only. Licences are granted for the specific use requested in the order and for no other use, subject to the conditions below.

1. 2. The Licensor warrants that it has, to the best of its knowledge, the rights to license reuse of the Licensed Material. However, you should ensure that the material you are requesting is original to the Licensor and does not carry the copyright of another entity (as credited in the published version).

1. 3. If the credit line on any part of the material you have requested indicates that it was reprinted or adapted with permission from another source, then you should also seek permission from that source to reuse the material.

2. Scope of Licence

ELSEVIER LICENSE
TERMS AND CONDITIONS

Dec 07, 2021

This Agreement between Dr. Amirali Shamsolhodaei ("You") and Elsevier ("Elsevier") consists of your license details and the terms and conditions provided by Elsevier and Copyright Clearance Center.

License Number	5203900927313
License date	Dec 07, 2021
Licensed Content Publisher	Elsevier
Licensed Content Publication	Materials Letters
Licensed Content Title	A novel laser welding method for the reliable joining of NiTi/301SS
Licensed Content Author	Xiao-Long Gao,Xiao-Qiang Wang,Jing Liu,Lun-kun Li
Licensed Content Date	Jun 1, 2020
Licensed Content Volume	268
Licensed Content Issue	n/a
Licensed Content Pages	1
Start Page	127573
End Page	0
Type of Use	reuse in a thesis/dissertation
Portion	figures/tables/illustrations

Number of figures/tables/illustrations	1
Format	both print and electronic
Are you the author of this Elsevier article?	No
Will you be translating?	No
Title	Dissimilar laser welding of NiTi shape memory alloys
Institution name	University of Waterloo
Expected presentation date	Dec 2021
Portions	Figure 1
Requestor Location	Dr. Amirali Shamsolhodaei 200 University Avenue West Waterloo, ON N2L 3G Canada Attn: Dr. Amirali Shamsolhodaei
Publisher Tax ID	GB 494 6272 12
Total	0.00 CAD

Terms and Conditions

INTRODUCTION

1. The publisher for this copyrighted material is Elsevier. By clicking "accept" in connection with completing this licensing transaction, you agree that the following terms and conditions apply to this transaction (along with the Billing and Payment terms and conditions established by Copyright Clearance Center, Inc. ("CCC"), at the time that you opened your Rightslink account and that are available at any time at http://myaccount.copyright.com).

GENERAL TERMS

2. Elsevier hereby grants you permission to reproduce the aforementioned material subject to the terms and conditions indicated.

3. Acknowledgement: If any part of the material to be used (for example, figures) has appeared in our publication with credit or acknowledgement to another source, permission

ELSEVIER LICENSE
TERMS AND CONDITIONS

Dec 07, 2021

This Agreement between Dr. Amirali Shamsolhodaei ("You") and Elsevier ("Elsevier") consists of your license details and the terms and conditions provided by Elsevier and Copyright Clearance Center.

License Number	5203901272404
License date	Dec 07, 2021
Licensed Content Publisher	Elsevier
Licensed Content Publication	Materials Science and Engineering: A
Licensed Content Title	Effects of post-weld heat treatment on the microstructure and mechanical properties of laser-welded NiTi/304SS joint with Ni filler
Licensed Content Author	Yuhua Chen,Songwei Sun,Timing Zhang,Xingwen Zhou,Shuhan Li
Licensed Content Date	Jan 13, 2020
Licensed Content Volume	771
Licensed Content Issue	n/a
Licensed Content Pages	1
Start Page	138545
End Page	0
Type of Use	reuse in a thesis/dissertation

Portion	figures/tables/illustrations
Number of figures/tables/illustrations	3
Format	both print and electronic
Are you the author of this Elsevier article?	No
Will you be translating?	No
Title	Dissimilar laser welding of NiTi shape memory alloys
Institution name	University of Waterloo
Expected presentation date	Dec 2021
Portions	Figure 2, Figure 4, Table 2
Requestor Location	Dr. Amirali Shamsolhodaei 200 University Avenue West Waterloo, ON N2L 3G Canada Attn: Dr. Amirali Shamsolhodaei
Publisher Tax ID	GB 494 6272 12
Total	0.00 CAD

Terms and Conditions

INTRODUCTION

1. The publisher for this copyrighted material is Elsevier. By clicking "accept" in connection with completing this licensing transaction, you agree that the following terms and conditions apply to this transaction (along with the Billing and Payment terms and conditions established by Copyright Clearance Center, Inc. ("CCC"), at the time that you opened your Rightslink account and that are available at any time at http://myaccount.copyright.com).

GENERAL TERMS

ELSEVIER LICENSE
TERMS AND CONDITIONS

Dec 07, 2021

This Agreement between Dr. Amirali Shamsolhodaei ("You") and Elsevier ("Elsevier") consists of your license details and the terms and conditions provided by Elsevier and Copyright Clearance Center.

License Number	5203901038212
License date	Dec 07, 2021
Licensed Content Publisher	Elsevier
Licensed Content Publication	Journal of the Mechanical Behavior of Biomedical Materials
Licensed Content Title	The effect of annealing temperature on microstructure and mechanical properties of dissimilar laser welded superelastic NiTi to austenitic stainless steels orthodontic archwires
Licensed Content Author	Saeed Asadi,Tohid Saeid,Alireza Valanezhad,Ikuya Watanabe,Jafar Khalil-Allafi
Licensed Content Date	Sep 1, 2020
Licensed Content Volume	109
Licensed Content Issue	n/a
Licensed Content Pages	1
Start Page	103818
End Page	0
Type of Use	reuse in a thesis/dissertation

Portion	figures/tables/illustrations
Number of figures/tables/illustrations	1
Format	both print and electronic
Are you the author of this Elsevier article?	No
Will you be translating?	No
Title	Dissimilar laser welding of NiTi shape memory alloys
Institution name	University of Waterloo
Expected presentation date	Dec 2021
Portions	Figure 10
Requestor Location	Dr. Amirali Shamsolhodaei 200 University Avenue West Waterloo, ON N2L 3G Canada Attn: Dr. Amirali Shamsolhodaei
Publisher Tax ID	GB 494 6272 12
Total	0.00 CAD

Terms and Conditions

INTRODUCTION

1. The publisher for this copyrighted material is Elsevier. By clicking "accept" in connection with completing this licensing transaction, you agree that the following terms and conditions apply to this transaction (along with the Billing and Payment terms and conditions established by Copyright Clearance Center, Inc. ("CCC"), at the time that you opened your Rightslink account and that are available at any time at http://myaccount.copyright.com).

GENERAL TERMS

SPRINGER NATURE LICENSE
TERMS AND CONDITIONS

Dec 07, 2021

This Agreement between Dr. Amirali Shamsolhodaei ("You") and Springer Nature ("Springer Nature") consists of your license details and the terms and conditions provided by Springer Nature and Copyright Clearance Center.

License Number	5203910176705
License date	Dec 07, 2021
Licensed Content Publisher	Springer Nature
Licensed Content Publication	ISSS Journal of Micro and Smart Systems
Licensed Content Title	NiTiPt shape memory alloy: microstructure and transformation behaviour
Licensed Content Author	K. V. Ramaiah et al
Licensed Content Date	Jul 18, 2019
Type of Use	Thesis/Dissertation
Requestor type	academic/university or research institute
Format	print and electronic
Portion	figures/tables/illustrations
Number of figures/tables/illustrations	3
Will you be translating?	no
Circulation/distribution	1 - 29

Author of this Springer Nature content	no
Title	Dissimilar laser welding of NiTi shape memory alloys
Institution name	University of Waterloo
Expected presentation date	Dec 2021
Portions	Figure 1, Figure 4 and Figure 6
Requestor Location	Dr. Amirali Shamsolhodaei 200 University Avenue West Waterloo, ON N2L 3G Canada Attn: Dr. Amirali Shamsolhodaei
Total	0.00 CAD

Terms and Conditions

Springer Nature Customer Service Centre GmbH
Terms and Conditions

This agreement sets out the terms and conditions of the licence (the **Licence**) between you and **Springer Nature Customer Service Centre GmbH** (the **Licensor**). By clicking 'accept' and completing the transaction for the material (**Licensed Material**), you also confirm your acceptance of these terms and conditions.

1. Grant of License

1. 1. The Licensor grants you a personal, non-exclusive, non-transferable, world-wide licence to reproduce the Licensed Material for the purpose specified in your order only. Licences are granted for the specific use requested in the order and for no other use, subject to the conditions below.

1. 2. The Licensor warrants that it has, to the best of its knowledge, the rights to license reuse of the Licensed Material. However, you should ensure that the material you are requesting is original to the Licensor and does not carry the copyright of another entity (as credited in the published version).

1. 3. If the credit line on any part of the material you have requested indicates that it was reprinted or adapted with permission from another source, then you should also seek permission from that source to reuse the material.

2. Scope of Licence

SPRINGER NATURE LICENSE
TERMS AND CONDITIONS

Dec 07, 2021

This Agreement between Dr. Amirali Shamsolhodaei ("You") and Springer Nature ("Springer Nature") consists of your license details and the terms and conditions provided by Springer Nature and Copyright Clearance Center.

License Number	5203910492942
License date	Dec 07, 2021
Licensed Content Publisher	Springer Nature
Licensed Content Publication	European Radiology
Licensed Content Title	Self-expanding nitinol stents: material and design considerations
Licensed Content Author	Dieter Stoeckel et al
Licensed Content Date	Sep 3, 2003
Type of Use	Thesis/Dissertation
Requestor type	academic/university or research institute
Format	print and electronic
Portion	figures/tables/illustrations
Number of figures/tables/illustrations	2
Will you be translating?	no
Circulation/distribution	1 - 29

Author of this Springer Nature content	no
Title	Dissimilar laser welding of NiTi shape memory alloys
Institution name	University of Waterloo
Expected presentation date	Dec 2021
Portions	Figure 21 and Figure 22
Requestor Location	Dr. Amirali Shamsolhodaei 200 University Avenue West Waterloo, ON N2L 3G Canada Attn: Dr. Amirali Shamsolhodaei
Total	0.00 CAD

Terms and Conditions

Springer Nature Customer Service Centre GmbH
Terms and Conditions

This agreement sets out the terms and conditions of the licence (the **Licence**) between you and **Springer Nature Customer Service Centre GmbH** (the **Licensor**). By clicking 'accept' and completing the transaction for the material (**Licensed Material**), you also confirm your acceptance of these terms and conditions.

1. Grant of License

1. 1. The Licensor grants you a personal, non-exclusive, non-transferable, world-wide licence to reproduce the Licensed Material for the purpose specified in your order only. Licences are granted for the specific use requested in the order and for no other use, subject to the conditions below.

1. 2. The Licensor warrants that it has, to the best of its knowledge, the rights to license reuse of the Licensed Material. However, you should ensure that the material you are requesting is original to the Licensor and does not carry the copyright of another entity (as credited in the published version).

1. 3. If the credit line on any part of the material you have requested indicates that it was reprinted or adapted with permission from another source, then you should also seek permission from that source to reuse the material.

2. Scope of Licence

JOHN WILEY AND SONS LICENSE
TERMS AND CONDITIONS

Dec 07, 2021

This Agreement between Dr. Amirali Shamsolhodaei ("You") and John Wiley and Sons ("John Wiley and Sons") consists of your license details and the terms and conditions provided by John Wiley and Sons and Copyright Clearance Center.

License Number	5203910589979
License date	Dec 07, 2021
Licensed Content Publisher	John Wiley and Sons
Licensed Content Publication	Advanced Engineering Materials
Licensed Content Title	Anisotropic Behavior of Radiopaque NiTiPt Hypotube for Biomedical Applications
Licensed Content Author	Kelly Pike, Boris Anukhin, David Mackiewicz, et al
Licensed Content Date	Nov 18, 2009
Licensed Content Volume	11
Licensed Content Issue	11
Licensed Content Pages	5
Type of use	Dissertation/Thesis
Requestor type	University/Academic
Format	Print and electronic

Portion	Figure/table
Number of figures/tables	1
Will you be translating?	No
Title	Dissimilar laser welding of NiTi shape memory alloys
Institution name	University of Waterloo
Expected presentation date	Dec 2021
Portions	Figure 2
Requestor Location	Dr. Amirali Shamsolhodaei 200 University Avenue West Waterloo, ON N2L 3G Canada Attn: Dr. Amirali Shamsolhodaei
Publisher Tax ID	EU826007151
Total	0.00 CAD

Terms and Conditions

TERMS AND CONDITIONS

This copyrighted material is owned by or exclusively licensed to John Wiley & Sons, Inc. or one of its group companies (each a"Wiley Company") or handled on behalf of a society with which a Wiley Company has exclusive publishing rights in relation to a particular work (collectively "WILEY"). By clicking "accept" in connection with completing this licensing transaction, you agree that the following terms and conditions apply to this transaction (along with the billing and payment terms and conditions established by the Copyright Clearance Center Inc., ("CCC's Billing and Payment terms and conditions"), at the time that you opened your RightsLink account (these are available at any time at http://myaccount.copyright.com).

Terms and Conditions

- The materials you have requested permission to reproduce or reuse (the "Wiley Materials") are protected by copyright.

ELSEVIER LICENSE
TERMS AND CONDITIONS

Dec 07, 2021

This Agreement between Dr. Amirali Shamsolhodaei ("You") and Elsevier ("Elsevier") consists of your license details and the terms and conditions provided by Elsevier and Copyright Clearance Center.

License Number	5203910723592
License date	Dec 07, 2021
Licensed Content Publisher	Elsevier
Licensed Content Publication	Scripta Materialia
Licensed Content Title	In situ W–NiTi shape memory alloy composite of high radiopacity
Licensed Content Author	S. Wang,F.M. Guo,D.Q. Jiang,Y. Liu,L.S. Cui
Licensed Content Date	Jun 15, 2014
Licensed Content Volume	81
Licensed Content Issue	n/a
Licensed Content Pages	4
Start Page	4
End Page	7
Type of Use	reuse in a thesis/dissertation
Portion	figures/tables/illustrations

Number of figures/tables/illustrations	1
Format	both print and electronic
Are you the author of this Elsevier article?	No
Will you be translating?	No
Title	Dissimilar laser welding of NiTi shape memory alloys
Institution name	University of Waterloo
Expected presentation date	Dec 2021
Portions	Figure 1
Requestor Location	Dr. Amirali Shamsolhodaei 200 University Avenue West Waterloo, ON N2L 3G Canada Attn: Dr. Amirali Shamsolhodaei
Publisher Tax ID	GB 494 6272 12
Total	0.00 CAD

Terms and Conditions

INTRODUCTION

1. The publisher for this copyrighted material is Elsevier. By clicking "accept" in connection with completing this licensing transaction, you agree that the following terms and conditions apply to this transaction (along with the Billing and Payment terms and conditions established by Copyright Clearance Center, Inc. ("CCC"), at the time that you opened your Rightslink account and that are available at any time at http://myaccount.copyright.com).

GENERAL TERMS

2. Elsevier hereby grants you permission to reproduce the aforementioned material subject to the terms and conditions indicated.

3. Acknowledgement: If any part of the material to be used (for example, figures) has appeared in our publication with credit or acknowledgement to another source, permission

SPRINGER NATURE LICENSE
TERMS AND CONDITIONS

Dec 07, 2021

This Agreement between Dr. Amirali Shamsolhodaei ("You") and Springer Nature ("Springer Nature") consists of your license details and the terms and conditions provided by Springer Nature and Copyright Clearance Center.

License Number	5203911067276
License date	Dec 07, 2021
Licensed Content Publisher	Springer Nature
Licensed Content Publication	Journal of Materials Engineering and Performance
Licensed Content Title	Effect of Laser Positioning on the Microstructure and Properties of NiTi-Copper Dissimilar Laser Welds
Licensed Content Author	A. Shamsolhodaei et al
Licensed Content Date	Feb 10, 2020
Type of Use	Thesis/Dissertation
Requestor type	academic/university or research institute
Format	print and electronic
Portion	full article/chapter
Will you be translating?	no
Circulation/distribution	1 - 29

Author of this Springer Nature content	yes
Title	Dissimilar laser welding of NiTi shape memory alloys
Institution name	University of Waterloo
Expected presentation date	Dec 2021
Requestor Location	Dr. Amirali Shamsolhodaei 200 University Avenue West Waterloo, ON N2L 3G Canada Attn: Dr. Amirali Shamsolhodaei
Total	0.00 CAD

Terms and Conditions

Springer Nature Customer Service Centre GmbH
Terms and Conditions

This agreement sets out the terms and conditions of the licence (the **Licence**) between you and **Springer Nature Customer Service Centre GmbH** (the **Licensor**). By clicking 'accept' and completing the transaction for the material (**Licensed Material**), you also confirm your acceptance of these terms and conditions.

1. Grant of License

1. 1. The Licensor grants you a personal, non-exclusive, non-transferable, world-wide licence to reproduce the Licensed Material for the purpose specified in your order only. Licences are granted for the specific use requested in the order and for no other use, subject to the conditions below.

1. 2. The Licensor warrants that it has, to the best of its knowledge, the rights to license reuse of the Licensed Material. However, you should ensure that the material you are requesting is original to the Licensor and does not carry the copyright of another entity (as credited in the published version).

1. 3. If the credit line on any part of the material you have requested indicates that it was reprinted or adapted with permission from another source, then you should also seek permission from that source to reuse the material.

2. Scope of Licence

2. 1. You may only use the Licensed Content in the manner and to the extent permitted by these Ts&Cs and any applicable laws.

SPRINGER NATURE LICENSE
TERMS AND CONDITIONS

Dec 07, 2021

This Agreement between Dr. Amirali Shamsolhodaei ("You") and Springer Nature ("Springer Nature") consists of your license details and the terms and conditions provided by Springer Nature and Copyright Clearance Center.

License Number	5203911245115
License date	Dec 07, 2021
Licensed Content Publisher	Springer Nature
Licensed Content Publication	Metallurgical and Materials Transactions A
Licensed Content Title	Laser Alloying as an Effective Way to Fabricate NiTiPt Shape Memory Alloys
Licensed Content Author	A. Shamsolhodaei et al
Licensed Content Date	Jul 17, 2021
Type of Use	Thesis/Dissertation
Requestor type	academic/university or research institute
Format	print and electronic
Portion	full article/chapter
Will you be translating?	no
Circulation/distribution	1 - 29
Author of this Springer Nature content	yes

Title	Dissimilar laser welding of NiTi shape memory alloys
Institution name	University of Waterloo
Expected presentation date	Dec 2021
Requestor Location	Dr. Amirali Shamsolhodaei 200 University Avenue West Waterloo, ON N2L 3G Canada Attn: Dr. Amirali Shamsolhodaei
Total	0.00 CAD

Terms and Conditions

Springer Nature Customer Service Centre GmbH
Terms and Conditions

This agreement sets out the terms and conditions of the licence (the **Licence**) between you and **Springer Nature Customer Service Centre GmbH** (the **Licensor**). By clicking 'accept' and completing the transaction for the material (**Licensed Material**), you also confirm your acceptance of these terms and conditions.

1. Grant of License

1. 1. The Licensor grants you a personal, non-exclusive, non-transferable, world-wide licence to reproduce the Licensed Material for the purpose specified in your order only. Licences are granted for the specific use requested in the order and for no other use, subject to the conditions below.

1. 2. The Licensor warrants that it has, to the best of its knowledge, the rights to license reuse of the Licensed Material. However, you should ensure that the material you are requesting is original to the Licensor and does not carry the copyright of another entity (as credited in the published version).

1. 3. If the credit line on any part of the material you have requested indicates that it was reprinted or adapted with permission from another source, then you should also seek permission from that source to reuse the material.

2. Scope of Licence

2. 1. You may only use the Licensed Content in the manner and to the extent permitted by these Ts&Cs and any applicable laws.

2. 2. A separate licence may be required for any additional use of the Licensed Material, e.g. where a licence has been purchased for print only use, separate permission must be obtained for electronic re-use. Similarly, a licence is only valid in the language selected and does not apply for editions in other languages unless additional translation rights have been granted separately in the licence. Any content